



## Copyright Undertaking

This thesis is protected by copyright, with all rights reserved.

**By reading and using the thesis, the reader understands and agrees to the following terms:**

1. The reader will abide by the rules and legal ordinances governing copyright regarding the use of the thesis.
2. The reader will use the thesis for the purpose of research or private study only and not for distribution or further reproduction or any other purpose.
3. The reader agrees to indemnify and hold the University harmless from and against any loss, damage, cost, liability or expenses arising from copyright infringement or unauthorized usage.

### IMPORTANT

If you have reasons to believe that any materials in this thesis are deemed not suitable to be distributed in this form, or a copyright owner having difficulty with the material being included in our database, please contact [lbsys@polyu.edu.hk](mailto:lbsys@polyu.edu.hk) providing details. The Library will look into your claim and consider taking remedial action upon receipt of the written requests.

**PARAMETRIC CONVERGENCE BOUND OF  
VOLTERRA SERIES EXPANSION AND  
APPLICATIONS USING NCOS-BASED  
ANALYSIS AND DESIGN**

XIAO ZHENLONG

Ph.D

The Hong Kong  
Polytechnic University

2015

THE HONG KONG POLYTECHNIC UNIVERSITY

Department of Mechanical Engineering

**Parametric Convergence Bound of Volterra Series  
Expansion and Applications using nCOS-based  
Analysis and Design**

Xiao Zhenlong

A thesis submitted in partial fulfilment of the requirements for the

degree of Doctor of Philosophy

January 2015

*This page intentionally left blank*

# CERTIFICATE OF ORIGINALITY

I hereby declare that this thesis is my own work and that, to the best of my knowledge and belief, it reproduces no material previously published or written, nor material that has been accepted for the award of any other degree or diploma, except where due acknowledgement has been made in the text.

---

Xiao Zhenlong

---

*This page intentionally left blank*

# Abstract

The Volterra series based nonlinear analysis and design methodology is a powerful tool that has been applied to various engineering practices. This study addresses several key issues of the Volterra series based methodology that have not been well developed in the literature, including its convergence, applications, and extensions.

Two novel concepts, i.e., the parametric bound of convergence (PBoC) and parametric convergence margin (PCM), are proposed for nonlinear systems described by nonlinear auto-regressive with exogenous input (NARX) models. The proposed PBoC can calculate the convergence bound not only for the input magnitude, but also for the parameters of interest. The PCM is developed as a quantitative assessment to examine the distance from a given nonlinear system to the bound of a convergent Volterra series expansion.

By applying the theoretical results above, the nonlinear characteristic output spectrum (nCOS) function can be well analysed and designed within a certain region of nonlinear parameters of interest. A nonlinear damping is proposed to overcome the well-known dilemma with respect to linear damping. The performance of the nonlinear damping is derived with the nCOS method, which also provides a straightforward and effective way to tackle the multiple-object nonlinear optimization problem.

Linear components or linear controllers are usually easier to implement in practice, and are thus of considerable interest for analysis and design to achieve a better performance when simultaneously considering a system that is inherently nonlinear. The existing nCOS method is only available for nonlinear parameters, and thus is extended to those linear parameters of interest. A symbolic algorithm for calculating the new nCOS function is developed for single-input single-output (SISO) systems. In case that the built symbolic algorithm is complicated for MIMO systems, a numerical identification method is developed.

The results above are established for nonlinear systems with polynomial nonlinearity. For those nonlinear systems with exponential-type nonlinearity, there would be too many parameters in the analysis and design because exponential nonlinearity is usually approximated by Taylor series expansions. An efficient algorithm with many fewer parameters for calculating the generalized frequency response function (GFRF) in the nonlinear analysis and design is then developed.

The contributions of this thesis lie in the following points. The results of PBoC and PCM are notable extensions of those convergence results in the literature, and can provide a more straightforward and useful guidance for the parameter design or feedback design of nonlinear systems via the nCOS method. The new nCOS function can provide a straightforward understanding of the effect of the linear parameters of interest on the nonlinear output spectrum and thereby greatly facilitate the analysis and design of linear components or controllers for nonlinear systems. The extension of the nCOS method to exponential-type nonlinear system will considerably ease the analysis and design of systems with exponential nonlinearity, such as amplifier circuits and neural networks, in the frequency domain.

# Publication List

## *Journal paper:*

*Xiao*, Jing, and Cheng, “The transmissibility of vibration isolators with cubic nonlinear damping under both force and base excitations,” *Journal of Sound and Vibration*, vol. 332, pp.1335-1354, 2013.

*Xiao*, Jing, and Cheng, “Parameterized convergence bounds for Volterra series expansion of NARX models,” *Signal Processing, IEEE Transactions on*, vol. 61, pp. 5026-5038, 2013.

*Xiao*, Jing, and Cheng, “Estimation of parametric convergence bounds for Volterra series expansion of nonlinear systems,” *Mechanical Systems and Signal Processing*, vol. 45, pp. 28-48, 2014.

*Xiao*, and Jing, “A SIMO nonlinear system approach to analysis and design of vehicle suspensions,” *Mechatronics, IEEE Transactions on*, DOI: 10.1109/TMECH. 2015. 2401631.

*Xiao*, and Jing, “Frequency-domain analysis and design of linear feedback of nonlinear systems and applications in vehicle suspensions,” *Mechatronics, IEEE Transactions on*, DOI:10.1109/TMECH.2015.2446519.

*Xiao*, and Jing, “A novel linear analysis and design approach to nonlinear circuit systems,” *Signal Processing, IEEE Transactions on*, revision.

## *Conference paper:*

*Xiao*, Jing, and Cheng, “Computation of parametric convergence bound and parametric convergence margin for Volterra series expansion,” the 9th ASCC 2013, Istanbul, Turkey, June23-26, 2013.

*Xiao*, Jing, and Cheng, “Parametric convergence bounds for Volterra series expansion of nonlinear MDoF systems”, The 9th International Conference on Vibration Engineering and Technology of Machinery, Nanjing, China, August 20-23, 2013

# Acknowledgments

I would like to express my deepest appreciation to my chief supervisor, Dr. Jing Xingjian, for his patience, creative thoughts, and professional guidance in my postgraduate study. I appreciate his vast knowledge and skills in many disciplines and his guidance in writing this dissertation. I am also would like to express my gratitude to my co-supervisor, Prof. Cheng Li, for his encouragement and discussion.

I would like to thank my friends, Xi Qiang, Yu Xiang, Hong Ming, Wang Zhibo, Liu Shuyuan, Dr. Wang Qiang, and Dr. Liang Wenyan, for their encouragement and useful discussion. I would also like to express my sincere thanks to the members of the Nonlinear System and Signal Processing (NSSP) group, Dr. Zhu Xiacong, Mr. Wu Keming, and Dr. Ning Hanwen, etc..

Finally, I am grateful to my parents for their understanding and support.

# Table of Contents

Certificate of originality .....	II
Abstract.....	IV
Publication List .....	VI
Acknowledgments .....	VII
Table of Contents.....	VIII
Figures and Tables.....	X
<b>1. Introduction .....</b>	<b>1</b>
1.1 Overview of nonlinear analysis methods .....	2
1.2 Motivation, Objectives and Contributions .....	15
1.3 Outline of the thesis .....	23
<b>2 Parametric convergence bound for Volterra series expansion of nonlinear systems .....</b>	<b>26</b>
2.1 Introduction .....	26
2.2 The parametric convergence bound for single-input single-output (SISO) nonlinear autoregressive with exogenous input (NARX) model.....	27
2.3 Parametric convergence bound for general input.....	57
2.4 Parametric convergence bound for single-input multiple-output (SIMO) system .....	67
2.5 Conclusion .....	75
<b>3 The nCOS method based analysis and design of nonlinear parameters, considering the parametric convergence bound (PBoC).....</b>	<b>76</b>
3.1 Introduction .....	76
3.2 nCOS method based analysis of nonlinear damping .....	79
3.3 Multiple-object nonlinear optimization based on the nCOS method....	96
3.4 Conclusions .....	114
<b>4 A new nCOS function for the analysis and design of linear parameters in a nonlinear system.....</b>	<b>115</b>
4.1 Introduction .....	115
4.2 New nCOS function for linear parameters of interest.....	117
4.3 The new nCOS function based linear feedback design for MIMO nonlinear systems .....	139
4.4 Conclusions .....	161
<b>5 An extension to exponential type nonlinear systems.....</b>	<b>162</b>
5.1 Introduction .....	162
5.2 Calculation of the GFRFs and the nCOS-based analysis of	

exponential-type nonlinear systems.....	164
5.3 Conclusion .....	183
<b>6 Conclusions and future work .....</b>	<b>184</b>
6.1 Conclusions .....	184
6.2 Future work .....	186
<b>7 Appendix .....</b>	<b>188</b>
<b>8 Reference.....</b>	<b>212</b>

# Figures and Tables

Table 1.1 Comparisons between different frequency methods.....	14
Table 3.1 Coefficients of (3.35).....	99
Table 3.2 Coefficients of (3.42).....	106
Table 4.1 Coefficients $\theta_1^{\alpha_2}(\omega_1)$ at $\omega_1 = 2\pi \times 5 \times 10^6 \text{ rad / s}$ .....	127
Table 4.2 Coefficients of $\theta_3^{\alpha_2}(\omega_3)$ .....	130
Table 4.3 Coefficients of (4.17).....	134
Table 4.4 Estimation of Parameters of Interest Independent Part.....	155
Figure 2.1 The PBoC of $C(3,0) =  c_{3,0}(1,1,1) $ .....	41
Figure 2.2 Comparison of the synthesized output and the original output at $\omega = 0.8\omega_0$ .....	42
Figure 2.3 The PBoCs for the input amplitude.....	43
Figure 2.4 The parametric convergence margin (PCM) .....	44
Figure 2.5 The PBoC of $C(1,2) =  c_{1,2}(1,1,1) $ .....	46
Figure 2.6 The PBoC of $C(3,0) =  c_{3,0}(1,1,1) $ .....	46
Figure 2.7 Comparison of the synthesized output and the original output at $\omega = 0.8\omega_0$ with $c_{3,0}(1,1,1) = -153.8223$ .....	47
Figure 2.8 Comparison of the synthesized output and the original output at $\omega = 0.8\omega_0$ with $c_{1,2}(1,1,1) = -1.5382 \times 10^{-4}$ .....	47
Figure 2.9 The parametric convergence margin (PCM) .....	48
Figure 2.10 The PBoC of $C(1,2) =  c_{1,2}(1,1,1) $ .....	50
Figure 2.11 Comparison of the synthesized output and the original output at $\omega = 0.8\omega_0$ with $c_{0,3}(1,1,1) = 0$ .....	50
Figure 2.12 Comparison of the synthesized output and the original output at $\omega = 0.8\omega_0$ with $c_{0,3}(1,1,1) = -2.5 \times 10^{-5}$ .....	51
Figure 2.13 The PCM.....	51
Figure 2.14 The PBoC of $C(3,0) =  c_{3,0}(1,1,1) $ .....	53

Figure 2.15 The PBoC of $C(0,3) =  c_{0,3}(1,1,1) $ .....	54
Figure 2.16 Comparison of the synthesized output and the original output at $\omega = 0.8\omega_0$ with $c_{0,3}(1,1,1) = -2.3073 \times 10^{-7}$ .....	54
Figure 2.17 Comparison of the synthesized output and the original output at $\omega = 0.8\omega_0$ with $c_{3,0}(1,1,1) = -153.8223$ .....	55
Figure 2.18 The PCM.....	56
Figure 2.19 The PBoC of the input magnitude.....	63
Figure 2.20 The normalized root mean square error .....	64
Figure 2.21 The PBoC of the model parameter $c_{3,0}(111)$ .....	65
Figure 3.1 Isolator subjected to force excitation .....	80
Figure 3.2 Isolator subjected to base excitation .....	80
Figure 3.3 The parametric convergence bound $\bar{\beta}_2$ for nonlinear isolator under force excitation (3.4).....	91
Figure 3.4 The parametric convergence bound $\bar{\beta}_2$ for nonlinear isolator under base excitation (3.8).....	91
Figure 3.5 The force transmissibility of a SDoF isolator under force excitation.....	93
Figure 3.6 The force transmissibility of the isolator under base displacement excitation .....	93
Figure 3.7 The absolute displacement transmissibility of the isolator under base displacement .	94
Figure 3.8 Equivalent damping coefficient of the cubic order nonlinear damping .....	95
Figure 3.9 A quarter vehicle suspension model.....	98
Figure 3.10 The PBoC of $C_{s3}$ .....	101
Figure 3.11 The normalized root mean square error when $f=4\text{Hz}$ .....	102
Figure 3.12 Comparison of vertical body acceleration under cosine road excitation.....	105
Figure 3.13 Multiple-object performance under cosine excitation: (a) at 4Hz, (b) at 8Hz.....	108
Figure 3.14 Multiple-object performance under cosine excitation at 4Hz with $\mu_1+\mu_2=1$ , the red ball is the MOP function by numerical simulation.....	110
Figure 3.15 Comparison of the performances with different strategies. (a) subject to C level road profile with 20 m/s, (b) subject to D level road profile with 20 m/s .....	112
Figure 3.16 Comparison of the Active forces.....	112
Figure 4.1 The equivalent circuit model of a common-gate amplifier .....	126
Figure 4.2 Validation of Proposition 4.2 with $c_{1,02}=C=63\text{pF}$ . 63pF adopted here because it is the optimal value for suppression of harmonic distortion in example 2. ....	128
Figure 4.3 Magnitude of $H_1(\omega_1)$ with different capacitance at $\omega_1 = 2\pi \times 5 \times 10^6 \text{ rad / s}$ .....	128
Figure 4.4 Magnitude of $H_3(\omega_1, \omega_2, \omega_3)$ with different capacitance at $\omega_1 = \omega_2 = \omega_3 = 2\pi \times 5 \times 10^6 \text{ rad / s}$ .....	132

Figure 4.5 $\Gamma_1 =  \hat{L}_1^{-1}(\omega_1)\delta(\omega_1) $ and $\Gamma_3 =  \hat{L}_3^{-1}(\omega_3)\delta(\omega_3) $ .....	132
Figure 4.6 Third-order harmonic distortion with different parameter of interest .....	135
Figure 4.7 Output spectrum with different parameter of interest at $\Omega$ .....	136
Figure 4.8 Output spectrum with different parameter of interest at $3\Omega$ .....	137
Figure 4.9 A nonlinear vehicle suspension systems .....	150
Figure 4.10 The estimated nCOS function by (4.44) with different sets of $k_3$ and $k_4$ at four frequencies of interest. The symbols (ball, star, cubic, and tetrahedron) stand for the acceleration at the corresponding frequency and parameters by numerical simulation. The red balls represent the acceleration with designed parameters.....	156
Figure 4.11 The value of $\rho =  \mathbf{K}\tilde{\mathbf{L}}_1^{-1}\mathbf{B}_2 $ .....	156
Figure 4.12 Performance function (4.46) with different feedback gain parameters. The red ball is the performance with optimal designed parameters.....	157
Figure 4.13 Comparison of the performance with/without controller when subjects to ISO C level road profile.....	158
Figure 4.14 (a) Comparison of the accelerations when subjects to ISO C level road profile in the time domain. (b) Comparison of the active force in time domain. ....	158
Figure 5.1 Equivalent model of bipolar amplifier .....	172
Figure 5.2 Comparison of third-order harmonic distortion with different methods .....	175
Figure 5.3 A three-layer radial-basis function neural network .....	177
Figure 5.4 Amplitude of $X_1(3\Omega)$ via different methods .....	180
Figure 5.5 Amplitude of $X_2(3\Omega)$ via different methods .....	180
Figure 5.6 Amplitude of $Y(3\Omega)$ with different parameters of interest .....	181

# 1. Introduction

Many practical systems have inherent nonlinearity. Examples can be observed in mechanical engineering, i.e., the leaf spring in a vehicle suspension [1], the magnetorheological fluid damper and the pneumatic spring in a vibration isolator [2-4], and also in electronic engineering, i.e., satellite communication channel modelling [5] and a radio frequency amplifier [6-11]. Even if all of the system components have ideal linear characteristics, the system characteristics can possess observable nonlinearity, for example, the quasi-zero stiffness isolator [12-20] and the recently developed scissor-like isolator [21, 22]. Moreover, many results show that some potential advantages or benefits can be achieved when nonlinearity is intentionally employed in the system, for example, the nonlinear damper investigated in [23, 24] to overcome the well-known dilemma associated with linear viscous damping.

From the above, system nonlinearity should be well taken into account in system analysis and design, but the existence of nonlinearity often introduces difficulties. An effective and efficient method for the analysis and design of nonlinear systems is increasingly demanded but is still a challenging topic in the literature.

In the following, the overview and comparison of different nonlinear analysis methods are first presented. Then, the motivation, objectives, and corresponding main contributions of this thesis are presented. Finally, an outline of this thesis is

given.

## 1.1 Overview of nonlinear analysis methods

A variety of methods (both time domain methods and frequency domain methods) have been independently developed for analysing nonlinear systems. A brief overview of the following nonlinear analysis methods is presented:

### Time domain methods

- Adomian Decomposition Method
- Homotopy Analysis Method

### Frequency domain methods

- Harmonic Balance Method
- Lindstedt-Poincare Method
- Describing Function Method
- Volterra Series Associated Method
- Nonlinear Characteristic Output Spectrum (nCOS) Method

### 1.1.1 Time Domain Methods

#### Adomian Decomposition Method

The Adomian decomposition method was introduced by Adomian [25] in the 1980s and has been widely used in various areas [26-29]. It is defined by the nonlinear equation

$$\mathcal{L}(y(t)) + \mathcal{N}(y(t)) = u(t) \quad (1.1)$$

where  $\mathcal{L}(\bullet)$  is a linear operator,  $\mathcal{N}(\bullet)$  is a nonlinear operator,  $y(t)$  is the system output, and  $u(t)$  is the system input. The Adomian decomposition method decomposes the solution  $y(t)$  and the nonlinear operator  $\mathcal{N}(\bullet)$  as,

$$y(t) = \sum_{n=0}^{\infty} \lambda^n y_n(t) \quad (1.2)$$

and

$$N(y(t)) = \sum_{n=0}^{\infty} \lambda^{n+1} A_n(y_0(t), y_1(t), \dots, y_n(t)) \quad (1.3)$$

where  $A_n(y_0(t), y_1(t), \dots, y_n(t))$  is referred to as Adomian polynomials, which can be analytically calculated. Substituting (1.2) and (1.3) into nonlinear equation (1.1) and equating the coefficients of  $\lambda^n$  on both sides, the nonlinear equation can be decomposed into a series of linear equations as

$$\begin{aligned} \mathcal{L}(y_0(t)) &= u(t) \\ \mathcal{L}(y_n(t)) &= A_{n-1}(y_0(t), y_1(t), \dots, y_{n-1}(t)), \quad n \geq 1. \end{aligned} \quad (1.4)$$

From(1.4),  $y_n(t)$  can be recursively calculated with  $y_0(t), y_1(t), \dots, y_{n-1}(t)$  . It should be noted that no perturbation theory or closure approximation is required for calculating  $y_n(t)$ , so the small parameters assumption is thus not needed, and the Adomian decomposition method is able to work in circumstances where the perturbation method fails. Supposing that (1.2) and (1.3) converge when  $\lambda = 1$ , the solution  $y$  can then be obtained via (1.2). This assumption works in many circumstances but with the problem that (1.2) and (1.3) are not always convergent [30, 31]. Thus, the Adomian decomposition method is only applicable to mild nonlinearities, although it is not restricted to a small parameters assumption [32].

## Homotopy Analysis Method

The homotopy analysis method was proposed by Liao [32] in the 1990s based on homotopy, a fundamental concept of topology. An auxiliary parameter and an auxiliary function are introduced in this method to adjust the convergence region and convergence rate, which enables its use for some strongly nonlinear cases. Considering the following nonlinear equation,  $\mathcal{N}(y(t))=0$ , Liao constructed a so-called homotopy,

$$(1-\kappa)\mathcal{L}[\pi(t,\kappa)-y_0(t)]=\kappa\hbar\mathcal{H}(t)\mathcal{N}[\pi(t,\kappa)] \quad (1.5)$$

where  $\mathcal{L}(\bullet)$  is an auxiliary linear operator with the property  $\mathcal{L}(0)=0$ , which need not be the linear part of nonlinear operator  $\mathcal{N}(\bullet)$ .  $y_0(t)$  is an initial guess output. The choice of a different auxiliary linear operator  $\mathcal{L}(\bullet)$  and initial guess output  $y_0(t)$  makes it possible to construct the system output  $y(t)$  with different sets of base functions.  $\hbar$  and  $\mathcal{H}(t)$  are the auxiliary parameter and auxiliary function for adjusting the convergence region and convergence rate, respectively.  $\kappa \in [0,1]$  is an embedding parameter, and  $\pi(t,\kappa)$  is a function of  $t$  and  $\kappa$ . When  $\kappa=0$  holds, we have  $\pi(t,0)=y_0(t)$ , and  $\pi(t,1)=y(t)$  holds when  $\kappa$  equals to 1. As the embedding parameter  $\kappa$  increases from 0 to 1, the solution  $\pi(t,\kappa)$  varies from the guess output  $y_0(t)$  to the exact output  $y(t)$ . Such a continuous variation is called deformation in topology.

The homotopy analysis method provides great freedom to choose the initial guess output  $y_0(t)$ , the auxiliary linear operator  $\mathcal{L}(\bullet)$ , the auxiliary parameter  $\hbar$ ,

and the auxiliary function  $\mathcal{H}(t)$ , but no rigorous guidance has been developed for choosing them. The choice of those auxiliary elements may require some prior knowledge about the nonlinear operator, and would not be easy if the nonlinear problem is completely new to engineers [32].

Most studies of homotopy analysis method focus on the initial value problem or the boundary value problem [33-36]. In a case with an external input, the homotopy analysis method also has the problem [37] that occurs in the harmonic balance method or the Lindstedt-Poincare method, which will be discussed later.

### **1.1.2 Frequency Domain Methods**

Although time domain methods for nonlinear problems are easy to implement, nonlinear phenomena such as super-harmonic, sub-harmonic, or intermodulation directly relate to the concepts in the frequency domain, making the use of frequency domain methods more straightforward, which has led to their popularity in the literature.

#### **Harmonic Balance Method**

The harmonic balance method is not restricted to mildly nonlinear problems and can easily be understood by transferring a nonlinear differential equation problem into a nonlinear algebraic problem [38]. Considering the nonlinear equation in (1.1), the harmonic balance method assumes that the solution is given

by a truncated Fourier series of the form

$$y = \sum_{m=0}^M A_m \cos(m\omega t + \varphi_m) \quad (1.6)$$

where  $M$  is the truncation order, and  $A_m$  and  $\varphi_m$  are the coefficients to be determined. First, approximate the nonlinear operator  $\mathcal{N}(\bullet)$  in (1.1) with a Taylor series expansion, and then substitute solution (1.6) into the approximated nonlinear equation. After equating the coefficients of the lowest  $M + 1$  harmonics to 0,  $2(M + 1)$  nonlinear algebraic equations involving  $A_m$ ,  $\varphi_m$ , and the input frequency variable  $\omega$  can be obtained. The solution is obtained by solving the algebraic equations, which would be much easier than directly solving nonlinear differential equations. The technical line of the harmonic balance method is straightforward and easy to understand.

One problem of the harmonic balance method is that the accuracy of the solution depends on the number of harmonics,  $M$ , in (1.6). One needs to use a large enough truncated order  $M$  or to understand a great deal of the solution a priori, or the solution would otherwise be inaccurate [39, 40]. However, a large truncated order  $M$  would cause a dimension problem of the nonlinear algebraic equations, which would be even worse when a multi-tone input or a general input acts on the system [41-43]. Hence, Nayfeh had the following comment—‘therefore we prefer not to use this technique’ [39].

## Lindstedt-Poincare Method

The Lindstedt-Poincare method was developed to eliminate the secular terms that exist in the perturbation method [38, 39]. Considering nonlinear equation (1.1) again, the Lindstedt-Poincare method expands the system output  $y$  and the frequency variable  $\omega$  as power series of the small parameter  $\varepsilon$  in the nonlinear operator  $\mathcal{N}(\cdot)$ ,

$$y(t) = y_0 + \varepsilon y_1 + \varepsilon^2 y_2 + \dots \quad (1.7)$$

$$\omega = \omega_0 + \varepsilon \omega_1 + \varepsilon^2 \omega_2 + \dots \quad (1.8)$$

where  $\omega_0$  is the resonant frequency in the linear operator  $\mathcal{L}(\cdot)$ . Substituting (1.7) and (1.8) into nonlinear equation (1.1) and equating the coefficient of each power of  $\varepsilon$  to zero, the nonlinear equation is then transferred into a series of linear differential equations. New nonlinear algebraic equations can be derived to eliminate the secular terms. After solving the nonlinear algebraic equations, the solution  $y(t)$  can be obtained.

The Lindstedt-Poincare method strongly depends on the small parameter assumption, so would fail if there exists no small parameter in the nonlinear equation. Usually, the approximation of the system output in (1.7) is truncated up to second-order or third-order because it is very complicated to derive the associated nonlinear algebraic equations of a higher-order approximation  $y_n$ . Another problem of the Lindstedt-Poincare method is that  $y_1, y_2, \dots$  are implicitly involved in the nonlinear algebraic equations, so it fails to provide an explicit relationship between the system output and the system input (or model

parameters of interest). Moreover, when nonlinear equation (1.1) is a multi-degree-of-freedom system or subject to a multi-tone input, it is not easy to derive the nonlinear algebraic equations based on the rule of eliminating secular terms, which limits the application of this method.

### **Describing Function Method**

The frequency response function (or transfer function) is a powerful tool in linear system analysis and design that does not work in nonlinear systems because the principles of superposition and homogeneity do not hold. The describing function method tries to extend the concept of the frequency response function to a nonlinear problem [44, 45]. Assuming that a single-tone input  $u(t) = Ue^{j\omega t}$  acts on the nonlinear operator  $\mathcal{N}(u(t))$ , the describing function is then defined as

$$D(U, \omega) = \frac{Y(U, \omega)}{U} \quad (1.9)$$

where  $Y(U, \omega)$  is the output of nonlinear operator  $\mathcal{N}(u(t))$  at frequency  $\omega$  with input amplitude  $U$ . The nonlinear operator  $\mathcal{N}(u(t))$  can then be approximated as a linear operator with transfer function  $D(U, \omega)$ . The describing function is a function of input amplitude  $U$ , which is different from the linear transfer function (that is independent of input).

From (1.9), the describing function only considers the output at the fundamental excitation frequency, so it fails to characterize the super-harmonic components, sub-harmonic components, and the intermodulation effect of the

nonlinear operator. The nonlinear operator  $\mathcal{N}(\bullet)$  is usually assumed to have odd-order nonlinearity, and the input is supposed to be single-tone in the literature to simplify the calculation, which limits the application of the describing function. The generalized describing function was then proposed to relax the input to be multi-tone [46, 47], but in this case, the nonlinear operator  $\mathcal{N}(\bullet)$  should be Volterra-type.

### Volterra series associated method

The Volterra series associated frequency method generalizes the concept of the frequency response function in linear systems to nonlinear systems. Initiated by Vito Volterra [48] and then developed by many researchers, for example, Brilliant [49], Brockett [50], Sandberg [51-54], and Boyd [55, 56], it was shown that the input-output relationship of the nonlinear operator  $\mathcal{N}(\bullet)$  can be approximated uniformly and to an arbitrary degree of precision by a sufficient high order Volterra series as

$$y(t) = \sum_{n=1}^N \int_0^{\infty} \cdots \int_0^{\infty} h_n(\tau_1, \cdots, \tau_n) \prod_{i=1}^n u(t - \tau_i) d\tau_i \quad (1.10)$$

where  $h_n(\tau_1, \cdots, \tau_n)$  is the  $n$ th-order Volterra kernel,  $N$  is the truncated order, and  $\tau_i$  is the convolution variable. In (1.10), the existence of the convolution variable  $\tau_i$  implies that the output of the nonlinear system at the given moment  $t$  via Volterra series expansion depends on the part input to the system, which provides the ability of the output via Volterra series expansion to capture the ‘memory’ effect of the nonlinear system. This is the fundamental difference between the

Volterra series expansion and the Taylor series expansion because the output of the nonlinear system via Taylor series expansion depends strictly on the input at that particular time. Therefore, the Volterra series associated method is more suitable for the devices/systems having ‘memory’ effect, for example, capacitors and inductors.

The generalized frequency response function (GFRF) was first introduced by George [57] and is defined as the  $n$ -dimensional Fourier transform of the Volterra kernel as

$$H_n(\omega_1, \dots, \omega_n) = \int_{-\infty}^{\infty} \dots \int_{-\infty}^{\infty} h_n(\tau_1, \dots, \tau_n) e^{j\omega_1\tau_1} \dots e^{j\omega_n\tau_n} d\tau_1 \dots d\tau_n . \quad (1.11)$$

The calculation of the  $n$ th-order generalized frequency response function (GFRF) was first developed for nonlinear autoregressive models with exogenous inputs (NARX) [58] using the probing method and then built for nonlinear integro-differential equations [59] and nonlinear rational models [60]. According to these results, higher-order GFRFs can be recursively calculated from lower-order GFRFs, which provides a powerful tool to calculate GFRFs from model parameters, greatly facilitating the analysis of nonlinear systems. The calculation of GFRFs for a nonlinear system with constant terms [61-63] was investigated thereafter, and algorithms for multiple-input single-output [64] and multiple-input multiple-output (MIMO) [65] nonlinear systems were also developed for a wide range of practical systems. The algorithm for determining the GFRFs of a nonlinear system was also studied with other methods, for example, the Adomian method [66] and the Diophantine equation method [67],

and techniques for simplifying and improving the computation efficiency of higher-order GFRFs were studied in [62, 68, 69].

The nonlinear output spectrum can be analytically calculated with the input spectrum and the calculated GFRFs as

$$Y(\Omega) = \sum_{n=1}^N \frac{1}{(2\pi)^n} \int \cdots \int_{\omega_1 + \cdots + \omega_n = \Omega} H_n(\omega_1, \dots, \omega_n) e^{\sum_{i=1}^n j\omega_i t} \prod_{i=1}^n U(j\omega_i) d\omega_1 \cdots d\omega_n \quad (1.12)$$

where  $\Omega$  is the output frequency,  $U(j\omega_i)$  is the input spectrum, and  $H_n(\omega_1, \dots, \omega_n)$  is the calculated GFRF. Lang and Billings studied the nonlinear output response function when a nonlinear system is subjected to a multi-tone harmonic input and general input [70]. The output frequency range was investigated in [70-73], and was found to be totally different from that in linear systems (in linear cases, the output frequency range is the same as the input frequency range), and important nonlinear output frequency properties were theoretically revealed in [73]. Studies were also attempted to visually interpret the nonlinear output frequency response characteristics in [74-78], and a theoretical understanding of the nonlinear influence on the output response in vibration control was given in [79]. The concept of nonlinear energy transfer was developed and discussed in [73, 80-83], which illustrated phenomena of nonlinear energy transfer from one frequency to others. Applications of nonlinear properties and the benefits of nonlinearity for vibration control were studied in [23, 24, 79, 84-86]. The concept of a nonlinear output frequency response function (NOFRF) was proposed by Lang [82], with applications in structural health monitoring and fault diagnosis [87-90]. A systematic method for the

analysis and design of nonlinear systems in the frequency domain was developed in the last 10 years [79, 91-93] based on the concept of GFRFs with a parametric characteristic approach, initially referred to as the output frequency response function based method [94, 95] and later called the nCOS method [92]. With this parametric characteristic approach, the magnitude-bound characteristics of nonlinear frequency response functions (i.e., GFRFs and output spectrum) were studied in [96-98]. These results provide the important basis for the results, including the novel parametric convergence bounds and the new nCOS function, to be established in this thesis.

Studies of the Volterra series associated frequency domain method were also conducted for time delay systems [59, 99, 100], time varying systems [101], spatial-temporal systems [102-106], and even systems with strong nonlinearity having sub-harmonic [107-109] or jump phenomena [110, 111].

### **Nonlinear Characteristic Output Spectrum (nCOS) Method**

As mentioned before, the nCOS method is developed with a parametric characteristic approach based on the GFRF concept [112]. One significant advantage of the nonlinear characteristic output spectrum (nCOS) method is that the nonlinear output spectrum can be expressed in the form of a polynomial function with respect to the nonlinear system model parameters, which provides an explicit and analytical relationship between the nonlinear output spectrum and the nonlinear model parameters of interest. The above several methods (both the

time domain methods and frequency domain methods) focus more on the nonlinear model analysis rather than the system design. With the constructed explicit and analytical relationship between the nonlinear output spectrum and the nonlinear model parameters, the nCOS method provides a straightforward insight into nonlinear system design that can greatly facilitate the process.

The nCOS method was proposed and developed by Jing and Lang [73, 79, 85, 86, 91-95, 113-117], as summarized in monograph [112]. The output spectrum is given as a polynomial function of nonlinear model parameters [95,113] as

$$Y(\Omega) = \sum_{j_1 \cdots j_{s_N}} \varphi_{j_1 \cdots j_{s_N}}(\Omega) k_1^{j_1} \cdots k_{s_N}^{j_{s_N}} \quad (1.13)$$

where  $k_1, \dots, k_{s_N}$  are  $s_N$  nonlinear parameters of interest, and  $\varphi_{j_1 \cdots j_{s_N}}(\Omega)$  are the coefficients of the corresponding terms  $k_1^{j_1} \cdots k_{s_N}^{j_{s_N}}$ . The terms related to the nonlinear parameters of interest and the corresponding coefficients can be symbolically calculated with the results in [93, 113-117]. Applications in vibration suppression were then studied with the developed characteristic relationship [85, 86, 94]. Further studies of the property of opposition of input nonlinearity and alternating series were then conducted in [73, 79]. An effective method for the identification of coefficients  $\varphi_{j_1 \cdots j_{s_N}}(\Omega)$  in (1.13) was theoretically investigated [91] with an efficient algorithm developed in [92], which would greatly facilitate the application of the nCOS method for nonlinear analysis and design.

### 1.1.3 Comparison

Table 1.1 Comparison between different frequency methods

	Multi-Degree-of-Freedom system	Multi-tone excitation	Input-output relationship	Response at non-excited frequencies <sup>2</sup>
Harmonic Balance	difficult	difficult	implicit	available
Lindstedt-Poincare method	difficult	difficult	implicit	available
Describing Function	easy	not available	partially explicit <sup>1</sup>	not available
Volterra series associated method	easy	easy	explicit	available

<sup>1</sup> only limited and specific model parameters are involved.

<sup>2</sup> Non-excited frequencies involve the inter-modulated frequencies and harmonic frequencies.

This section concludes with some comparisons between the different frequency domain methods discussed above. From Table 1.1, it can be observed that both the harmonic balance method and Lindstedt-Poincare method have difficulty analysing multi-degree-of-freedom (MDoF) systems or nonlinear systems with a multi-tone input. The reason for this is that the input-output relationship via these two methods is implicitly involved in a set of nonlinear algebraic equations, whose derivation would be very complicated. The describing function method usually requires that the input be a single tone sinusoid input and only considers the response at the excited frequency. The generalized describing function (GDF) method can relax the single tone input to a multi-tone input when the nonlinear system is Volterra-type nonlinear, but for this case, the GDF method is in essence a Volterra series associated method. The Volterra series associated method thus show great advantages over the other methods.

The nCOS method provides a more straightforward and explicit relationship between the output spectrum and the nonlinear parameters of interest (equation (1.13)) than the traditional Volterra series associated method (equation (1.12)). Moreover, a new recursive calculation for the output spectrum is required via (1.12) when the nonlinear parameters of interest change, but not for the nCOS method via (1.13). These advantages of the nCOS method are the motivation for this thesis work.

## **1.2 Motivation, Objectives and Contributions**

### **1.2.1 Motivation of study**

The nonlinear characteristic output spectrum (nCOS) method explicitly defines an analytical relationship between the output spectrum and the system nonlinear parameters of interest and shows great advantages over other nonlinear analysis methods for the analytical study and design of a wide class of nonlinear systems, but it requires that the nonlinear system be Volterra-type. A nonlinear system is defined as possessing Volterra-type nonlinearity if the input-output relationship of the nonlinear system has a convergent Volterra series expansion.

The nonlinearity degree of a given nonlinear system relates to the model parameters, the input magnitude, and the excited frequency. For example, upon applying a given input to a nonlinear system at the resonant frequency, strongly nonlinear behaviours such as jump phenomena, bifurcation, or chaos may occur

in the system output, but the nonlinearity degree of the system may be very weak when the system is excited at a frequency far away from the resonant frequency with the same input magnitude. The model parameters, input magnitude, and frequency variable are denoted as the characteristic parameters that affect the nonlinearity degree of a given nonlinear system.

Determining under what range the characteristic parameters can freely take values such that the system input-output relationship is always valid for a convergent Volterra series expansion is very important not only for the nonlinear characteristic output spectrum (nCOS) method, but also for other Volterra series associated time domain and frequency domain methods. Although the convergence problem is a fundamental issue in this area, it still has not been completely solved. The convergence criteria for fading memory systems or nonlinear operators were theoretically given by Boyd [55, 56] and Sandberg [51, 53, 54], but may not be easy to implement in practice. Similarly, the convergence criterion for analytic systems in  $L^p$  space was established in [118]. For a specific nonlinear system such as a Duffing oscillator, the convergence criteria in the frequency domain were discussed in [110, 119, 120], but almost all of the results are obviously over-estimated (the computed convergence bound for the input magnitude is larger than the real bound), and only one of the results can catch the convergence bound at the  $1/3$  super resonant frequency [120]. Recently, the results were developed for the convergence bound of the input magnitude, but they require the system to be input analytic [121, 122], i.e., with an input

nonlinear degree not larger than 1, which shows limitations in practical application (only for the input magnitude and only for an input analytic system).

The system always suffers from various perturbations. If the design parameters are chosen very close to the convergence bound, the system would easily go out of convergence. If the designed nonlinear system is out of the convergence region, the real output of the designed system may be very different from the design output. Therefore, for any characteristic parameter, it is reasonable to develop a measure for accessing the convergence margin in terms of this characteristic parameter, which is referred to here as the parametric convergence margin (PCM). A large PCM implies that the system dynamics stay far from divergence in terms of the concerned parameters and in the sense of a convergent Volterra series expansion.

With the parametric bound of convergence (PBoC) and parametric convergence margin (PCM) developed in this thesis, the system output response can be freely studied in the computed convergence region using the nonlinear characteristic output spectrum (nCOS) method. The nonlinear benefits or advantages can then be studied with the intentionally introduced nonlinearity or nonlinear controller based on this powerful tool.

A well-known dilemma for linear damping is that a large linear damping can suppress the vibration around the resonant frequency but deteriorate the performance at the frequencies away from the resonant frequencies. Overcoming this issue is a hot topic in the literature. Nonlinear damping or a nonlinear

controller would be potential technique to achieve this aim.

In the analysis and design of vibration control systems, multiple-objects are often required for a full assessment of the design. One problem of multiple-object analysis and optimization for nonlinear systems is that complex nonlinear phenomena may exist. To avoid such complex dynamics as chaos, bifurcation, sub-harmonics, and jump phenomena, one can design a nonlinear system to be Volterra-type nonlinear because the Volterra series theory works only for mild nonlinearity, which can be easily ensured by taking the parameters in the computed convergence region via the parametric bound of convergence (PBoC) developed in the thesis. Another problem is that the calculation of the nonlinear system performance is difficult and not straightforward in the literature, especially when a multi-degree of freedom system or a multi-tone input is considered.

For those systems with inherent nonlinearity, the design of a linear components or linear controller is sometimes preferable because of the ease in implementation. The nonlinear characteristic output spectrum (nCOS) method developed in (1.13) is only available for nonlinear parameters of interest, and fails in the analysis and design of linear parameters of interest. This thesis thus aims to extend the nonlinear characteristic output spectrum (nCOS) method to analyse and design those linear parameters of interest.

Note that the nCOS method is developed for polynomial nonlinearities, so exponential nonlinearities should first be transformed into polynomial

nonlinearities via a Taylor series expansion. Higher accuracy Taylor series approximations require a larger truncation order, which obviously leads to a large number of parameters in the analysis and design and would significantly complicate the application of the nCOS method. An effective and straightforward method for the analysis and design of an exponential nonlinear system is thus targeted in this thesis.

### **1.2.2 Objectives**

The research in this thesis aims to contribute an effective and efficient method for the analysis and design of nonlinear systems. The following two objectives are addressed:

- 1. To study the parametric convergence problem of the Volterra series expansion.**
- 2. To apply, develop, and extend the existing nCOS method.**

The first objective is to address under what parametric conditions the input-output relationship of a nonlinear dynamic system has a convergent Volterra series expansion. Obviously, only when we know this clear can we confidently apply the nonlinear characteristic output spectrum (nCOS) method mentioned above to any nonlinear analysis and design in any context of signal processing or control.

The second objective involves the following three parts:

- 1. Applying the nCOS method to the analysis and design of nonlinear**

**parameters considering the parametric convergence bound.** First, a nonlinear damping is proposed and studied using the nCOS method to overcome the well-known dilemma of linear damping. It is shown that the nCOS method can provide a straightforward insight into the analysis and design of such a system. Then, the nCOS method is applied to a nonlinear optimization problem. By mapping the multiple-object performance function into the nonlinear characteristic function as shown in (1.13), the multiple-object analysis and optimization problem is then ready for analysis and design in the convergence region computed by the developed algorithm for PBoC, which shows straightforward insight and can greatly facilitate the nonlinear analysis and optimization problem. A systematic and novel method for the nonlinear analysis and optimization problem is then developed in this thesis.

2. **Developing a new nCOS function for the analysis and design of linear parameters of interest.** The existing nCOS method is only developed for nonlinear parameters of interest. The issue is how to express the output spectrum as an explicit and analytical function of those linear parameters of interest such as that built for nonlinear parameters in (1.13). The development of such an expression that maintains the independence between the coefficients  $\varphi_{j_1 \dots j_{s_N}}(\Omega)$  and the linear parameters of interest is not straightforward. An algorithm is thus built for the symbolic calculation of the independent coefficients  $\varphi_{j_1 \dots j_{s_N}}(\Omega)$  for single-input

single-output nonlinear systems, and a numerical identification method is developed for multiple-input multiple-output (MIMO) nonlinear systems described in state space. After these, a systematic method can be built for the analysis and design of linear parameters of interest.

3. **Extending the nCOS method and the new nCOS function to exponential nonlinearities.** To this aim, an effective and efficient algorithm is developed to determine the generalized frequency response function (GFRF) of exponential nonlinearities with many fewer parameters. The proposed algorithm can greatly facilitate the application of the new nCOS function to the analysis and design of exponential nonlinear systems in practical engineering applications.

### 1.2.3 Contributions

The main contributions of this thesis are summarized as:

1. The parametric bound of convergence (PBoC) and parametric convergence margin (PCM) are proposed for nonlinear systems, and the corresponding algorithms for calculations are also developed. It should be noted that the computation of PBoC is not only for the input magnitude but also for the model parameters and frequency variables. All of the result in the literatures were focused only on the convergence bound of the input magnitude. This study thus would be the first one on the convergence bound of the model parameters, and it provides a solid basis for the analysis and design of

nonlinear systems via the nonlinear characteristic output spectrum (nCOS) method.

2. A systematic and novel method for multiple-object nonlinear analysis and optimization problems is proposed by mapping the multiple-object function onto the nonlinear characteristic output spectrum function. The proposed concept of the parametric bound of convergence (PBoC) or parametric convergence margin (PCM) can help guarantee that the designed or optimized system is Volterra-type nonlinear to avoid the complex dynamics of strong nonlinearity.
3. The nonlinear characteristic output spectrum (nCOS) function is extended to those linear parameters of interest, which shows great significance in practical engineering applications because the design of linear components or a linear controller would be easier for implementation. The algorithm for the symbolic calculation of the independent coefficients is developed for a single-input single-output (SISO) nonlinear system, and a procedure is built for the numerical identification of the independent coefficients in state feedback controller design.
4. An algorithm for calculating the generalized frequency response function (GFRF) of exponential nonlinearities is proposed by introducing two auxiliary equations, which has many fewer parameters of interest than that necessary upon approximating the exponential nonlinearity with a truncated Taylor series expansion. The newly developed algorithm can greatly facilitate

the analysis and design of many exponential nonlinear problems with the nCOS method in practical engineering applications such as the design of power amplifiers or the analysis of a neural network.

### **1.3 Outline of the thesis**

All of the results in this thesis aim to provide effective and efficient methods for the analysis, design, and optimization of nonlinear systems. The other parts of this thesis are organized as follows.

In Chapter 2, the parametric bound of convergence (PBoC) and parametric convergence margin (PCM) are proposed. The algorithms for calculating the PBoC and PCM are first developed for single-input single-output nonlinear systems with a harmonic input. The results are then extended to single-input multiple-output nonlinear systems and also to nonlinear systems with a general input, which are thus applicable to a wide class of nonlinear systems in practical applications such as those multi-degree of freedom (MDoF) systems or multiple-input multiple-output (MIMO) systems.

Chapter 3 involves two applications of the nCOS method to the analysis and design of nonlinear parameters considering the result of PBoC in Chapter 2. First, a nonlinear damping defined as a function of both position and velocity is proposed to overcome the well-known linear damping dilemma. This part focuses on the qualitative analysis of nonlinear damping based on the nonlinear characteristic output spectrum (nCOS) method. Then, the multiple-object

optimization problem is investigated by mapping the nonlinear multiple-object function onto a nonlinear characteristic output spectrum function. This method provides a straightforward insight into the nonlinear optimization problem. A procedure is given, and an application to nonlinear suspension vibration control is presented to demonstrate this systematic and novel method.

In Chapter 4, the analysis and design of linear parameters of interest in a nonlinear system is studied. The traditional nCOS method cannot be applied to this problem because it is developed only for nonlinear parameters of interest. It is shown that the generalized frequency response function (GFRF) and the nonlinear output spectrum can both be expressed as a polynomial function with respect to linear parameters of interest. The coefficients of the polynomial function are independent of those linear parameters of interest, which is similar to that in the traditional nCOS method in (1.14). The newly developed method for linear parameters of interest can thus be observed as an extension of the traditional nCOS method. An algorithm for the symbolic calculation of the independent coefficients is developed for single-input single-output nonlinear systems, and a numerical identification procedure for the independent coefficients is built for multiple-input multiple-output (MIMO) nonlinear systems (expressed in state space with state feedback control). Applications for the improvement of the harmonic distortion of the common-gate amplifier and linear state feedback controller for nonlinear suspension systems are presented to demonstrate the effectiveness and efficiency of the proposed method.

In Chapter 5, two auxiliary equations are introduced to facilitate the calculation of the generalized frequency response function (GFRF) of the exponential-type nonlinearity. With the auxiliary equations, the exponential-type nonlinear equation is transformed into polynomial-type nonlinear equations but with many fewer parameters of interest than that obtained by Taylor series expansion. Examples, the design of a common-gate amplifier and the analysis of a neural network with the new nCOS function, are presented to illustrate the advantages of the proposed algorithm.

Finally, in Chapter 6, the conclusion is given, and some recommendations for further study are presented.

## 2 Parametric convergence bound for Volterra series expansion of nonlinear systems

### 2.1 Introduction

For a large class of nonlinear systems, the input-output relationship allows a Volterra series expansion [51, 53, 56, 57]. The Volterra series and its associated nonlinear analysis methods have been extensively applied in practice for control designing, signal processing, system identification, and system analysis [123-129].

Whether a nonlinear system has a convergent Volterra series expansion is determined by the input magnitude, the input frequencies, and the model parameters, referred to as the characteristic parameters. When applying the Volterra series based methods to the nonlinear analysis and design, a fundamental issue is to ensure that the underlying nonlinear dynamics can be approximated by the Volterra series, which requires the characteristic parameters be within certain appropriate ranges. Several results in the literature attempted to address this issue only focusing on the input magnitude bound. That is to estimate a bound of input magnitude for a given nonlinear system to guarantee the nonlinear system has a convergent Volterra series expansion. The results in [51, 53, 56] are general operator theory based results, which theoretically prove the existence of the Volterra series expansion for a class of nonlinear systems but fail to provide a

detailed parametric convergent bound for any characteristic parameter. Some other works can be found in [110, 119, 120], which were studied only for a specific nonlinear system, the Duffing oscillator. A recent result in [121] tackled the input-analytic nonlinear systems. All the results above are either conservative or obviously over-estimated and only focus on a convergent criterion for the input magnitude.

In the analysis and design of a nonlinear system, a fundamental problem could be: in what parameter ranges (in terms of the input magnitude, the model parameters, and the input frequencies) can the nonlinear system has a convergent Volterra series expansion? More specifically, for the parameter design of a nonlinear system, the question could be: under what range can a parameter freely take its value such that the system is valid for a convergent Volterra series expansion? These practical questions are clear the key issues before any nonlinear analysis and design based on the Volterra series based methods but are still not well addressed.

## **2.2 The parametric convergence bound for single-input single-output (SISO) nonlinear autoregressive with exogenous input (NARX) model**

Many nonlinear systems can be identified into a NARX model [130-132] , which includes several commonly-used nonlinear models as special cases. The NARX model actually provides a generic and convenient platform for the analysis and design of a nonlinear system in practice. Consider the NARX model

$$y(k) = \sum_{m=1}^M \sum_{p=0}^m \sum_{(k_1, \dots, k_m)} c_{p, m-p}(k_1, \dots, k_m) \prod_{i=1}^p y(k-k_i) \prod_{i=p+1}^m u(k-k_i) \quad (2.1)$$

where  $M$  is the maximum nonlinear degree in terms of  $y(k)$  and  $u(k)$ ,  $p$  is the nonlinear degree in terms of  $y(k)$ , and  $m-p$  is the nonlinear degree in terms of  $u(k)$  which is denoted later by  $q = m-p$ .  $(k_1, \dots, k_m)$  denotes all of the combinations of nonlinear terms in terms of input and output, which can be expressed as  $(k_1, \dots, k_m) \in \mathfrak{V}_m = \{(k_1, \dots, k_m) | 1 \leq k_i \leq K, p \leq k_1 + \dots + k_p \leq pK, q \leq k_{p+1} + \dots + k_m \leq qK\}$ , where  $K$  is the maximum order of the derivative, and

$c_{p, m-p}(k_1, \dots, k_m)$  is the corresponding coefficient of  $\prod_{i=1}^p y(t-k_i) \prod_{i=p+1}^m u(t-k_i)$ .

The NARX model (2.1) can be approximated by a Volterra series expansion as

$$y(k) = \sum_{n=1}^N \int_{-\infty}^{\infty} \dots \int_{-\infty}^{\infty} h_n(\tau_1, \dots, \tau_n) \prod_{i=1}^n u(k-\tau_i) d\tau_i \quad (2.2)$$

where  $N$  is the truncation order, and  $h_n(\tau_1, \dots, \tau_n)$  is the  $n$ th order Volterra kernel.

The following comes to study the convergence bound of the characteristic parameters (the input magnitude, the input frequencies, and the model parameters  $c_{p, m-p}(k_1, \dots, k_m)$ ) in the frequency domain to guarantee the Volterra series expansion in (2.2) holds for the NARX model given in (2.1).

### 2.2.1 The GFRFs and the nonlinear output spectrum

The  $n$ th order GFRF of the NARX model can be recursively calculated as

$$H_n(j\omega_1, \dots, j\omega_n) = \frac{1}{L_n(\omega_1, \dots, \omega_n)} \times \sum_{m=1}^n \sum_{p=0, q=m-p}^m \sum_{(k_1, \dots, k_m)} c_{p,q}(k_1, \dots, k_m) e^{-\sum_{i=1}^q j\omega_{n-q+i} k_{p+i}} H_{n-q,p}(j\omega_1, \dots, j\omega_{n-q}) \quad (2.3)$$

$$L_n(\omega_1, \dots, \omega_n) = 1 - \sum_{k_1=1}^K c_{1,0}(k_1) e^{-jk_1 \sum_{i=1}^n \omega_i} \quad (2.4)$$

$$H_{n,p}(j\omega_1, \dots, j\omega_n) = \sum_{r_1, \dots, r_p=1, \sum r_i=n}^{n-p+1} \prod_{i=1}^p H_{r_i}(j\omega_{X+1}, \dots, j\omega_{X+r_i}) e^{-jk_1 \sum_{j=1}^n \omega_{X+j}} \quad (2.5)$$

$$H_{n,1}(j\omega_1, \dots, j\omega_n) = H_n(j\omega_1, \dots, j\omega_n) e^{-jk_1 \sum_{j=1}^n \omega_j} \quad (2.6)$$

Where  $H_{0,0}(\bullet) = 1$ ,  $H_{n,0}(\bullet) = 0$  for  $n > 0$ ,  $H_{n,p}(\bullet) = 0$  for  $n < p$ ,  $X = \sum_{j=1}^{i-1} r_j$ ,

and

$$\exp\left(\sum_{i=1}^q j\omega_{n-q+i} k_{p+i}\right) = \begin{cases} 1 & q=0, p>1 \\ 0 & q=0, p \leq 1 \end{cases} \quad (2.7)$$

When  $n=1$ , the first-order GFRF is the linear transfer function as

$$H_1(j\omega_1) = \frac{\sum_{k_1=1}^K c_{0,1}(k_1) e^{-j\omega_1 k_1}}{1 - \sum_{k_1=1}^K c_{1,0}(k_1) e^{-j\omega_1 k_1}} = \frac{\sum_{k_1=1}^K c_{0,1}(k_1) e^{-j\omega_1 k_1}}{L_1(j\omega_1)} \quad (2.8)$$

The nonlinear output spectrum when the system is subject to a harmonic input

$$u(k) = U \cos(\omega T_s k + \angle A) = \frac{A}{2} e^{j\omega T_s k} + \frac{A^*}{2} e^{-j\omega T_s k} \quad (2.9)$$

where  $T_s$  is the sampling interval can be computed as

$$Y(j\Omega) = \sum_{n=1}^{+\infty} \frac{1}{2^n} \sum_{\omega_1 + \dots + \omega_n = \Omega} H_n(j\omega_1, \dots, j\omega_n) \prod_{i=1}^n A(\omega_i) \quad (2.10)$$

where  $\omega_i \in \{\omega, -\omega\}$ ,  $A(\omega) = A$ ,  $A(-\omega) = A^*$ , and  $U = |A|$ .

### 2.2.2 Notations and definitions

The operator  $\|\cdot\|$  denotes the absolute value for scalars and Euclidian norm  $\|\cdot\|_2$  for vectors.  $\mathbb{N}$  is the set for all nonnegative integers, and  $\mathbb{N}^+$  for positive integers. Define

$$\underline{L}(\omega) = \inf_{\Omega \in W_\infty} \{\|L_n(j\omega_1, \dots, j\omega_n)\|\} \quad (2.11)$$

where  $W_\infty = \bigcup_{k=1}^{\infty} W_k = \bigcup_{k=1}^{\infty} \{\Omega \mid \Omega = \omega_1 + \dots + \omega_k, \omega_i \in \{\omega, -\omega\}\}$ .  $W_k$  is the set of all of the output frequencies in the  $k$ th order output spectrum, and  $W_\infty$  represents the whole output frequency range when the NARX model is subject to the input (2.9). Define

$$C(p, q) = \sum_{(k_1, \dots, k_m)} \|c_{p,q}(k_1, \dots, k_m)\| \quad (2.12)$$

where  $c_{p,q}(k_1, \dots, k_m)$  is the coefficient of the NARX model (2.1), and clear  $C(p, q)$  is a nonnegative function. Denote

$$\bar{H}_1(j\omega_1) = \|H_1(j\omega_1)\| \quad (2.13)$$

### 2.2.3 The bound results of output spectrum

**Lemma 2.1:** The upper bound of the  $n$ th order GFRF can be obtained as

$$\begin{aligned} & \sup \left\{ \|H_n(j\omega_1, \dots, j\omega_n)\| \mid \forall \omega_1, \dots, \omega_n \in \{\omega, -\omega\} \right\} \leq \bar{H}_n(j\omega_1, \dots, j\omega_n) \\ & = \frac{1}{\underline{L}(\omega)} \left( C(0, n) + \sum_{m=2}^n \sum_{p=1}^m C(p, q) \sum_{r_1, \dots, r_p=1, \sum r_i=n-q}^{n-m+1} \prod_{i=1}^p \bar{H}_{r_i}(\omega_{X+1}, \dots, \omega_{X+r_i}) \right), \quad n \geq 2 \end{aligned} \quad (2.14)$$

**Proof:** See Lemma 1 in [98].

**Lemma 2.2:** The upper bound of the nonlinear output spectrum involving the

whole output frequency range  $W_\infty$  is given as

$$\bar{Y}(U)_\omega = \sum_{k=0}^{\infty} \bar{Y}_{\Omega=k\omega}(U) = \sum_{\Omega \in W_\infty} \bar{Y}_\Omega(U) = \sum_{n=1}^{\infty} \left\| \sum_{\Omega \in W_n} \bar{Y}_n(j\Omega) \right\| = \sum_{n=1}^{+\infty} \bar{H}_n(j\omega_1, \dots, j\omega_n) U^n \quad (2.15)$$

where  $\bar{Y}_{\Omega=k\omega}(U)$  is the upper bound of the output spectrum at frequency

$\Omega = k\omega, k \in \mathbb{N}$ , which is given as

$$\begin{aligned} |Y(j\Omega)| \leq \bar{Y}_{\Omega=k\omega}(U) &= \sum_{n=1}^{\infty} \frac{C_{k+2(n-1)}^{n-1}}{2^{k+2(n-1)-1}} \bar{H}_{k+2(n-1)}(j\omega_1, \dots, j\omega_{k+2(n-1)}) U^{k+2(n-1)} \quad k \in \mathbb{N}^+ \\ |Y(j\Omega)| \leq \bar{Y}_{\Omega=k\omega}(U) &= \sum_{n=1}^{\infty} \frac{C_{2n}^n}{2^{2n}} \bar{H}_{2n}(j\omega_1, \dots, j\omega_{2n}) U^{2n} \quad k = 0 \end{aligned} \quad (2.16)$$

**Proof:** For  $k \in \mathbb{N}^+$ ,

$$\begin{aligned} Y_{\bar{\omega}=k\omega}(U) &\leq \sum_{n=1}^{+\infty} \frac{2}{2^{k+2(n-1)}} \sum_{\bar{\omega}=k\omega} \bar{H}_{k+2(n-1)}(j\omega_1, \dots, \omega_n) \prod_{i=1}^{k+2(n-1)} \|A(\omega_i)\| \\ &\leq \sum_{n=1}^{\infty} \frac{C_{k+2(n-1)}^{n-1}}{2^{k+2(n-1)-1}} \bar{H}_{k+2(n-1)}(j\omega_1, \dots, j\omega_{k+2(n-1)}) U^{k+2(n-1)}, \end{aligned}$$

For  $k=0$ , the result is straightforward.

**Proposition 2.1:** The analytical relationship among the upper bound of nonlinear output spectrum, the model parameters, magnitude bound of the first-order GFRF, the input magnitude, and frequency variable can be obtained as

$$\sum_{p=1}^{M_p} \left( \sum_{q=0}^{\infty} C(p, q) U^q \right) x^p - \underline{L}(\omega) x + \left( \underline{L}(\omega) \bar{H}_1(j\omega) U + \sum_{m=2}^{\infty} C(0, m) U^m \right) = 0, \quad p + q \geq 2 \quad (2.17)$$

where  $x$  is simplified for  $x(\omega, U)$ . Denote

$$x(\omega, U) = \bar{Y}(U)_\omega = \sum_{n=1}^{+\infty} \bar{H}_n(j\omega_1, \dots, j\omega_n) U^n, \quad \text{and } M_p \text{ is the maximum nonlinear}$$

degree in terms of output  $y(k)$ . Specifically, when the NARX model only

involves those nonlinear terms with  $p = 1$  or together with the pure input nonlinearity, the upper bound of the nonlinear output spectrum  $x$  can be obtained directly as

$$x = \frac{\bar{H}_1(j\omega)U + \frac{1}{\underline{L}(\omega)} \sum_{q=m=2}^{\infty} C(0, m)U^m}{1 - \frac{1}{\underline{L}(\omega)} \sum_{q=1}^{\infty} C(1, q)U^q} \quad (2.18)$$

**Proof:** See Appendix 2.1.

**Remark 2.1:** The output bound  $x$  in (2.17) should be a real nonnegative number. If (2.17) possesses only one positive root, this positive root is the output bound; when (2.17) has more than two positive roots, the parametric convergence margin proposed later can help to determine the true output bound.

#### 2.2.4 Parametric bound of Convergence (PBoC)

The parametric bound of convergence (PBoC) is referred to as a bound (e.g.,  $\bar{C}$ ) for any characteristic parameter  $C$  (i.e.,  $\|C\| \leq \bar{C}$ ) under which the NARX model has a convergent Volterra series expansion.

**Proposition 2.2:** Denote the formal function  $\Gamma(x; C, U, \omega)$  as

$$\Gamma = \frac{1}{\underline{L}(\omega)} \sum_{p=1}^{M_p} \sum_{q=0}^{\infty} pC(p, q)U^q x^{p-1}, \quad p + q \geq 2 \quad (2.19)$$

The upper bound of the nonlinear output spectrum, the power series

$x = \sum_{n=1}^{+\infty} \bar{H}_n(j\omega_1, \dots, j\omega_n)U^n$ , is convergent when  $0 \leq \Gamma < 1$  holds and divergent

when  $\Gamma \geq 1$  holds.

**Proof:** See Appendix 2.2.

**Remark 2.2:** The function  $\Gamma$  is a non-negative continuous and monotonically increasing function of  $C(p, q)$  or the input magnitude  $U$ .

**Remark 2.3:** When the NARX model (2.1) has only pure input nonlinearity, then the whole input part can be considered as a new input. In this case, the model can be regarded as a linear model with this new input, which is not focused on in this study.

**Proposition 2.3:** Consider the NARX model except the case that the NARX model involves only the nonlinear terms with index  $p = 1$  or together with only pure input nonlinear terms, the analytical PBoC can be obtained by solving the following equation

$$\begin{array}{l}
 M_p - 1 \text{ rows} \\
 \\
 \\
 \\
 \\
 \\
 M_p \text{ rows}
 \end{array}
 \left\{ \begin{array}{cccccccc}
 a_{1, M_p} & a_{1, M_p - 1} & \cdots & a_{1, 0} & 0 & \cdots & 0 \\
 0 & a_{1, M_p} & a_{1, M_p - 1} & \cdots & a_{1, 0} & \cdots & 0 \\
 & & \cdots & & & & \\
 0 & 0 & \cdots & a_{1, M_p} & a_{1, M_p - 1} & \cdots & a_{1, 0} \\
 \\
 a_{2, M_p - 1} & a_{2, M_p - 2} & \cdots & a_{2, 0} & 0 & \cdots & 0 \\
 0 & a_{2, M_p - 1} & a_{2, M_p - 2} & \cdots & a_{2, 0} & \cdots & 0 \\
 & & \cdots & & & & \\
 0 & 0 & \cdots & a_{2, M_p - 1} & a_{2, M_p - 2} & \cdots & a_{2, 0}
 \end{array} \right. = 0 \quad (2.20)$$

where  $M_p$  takes the same definition as in Proposition 1, and

$$a_{1, p} = \left( (p-1) \sum_{q=0}^{\infty} C(p, q) U^q \right), \quad 1 \leq p \leq M_p, p+q \geq 2, \quad (2.21)$$

$$a_{1, 0} = - \left( \underline{L}(\omega) \bar{H}_1(j\omega) U + \sum_{m=2}^{\infty} C(0, m) U^m \right), \quad (2.22)$$

$$a_{2, p-1} = p \sum_{q=0}^{\infty} C(p, q) U^q, \quad 2 \leq p \leq M_p, \quad (2.23)$$

$$a_{2, 0} = \sum_{q=1}^{\infty} C(1, q) U^q - \underline{L}(\omega). \quad (2.24)$$

When the NARX model (2.1) involves only the nonlinear terms with  $p = 1$  or together with the pure input nonlinear terms with  $p=0$ , the PBoC can be obtained by directly solving  $F=1$  as

$$\frac{1}{\underline{L}(\omega)} \sum_{q=1}^{\infty} C(1,q)U^q = 1 \quad (2.25)$$

**Proof:** See Appendix 2.3.

**Remark 2.4:** If the NARX model only involves the nonlinear terms with index  $p = 1$  or together with  $p = 0$ , the coefficients of the pure input nonlinearity do not play a role in (2.19), which means that these pure input nonlinearities do not affect the convergence bound. Otherwise, the pure input nonlinearities could have great influence on the convergence bound, which can be seen in (2.20) and (2.22) and will be validated in Examples 2.2.6.3 and 2.2.6.4.

**Remark 2.5:** When the input amplitude  $U$  is given, the PBoC of any model parameter of interest can be obtained from (2.20). When the parameter values are selected under the bound calculated by (2.20), the nonlinear system can be well approximated by a convergent Volterra series. When all of the model parameters are given, the PBoC of the input amplitude can be obtained. The latter has been studied in [110, 118-121] for some specific nonlinear systems. The result in Proposition 2.3 is more general, not restrictive to any specific nonlinear system, and less conservative due to the frequency dependent bound used.

**Algorithm 2.1 (Computation of PBoC) :**

**Step 1.** Calculate  $\underline{L}(\omega)$  according to (2.4) and (2.11); Calculate  $\bar{H}_1(j\omega_1)$

according to (2.8) and (2.13); Calculate  $C(p,q)$  using (2.12).

**Step 2.** Compute (2.21)-(2.24) to construct (2.20) for the applicable case.

**Step 3.** Solve (2.20) or (2.25) for the applicable case to obtain the PBoC .

### 2.2.5 The parametric convergence margin (PCM)

For any characteristic parameter, it is reasonable to develop a measure to assess the convergence margin with respect to this parameter, referred to as the parametric convergence margin (PCM), before the Volterra series expansion diverges. A larger PCM implies that the system dynamics can be well approximated by a Volterra series expansion and stays away from its divergence.

Considering the function  $\Gamma$  in (2.19), when all of the nonlinear coefficients in the NARX model are equal to 0 or the input amplitude  $U=0$ , then  $\Gamma=0$ ; when the nonlinear coefficients or the input amplitude reach the PBoC, then  $\Gamma=1$ ; when the nonlinear coefficients or the input amplitude is out of the PBoC, then  $\Gamma>1$ . Because of these properties, the function  $\Gamma$  can be used as an overall indicator to the convergence margin of the NARX model. Therefore, the PCM is defined as

$$\text{PCM} = 1 - \Gamma \quad (2.26)$$

When the PCM is very close to 1, the NARX model possesses the largest convergence margin; when the PCM is close to 0, the NARX model is very close to the convergent bound and has smaller convergence margin; when the PCM is

negative, the system cannot be expanded by a Volterra series and thus is not a Volterra-type system.

**Proposition 2.4:** When the NARX model does not only possess nonlinearities with index  $p = 1$  or together with pure input nonlinearity, the indicator  $\Gamma$  can be obtained by solving (2.20) with

$$a_{1,p} = \sum_{q=0}^{\infty} C(p,q)U^q, \quad (2.27)$$

$$a_{1,1} = \sum_{q=1}^{\infty} C(1,q)U^q - \underline{L}(\omega), \quad (2.28)$$

$$a_{1,0} = \underline{L}(\omega)\bar{H}_1(j\omega)U + \sum_{m=2}^{\infty} C(0,m)U^m, \quad (2.29)$$

$$a_{2,p-1} = p \sum_{q=0}^{\infty} C(p,q)U^q, \quad (2.30)$$

$$a_{2,0} = \sum_{q=1}^{\infty} C(1,q)U^q - \Gamma \underline{L}(\omega). \quad (2.31)$$

where  $2 \leq p \leq M_p$ . When the NARX model possesses only nonlinear terms with index  $p = 1$  or together with pure input nonlinearity,  $\Gamma$  can be directly obtained according to (2.19).

**Proof:** See Appendix 2.4.

**Remark 2.6:** When  $0 \leq \Gamma < 1$  ( $0 < PCM \leq 1$ ), the NARX model possesses unique steady state and can be well approximated by a convergent Volterra series; when  $\Gamma \geq 1$ , i.e.,  $PCM \leq 0$ , the Volterra series becomes divergent, and therefore cannot approximate to the NARX model. From (2.19), it is clear that  $\Gamma$  is a real nonnegative number. Therefore, if (2.20) has no real positive root, the nonlinear system can be seen as divergent in the sense of Volterra series

expansion. If there exists more than one real positive root, the PBoC can be used to determine the true  $\Gamma$ . That is, when the nonlinear coefficients are out of the PBoC, the solution that is larger than 1 should be the true  $\Gamma$ ; otherwise, the solution that is smaller than 1 would be the true one. Similarly, when there exists more than one real positive solutions in (2.17),  $\Gamma$  can be calculated by substituting the solutions into (2.19), the true solution for the output bound  $x$  should be the one who has the same  $\Gamma$  by (2.19) as that obtained by (2.20).

**Remark 2.7:** The PBoC and PCM provide a novel view for understanding the nonlinear influences on a system dynamic response (such as super/sub harmonics and inter-modulation) incurred by different characteristic parameters. Some other recent advances also vindicate that the Volterra series approach can also be used for interpretation of complicated nonlinear behaviour such as bifurcation and even chaos [107, 109, 110].

**Remark 2.8:** There are some other nonlinear analysis methods, for example, the harmonic balance method and the nonlinear normal mode [133], which are often computationally intensive as the nonlinear degree of the system increases [134, 135]. This study presents a simple and novel evaluation on the nonlinear influence in terms of the characteristic parameters and on the parametric convergence bound of a nonlinear system in the sense of Volterra series expansion. This provides a very fundamental and significant basis for the nonlinear analysis and design using the Volterra series based methods [58, 70, 73, 98, 113, 116, 117].

To facilitate the computation of the PCM, the procedure is summarized as

**Algorithm 2.2 (Computation of PCM) :**

**Step 1.** Calculate  $\underline{L}(\omega)$  according to (2.4) and (2.11); Calculate  $\bar{H}_1(j\omega)$  according to (2.8) and (2.13); Calculate  $C(p, q)$  from (2.12).

**Step 2.** Compute (2.27)-(2.31) to construct (2.20) for the applicable case.

**Step 3.** Solve (2.20) or (2.19) for the applicable case to obtain the indicator  $\Gamma$ .

**Step 4.** Calculate (2.26) for the applicable case to obtain the PCM.

**2.2.6 Examples and discussion**

In order to illustrate the theoretical results, the NARX model in four cases with different nonlinear terms are discussed, which is given with zero initial conditions as

$$y(k) = c_{1,0}(1)y(k-1) + c_{1,0}(2)y(k-2) + c_{3,0}(1,1,1)y^3(k-1) + c_{1,2}(1,1,1)y(k-1)u^2(k-1) + c_{0,3}(1,1,1)u^3(k-1) + c_{0,1}(1)u(k-1) \quad (2.32)$$

The model in (2.32) can be obtained by discretizing in a backward manner the following nonlinear differential equation

$$m\ddot{y}(t) + c\dot{y}(t) + k_1y(t) + k_{30}y^3(t) + k_{12}y(t)u^2(t) + k_{03}u^3(t) = u(t) \quad (2.33)$$

where the linear coefficients are given as  $m=1, c=0.01\omega_0, k_1=\omega_0^2, \omega_0=20\pi$ ,

and  $u(t) = U \cos(\omega t)$ . Setting  $T_s = 1 / 2000s$ , then  $u(k) = U \cos(\Omega k)$

$$= U \cos(\omega T_s k) \text{ and } c_{1,0}(1) = 2 - \frac{cT_s}{m} - \frac{kT_s^2}{m} = 1.9987, c_{1,0}(2) = \frac{cT_s}{m} - 1 = -0.9997, c_{0,1}(1) = \frac{T_s^2}{m}$$

$$= 2.5 * 10^{-7}, c_{3,0}(1,1,1) = -\frac{k_{30}T_s^2}{m}, c_{1,2}(1,1,1) = -\frac{k_{12}T_s^2}{m}, c_{0,3}(1,1,1) = -\frac{k_{03}T_s^2}{m}.$$

The discussion starts with the case that the NARX model only possesses pure output nonlinear terms, that is,  $c_{1,2}(1,1,1) = c_{0,3}(1,1,1) = 0$ , which can be obtained by discretizing the well-known Duffing oscillator equation. Several existing results available in the literature are compared with this example. However, no existing results can be applied to all the other examples. In example 2.2.6.2, the nonlinear term with coefficient  $c_{1,2}(1,1,1)$  is considered in the discussion, and only  $c_{0,3}(1,1,1)$  is set to be zero in (2.32). Example 2.2.6.3 and example 2.2.6.2 are presented to illustrate and validate Remark 2.4 (how and in what conditions can the pure input nonlinearities affect the PBoC and PCM of a given nonlinear system).

When all of the parameters of the NARX model are given, (2.20) or (2.25) can also give an estimation of the PBoC for the input amplitude. But this thesis focuses on the PBoC for model parameters and the PCM in the following discussion.

In order to indicate the error between the synthesized output using Volterra series and the true output, the normalized root mean square error (NRMSE) is introduced,

$$NRMSE = \sqrt{\frac{\sum (y_{synthesized}(k) - y_{true}(k))^2}{\sum (y_{true}(k))^2}} \quad (2.34)$$

where  $y_{synthesized}$  is the synthesized output and  $y_{true}(k)$  is the true output.

### 2.2.6.1 The NARX model with pure output nonlinearity

The model is given as

$$y(k) = c_{1,0}(1)y(k-1) + c_{1,0}(2)y(k-2) + c_{3,0}(1,1,1)y^3(k-1) + c_{0,1}(1)u(k-1) \quad (2.35)$$

which can be obtained by discretizing the well-known Duffing equation. The PBoC of  $c_{3,0}(1,1,1)$  is calculated first, and then the PCM is discussed when the coefficient  $c_{3,0}(1,1,1)$  and the input are given.

The PBoC of  $c_{3,0}(1,1,1)$  can be computed via Algorithm 2.1. According to (2.21)-(2.24), it gives

$$\begin{aligned} a_{1,3} &= 2C(3,0), a_{1,0} = -\bar{H}_1(j\omega)U\underline{L}(\omega), \\ a_{2,2} &= 3C(3,0), a_{2,0} = -\underline{L}(\omega), \\ a_{1,2} &= a_{1,1} = a_{2,1} = 0. \end{aligned}$$

where  $C(3,0) = |c_{3,0}(1,1,1)|$ . Then from (2.20), the following equation holds

$$\begin{vmatrix} 2C(3,0) & 0 & 0 & -\bar{H}_1(j\omega)U\underline{L}(\omega) & 0 \\ 0 & 2C(3,0) & 0 & 0 & -\bar{H}_1(j\omega)U\underline{L}(\omega) \\ 3C(3,0) & 0 & -\underline{L}(\omega) & 0 & 0 \\ 0 & 3C(3,0) & 0 & -\underline{L}(\omega) & 0 \\ 0 & 0 & 3C(3,0) & 0 & -\underline{L}(\omega) \end{vmatrix} = 0 \quad (2.36)$$

Denoting  $A = \begin{pmatrix} 2C(3,0) & 0 \\ 0 & 2C(3,0) \end{pmatrix}$ ,  $B = \begin{pmatrix} 0 & -\bar{H}_1(j\omega)U\underline{L}(\omega) & 0 \\ 0 & 0 & -\bar{H}_1(j\omega)U\underline{L}(\omega) \end{pmatrix}$ ,

$$C = \begin{pmatrix} 3C(3,0) & 0 \\ 0 & 3C(3,0) \\ 0 & 0 \end{pmatrix}, D = \begin{pmatrix} -\underline{L}(\omega) & 0 & 0 \\ 0 & -\underline{L}(\omega) & 0 \\ 3C(3,0) & 0 & -\underline{L}(\omega) \end{pmatrix}, (2.36) \text{ is equivalent}$$

to  $|A||D - CA^{-1}B| = 0$ . The following equation can be obtained

$$\underline{L}(\omega) - \frac{27}{4}C(3,0)(\bar{H}_1(j\omega)U)^2 = 0 \quad (2.37)$$

From Eq. (2.37),  $C(3,0)$  can be solved.

In the discussion, the input amplitude is given as  $U = 0.5$ .  $\underline{L}(\omega)$  and

$\bar{H}_1(j\omega)$  can be obtained from (2.11) and (2.13), respectively. From (2.11), it can be obtained that  $\underline{L}(\omega) = \inf \{L(\omega), L(3\omega), L(5\omega), L(7\omega), \dots\}$  [117]. Since the first several orders of output spectra take the dominant roles, it can be simplified as  $\underline{L}(\omega) = \inf \{L(\omega), L(3\omega), L(5\omega), L(7\omega)\}$  [73, 117]. The estimated PBoC of  $|c_{3,0}(1,1,1)|$  is shown in Fig. 2.1, indicating a very close estimation to the real ones (obtained by numerical simulations) at different frequencies. The estimated bound varies at different frequencies and is very small at or around the harmonic resonant frequencies, which shows the nonlinear influence and potential behaviour due to this specific nonlinearity.

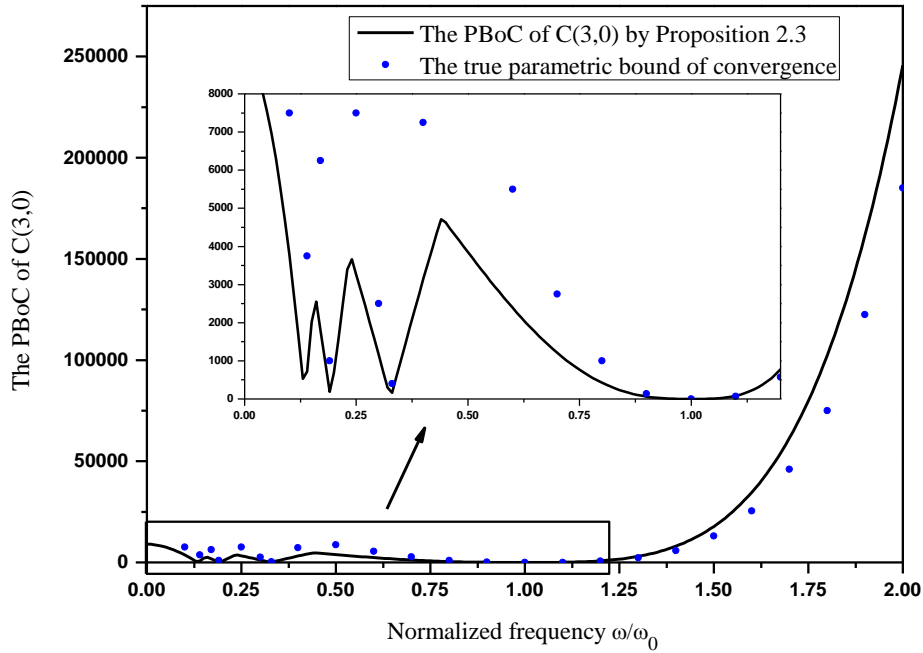


Figure 2.1 The PBoC of  $C(3,0) = |c_{3,0}(1,1,1)|$

To validate the effectiveness of the convergent bound above, a comparison with different nonlinear coefficients  $|c_{3,0}(1,1,1)|$  at  $\omega = 0.8\omega_0$  is given in Fig. 2.2. The estimated PBoC is  $C(3,0) = 426.0788$ . Fig. 2.2 shows that when the coefficient  $|c_{3,0}(1,1,1)| < C(3,0)$  holds, the synthesized output and the true output

has good agreement with each other (with the NRMSE quickly decrease to 0 as the synthesized order increases), while a larger nonlinear coefficient  $|c_{3,0}(1,1,1)|$  leads to the divergence of the synthesized output with an observable increasing NRMSE.

For the comparison with the other existing results [110, 119-121], the PBoCs of the input amplitude are given in Fig. 2.3, which indicates that our result provides the closest estimation.

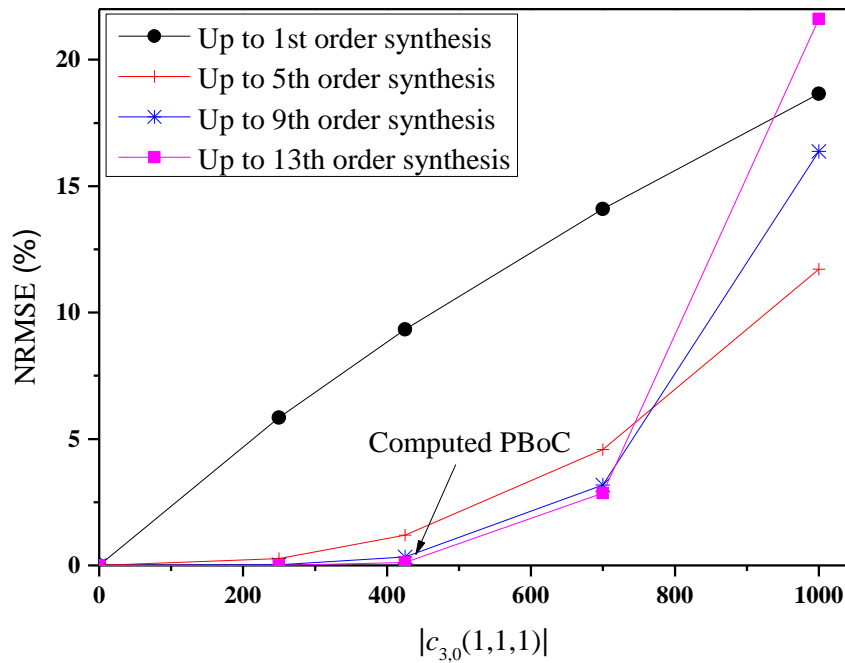


Figure 2.2 Comparison of the synthesized output and the true output at  $\omega = 0.8\omega_0$ .

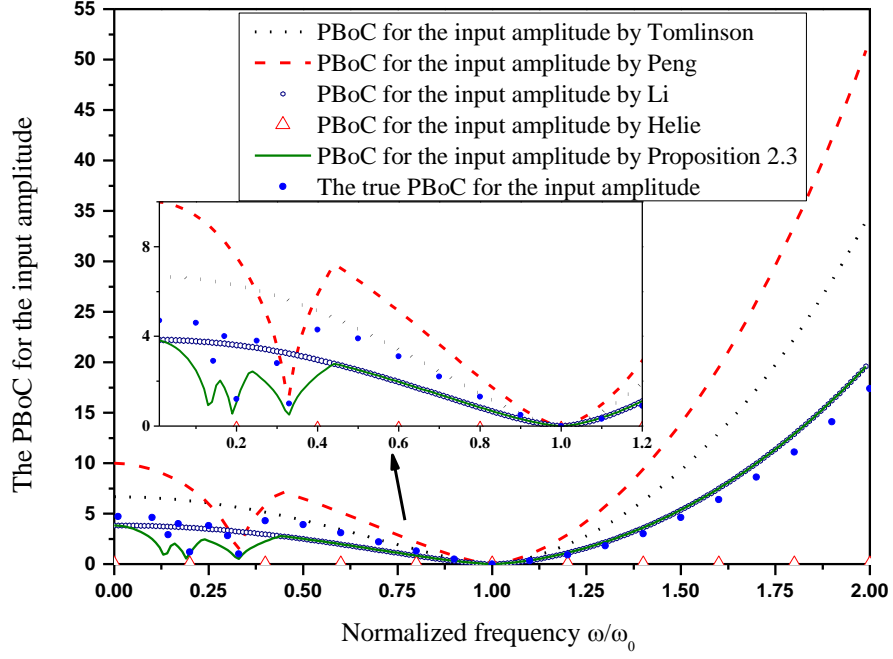


Figure 2.3 The PBoCs for the input amplitude

The following is to show the parametric convergence margin (PCM).

According to (2.27)-(2.31), the following equations hold

$$\begin{aligned}
 a_{1,3} &= C(3,0), a_{1,1} = -\underline{L}(\omega), a_{1,0} = \bar{H}_1(j\omega)U\underline{L}(\omega) \\
 a_{2,2} &= 3C(3,0), a_{2,0} = -\Gamma\underline{L}(\omega) \\
 a_{1,2} &= a_{2,1} = 0.
 \end{aligned}$$

Then  $\Gamma$  can be estimated from (2.20) as

$$\begin{vmatrix}
 C(3,0) & 0 & -\underline{L}(\omega) & \bar{H}_1(j\omega)U\underline{L}(\omega) & 0 \\
 0 & C(3,0) & 0 & -\underline{L}(\omega) & \bar{H}_1(j\omega)U\underline{L}(\omega) \\
 3C(3,0) & 0 & -\Gamma\underline{L}(\omega) & 0 & 0 \\
 0 & 3C(3,0) & 0 & -\Gamma\underline{L}(\omega) & 0 \\
 0 & 0 & 3C(3,0) & 0 & -\Gamma\underline{L}(\omega)
 \end{vmatrix} = 0 \tag{2.38}$$

From (2.38), the following equation can be obtained

$$\Gamma^3 - 6\Gamma^2 + 9\Gamma - \frac{27C(3,0)(\bar{H}_1(j\omega)U)^2}{\underline{L}(\omega)} = 0 \tag{2.39}$$

$\Gamma$  can then be solved, and the PCM can be obtained according to (2.26). The

convergence margin with  $c_{3,0}(1,1,1) = -153.8223$  and  $U = 0.5$  is presented in Fig. 2.4.

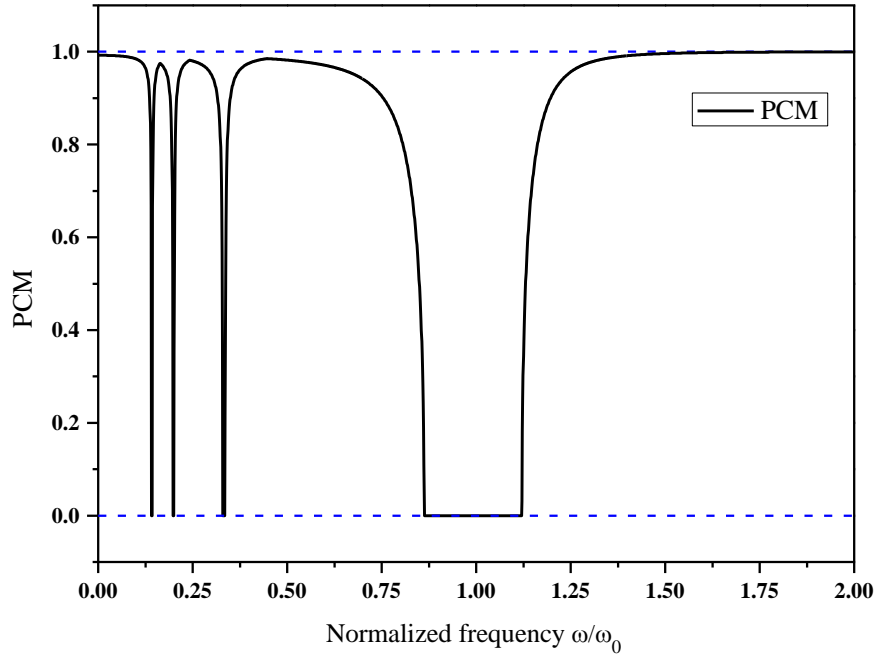


Figure 2.4 The parametric convergence margin (PCM)

The PCM is equal to zero around the resonant frequency, which means that the nonlinear system with given coefficients and input is divergent in the sense of Volterra series expansion, while at high frequencies the PCM is near to 1. This is consistent with the previous PBoC results, and also confirms the existing knowledge about the Duffing equation [110, 119]. Numerical simulations show that complicated nonlinear behaviours can be observed at the frequencies where  $PCM = 0$ .

### 2.2.6.2 The NARX model with pure output nonlinearity and cross nonlinearity

In this example, the NARX model has a nonlinear cross-term with  $p = 1$  and

a pure output nonlinear term with  $p = 3$  as

$$y(k) = c_{1,0}(1)y(k-1) + c_{1,0}(2)y(k-2) + c_{3,0}(1,1,1)y^3(k-1) \\ + c_{1,2}(1,1,1)y(k-1)u^2(k-1) + c_{0,1}(1)u(k-1) \quad (2.40)$$

From (2.21)-(2.24), it can be obtained that

$$a_{1,3} = 2C(3,0), a_{1,0} = -\bar{H}_1(j\omega)U\underline{L}(\omega), \\ a_{2,2} = 3C(3,0), a_{2,0} = C(1,2)U^2 - \underline{L}(\omega), \\ a_{1,2} = a_{1,1} = a_{2,1} = 0.$$

where  $C(3,0) = |c_{3,0}(1,1,1)|$ , and  $C(1,2) = |c_{1,2}(1,1,1)|$ . Then according to (2.20), it gives

$$\left(C(1,2)U^2 - \underline{L}(\omega)\right)^3 + \frac{27}{4}C(3,0)\left(\bar{H}_1(j\omega)U\underline{L}(\omega)\right)^2 = 0 \quad (2.41)$$

Clearly, (2.41) provides an analytical relationship among the parametric bounds ( $C(3,0)$ ,  $C(1,2)$ , and  $U$ ), and the linear part of the model. It can be obtained that

$$C(1,2) = \frac{\underline{L}(\omega) - \sqrt[3]{\frac{27}{4}C(3,0)\left(\bar{H}_1(j\omega)U\underline{L}(\omega)\right)^2}}{U^2} \quad (2.42)$$

$$C(3,0) = \frac{4\left(\underline{L}(\omega) - C(1,2)U^2\right)^3}{27\left(\bar{H}_1(j\omega)U\underline{L}(\omega)\right)^2} \quad (2.43)$$

In the discussion, the input amplitude is given as  $U = 0.5$ , and give  $c_{3,0}(1,1,1) = -153.8223$  for (2.42), and  $c_{1,2}(1,1,1) = -1.5382 \times 10^{-4}$  for (2.43). The estimated bound results are presented in Fig. 2.5 and Fig. 2.6. Fig. 2.5 shows that at or around the resonant frequency or some harmonic resonant frequencies, the PBoC  $C(1,2)$  is zero, which means that the Volterra series expansion of the model with  $c_{3,0}(1,1,1) = -153.8223$ ,  $c_{1,2}(1,1,1) = 0$ , and  $U = 0.5$  diverges; Similar phenomena can also be observed in Fig. 2.6 for the PBoC of  $C(3,0)$ .

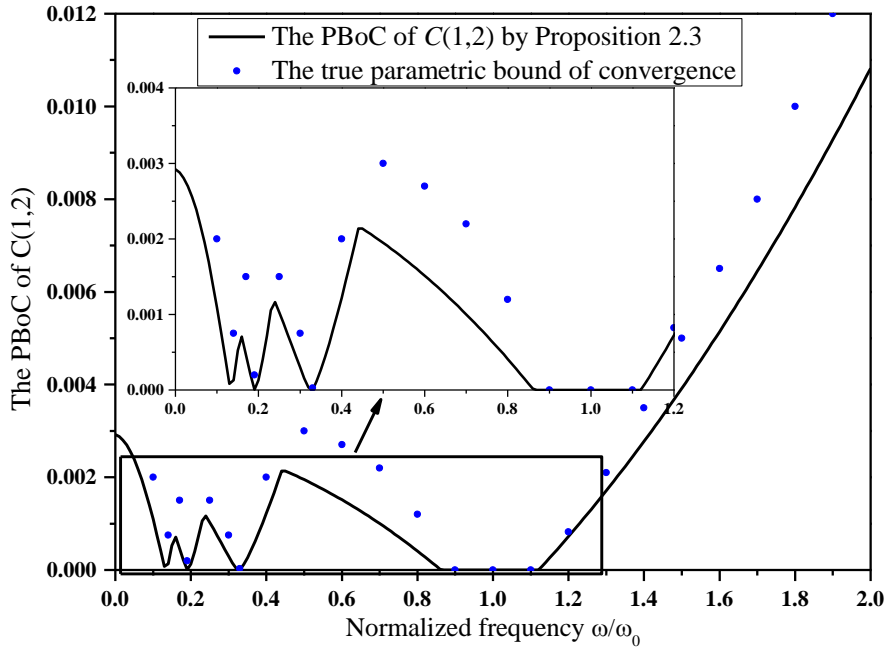


Figure 2.5 The PBoC of  $C(1,2) = |c_{1,2}(1,1,1)|$

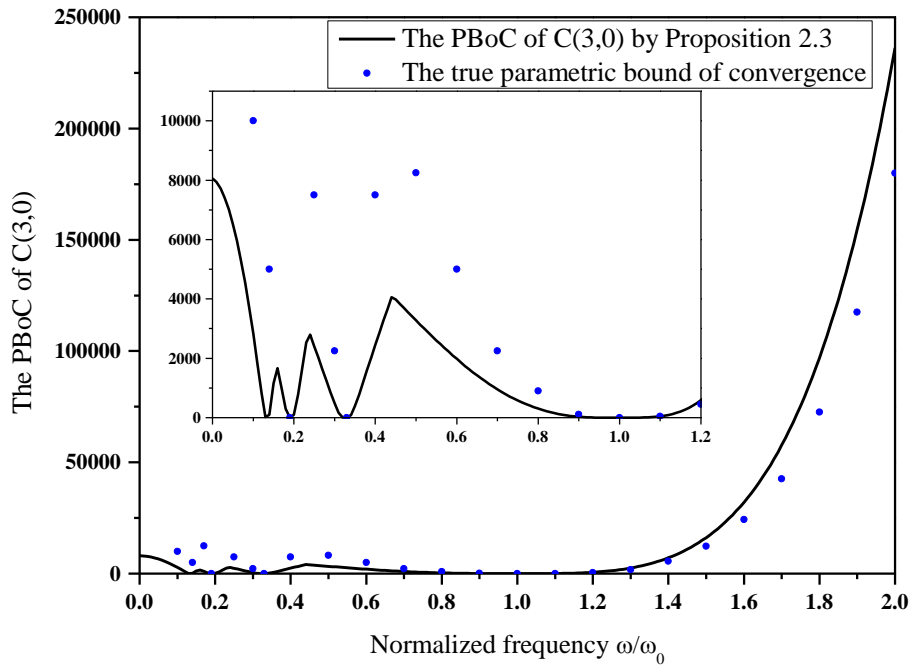


Figure 2.6 The PBoC of  $C(3,0) = |c_{3,0}(1,1,1)|$

Fig. 2.7-2.8 show that when the nonlinear parameter is selected under the estimated bound, the synthesized output can well approximate to the true output, while the synthesized output becomes divergent when the parameter takes a value larger than the estimated bound.

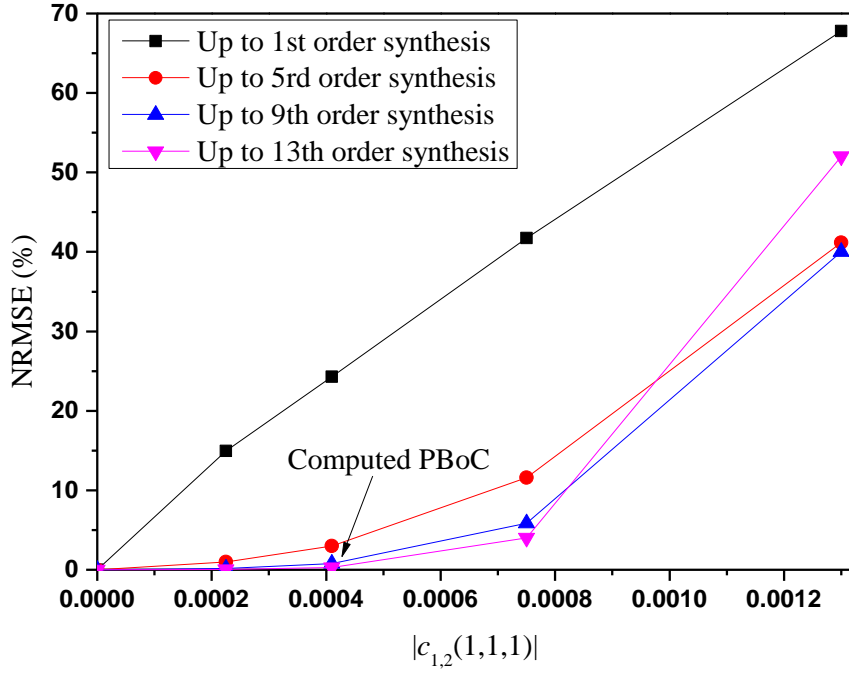


Figure 2.7 Comparison of the synthesized output and the true output at  $\omega = 0.8\omega_0$  with  $c_{3,0}(1,1,1) = -153.8223$ .

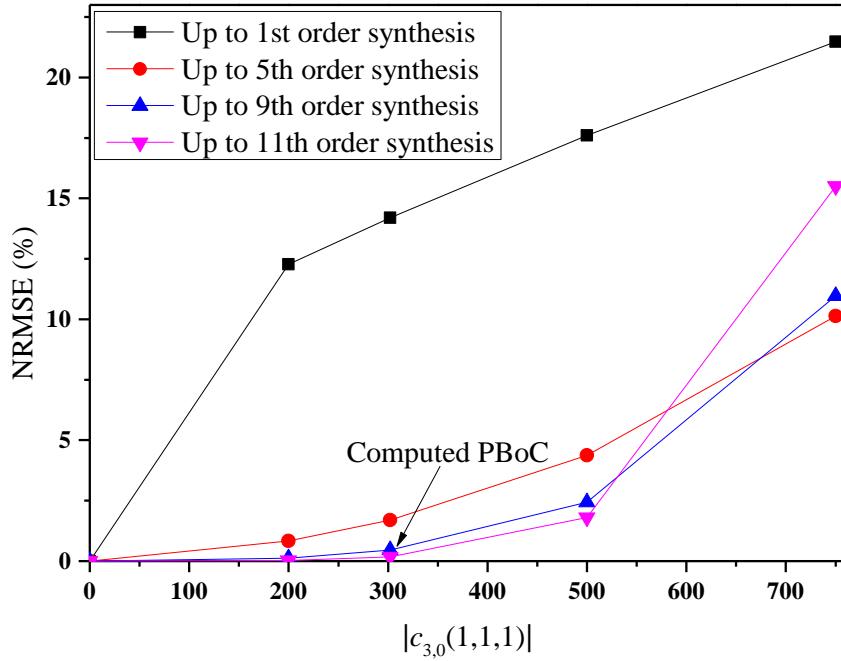


Figure 2.8 Comparison of the synthesized output and the true output at  $\omega = 0.8\omega_0$  with  $c_{1,2}(1,1,1) = -1.5382 \times 10^{-4}$ .

According to (2.27)-(2.31), the following equations hold

$$\begin{aligned}
 a_{1,3} &= C(3,0), a_{1,1} = C(1,2)U^2 - \underline{L}(\omega), a_{1,0} = \bar{H}_1(j\omega)U\underline{L}(\omega), \\
 a_{2,2} &= 3C(3,0), a_{2,0} = (C(1,2)U^2 - \underline{L}(\omega))\Gamma, \\
 a_{1,2} &= a_{2,1} = 0.
 \end{aligned}$$

Then  $\Gamma$  satisfies the following equation according to (2.20)

$$\begin{aligned} (\underline{L}(\omega))^3 \Gamma^3 - 3(\underline{L}(\omega))^2 C(1,2)U^2 \Gamma^2 + 3\underline{L}(\omega)(C(1,2)U^2)^2 \Gamma \\ - (C(1,2)U^2)^3 + \frac{27C(3,0)(\underline{L}(\omega)\bar{H}_1(j\omega)U)^2}{4} = 0 \end{aligned} \quad (2.44)$$

The convergence margin indicator  $\Gamma$  can then be solved. When  $\Gamma \geq 1$ , the Volterra series expansion is divergent with  $\text{PCM} < 0$ , which is denoted by  $\text{PCM} = 0$  in the Figures. The PCM can then be calculated according to (2.26) and is presented in Fig. 2.9 with  $U = 0.5$ ,  $c_{3,0}(1,1,1) = -153.8223$ , and  $c_{1,2}(1,1,1) = -1.5382 * 10^{-4}$ .

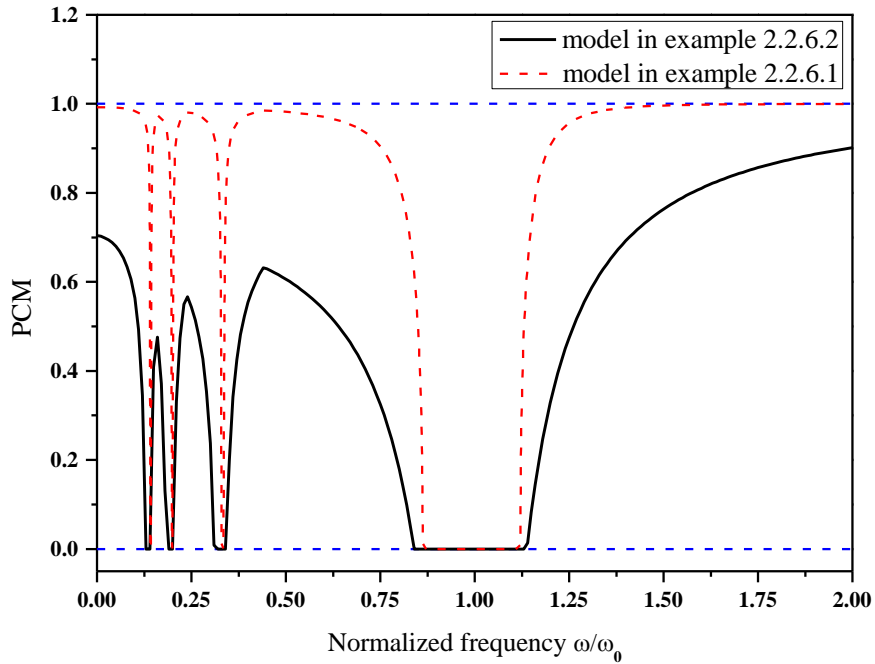


Figure 2.9 The parametric convergence margin (PCM)

From Fig. 2.9, the convergence margin PCM with given coefficients and input amplitude is equal to 0 around the resonant and super-harmonic resonant frequencies, and the influence of the nonlinear cross-term with index  $p = 1$  can be seen. The nonlinear cross-term gives rise to a stronger nonlinear behavior, which can be observed from the smaller PCM. The frequency bandwidth where the  $\text{PCM} = 0$  around the resonant frequency increases (compared with the case in

Example A). This means that the nonlinear dynamic response of the NARX model becomes more complicated after introducing a new nonlinear term.

### 2.2.6.3 The NARX model with pure input nonlinearity and cross nonlinearity

The system model is given by

$$y(k) = c_{1,0}(1)y(k-1) + c_{1,0}(2)y(k-2) + c_{1,2}(1,1,1)y(k-1)u^2(k-1) + c_{0,3}(1,1,1)u^3(k-1) + c_{0,1}(1)u(k-1) \quad (2.45)$$

Eqs (2.25) and (2.19) can be used for the computation of the PBoC and PCM, respectively. It is interesting to see that the pure input nonlinear term with the coefficient  $c_{0,3}(1,1,1)$  does not affect the PBoC of  $c_{1,2}(1,1,1)$ , the PBoC of the input magnitude, and the PCM.

From (2.25), the convergent bound can be obtained

$$\frac{C(1,2)U^2}{\underline{L}(\omega)} = 1 \quad (2.46)$$

The PBoC for  $c_{1,2}(1,1,1)$  with  $U = 0.5$  is presented in Fig. 2.10. The PBoC of  $c_{1,2}(1,1,1)$  is very close to 0 at or around harmonic resonance frequencies. In order to validate that the convergent bound (PBoC of  $C(1,2) = |c_{1,2}(1,1,1)|$ ) is independent of the pure input nonlinear parameter, the case that  $c_{0,3}(1,1,1) = 0$  and the case that  $c_{0,3}(1,1,1) = -2.5 * 10^{-5}$  are compared. In both cases, the simulations take the same input magnitude and consider the same frequency point, for example,  $U = 0.5$ , and  $\omega = 0.8\omega_0$ . The PBoC of  $C(1,2)$  is computed as 0.00142. The results are presented in Figs. 2.11-2.12, which show that when

$|c_{1,2}(1,1,1)|$  is out of the estimated bound, the synthesized output is divergent, and the convergent bound is independent of  $c_{0,3}(1,1,1)$ .

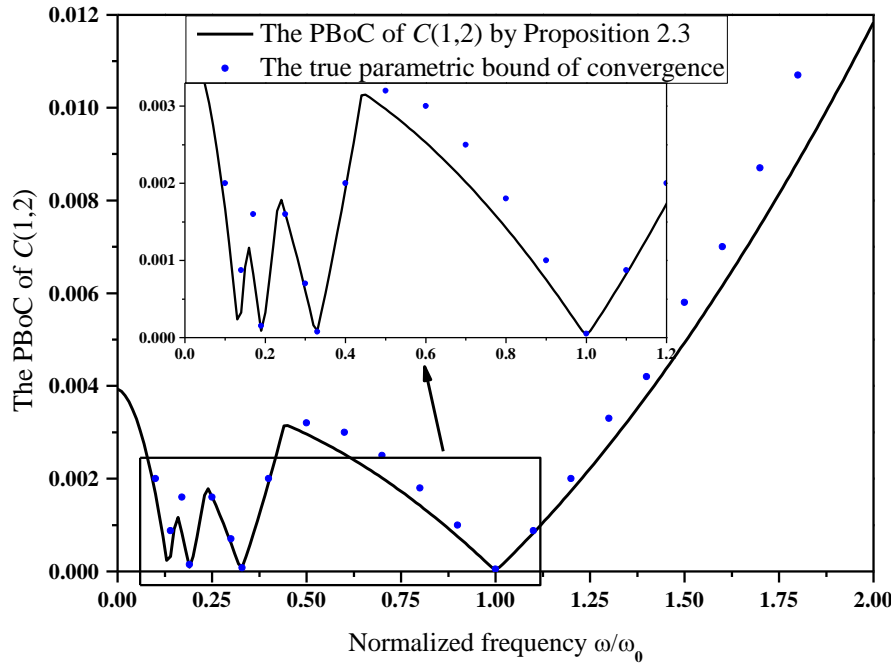


Figure 2.10 The PBoC of  $C(1,2) = |c_{1,2}(1,1,1)|$

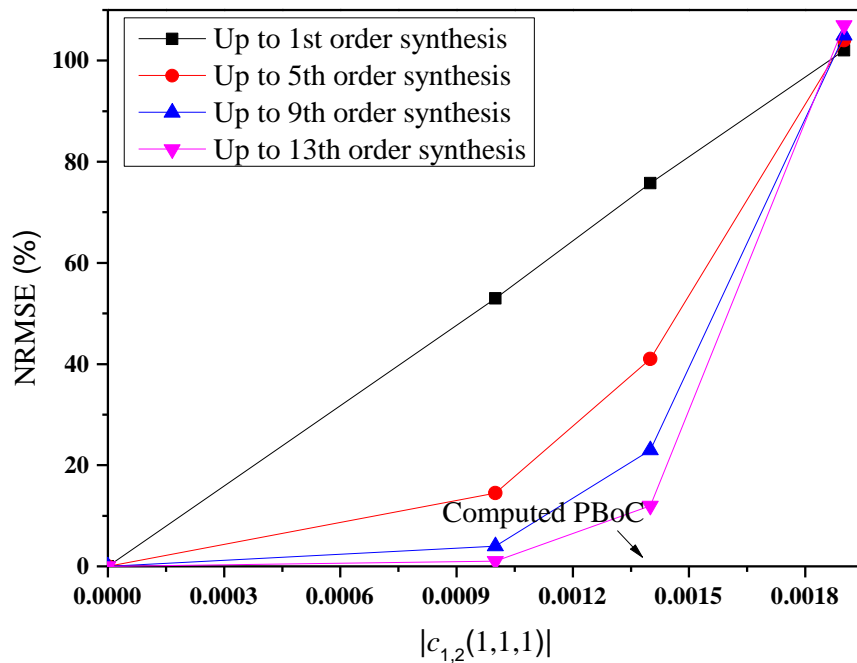


Figure 2.11 Comparison of the synthesized output and the true output at  $\omega = 0.8\omega_0$  with  $c_{0,3}(1,1,1) = 0$

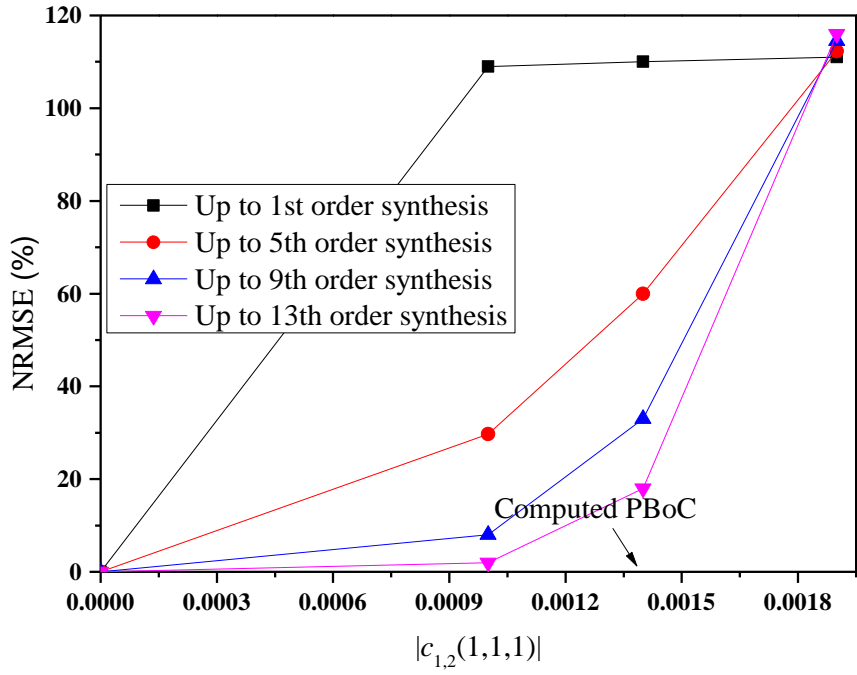


Figure 2.12 Comparison of the synthesized output and the true output at  $\omega = 0.8\omega_0$  with  $c_{0,3}(1,1,1) = -2.5 \times 10^{-5}$

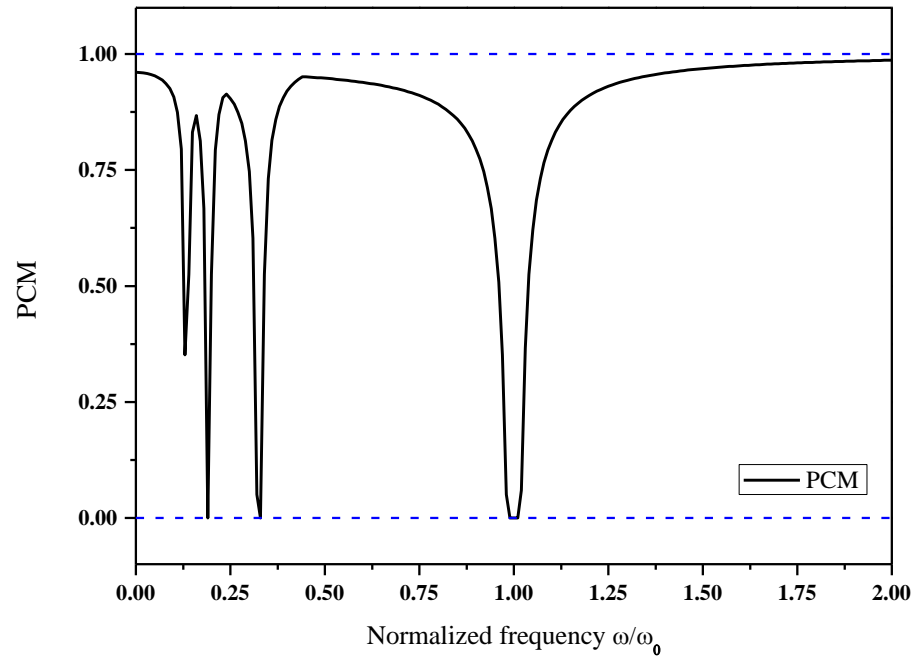


Figure 2.13 The PCM

The indicator  $\Gamma$  can be obtained from (2.19). When  $c_{1,2}(1,1,1) = -1.5382 \times 10^{-4}$  and  $U = 0.5$ , the result of the PCM is shown in Fig. 2.13. The PCM at/around the resonant frequency decreases to 0, indicating the

complicated nonlinear dynamics there.

#### 2.2.6.4 The NARX model with pure input nonlinearity and pure output nonlinearity

The system model is given by

$$y(k) = c_{1,0}(1)y(k-1) + c_{1,0}(2)y(k-2) + c_{3,0}(1,1,1)y^3(k-1) + c_{0,3}(1,1,1)u^3(k-1) + c_{0,1}(1)u(k-1) \quad (2.47)$$

This example is given as a comparison with example 2.2.6.1 and 2.2.6.3 to further show how the pure input nonlinearity affects the PBoC and the PCM. In this case, (2.20) can be used to calculate the PBoC. From (2.21)-(2.24),

$$\begin{aligned} a_{1,3} &= 2C(3,0), a_{1,0} = -C(0,3)U^3 - \bar{H}_1(j\omega)U\underline{L}(\omega), \\ a_{2,2} &= 3C(3,0), a_{2,0} = -\underline{L}(\omega), \\ a_{1,2} &= a_{1,1} = a_{2,1} = 0. \end{aligned}$$

the following equation holds

$$(\underline{L}(\omega))^3 - \frac{27}{4}C(3,0)(\bar{H}_1(j\omega)U\underline{L}(\omega) + C(0,3)U^3)^2 = 0. \quad (2.48)$$

Then, the PBoCs can be obtained as

$$C(3,0) = \frac{4}{27} \frac{(\underline{L}(\omega))^3}{(\bar{H}_1(j\omega)U\underline{L}(\omega) + C(0,3)U^3)^2} \quad (2.49)$$

$$C(0,3) = \frac{\sqrt{\frac{4(\underline{L}(\omega))^3}{27C(3,0)} - \bar{H}_1(j\omega)U\underline{L}(\omega)}}{U^3} \quad (2.50)$$

From (2.49), it is clear that the coefficient of the pure input nonlinearity (i.e.,  $c_{0,3}(1,1,1)$ ) does affect the the bound  $C(3,0)$ . This is different from the case in example 2.2.6.3 where the pure input nonlinearity does not affect the PBoC.

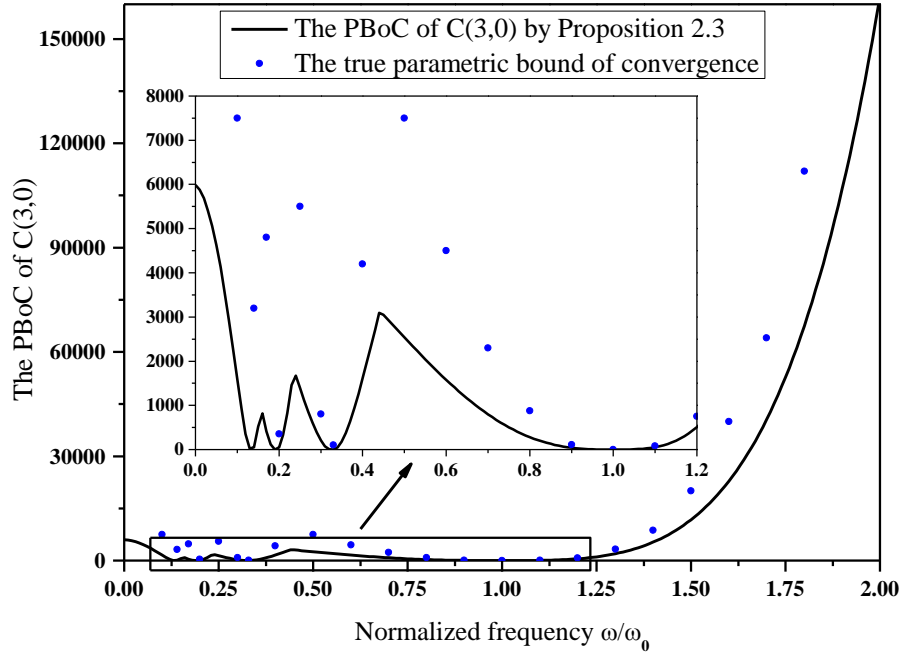


Figure 2.14 The PBoC of  $C(3,0) = |c_{3,0}(1,1,1)|$

The estimated PBoCs for  $C(3,0)$  and  $C(0,3)$  are shown in Figs. 2.14-2.15 respectively, with  $c_{0,3}(1,1,1) = -2.3073 \cdot 10^{-7}$  in Fig. 2.14 and  $c_{3,0}(1,1,1) = -153.8223$  in Fig. 2.15. In Fig. 2.14 and Fig. 2.15, the computed PBoC  $C(3,0)$  is very close to 0 around the resonant frequency and super-harmonic resonant frequencies.

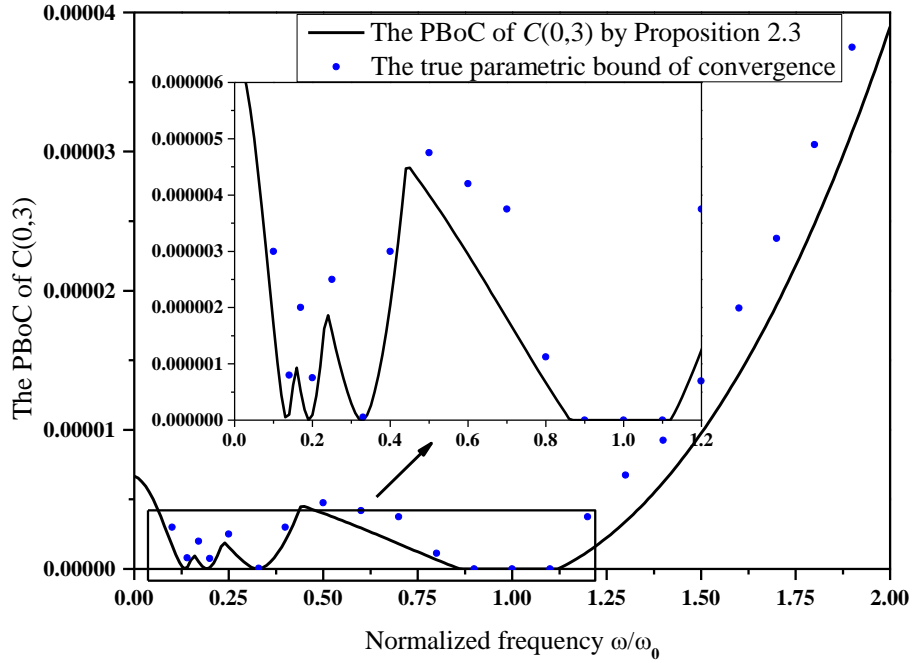


Figure 2.15 The PBoC of  $C(0,3) = |c_{0,3}(1,1,1)|$

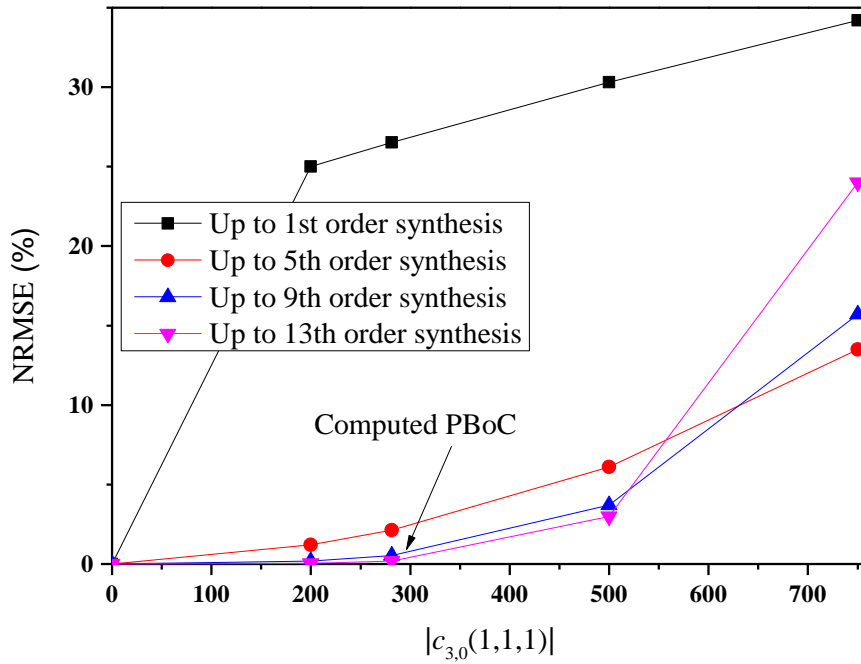


Figure 2.16 Comparison of the synthesized output and the true output at  $\omega = 0.8\omega_0$  with  $c_{0,3}(1,1,1) = -2.3073 \times 10^{-7}$

The validation of these estimated bounds is given in Figs. 2.16-2.17 with  $\omega = 0.8\omega_0$  and  $U = 0.5$ . Given the model parameters  $c_{0,3}(1,1,1) = -2.3073 \times 10^{-7}$  for (2.49) and  $c_{3,0}(1,1,1) = -153.8223$  for (2.50),

The PBoCs are computed as  $C(3,0)=281.2949$  and  $C(0,3)=6.6431 \times 10^{-7}$ . Fig. 2.16 and Fig. 2.17 show that the estimated bound is effective, and the synthesized output becomes slowly divergent when the nonlinear coefficients are out of the estimated bound.

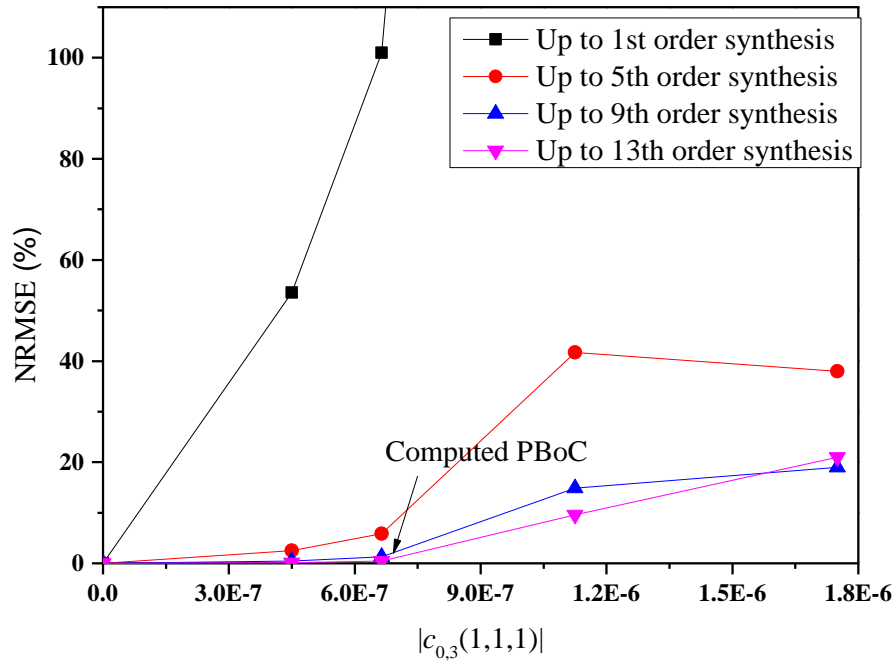


Figure 2.17 Comparison of the synthesized output and the true output at  $\omega = 0.8\omega_0$  with  $c_{3,0}(1,1,1) = -153.8223$

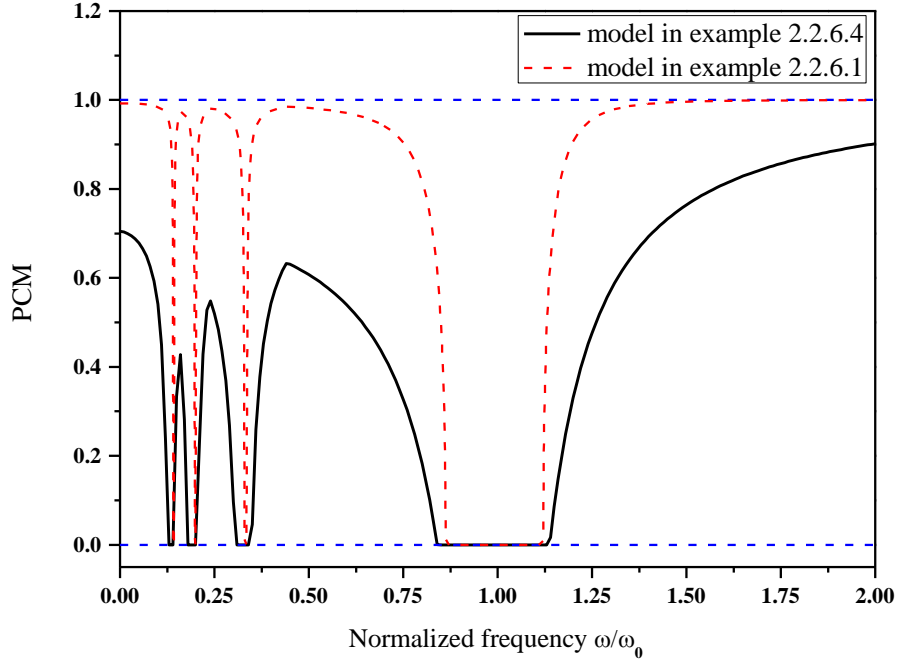


Figure 2.18 The PCM

For the calculation of the PCM , the following equations hold from (2.27)

-(2.31)

$$\begin{aligned}
 a_{1,3} &= C(3,0), a_{1,1} = -\underline{L}(\omega), a_{1,0} = C(0,3)U^3 + \bar{H}_1(j\omega)U\underline{L}(\omega) \\
 a_{2,2} &= 3C(3,0), a_{2,0} = -\Gamma\underline{L}(\omega), \\
 a_{1,2} &= a_{2,1} = 0.
 \end{aligned}$$

Then from (2.20), it can be obtained that

$$\Gamma = \frac{1}{\underline{L}(\omega)} \times \left( \frac{27C(3,0)(\underline{L}(\omega)\bar{H}_1(j\omega)U + C(0,3)U^3)^2}{4} \right)^{\frac{1}{3}} \quad (2.51)$$

Given  $U = 0.5$  ,  $c_{3,0}(1,1,1) = -153.8223$  and  $c_{0,3}(1,1,1) = -2.3073 \cdot 10^{-7}$  ,

the convergence margin is presented in Fig. 2.18, which shows that the pure input nonlinearity leads to a smaller PCM, indicating a stronger nonlinear behaviour. The PCM around the super-resonant frequencies decreases to 0, and the region where  $\text{PCM} = 0$  becomes wider, implying that the nonlinear dynamics become more complicated.

## 2.3 Parametric convergence bound for general input

### 2.3.1 Notations and definitions

Let  $R_\omega$  as the input frequency range of a input signal  $u(t)$ , and  $W_\omega$  is the output frequency range. The latter can be determined with the method in [71, 73].  $C(p, q)$  is a non-negative function of parameter  $c_{p,q}(\cdot)$  ( $0 \leq p, q \leq n$ ) defined in (2.12).

Define

$$\overline{H}_n = \max_{\omega_1 \cdots \omega_n \in R_\omega} (|H_n(\cdot)|) \quad (2.52)$$

For any input  $U(j\omega)$  defined in  $R_\omega$ , and denote the minimum value of  $|L(j\omega)|$  as

$$\underline{L}_{R_\omega} = \min_{\Omega \in W_\omega} \{|L(j\Omega)|\} \quad (2.53)$$

Obviously, different input  $U(j\omega)$  leads to different  $\underline{L}_{R_\omega}$ . For any input signal  $r(t)$ ,

denote  $R(j\omega)$  as the spectrum of  $r(t)$ , and

$$\rho = \max |R(j\omega)| \quad (2.54)$$

$$U(j\omega) = R(j\omega) / \rho \quad (2.55)$$

It is clear that  $U(j\omega)$  is the normalized spectrum of  $R(j\omega)$ , and  $\max|U(j\omega)|=1$ . The output frequency response of the nonlinear system can be obtained as [71, 136]

$$Y(j\omega) = \sum_{n=1}^N \frac{1}{(2\pi)^{n-1}} \underbrace{\int_{-\infty}^{\infty} \cdots \int_{-\infty}^{\infty}}_{n-1} \mathcal{E} d\omega_1 \cdots d\omega_{n-1} \quad (2.56)$$

where  $\mathcal{E} = H_n(j\omega_1, \cdots, j\omega_{n-1}, j(\omega - \omega_1 - \cdots - \omega_{n-1})) U_n(j\omega, j\omega_1, \cdots, j\omega_{n-1})$  and

$$U_n(j\Omega, j\omega_1, \cdots, j\omega_{n-1}) = U_1(j\omega_1) \cdots U_1(j\omega_{n-1}) U_1(j(\Omega - \omega_1 - \cdots - \omega_{n-1})) \quad .$$

### 2.3.2 The main result

Magnitude bounds of nonlinear frequency response functions including the GFRFs and output spectrum have been studied in [96-98] with a parametric characteristic point of view, where the magnitude bounds are expressed as polynomial functions of the magnitude bound of the first-order GFRF  $H_1(j\omega)$ . In this study, the bound of the output spectrum in (2.56) is formulated into a frequency-dependent polynomial function of the input magnitude, and this polynomial function is actually an infinite power series with respect to the input magnitude. The closed form polynomial function in (2.58) explicitly involves the frequency variable, wave form information of the input, input magnitude, and also the model parameters, which provides a novel insight into the bound of output spectrum and leads to the new parametric convergence criterion in Proposition 2.5 based on the analytic inversion lemma in [137].

**Lemma 2.3:** The bound of the output frequency response in (2.56) subjected to a general input having the Fourier transform  $\rho \cdot U(j\omega)$  ( $\omega \in R_\omega$ ) is given by

$$|Y(j\omega)| \leq \bar{Y} = \frac{1}{\sigma} \sum_{n=1}^{\infty} \bar{H}_n \gamma^n \quad (2.57)$$

which can be further written into a closed form as

$$\tilde{Y} = \bar{H}_1 \gamma + \frac{1}{L_{R_\omega}} \sum_{m=2}^M \sum_{\substack{p+q=m \\ 0 \leq p, q \leq m}} C(p, q) \tilde{Y}^p \gamma^q \quad (2.58)$$

where

$$\sigma = \frac{1}{\pi} \int_{\omega_1 \in R_\omega} |U(j\omega_1)| d\omega_1, \quad \tilde{Y} = \sigma \bar{Y}, \quad \gamma = \sigma \rho \quad (2.59)$$

Specifically, if  $u(t) = \sum_{i=1}^{\bar{K}} |F_i| \cos(\omega_i t + \angle F_i)$  with  $\max |F_i| = 1$ ,  $\sigma$  in (2.59) is given

by

$$\sigma = \sum_{\omega_{k_1} \in R_\omega} |F(j\omega_{k_1})| \quad (2.60)$$

with  $R_\omega = \{\omega_1, \omega_2, \dots, \omega_{\bar{K}}\}$  and  $F(\omega_{k_1}) = |F_{k_1}| e^{j\angle F_{k_1}}$  for  $k_1 \in \{1, \dots, \bar{K}\}$ . For a single-tone input, i.e.,  $\bar{K} = 1$ ,  $\bar{H}_1$  can be replaced by  $|H_1(j\omega)|$  in (2.57) and (2.58).

**Proof:** See Appendix 2.5.

**Remark 2.9:**  $\sigma$  in (2.59) involves the wave form information of the input,  $\tilde{Y}$  and  $\gamma$  can then be considered as a new bound for the output spectrum and the new input magnitude having wave form information, respectively. The input wave form information involved in  $\sigma$  makes the result in this section available for a general input.

In [137], it is shown that an analytic function locally admits an analytic inverse near any point where the first derivative of the inverse is non-zero. However, a function cannot be analytically inverted in a neighbourhood of a point where the first derivative vanishes.

The output bound in (2.57),  $\bar{Y} = \frac{1}{\sigma} \sum_{n=1}^{\infty} \bar{H}_n \gamma^n$ , is analytic in its convergence region, which allows an analytic inverse. That is, in the convergence region, there exists an inverse  $f^{-1}$  such that  $\gamma = f^{-1}(\bar{Y})$ . Therefore, the minimum input magnitude bound where the first derivative of the inverse is zero, i.e.,  $\partial\gamma/\partial\bar{Y} = 0$ , can be regarded as the convergence bound of the power series (2.57) (where the analytic inverse does not exist). The following proposition can be obtained.

**Proposition 2.5** The parametric convergence bound of the Volterra series expansion of the NARX system subjected to any input  $\rho u(t)$  with a Fourier transform  $\rho U(j\omega)$  (satisfying  $|U(j\omega)| \leq 1$  for all  $\omega$ ) for any model parameters (with  $p+q>1$ ) and input magnitude  $\rho$  can be obtained by solving the following equations:

$$\begin{cases} \bar{H}_1 \gamma + \frac{1}{\underline{L}_{R_\omega}} \sum_{m=2}^M \sum_{\substack{p+q=m \\ 0 \leq p, q \leq m}} C(p, q) \tilde{Y}^p \gamma^q = \tilde{Y} \\ \frac{1}{\underline{L}_{R_\omega}} \sum_{m=2}^M \sum_{\substack{p+q=m \\ 0 \leq p, q \leq m}} p C(p, q) \tilde{Y}^{p-1} \gamma^q = 1 \end{cases} \quad (2.61)$$

**Proof:** To ensure the convergence of the power series in (2.57) is to guarantee the existence of analytic inverse and thus to find the singular point where the first derivative of the inverse is zero. Therefore, applying the first derivative operation to both sides of (2.57) with respect to  $\tilde{Y}$ , and setting it to be  $d\gamma/d\tilde{Y} = 0$ , it yields the second equation of (2.61). Together with (2.57), the convergence bound for  $\gamma$  can be obtained and thus the bound of  $\rho$  can be computed by (2.59). If the input magnitude  $\rho$  is given, solving (2.61) can give a bound for any model parameters with  $p+q>1$ .  $\square$

**Remark 2.10** Proposition 2.5 presents a more general result, which is applicable to any input signal (not just for single-tone harmonic input as those in [110, 119, 120, 138, 139]), and can achieve a convergence bound for both input magnitude and any model parameter (with  $p+q>1$ ). Due to the definition of  $\gamma$  in (2.59), the convergence bound obtained with Proposition 2.5 is dependent on the wave form of the input (not just input magnitude in all of the existing results). Also, due to the definition of  $\underline{L}_{R_\omega}$  in (2.53), different input frequencies may result in different

values of  $\underline{L}_{R_o}$ , and thus the bound result by Proposition 2.5 is also frequency-dependent.

**Remark 2.11** A convergence bound (denoted by  $\bar{\gamma}$ ) for  $\gamma$  can be obtained via Proposition 2.5. From (2.59), the input magnitude bound for  $\rho$  can be calculated with  $\bar{\rho} = \bar{\gamma}/\sigma$ . For a single-tone harmonic input  $u(t) = \rho \cos(\omega t + \angle F_1)$ ,  $\sigma = 1$  in (2.59) and the input magnitude bound is  $\bar{\rho} = \bar{\gamma}/1 = \bar{\gamma}$ , which is the input magnitude bound obtained in last section. For a general input, the convergence bound of input magnitude in [121] is a constant that close to the worst case in this frequency-dependent bound.

The convergence bound results obtained by Proposition 2.5 is dependent of the frequency, the magnitude and wave form information of input signals, and is available to any characteristic parameters (including input magnitude and model parameters with  $p+q>1$ ). This cannot be achieved by all the existing methods. To compute the parametric convergence bound, the following procedure can be used

**Algorithm 2.3:**

**Step 1.** Compute the bounds  $\bar{H}_1$  and  $\underline{L}_{R_o}$  with (2.4), (2.8), (2.52), and (2.53).

**Step 2.** Solve (2.61) to find the bound for  $\gamma$  or any model parameters  $c_{p,q}(\cdot)$  with  $p+q>1$ .

**Step 3.** If all model parameters are known, the parametric convergence bound of input magnitude  $\rho$  can be obtained with the computed bound of  $\gamma$ , and (2.59); if input magnitude  $\rho$  is given, then  $\gamma$  can be computed with (2.59), and a convergence bound for any specific model parameter  $c_{p,q}(\cdot)$  with  $p+q>1$  can be

obtained from (2.61).

### 2.3.3 Examples and discussion

Consider that model (2.35) is subject to a multi-tone input

$$u(k) = \rho(\cos(\omega_1 k) + \beta \cos(\omega_2 k)) \quad (2.62)$$

where  $\beta \cos(\omega_2 k)$  can be seen as a disturbance of  $\cos(\omega_1 k)$ , satisfying  $0 < \beta < 1$ . Similar conclusions can be drawn for any other input signals.

#### 2.3.3.1 Computation of the convergence bound of input

The parametric bound of convergence (PBoC) of input magnitude  $\rho$  can be computed according to Algorithm 2.3. From (2.61), the following equations hold,

$$\begin{cases} C(3,0)\tilde{Y}^3 - \underline{L}_{R_\omega} \tilde{Y} + \underline{L}_{R_\omega} \bar{H}_1 \gamma = 0 \\ 3C(3,0)\tilde{Y}^2 - \underline{L}_{R_\omega} = 0 \end{cases} \quad (2.63)$$

From the second equation of (2.63), it gives  $\tilde{Y} = \sqrt{\underline{L}_{R_\omega}/3C(3,0)}$ . Substituting  $\tilde{Y}$  into the first equation of (2.63), the convergence bound of  $\gamma$  can be obtained. Then according to (2.59), the PBoC of  $\rho$  is straightforward as

$$\bar{\rho} = \frac{\gamma}{1+\beta} = \frac{2\sqrt{\underline{L}_{R_\omega}}}{3(1+\beta)\bar{H}_1\sqrt{3C(3,0)}} \quad (2.64)$$

Given  $c_{3,0}(1,1,1)=-153.8$ ,  $k_{30}=0.01\omega_0^2$ ,  $\beta=0.2$ , and  $\omega_2=\omega_1+2\pi \cdot 1 \cdot T_s$ , the computed PBoC of input magnitude is presented in Fig. 2.19. From Fig. 2.19, it can be seen that the computed PBoC of the input magnitude  $\rho$  is very close to the convergence bound by numerical simulations. As a comparison, the PBoC of input magnitude when model (2.35) is subject to a single-tone input, setting  $\beta$  to 0 in (2.62), is also presented in Fig. 2.19. It can be seen that even though  $\beta$  is very small, for example,

0.2 in this case, the PBoC with a multi-tone input is obviously smaller than the PBoC with a single-tone input because of the inter-modulation between the two input frequencies [39, 73]. When the model (2.35) is subject to a multi-tone input, the results in [110, 119, 120, 138, 139] are not applicable, and the convergence bound according to [121] is  $5.3895 \times 10^{-6}$ , which is more conservative compared with the PBoC via Proposition 2.5 at the resonant frequency (0.0032 in this case).

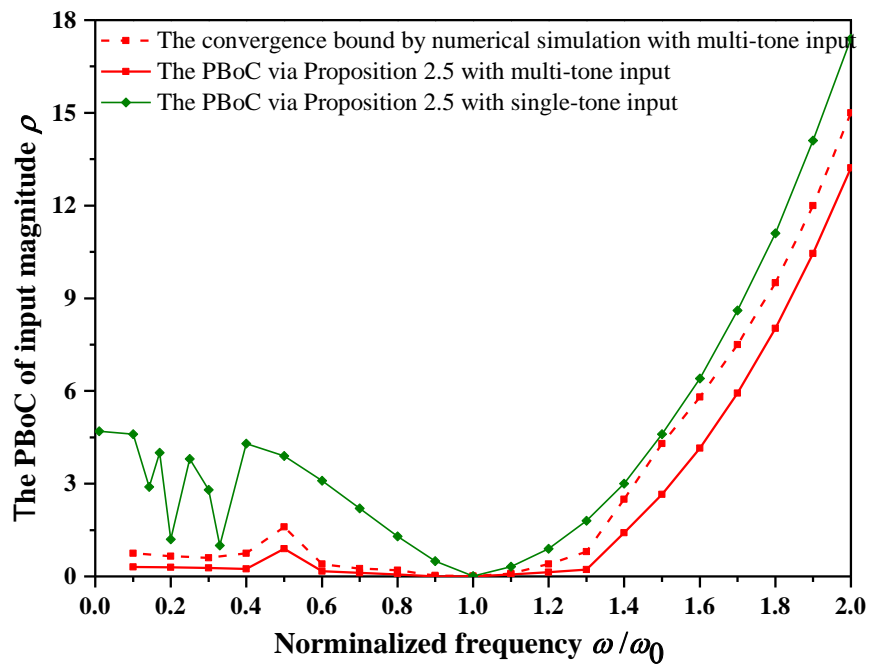


Figure 2.19 The PBoC of the input magnitude

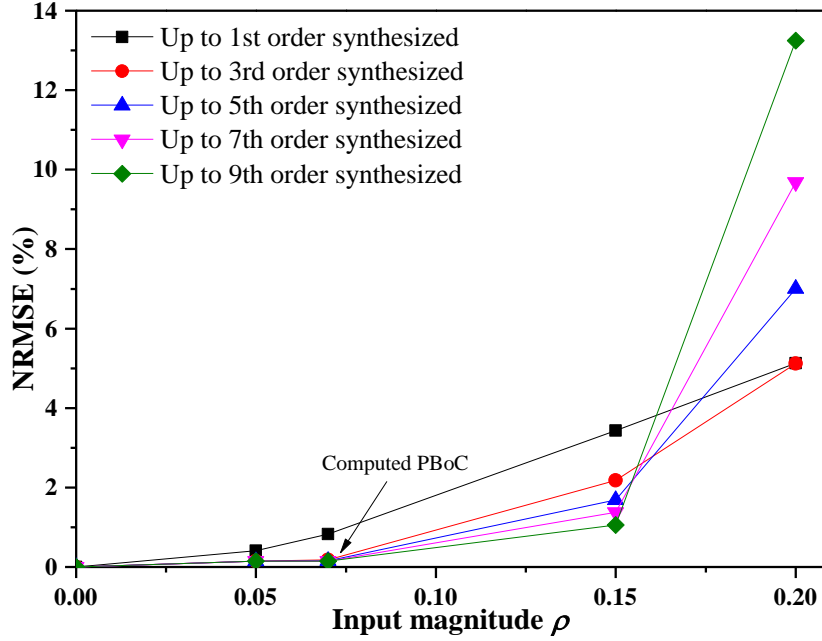


Figure 2.20 The normalized root mean square error

The normalized root mean square error is again given to validate the effectiveness of the bound result above. The  $NRMSE$  taken at  $\omega_1=1.1\omega_0$  as an example is presented in Fig. 2.20. It can be seen that when the input magnitude is smaller than the computed PBoC, the  $NRMSE$  dramatically decreases to 0 as the synthesized order increases, but the synthesized output  $y_{synthesized}(k)$  becomes divergent with an observed increasing  $NRMSE$  when the input magnitude is larger than the computed PBoC.

### 2.3.3.2 The convergence bound of model parameters

The computation of the PBoC of model parameter  $c_{3,0}(1,1,1)$  is given as

$$C(3,0) = \frac{4\underline{L}_{R_\omega}^2}{27(1+\beta)^2 \rho^2 \bar{H}_1^2}. \quad (2.65)$$

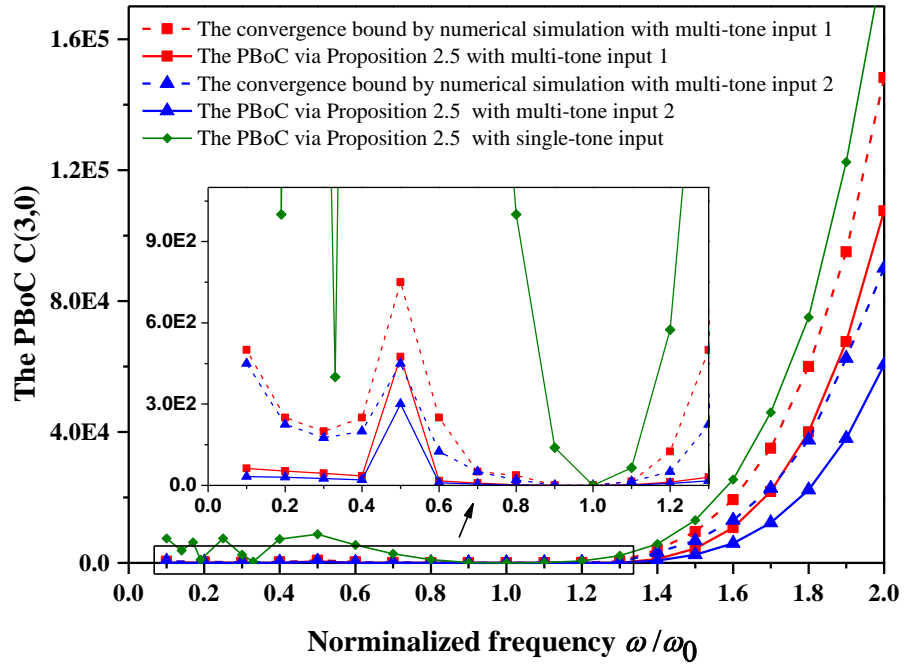


Figure 2.21 The PBoC of the model parameter  $c_{3,0}(111)$

For the computation of the PBoC, the method in [121] is not applicable. Considering the input magnitude as  $\rho=0.5$ , the computed PBoC is presented in Fig. 2.21. In Fig. 2.21, the multi-tone input 1, multi-tone input 2, and single-tone input correspond to the input in (2.62) with  $\beta=0.1$ ,  $\beta=0.3$ , and  $\beta=0$ , respectively. The PBoC of the model parameter with the multi-tone input is also smaller than that with a single-tone input. When  $\beta$  varies from 0.1 to 0.3, the nonlinearity degree of model (2.35) increases, which leads to a smaller PBoC of the parameter (see Fig. 2.21).

## 2.4 Parametric convergence bound for single-input multiple-output (SIMO) system

Consider a SIMO NARX model with  $M$  subsystems as [65]

$$y_{j_k}(k) = \sum_{p+q=1}^{N_l} \sum_{p=0}^{p+q} \sum_{j_1=1}^M \sum_{j_2=j_1}^M \cdots \sum_{j_p=j_{p-1}}^M \sum_{k_1, \dots, k_{p+q}=0}^K \left( c_{p,q}^{j_p j_{p-1} \cdots j_1}(k_1, \dots, k_{p+q}; j_k) \prod_{i=1}^p y_{j_i}(k-k_i) \prod_{i=p+1}^{p+q} u(k-k_i) \right) \quad (2.66)$$

where  $y_{j_k}(k)$  is the  $j_k$ th output,  $j_k=1,2,\dots,M$ .  $M$  is the number of subsystems, and  $N_l$  is the maximum nonlinear order in terms of output  $y(k)$  and input  $u(k)$ .  $c_{p,q}^{j_p j_{p-1} \cdots j_1}(k_1, \dots, k_{p+q}; j_k)$  is the model parameter of the corresponding term  $\prod_{i=1}^p y_{j_i}(k-k_i) \prod_{i=p+1}^{p+q} u(k-k_i)$  in the  $j_k$ th subsystem, which has a nonlinearity degree  $p+q$  ( $p$  order in terms of the output and  $q$  order in terms of the input), and  $k_i$  is the difference order with the maximum order  $K$ . The superscript  $j_i, i=1,2,\dots,p$  in the model parameter  $c_{p,q}^{j_p j_{p-1} \cdots j_1}(k_1, \dots, k_{p+q}; j_k)$  means that the  $j_i$ th output,  $y_{j_i}(k)$ , is in the corresponding term  $\prod_{i=1}^p y_{j_i}(k-k_i) \prod_{i=p+1}^{p+q} u(k-k_i)$ . Denote  $m=p+q$ , which is, clearly from the above, the nonlinear degree in NARX model (2.66). An example for a single-input four-output NARX model can be seen in Section 3.3.

The  $j_k$ th output of the SIMO NARX model in (2.66) can be approximated by the Volterra series (truncated up to the order  $N$ ) as,

$$y_{j_k}(k) = \sum_{n=1}^N \int_{-\infty}^{\infty} \cdots \int_{-\infty}^{\infty} h_n^{(j_k)}(\tau_1, \dots, \tau_n) \prod_{i=1}^n u(t-\tau_i) d\tau_i \quad (2.67)$$

where  $h_n^{(j_k)}(\tau_1, \dots, \tau_n)$  is the  $n$ th-order Volterra kernel of the  $j_k$ th subsystem.

### 2.4.1 The $n$ th-order GFRF and nonlinear output spectrum

The  $n$ th-order generalized frequency response function (GFRF) can be recursively calculated [65] as,

$$H_n = \begin{bmatrix} H_n^{(1)}(j\omega_1, \dots, j\omega_n) \\ H_n^{(2)}(j\omega_1, \dots, j\omega_n) \\ \vdots \\ H_n^{(M)}(j\omega_1, \dots, j\omega_n) \end{bmatrix} = \begin{bmatrix} l_{1,1} & l_{1,2} & \dots & l_{1,M} \\ l_{2,1} & l_{2,2} & \dots & l_{2,M} \\ \vdots & \vdots & \ddots & \vdots \\ l_{M,1} & l_{M,2} & \dots & l_{M,M} \end{bmatrix}^{-1} \begin{bmatrix} A_{1,n} \\ A_{2,n} \\ \vdots \\ A_{M,n} \end{bmatrix} \quad (2.68)$$

$$= L_n^{-1}(j\omega_1, \dots, j\omega_n) A_n$$

where  $H_n^{(j_k)}(j\omega_1, \dots, j\omega_n)$  is the  $n$ th-order GFRF of the  $j_k$ th subsystem,  $A_{i,n}$  represents the  $i$ th element of  $A_n$ .  $\omega_i$ ,  $i=1, \dots, n$  is the frequency variable in the  $n$ th-order GFRF,

$$l_{j_k, j_i} = \begin{cases} -\sum_{k_1=1}^K c_{1,0}^{j_i}(k_1; j_k) e^{-k_1(j\omega_1 + \dots + j\omega_n)} & j_i \neq j_k, \\ 1 - \sum_{k_1=1}^K c_{1,0}^{j_i}(k_1; j_k) e^{-k_1(j\omega_1 + \dots + j\omega_n)} & j_i = j_k. \end{cases} \quad (2.69)$$

Equation (2.69) involves only the linear model parameters, e.g.,  $c_{1,0}(\cdot)$ .  $A_{j_k, n}$  in

(2.68) is given by,

$$A_{j_k, n} = \sum_{m=2}^n \sum_{p=1}^m \sum_{j_1=1}^M \sum_{j_2=j_1}^M \dots \sum_{j_p=j_{p-1}}^M \sum_{k_1, \dots, k_{p+q}=0}^K \left[ \sum_{k_1, \dots, k_n=0}^K c_{0,n}(k_1, \dots, k_n; j_k) \right. \\ \times e^{-j(k_1\omega_1 + \dots + k_n\omega_n)} + \sum_{k_1, \dots, k_{p+q}=0}^K c_{p,q}^{j_p j_{p-1} \dots j_1}(k_1, \dots, k_{p+q}; j_k) \\ \left. \times e^{-j(k_{p+1}\omega_{n-q+1} + \dots + k_{p+q}\omega_n)} H_{n-q,p}^{(j_p j_{p-1} \dots j_1)}(j\omega_1, \dots, j\omega_{n-q}) \right] \quad (2.70)$$

where  $m=p+q$ , and

$$H_{n-q,p}^{(j_p j_{p-1} \dots j_1)}(j\omega_1, \dots, j\omega_n) = \sum_{r_1, \dots, r_p=1; r_1 + \dots + r_p = n-q}^{n-p+1} \prod_{i=1}^p \left[ H_{r_i}^{(j_i)}(j\omega_{X_i+1}, \dots, j\omega_{X_i+r_i}) e^{-jk_i(\omega_{X_i+1} + \dots + \omega_{X_i+n})} \right] \quad (2.71)$$

$\sum_{r_1, \dots, r_p=1; r_1+\dots+r_p=n-q}^{n-p+1}$  is the summation of all different combination of  $(\gamma_1, \gamma_2, \dots, \gamma_p)$

which satisfy ,  $1 \leq \gamma_1, \gamma_2, \dots, \gamma_p \leq n-p+1$  and  $\gamma_1 + \gamma_2 + \dots + \gamma_p = n-q$ .

$$H_{n,1}^{(j_k)}(j\omega_1, \dots, j\omega_n) = H_n^{(j_k)}(j\omega_1, \dots, j\omega_n) e^{-k_1(j\omega_1 + \dots + j\omega_n)} \quad (2.72)$$

$$e^{-j(k_{p+1}\omega_{n-q+1} + \dots + k_{p+q}\omega_n)} = \begin{cases} 1 & q=0, p>1 \\ 0 & q=0, p \leq 1 \end{cases} \quad (2.73)$$

In (2.71),  $X_i = \gamma_1 + \gamma_2 + \dots + \gamma_{i-1}$ , and  $\gamma_1 + \gamma_2 + \dots + \gamma_p = n-q$  for all  $p \geq 2$  and positive integer  $\gamma_i$ .

It is clear that higher-order GFRFs can be recursively calculated from the lower-order GFRFs, and the recursion terminates at the first-order GFRF, i.e.,

$H_1^{(j_k)}(j\omega_1)$ . To compute the first-order GFRF via (2.68), (2.70) is then defined by

$$A_{j_k,1} = \sum_{k_1=0}^K c_{0,1}(k_1; j_k) e^{-j\omega_1 k_1}. \quad (2.74)$$

When the SIMO NARX model is subject to the harmonic input (2.9), the nonlinear output spectrum of the  $j_k$ th subsystem (truncated at the order  $N$ ) can be obtained as [70, 73, 79, 117]

$$Y_{j_k}(j\Omega) = \sum_{n=1}^N \left[ \frac{1}{2^n} \sum_{\omega_1 + \dots + \omega_n = \Omega} \left( H_n^{(j_k)}(j\omega_1, \dots, j\omega_n) \prod_{i=1}^n A(\omega_i) \right) \right] \quad (2.75)$$

where  $|A|$  is the magnitude of the input  $u(k)$ , which is denoted by  $U$  latter,  $\Omega$  is the output frequency,  $\omega$  is the input frequency,  $\omega_i \in \{\omega, -\omega\}$ .

## 2.4.2 Notations and Definitions

$\|\cdot\|$  is denoted for matrix  $A$  as  $\|A\| = \sup_{\|x\|=1} \|Ax\|$ . Denote the upper bound of  $L_n^{-1}(j\omega_1, \dots, j\omega_n)$ , which is defined in (2.68), over the whole output frequency range  $W_\infty$  as

$$\bar{L}^{-1}(\omega) = \sup_{\Omega \in W_\infty} \left\{ \left\| L_n^{-1}(j\omega_1, \dots, j\omega_n) \right\| \right\} \quad (2.76)$$

where  $W_\infty = \bigcup_{n=1}^{\infty} W_n = \bigcup_{n=1}^{\infty} \{ \Omega \mid \Omega = \omega_1 + \dots + \omega_n, \omega_i \in \{ \omega, -\omega \} \}$  represents the output frequency range when the NARX model (2.66) is excited by (2.9), and  $W_n$  is the output frequency range of the  $n$ th-order output (see more discussion in [73]).

Define

$$C_{(p,q;j_k)}^{j_p j_{p-1} \dots j_1} = \sum_{k_1, \dots, k_{p+q}=0}^K \left\| c_{p,q}^{j_p j_{p-1} \dots j_1}(k_1, \dots, k_{p+q}; j_k) \right\| \quad (2.77)$$

Obviously,  $C_{(p,q;j_k)}^{j_p j_{p-1} \dots j_1}$  is a nonnegative function of the model parameters

$$c_{p,q}^{j_p j_{p-1} \dots j_1}(\bullet; j_k).$$

### 2.4.3 Boundedness of the GFRF and nonlinear output spectrum

**Lemma 2.4:** The upper bound of the nonlinear output spectrum of the  $j_k$ th subsystem at  $\Omega=k\omega$  is given by

$$\begin{aligned} \bar{Y}_{\Omega=k\omega}^{(j_k)}(U) &= \sum_{n=1}^{\infty} \left( C_{k+2(n-1)}^{n-1} / 2^{k+2(n-1)-1} \right. \\ &\quad \left. \times \bar{H}_{k+2(n-1)}^{(j_k)}(j\omega_1, \dots, j\omega_{k+2(n-1)}) U^{k+2(n-1)} \right) \quad k \in \mathbb{N}^+ \end{aligned} \quad (2.78)$$

$$\bar{Y}_{\Omega=k\omega}^{(j_k)}(U) = \sum_{n=1}^{\infty} \left( \frac{C_{2n}^n}{2^{2n}} \bar{H}_{2n}^{(j_k)}(j\omega_1, \dots, j\omega_{2n}) U^{2n} \right), \quad k = 0. \quad (2.79)$$

where  $\bar{H}_n^{(j_k)}(j\omega_1, \dots, j\omega_n)$  is the upper bound of the  $n$ th-order GFRF, which satisfies the following equation

$$\begin{aligned} \sum_{j_k=1}^M \bar{H}_n^{(j_k)}(j\omega_1, \dots, j\omega_n) &= \bar{L}(\omega) \sum_{j_k=1}^M \left[ C_{(0,n;j_k)} + \sum_{m=2}^n \sum_{p=1}^m \sum_{j_1=1}^M \sum_{j_2=j_1}^M \dots \sum_{j_p=j_{p-1}}^M \right. \\ &\quad \left. \left( C_{(p,q;j_k)}^{j_p j_{p-1} \dots j_1} \sum_{r_1, \dots, r_p=1, \sum r_i=n-q}^{n-m+1} \prod_{i=1}^p \bar{H}_{r_i}^{(j_i)}(j\omega_{X+1}, \dots, j\omega_{X+r_i}) \right) \right], n > 1 \end{aligned} \quad (2.80)$$

and

$$\bar{H}_1^{(j_k)}(j\omega_1) = \left\| H_1^{(j_k)}(j\omega_1) \right\|, \quad n = 1. \quad (2.81)$$

**Proof:** See Appendix 2.6.

**Lemma 2.5:** The upper bound of the nonlinear output spectrum of the  $j_k$ th subsystem involving all of the frequencies in the output frequency range  $W_\infty$  is given as

$$\begin{aligned} \bar{Y}_\omega^{(j_k)}(U) &= \sum_{k=0}^{\infty} \bar{Y}_{\Omega=k\omega}^{(j_k)}(U) = \sum_{\Omega \in W_\infty} \bar{Y}_\Omega^{(j_k)}(U) \\ &= \sum_{n=1}^{\infty} \left\| \sum_{\Omega \in W_n} \bar{Y}_n^{(j_k)}(j\bar{\omega}) \right\| = \sum_{n=1}^{+\infty} \bar{H}_n^{(j_k)}(j\omega_1, \dots, j\omega_n) U^n \end{aligned} \quad (2.82)$$

**Proof:** Following Lemma 2.2 .

**Lemma 2.6:** When  $\bar{L}(\omega) < \infty$  holds, and the upper bound of the nonlinear output spectrum of any subsystem is divergent, the upper bounds of the nonlinear output spectrum of all of the other subsystems also diverge.

**Proof:** See Appendix 2.7.

**Remark 2.12:** The bound results above can be seen as an extension of the results for SISO case in section 2. The upper bound of the nonlinear output spectrum of the  $j_k$ th subsystem in (2.82) is expressed as the summation of an infinite power series, which can also be seen as the summation of the power series (with nonnegative coefficients) in (2.78) and (2.79). If the upper bound of the nonlinear output spectrum in (2.82) converges, the upper bound of the nonlinear output spectrum at any frequency for any subsystem converges. Obviously, this indicates a convergent Volterra series expansion.

**Lemma 2.7:** The upper bounds of the nonlinear output spectrum of all of the  $M$  subsystems satisfy

$$\begin{aligned} & \bar{L}(\omega) \sum_{j_k=1}^M \sum_{m=2}^{+\infty} \sum_{p=1}^m \sum_{j_1=1}^M \sum_{j_2=j_1}^M \cdots \sum_{j_p=j_{p-1}}^M \left( U^q C_{(p,q;j_k)}^{j_p j_{p-1} \cdots j_1} \prod_{i=1}^p \bar{Y}_\omega^{(j_i)}(U) \right) \\ & - \sum_{j_k=1}^M \bar{Y}_\omega^{(j_k)}(U) + \bar{L}(\omega) \sum_{j_k=1}^M \sum_{m=2}^{+\infty} \left( C_{(0,m;j_k)} U^m \right) + \sum_{j_k=1}^M \left( \bar{H}_1^{(j_k)}(j\omega_1) U \right) = 0. \end{aligned} \quad (2.83)$$

**Proof:** See Appendix 2.8.

#### 2.4.4 Parametric bound of convergence (PBoC)

The parametric bound of convergence (PBoC) is defined as the upper bound of a characteristic parameter in which a given nonlinear system has a convergent Volterra series expansion.

**Proposition 2.6:** The PBoC can be obtained by solving (2.20), with

$$a_{1,p} = \bar{L}(\omega) \sum_{j_k=1}^M \sum_{q=0}^{+\infty} \sum_{j_1=1}^M \sum_{j_2=j_1}^M \cdots \sum_{j_p=j_{p-1}}^M \left[ U^q C_{(p,q;j_k)}^{j_p j_{p-1} \cdots j_1} \left( \prod_{i=1}^p \frac{\bar{H}_1^{(j_i)}(\omega)}{\bar{H}_1^{(j)}(\omega)} \right) \right], 2 \leq p \leq M_p \quad (2.84)$$

$$a_{1,1} = \bar{L}(\omega) \sum_{j_k=1}^M \sum_{q=1}^{+\infty} \sum_{j_1=1}^M \left( U^q C_{(1,q;j_k)}^{j_1} \frac{\bar{H}_1^{(j_1)}(\omega)}{\bar{H}_1^{(j)}(\omega)} \right) - \sum_{j_k=1}^M \frac{\bar{H}_1^{(j_k)}(\omega)}{\bar{H}_1^{(j)}(\omega)}, p=1, p+q \geq 2 \quad (2.85)$$

$$a_{1,0} = \sum_{j_k=1}^M \left( \bar{H}_1^{(j_k)}(j\omega_1) U \right) + \bar{L}(\omega) \sum_{j_k=1}^M \sum_{m=2}^{+\infty} \left( C_{(0,m;j_k)} U^m \right), \quad (2.86)$$

$$a_{2,p-1} = \bar{L}(\omega) \sum_{j_k=1}^M \sum_{q=0}^{+\infty} \sum_{j_1=1}^M \sum_{j_2=j_1}^M \cdots \sum_{j_p=j_{p-1}}^M \left[ U^q C_{(p,q;j_k)}^{j_p j_{p-1} \cdots j_1} p \left( \prod_{i=1}^p \frac{\bar{H}_1^{(j_i)}(\omega)}{\bar{H}_1^{(j)}(\omega)} \right) \right], 2 \leq p \leq M_p \quad (2.87)$$

$$a_{2,0} = \bar{L}(\omega) \sum_{j_k=1}^M \sum_{q=1}^{+\infty} \sum_{j_1=1}^M \left( U^q C_{(1,q;j_k)}^{j_1} \frac{\bar{H}_1^{(j_1)}(\omega)}{\bar{H}_1^{(j)}(\omega)} \right) - \sum_{j_k=1}^M \frac{\bar{H}_1^{(j_k)}(\omega)}{\bar{H}_1^{(j)}(\omega)}, p=1, p+q \geq 2. \quad (2.88)$$

where  $j \in \{1, \dots, M\}$  which means that  $\bar{H}_1^{(j)}(\omega)$  can be any one of  $\{\bar{H}_1^{(1)}(\omega), \dots, \bar{H}_1^{(M)}(\omega)\}$ .

**Proof:** See Appendix 2.9.

Note that the PBoC in Proposition 2.6 can be computed via any subsystem of the SIMO model, and the PBoCs by different subsystems will be the same with each other, which is consistent with the result in Lemma 2.6, that is, if one of the subsystem is not Volterra-type, then all of the other subsystems are also not Volterra-type.

**Remark 2.13:** If (2.20) has only one positive root, this positive root is the computed PBoC. If there exists more than one positive roots, then the smallest one is the computed PBoC. Otherwise, if there does not exist any positive root, the computed PBoC is 0, which means that the nonlinear model under study is already out of the convergence bound, and the system is not Volterra-type. Although the PBoC estimated here is derived for harmonic input signal, it can act as a useful reference or guidance for parameter optimization and design in practice for any input signals.

**Remark 2.14:** The bound result in (2.83) is an explicit expression of the output bound of all of the  $M$  subsystems, which is for the first time developed for a multi-output system and cannot be simply extended from the result in for SISO case. The result in Proposition 2.6 holds for any  $j$  from 1 to  $M$ , which is in compliance with Lemma 2.6. With Lemma 2.6 and the approximation (I-1) in Appendix 2.9, the bound result of the nonlinear output spectrum in (2.83) for a single-input multiple-output (SIMO) model can then be cast into the SISO case as shown in (I-2) in Appendix 2.9.

The procedures for calculating the PBoC is summarized as:

**Algorithm 2.4 Computation of PBoC:**

**Step 1.** Calculate  $\bar{L}^{-1}(\omega)$  according to (2.69) and (2.76); Calculate  $C_{(p,q;j)}^{j_p j_{p-1} \dots j_1}$  according to (2.77).

**Step 2.** Calculate  $\bar{H}_1^{(j_k)}$  according to (2.68)-(2.70), (2.74), and (2.81).

**Step 3.** Solving (2.20), the PBoC can then be obtained.

## 2.5 Conclusion

In this chapter, the parametric bound of convergence (PBoC) is studied for the single-input single-output (SISO) nonlinear systems, the single-input multiple-output (SIMO) nonlinear systems, and also the nonlinear systems with a general input. The developed algorithms for calculating the PBoC not only determine the convergence bound of input magnitude (the results existed in the literatures) but also determine the convergence bound of model parameters of interest. These results can provide a straightforward and useful guidance for the analysis and design of nonlinear systems with the nCOS method, which will be illustrated in the following chapter.

# **3 The nCOS method based analysis and design of nonlinear parameters, considering the parametric convergence bound (PBoC)**

## **3.1 Introduction**

Nonlinearities are complex phenomena in practice for analysis and design. If a nonlinear system has multiple steady states, the dynamic response could be very complicated, and even a simple harmonic excitation could lead to complex bifurcation or chaos. This could greatly complicate nonlinear analysis and design.

In vibration control problems, system nonlinearity usually comes from two sources: inherent nonlinearity such as in a vehicle suspension [140-142] or robotic manipulators [143-145] and externally introduced nonlinearity for performance improvement, which can be observed in nonlinear stiffness and damping design [23, 73, 79, 92], energy harvesting systems [146], hard disk drivers [147], elastic drives [148], and power invertors [149].

As discuss in Chapter 1, there are several methods for the analysis and design of nonlinear systems, for example, the harmonic balance method and perturbation method [39]. Difficulties such as analysis complexity and computation burden can often be observed, especially when these methods are applied to a multi-degree-of-freedom (MDoF) system or a multiple input multiple output (MIMO) system. Compared with the harmonic balance or the perturbation method,

the Volterra series associated frequency domain method has an obvious advantage, i.e., the output spectrum of the system can be expressed as a polynomial function with respect to the nonlinear model parameters of interest [92, 95, 113, 115], which is referred to as the nonlinear characteristic output spectrum (nCOS) function in [92].

The nCOS function can be any system output function or multiple-object performance function to be optimized, it is therefore obvious that the nCOS function based method can provide a straightforward insight into the analysis and design of nonlinear systems and also greatly facilitate the applications in practice, especially for MDoF or MIMO systems.

In this chapter, two applications of the nCOS method to the analysis and design of nonlinear parameters are presented:

1. In section 3.2, a nonlinear damper is proposed to overcome the dilemma associated with linear viscous damping. The system performance (force transmissibility and displacement transmissibility) is analytically derived in the form of the nCOS function with respect to the nonlinear damping coefficient. The transmissibility performance can then be easily studied, and the superior performance of the proposed nonlinear damping relative to that of linear viscous damping can be well demonstrated.
2. In section 3.3, a nonlinear optimization problem is studied. The multiple-object performance function is constructed and mapped onto an nCOS function with respect to nonlinear parameters of interest. The

optimization can then be straightforwardly conducted within the determined parametric convergence region, i.e., the PBoC proposed in Chapter 2.

In these two cases, the nCOS method works only when the system input-output relationship allows a convergent Volterra series expansion, which can be guaranteed via the PBoC or PCM proposed in Chapter 2. These two cases show that:

1. The results in Chapter 2 can provide a useful guidance for Volterra series associated methods such as the nCOS method.
2. The nCOS method can provide a straightforward and effective way for the analysis and design of nonlinear parameters or nonlinear components.

### 3.2 nCOS method based analysis of nonlinear damping

There is a well-known dilemma associated with linear viscous damping systems, i.e., a larger damping coefficient leads to performance improvement at/around the resonant frequency  $\omega_0$  but deteriorates the performance at frequency  $\Omega > \sqrt{2}\omega_0$  [150, 151]. To overcome this dilemma, isolators with nonlinear stiffness and/or nonlinear damping have been widely studied to explore the potential nonlinear benefits in vibration control [24, 95, 152-156].

In [153], vibration isolators with nonlinear stiffness and nonlinear damping have been investigated. The transmissibility was derived using the harmonic balance method. Jump phenomena can be observed because of the nonlinear stiffness. Nonlinear damping defined as a pure function of velocity is studied under force excitation [24, 85, 86] via the Volterra series associated method [94, 95, 113]. The cubic-order nonlinear damping can produce an ideal vibration isolation, i.e., the force transmissibility is suppressed only in/around the resonant frequency but remains almost unaffected in the non-resonant frequency region. Milovanovic [157] studied vibration isolators with cubic-order nonlinear stiffness and damping under base excitation. The absolute displacement transmissibility of the isolator with cubic-order nonlinear damping approaches 1 as  $\Omega \rightarrow \infty$ , which corresponds to a rigidly connected system.

In this section, a cubic-order nonlinear damping (i.e.,  $(\dot{\cdot})^2 \frac{d(\cdot)}{dt}$ ) is investigated. The performance (force and absolute displacement transmissibility) is derived to be an explicit and analytical polynomial function with respect to the nonlinear

damping coefficient (defined as nonlinear parameter of interest). With these transmissibilities developed in the form of the nCOS function, it is then straightforwardly and analytically shown that the nonlinear damping  $(\cdot)^2 \frac{d(\cdot)}{dt}$  can produce much better vibration isolation performance under both force excitation and base excitation.

### 3.2.1 Nonlinear isolators and transmissibility functions

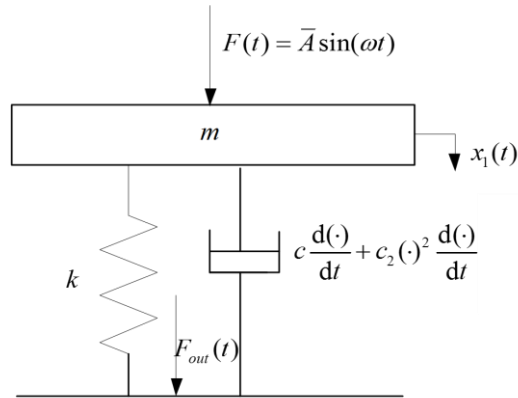


Figure 3.1 Isolator subjected to force excitation

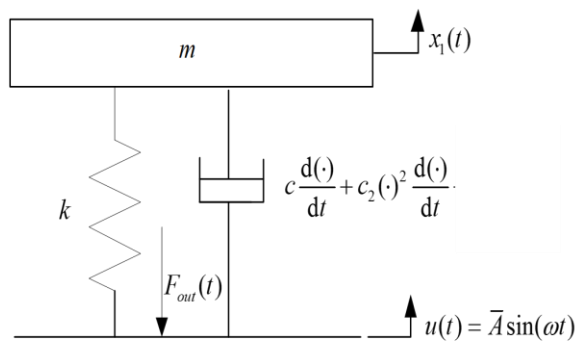


Figure 3.2 Isolator subjected to base excitation

The nonlinear damping force is denoted as:

$$F_{nd} = c \frac{d(\cdot)}{dt} + c_2 (\cdot)^2 \frac{d(\cdot)}{dt} \quad (3.1)$$

where  $c$  is the linear damping coefficient and  $c_2$  is the cubic order nonlinear

damping parameter.

### 3.2.1.1 The isolator subjected to force excitation and the force transmissibility

From Fig. 3.1, the governing equation of an isolator under force excitation can be given as

$$m\ddot{x}_1 = -kx_1 - c\dot{x}_1 - c_2x_1^2\dot{x}_1 + \bar{A}\sin(\omega t) \quad (3.2)$$

The force ratio  $T_{fr}(t)$  is then defined as

$$T_{fr}(t) = \frac{F_{out}}{A} = \frac{kx_1}{A} + \frac{c\dot{x}_1}{A} + \frac{c_2x_1^2\dot{x}_1}{A} \quad (3.3)$$

These two equations can be non-dimensionalized as

$$\begin{cases} \ddot{y}_1 + y_1 + \xi_1\dot{y}_1 + \beta_2y_1^2\dot{y}_1 = \sin(\Omega\tau) \\ y_2 = y_1 + \xi_1\dot{y}_1 + \beta_2y_1^2\dot{y}_1 \end{cases} \quad (3.4)$$

with

$$\begin{aligned} \omega_0 t = \tau, \omega_0 = \sqrt{k/m}, \Omega = \omega/\omega_0, z_1(\tau) = x_1(t) = x_1\left(\frac{\tau}{\omega_0}\right), \\ \dot{x}_1(t) = \omega_0 \dot{z}_1(\tau), \ddot{x}_1(t) = \omega_0^2 \ddot{z}_1(\tau), y_1(\tau) = \frac{kz_1(\tau)}{A}, \\ y_2(\tau) = T_f(\tau), \xi_1 = \frac{c}{\sqrt{km}}, \beta_2 = \frac{c_2\bar{A}^2}{\sqrt{k^5m}} \end{aligned}$$

### 3.2.1.2 The isolator subjected to base excitation, and the force and displacement transmissibility

The governing equation of an isolator in Fig. 3.2 under base excitation can be written as:

$$m\ddot{x}_1 = k(u - x_1) + c(\dot{u} - \dot{x}_1) + c_2(u - x_1)^2(\dot{u} - \dot{x}_1) \quad (3.5)$$

where  $u = \bar{A}\sin(\omega t)$ . The force ratio  $T_{fr}(t)$  is denoted by:

$$T_{fr}(t) = \frac{-F_{out}}{kA} = \frac{-1}{A}(u - x_1) - \frac{c}{kA}(\dot{u} - \dot{x}_1) - \frac{c_2}{kA}(u - x_1)^2(\dot{u} - \dot{x}_1) \quad (3.6)$$

Denote the relative displacement  $x$  of the isolator as:

$$x = x_1 - u \quad (3.7)$$

The following non-dimensional equations can be obtained:

$$\begin{cases} \ddot{y}_1 + y_1 + \xi_1 \dot{y}_1 + \beta_2 y_1^2 \dot{y}_1 = \Omega^2 \sin(\Omega \tau) \\ y_2 = y_1 + \xi_1 \dot{y}_1 + \beta_2 y_1^2 \dot{y}_1 \end{cases} \quad (3.8)$$

with

$$\begin{aligned} \omega_0 t = \tau, \omega_0 = \sqrt{k/m}, \Omega = \omega/\omega_0, z(\tau) = x(t) = x\left(\tau/\omega_0\right), \\ \dot{x}(t) = \omega_0 \dot{z}(\tau), \ddot{x}(t) = \omega_0^2 \ddot{z}(\tau), y_1(\tau) = z(\tau)/A, \\ y_2(\tau) = T_f(\tau), \xi_1 = c/\sqrt{km}, \beta_2 = c_2 \bar{A}^2 / \sqrt{km} \end{aligned}$$

From (3.4) and (3.8), it can be observed that the base excitation can be equivalent to a force excitation when the magnitude of the disturbing force is proportional to the square of the exciting frequency  $\Omega^2$ .

In the following, the absolute displacement transmissibility is derived. The displacement ratio is defined by:

$$T_{dr}(t) = \frac{x_1}{A} = \frac{x+u}{A} \quad (3.9)$$

which is non-dimensionalized as:

$$y_3 = y_1 + \sin(\Omega \tau) \quad (3.10)$$

where  $y_1$  is defined in (3.8).

In the next section, an explicit and analytical relationship between the force or displacement transmissibility and the nonlinear damping coefficient  $\beta_2$  will be developed in the frequency domain using the nCOS method.

### 3.2.2 The force and displacement transmissibility in the frequency domain

The concept of the nonlinear characteristic output spectrum (nCOS) was recently proposed [5, 12-13]. The advantage of this concept is that the output spectrum can be given as an explicit and analytical polynomial function with respect to the nonlinear parameters of interest. The analytical relationships between the transmissibilities, i.e., the force transmissibility  $T_f(\Omega)$  and displacement transmissibility  $T_d(\Omega)$ , and the nonlinear damping coefficients  $\beta_2$  are developed in this section, which can provide a straightforward understanding of the proposed nonlinear damping.

#### 3.2.2.1 Force transmissibility $T_f(\Omega)$

From system (3.4) and system (3.8), it can be observed that the force ratio under base displacement excitation has the same form as that under force excitation. The only difference is that the input magnitude is 1 for force excitation but  $\Omega^2$  for base excitation. These two transmissibilities will be developed in the frequency domain in this section.

According to [65, 85, 114], system (3.4) and system (3.8) can be regarded as a single-input-double-output system, with the output spectrum obtained as

$$Y_J(j\omega) = \sum_{n=1}^N \frac{1}{2^{n-1}} \sum_{\omega_1 + \dots + \omega_n = \omega} H_n^J(j\omega_1, \dots, j\omega_n) U(\omega_1) \cdots U(\omega_n) \quad J = 1, 2 \quad (3.11)$$

where  $H_n^J(j\omega_1, \dots, j\omega_n)$  is the  $n$ th-order generalized frequency response function

(GFRF),  $N$  is the truncation order, and  $U(\omega_i)$  is the input spectrum. For system

(3.4),

$$U(\omega_i) = \begin{cases} -j & \text{when } \omega_i = \Omega, i = 1, \dots, n \\ 0 & \text{otherwise} \\ j & \text{when } \omega_i = -\Omega, i = 1, \dots, n \end{cases} \quad (3.12)$$

For system (3.8),

$$U(\omega_i) = \begin{cases} -j\Omega^2 & \text{when } \omega_i = \Omega, i = 1, L, n \\ 0 & \text{otherwise} \\ j\Omega^2 & \text{when } \omega_i = -\Omega, i = 1, L, n \end{cases} \quad (3.13)$$

(3.11) involves the computation of the  $n$ th-order GFRFs  $H_n^J(j\omega_1, \dots, j\omega_n)$ , which can be referred to Appendix 3.1. With the results in Appendix 3.1, the output spectrum  $Y_2(j\omega)$  in system (3.4) and system (3.8) can be written as

$$Y_2(j\omega) = P_0(j\omega) + \sum_{n=1}^{\lfloor N/2 \rfloor} P_n(j\omega) \beta_2^n \quad (3.14)$$

where

$$P_0(j\omega) = H_1^2(j\omega)U(j\omega) \quad (3.15)$$

$$P_n(j\omega) = \frac{1}{2^{2n}} \frac{-(j\omega)^2}{L(j\omega)} \sum_{\omega_1 + \dots + \omega_{2n+1} = \omega} \prod_{i=1}^{2n+1} H_1^1(j\omega_i) U(\omega_i) \sum_{z=1}^{N_{\bar{n}}} \frac{\prod_{k=1}^n \left[ j\omega_{l_k(1)}^z + \dots + j\omega_{l_k(j_k^n)}^z \right]}{\prod_{i=1}^{n-1} L \left[ j\omega_{l_i(1)}^z + \dots + j\omega_{l_i(j_i^n)}^z \right]} \quad (3.16)$$

The definition of  $L(j\omega)$  is also given in Appendix 3.1. (3.14) presents an analytical relationship between the output spectrum and the nonlinear parameters  $\beta_2$ . The force transmissibility can then be given by

$$T_f(\Omega) = |Y_2(j\Omega)| = \left| P_0(j\Omega) + \sum_{n=1}^{\lfloor N/2 \rfloor} P_n(j\Omega) \beta_2^n \right| \quad (3.17)$$

It can be observed that (3.14) and (3.17) are explicit polynomial functions of the

input and first-order GFRE. Substituting (3.12) into (3.15) and (3.16), for system (3.4) (nonlinear isolator subjected to force excitation), it can be obtained that

$$P_0(j\Omega) = \frac{j(1 + j\xi_1\Omega)}{L(j\Omega)} \quad (3.18)$$

$$P_n(j\Omega) = \frac{1}{2^{2n}} \frac{j\Omega^2}{|L(j\Omega)|^{2n} [L(j\Omega)]^2} \sum_{\omega_1 + \dots + \omega_{2n+1} = \Omega} \sum_{z=1}^{N_{\bar{n}}} \frac{\prod_{k=1}^n [j\omega_{l_k(z)}^{z_{l_k(1)}} + \dots + j\omega_{l_k(z)}^{z_{l_k(n)}}]}{\prod_{i=1}^{n-1} L[j\omega_{l_i(z)}^{z_{l_i(1)}} + \dots + j\omega_{l_i(z)}^{z_{l_i(n)}}]} \quad (3.19)$$

where  $\omega_i \in \{-\Omega, \Omega\}$ ,  $i = 1, \dots, 2n + 1$

Similarly for system (3.8) (the nonlinear isolator subjected to base excitation), it can be obtained that

$$P_0(j\Omega) = \frac{j\Omega^2(1 + j\xi_1\Omega)}{L(j\Omega)} \quad (3.20)$$

$$P_n(j\Omega) = \frac{1}{2^{2n}} \frac{j\Omega^{4n+4}}{|L(j\Omega)|^{2n} [L(j\Omega)]^2} \sum_{\omega_1 + \dots + \omega_{2n+1} = \Omega} \sum_{z=1}^{N_{\bar{n}}} \frac{\prod_{k=1}^n [j\omega_{l_k(z)}^{z_{l_k(1)}} + \dots + j\omega_{l_k(z)}^{z_{l_k(n)}}]}{\prod_{i=1}^{n-1} L[j\omega_{l_i(z)}^{z_{l_i(1)}} + \dots + j\omega_{l_i(z)}^{z_{l_i(n)}}]} \quad (3.21)$$

where  $\omega_i \in \{-\Omega, \Omega\}$ ,  $i = 1, \dots, 2n + 1$ .

From (3.17), when there exists no nonlinear damping coefficients, i.e.,  $\beta_2 = 0$  and  $\beta_4 = 0$ , the nonlinear isolator turns into a linear isolator. The force transmissibility is easy to obtain as

For system (3.4), the linear isolator under force excitation,

$$T_f(\Omega) = |Y_2(j\Omega)| = |P_0(j\Omega)| = \left| \frac{j(1 + j\xi_1\Omega)}{L(j\Omega)} \right| = \sqrt{\frac{1 + (\xi_1\Omega)^2}{(1 - \Omega^2)^2 + (\xi_1\Omega)^2}} \quad (3.22)$$

For system (3.8), the linear isolator under base displacement excitation,

$$T_f(\Omega) = |Y_2(j\Omega)| = |P_0(j\Omega)| = \left| \frac{j\Omega^2(1 + j\xi_1\Omega)}{L(j\Omega)} \right| = \Omega^2 \sqrt{\frac{1 + (\xi_1\Omega)^2}{(1 - \Omega^2)^2 + (\xi_1\Omega)^2}} \quad (3.23)$$

### 3.2.2.2 Absolute displacement transmissibility $T_d(\Omega)$

The output spectrum of  $y_3$  in (3.10) is given as

$$Y_3(j\omega) = Y_1(j\omega) + (-j) = P_0(j\omega) + \sum_{n=1}^{\lfloor N/2 \rfloor} P_n(j\omega) \beta_2^n \quad (3.24)$$

where

$$P_0(j\omega) = -j - \frac{-j\omega^2}{L(j\omega)} \quad (3.25)$$

$$P_n(j\omega) = \frac{1}{2^{2n}} \frac{1}{L(j\omega)} \sum_{\omega_1 + \dots + \omega_{2n+1} = \omega} \prod_{i=1}^{2n+1} H_1^1(j\omega_i) U(\omega_i) \sum_{z=1}^{N_n} \frac{\prod_{k=1}^n \left[ j\omega_{l_k(1)}^z + \dots + j\omega_{l_k(j_k)}^z \right]}{\prod_{i=1}^{n-1} L \left[ j\omega_{l_i(1)}^z + \dots + j\omega_{l_i(j_i)}^z \right]} \quad (3.26)$$

The absolute displacement transmissibility can be obtained as

$$T_d(\Omega) = |Y_3(j\Omega)| = \left| P_0(j\Omega) + \sum_{n=1}^{\lfloor N/2 \rfloor} P_n(j\Omega) \beta_2^n \right| \quad (3.27)$$

### 3.2.3 Effects of nonlinear damping coefficients on vibration isolation

The force transmissibility and the absolute displacement transmissibility are derived in section 3.2.2. All of these transmissibilities have an explicit analytical polynomial relationship with the nonlinear damping coefficient  $\beta_2$ . The performance of the proposed nonlinear damping can then be easily investigated with the explicit nCOS function. The following results can be obtained

**Proposition 3.1:** For force excitation, the nonlinear damping  $(\cdot)^2 \frac{d(\cdot)}{dt}$  can produce the following performance for force transmissibility:

- (I) When  $\Omega \gg 1$  or  $\Omega \ll 1$ ,

$$T_f(\Omega) \approx |P_0(j\Omega)| = \sqrt{\frac{1 + (\xi_1 \Omega)^2}{(1 - \Omega^2)^2 + (\xi_1 \Omega)^2}} \quad (3.28)$$

(II) When  $\Omega \approx 1$ , there exists a  $\beta$  such that the force transmissibility can be expressed by an alternating series with respect to the nonlinear coefficient  $\beta_2$  if  $0 < \beta_2 < \beta$ . The force transmissibility can therefore be suppressed by exploiting the properties of alternating series.

**Proof:** See Appendix 3.2.

Proposition 3.1 indicates that the nonlinear damping term  $(\cdot)^2 \frac{d(\cdot)}{dt}$  has almost no effect on the force transmissibility over the non-resonant frequency regions, i.e., a frequency much lower or much higher than the resonant frequency, and the force transmissibility is obviously suppressed at/around the resonant frequency.

**Proposition 3.2:** When the isolator is under base excitation, the following performance for the force excitation can be obtained:

(I) When  $\Omega \gg 1$  or  $\Omega \ll 1$ , nonlinear damping  $(\cdot)^2 \frac{d(\cdot)}{dt}$  leads to

$$T(\Omega) \approx |P_0(j\Omega)| = \Omega^2 \sqrt{\frac{1 + (\xi_1 \Omega)^2}{(1 - \Omega^2)^2 + (\xi_1 \Omega)^2}} \quad (3.29)$$

(II) When  $\Omega \approx 1$ , there exists a  $\beta$  such that the force transmissibility can be expressed as an alternating series with respect to the nonlinear coefficient  $\beta_2$  where  $0 < \beta_2 < \beta$ . The force transmissibility can therefore be suppressed by exploiting the properties of alternating series.

**Proof:** See Appendix 3.3.

Proposition 3.2 shows that the proposed nonlinear damping can significantly

reduce the force transmissibility over the resonant frequency while leaving it almost unaffected in the non-resonant frequency region.

The absolute displacement transmissibility under base displacement excitation is very similar to the force transmissibility discussed above.

**Proposition 3.3:** The proposed nonlinear damping  $(\cdot)^2 \frac{d(\cdot)}{dt}$  leads to the following performance for the absolute displacement transmissibility:

(I) When  $\Omega \gg 1$  or  $\Omega \ll 1$ , nonlinear damping  $(\cdot)^2 \frac{d(\cdot)}{dt}$  can make

$$T(\Omega) \approx |P_0(j\Omega)| = \sqrt{\frac{1 + (\xi_1 \Omega)^2}{(1 - \Omega^2)^2 + (\xi_1 \Omega)^2}} \quad (3.30)$$

(II) When  $\Omega \approx 1$ , there exists a  $\beta > 0$  such that

$$\frac{d[T(\Omega)]^2}{d\beta_2} < 0, \text{ for } 0 < \beta_2 < \beta \quad (3.31)$$

**Proof:** See Appendix 3.4.

In this section, the performance of the nonlinear damping is theoretically investigated with the nCOS method. When the harmonic balance method or perturbation method is used to analyse the proposed nonlinear damping, the isolator performance (the force transmissibility and absolute displacement transmissibility) and the input are involved in a set of nonlinear algebraic equations that must be numerically solved to obtain the performance. The derivation of the isolator performance in Proposition 3.1-Proposition 3.3 via nCOS method is thus more straightforward.

### 3.2.4 Examples and Discussion

The following simulations via the Runge-Kutta method are given to verify the theoretical results above. The demonstrations of the results in section 3.2.3 are based on the nCOS functions developed between the system performance (force transmissibility and displacement transmissibility) and the nonlinear damping coefficient, so the convergent Volterra series expansion relationship between the system performance and the system input should thus be studied first. The parametric convergence bound for the nonlinear damping coefficient  $\beta_2$  is computed.

#### 3.2.4.1 Compute the PBoC of the nonlinear damping coefficient $\beta_2$

From (3.4) and (3.8), it can be observed that the only difference between the dimensionless governing equation of force excitation and that of base excitation is that the input magnitude for force excitation is 1 but the input magnitude for base excitation is  $\Omega^2$ . Thus, the parametric convergence bounds, i.e., PBoC, for the nonlinear damping coefficient  $\beta_2$  in these two cases can be computed in the same way but with different input magnitudes.

The first equation of the governing equations ((3.4) or (3.8)) is transformed into a SIMO NARX model as

$$\begin{cases} x(k) + y_1(k) + \xi_1 z(k) + \beta_2 y_1^2(k) z(k) + \beta_4 z^3(k) = U \sin(\Omega \tau) \\ z(k) = \frac{y_1(k) - y_1(k-1)}{T_s} \\ x(k) = \frac{y_1(k) - 2y_1(k-1) + y_1(k-2)}{T_s^2} \end{cases} \quad (3.32)$$

where  $U = 1$  for (3.4) and  $U = \Omega^2$  for (3.8), and  $x(k)$  and  $z(k)$  denote the acceleration and velocity of  $y_1(k)$ , respectively.  $T_s$  is the sample time.

According to Proposition 2.6, and denoting  $\bar{\beta}_2$  as the parametric bound of nonlinear damping coefficient  $\beta_2$ , the following equations hold

$$\begin{aligned} a_{1,3} &= \bar{\beta}_2 \bar{L}(j\omega) \frac{\bar{H}_1^{(z)}(j\omega)}{\bar{H}_1^{(y1)}(j\omega)}, a_{1,1} = - \left[ 1 + \frac{\bar{H}_1^{(x)}(j\omega)}{\bar{H}_1^{(y1)}(j\omega)} + \frac{\bar{H}_1^{(z)}(j\omega)}{\bar{H}_1^{(y1)}(j\omega)} \right], a_{1,2} = 0, \\ a_{1,0} &= \left[ \bar{H}_1^{(y1)}(j\omega) + \bar{H}_1^{(z)}(j\omega) + \bar{H}_1^{(x)}(j\omega) \right] U, a_{2,2} = 3a_{1,3}, a_{2,1} = 2a_{1,2}, a_{2,0} = a_{1,1}. \end{aligned}$$

From (2.20), the following equation can be obtained:

$$27a_{1,0}^2 a_{1,3}^2 + 4a_{1,1}^3 a_{1,3} = 0$$

Then, the parametric bound for the nonlinear damping coefficient  $\beta_2$  can be obtained as

$$\bar{\beta}_2 = - \frac{4}{27\bar{L}(j\omega)} \frac{\bar{H}_1^{(y1)}(j\omega)}{\bar{H}_1^{(x)}(j\omega)} \frac{a_{1,1}^3}{a_{1,0}^2} \quad (3.33)$$

In Figure 3.3 and Figure 3.4, the parameter is given as  $\xi_1 = 0.1, T_s = 1/2000$  s.

It can be observed that the computed parametric convergence bound for the nonlinear damping coefficient  $\beta_2$  has good agreement with that obtained by numerical simulations, thereby validating the results proposed in Chapter 2, i.e., the parametric convergence bound for the Volterra series expansion of nonlinear systems.

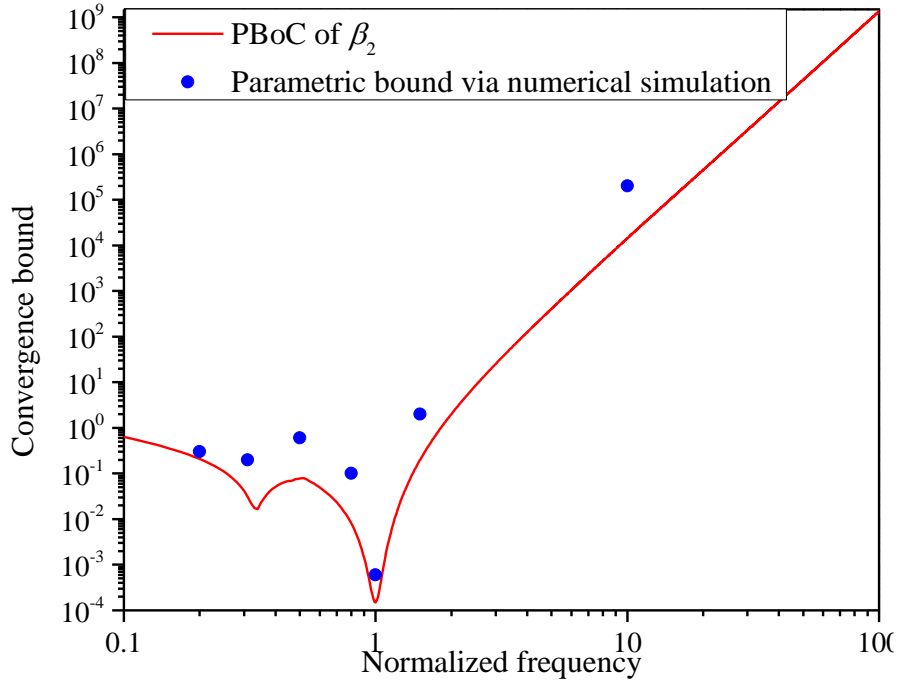


Figure 3.3 The parametric convergence bound  $\bar{\beta}_2$  for a nonlinear isolator under force excitation (3.4)

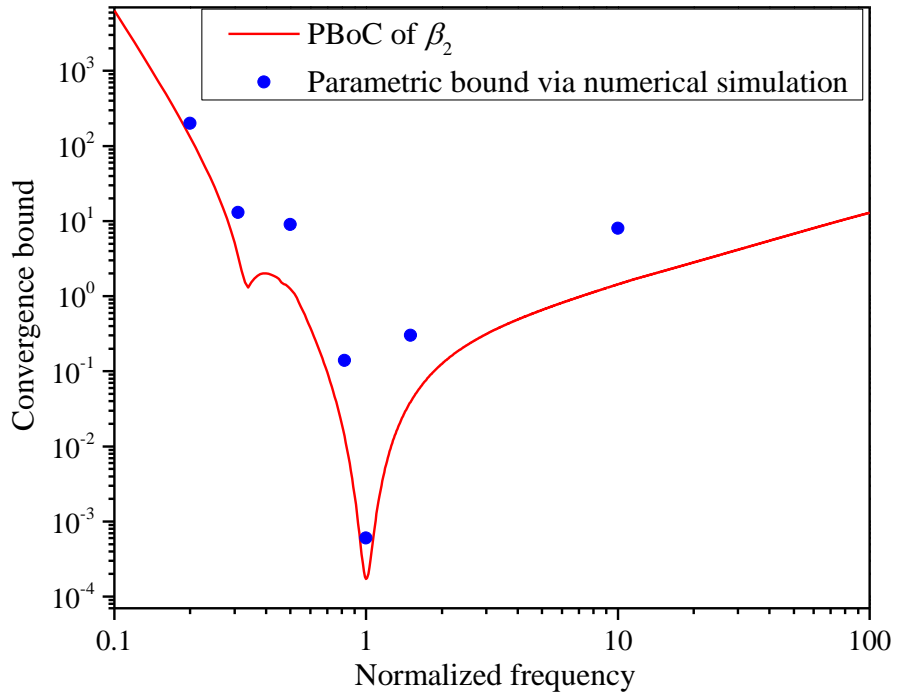


Figure 3.4 The parametric convergence bound  $\bar{\beta}_2$  for a nonlinear isolator under base excitation (3.8)

### 3.2.4.2 Isolator performance

Figure 3.5 presents the force transmissibility of an isolator under force excitation. The solid line and dash line are the force transmissibilities with linear damping coefficients  $\xi_1 = 0.1$  and  $\xi_1 = 0.325$ , respectively. The star line presents the performance when the cubic order nonlinear damping  $(\dot{\cdot})^2 \frac{d(\cdot)}{dt}$  is introduced into an isolator with nonlinear damping coefficient  $\beta_2 = 0.1$ . It can be observed that the force transmissibility over the resonant frequency is obviously suppressed but remains almost unaffected over the non-resonant regions. The dash line is presented as a reference case. To reach the same force transmissibility in the resonant frequency as that by cubic-order nonlinear damping, the linear damping coefficient  $\xi_1$  increases from 0.1 to 0.325, which obviously leads to performance deterioration at high frequency.

The nonlinear damping coefficient is chosen as  $\beta_2 = 0.1$  in the following discussion. This is because that the convergence bound for the nonlinear damping coefficient,  $\bar{\beta}_2$ , is larger than 0.1 in almost the whole frequency range except around the resonant frequency. For the case in/around the resonant frequency, the equivalent damping coefficient, i.e.,  $\xi_1 + \beta_2 (\dot{\cdot})^2$ , is a positive damping coefficient that is always larger than  $\xi_1$ , which will obviously lead to a superior vibration suppression, so the discussion are thus still reasonable and meaningful.

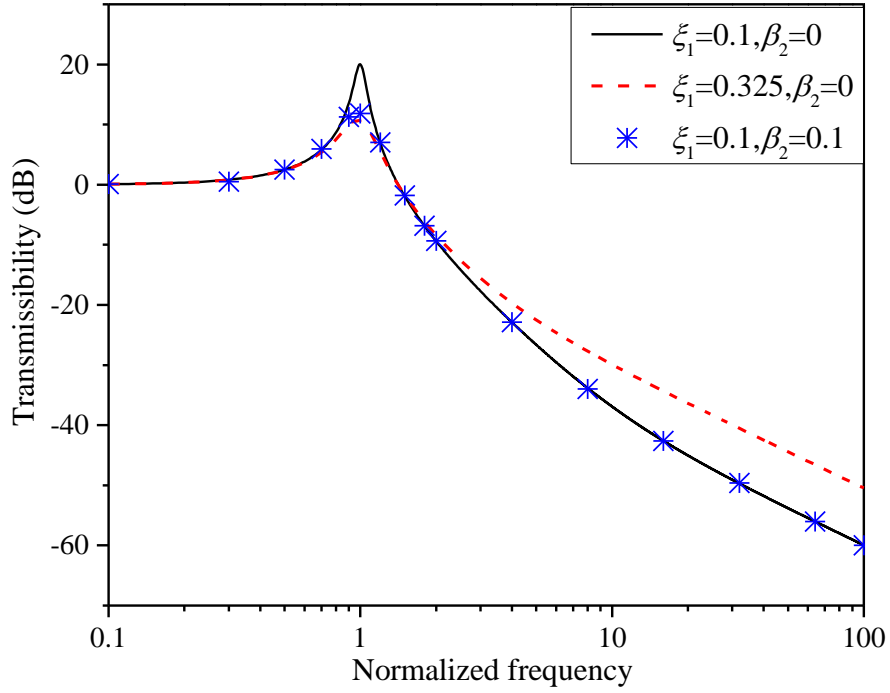


Figure 3.5 The force transmissibility of an SDoF isolator under force excitation

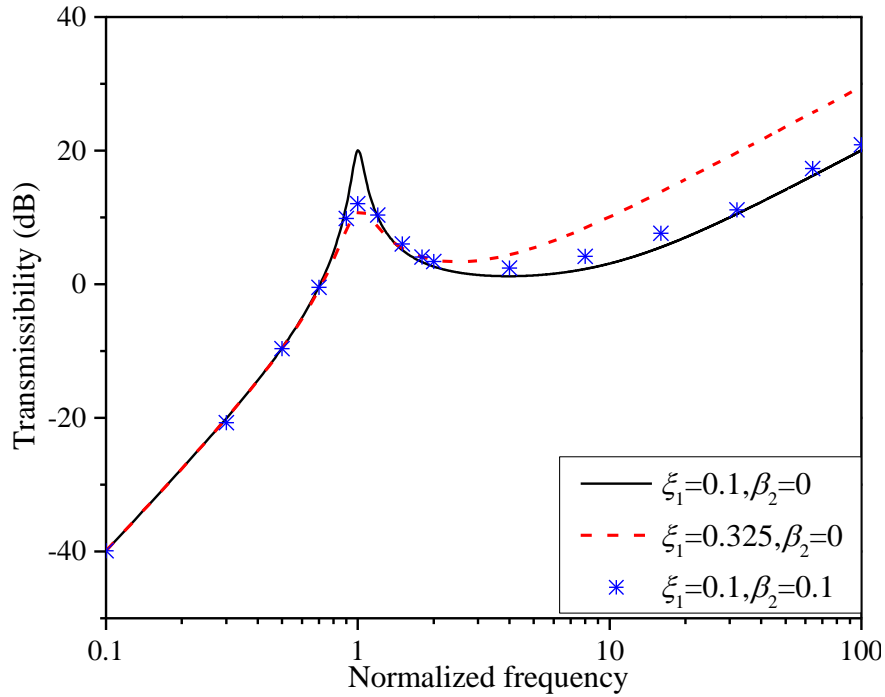


Figure 3.6 The force transmissibility of an isolator under base displacement excitation

In Figure 3.6, the force transmissibilities under base displacement excitation are presented. The proposed nonlinear damping can significantly suppress the force transmissibility over the resonant frequency and keep the performance very close to that with a small linear damping coefficient over the non-resonant regions.

The dash line is also presented as a reference case, from which it can be observed that the force transmissibility can reach the same performance as that by cubic-order nonlinear damping at the resonant frequency but results in performance deterioration at high frequency.

In Figure 3.7, the absolute displacement transmissibility with cubic-order nonlinear damping  $(\dot{\cdot})^2 \frac{d(\cdot)}{dt}$  is presented. Superior performance for the absolute displacement transmissibility relative to that by a larger linear damping coefficient can also be observed.

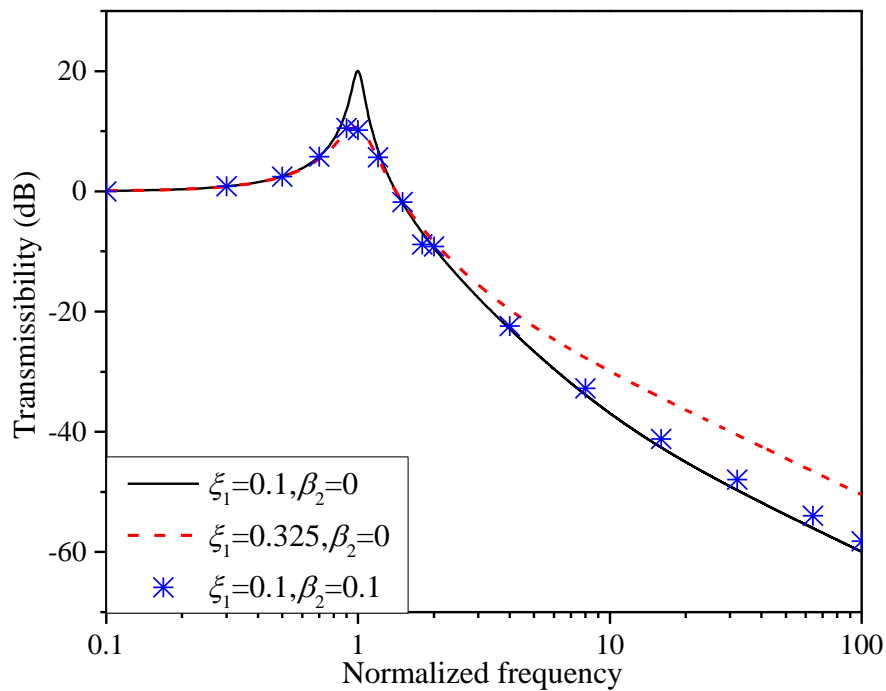


Figure 3.7 The absolute displacement transmissibility of an isolator under base displacement

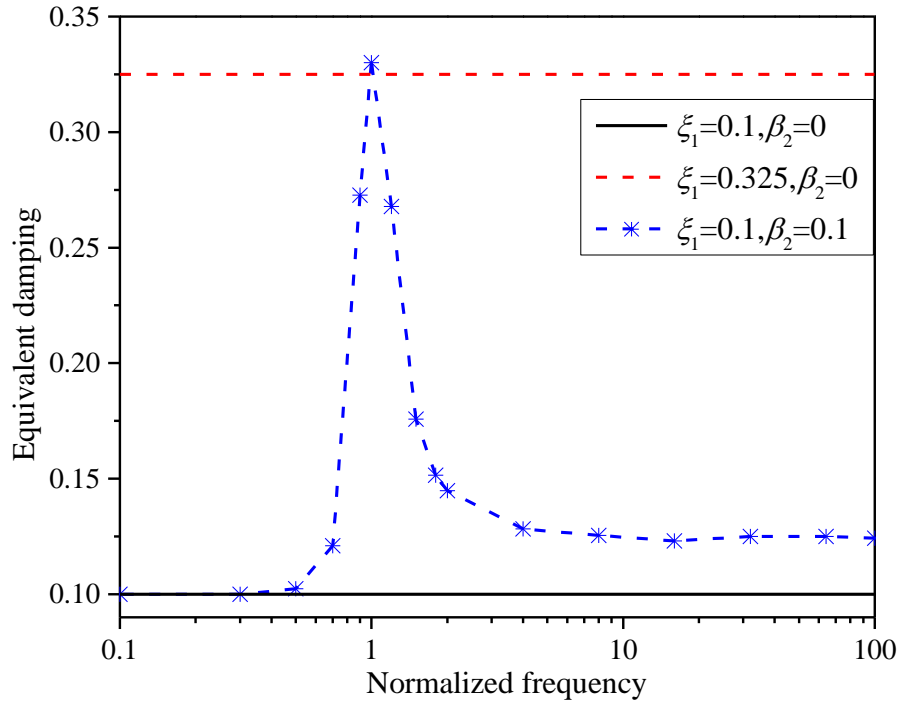


Figure 3.8 Equivalent damping coefficient of the cubic order nonlinear damping

To provide a more straightforward insight into the nonlinear mechanism in vibration suppression, the equivalent damping coefficient of the isolator is provided in Figure 3.8. As shown in Figure 3.8, the cubic order nonlinear damping  $(\cdot)^2 \frac{d(\cdot)}{dt}$  has an equivalent linear damping coefficient very close to 0.325 at the resonant frequency and near 0.1 in non-resonant frequency region. The better performance of the nonlinear damping  $(\cdot)^2 \frac{d(\cdot)}{dt}$  at high frequency presented in Figure 3.5 to Figure 3.7 therefore straightforwardly results from this small equivalent damping coefficient.

### 3.3 Multiple-object nonlinear optimization based on the nCOS method

Vibration control of a vehicle suspension is a multiple-object (body acceleration, relative tire load, and suspension stroke) optimization problem. This multiple-object problem is often nonlinear because of the inherent nonlinearity of the spring [158, 159] and damper [160], and also the actuator saturation [161]. Controller designs that neglecting these inherent system nonlinearities may therefore lead to performance deterioration, so an effective and efficient method for the analysis and design of nonlinear suspension systems is needed.

The body acceleration, relative tire load, and suspension stroke are three indicators for assessing the vehicle suspension performance. Note that 4-8Hz is suggested by ISO2361 as nominal frequency range for assessing the ride comfort; a systematic methodology in the frequency domain for the analysis and design of the vehicle suspension may provide straightforward information for the engineers. The existence of nonlinearity makes it more difficult to analyse and design the suspension system, and the nCOS method could be a powerful tool for the nonlinear analysis and design of this multiple-object optimization problem.

First, the PBoC can be computed to indicate whether the system is Volterra-type or has strong nonlinear dynamics such as bifurcation or chaos. By guaranteeing that the system nonlinearity is Volterra-type, the system nonlinear dynamics can be well analysed using the nCOS method. Second, the multiple-object performance (MOP) function (including the ride comfort, suspension stroke, and relative tire load) is constructed. The MOP function is regarded as a nonlinear output function

and expressed as a polynomial function of model parameters with the nCOS method [92]. How the model parameters of interest affect the MOP can then be studied in the frequency domain, and the design and optimization of the MOP function can be conducted directly within the computed PBoC.

In this section, a nonlinear controller based on  $\ddot{x}_s^3$  is deliberately introduced into the suspension system for performance improvement. Compared with the sprung mass acceleration adopted here, the absolute sprung mass displacement and velocity based control strategies [162-165] (for example, the skyhook control, ground hook control, acceleration driven damper (ADD), mixed skyhook and ADD strategy, and state feedback control) may have a limitation in that required motion signals such as absolute displacement and velocity are not readily available for measurement on a moving vehicle. Usually, these motion signals can be obtained by state estimation methods or filters (e.g., integration of acceleration signal or Kalman filters), which will introduce estimation error and control delay to the system, and increase development or manufacturing cost. However, by employing beneficial nonlinearity in vibration control, a simple nonlinear controller with measurable signals could provide the same or even better performance.

### **3.3.1 Model under consideration**

According to Figure 3.9, the governing equation of the quarter vehicle suspension model is given as,

$$\begin{cases} m_t \ddot{x}_t = k_t u + c_t \dot{u} - k_t x_t - c_t \dot{x}_t - m_s \ddot{x}_s \\ m_s \ddot{x}_s = -c_s (\dot{x}_s - \dot{x}_t) - c_{s3} \ddot{x}_s^3 - f_s \end{cases} \quad (3.34)$$

where  $f_s = k_{s1}(x_s - x_t) + k_{s2}(x_s - x_t)^2 + k_{s3}(x_s - x_t)^3$ . The model parameters are borrowed from [141], which are obtained by curve fitting with measurement data from a Hyundai Elantra front suspension and given as  $m_s = 240 \text{ kg}$ ,  $m_t = 25 \text{ kg}$ ,  $k_t = 160 \text{ kN/m}$ ,  $k_{s1} = 12 \text{ kN/m}$ ,  $c_t = 10 \text{ N}\cdot\text{s/m}$ ,  $k_{s2} = -73696 \text{ N/m}^2$ ,  $k_{s3} = 3170400 \text{ N/m}^3$ ,  $c_s = 1385.4 \text{ N}\cdot\text{s/m}$ . Here only the model parameter  $c_{s3}$  is unknown, which is considered a characteristic parameter of interest. To compute the PBoC of  $c_{s3}$ , the road input is assumed to be a cosine input  $u = U \cos(2\pi ft)$ .

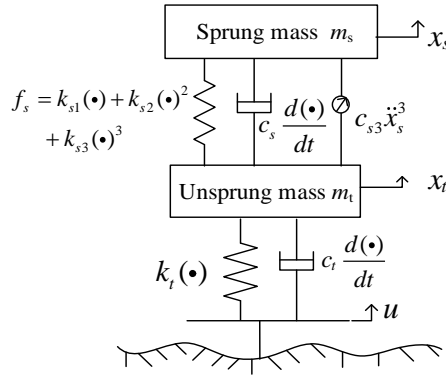


Figure 3.9 A quarter vehicle suspension model

### 3.3.2 Compute the PBoC of $c_{s3}$

The suspension model in (3.34) can be transformed into a SIMO (single-input four-output) NARX model by backward discretization as,

$$\left\{ \begin{array}{l} x_1(k) = c_{1,0}^1(1;1)x_1(k-1) + c_{1,0}^1(2;1)x_1(k-2) + c_{1,0}^4(0;1)x_4(k) \\ \quad + c_{0,1}(0;1)u(k) + c_{0,1}(1;1)u(k-1) \\ x_2(k) = c_{1,0}^2(1;2)x_2(k-1) + c_{1,0}^2(2;2)x_2(k-2) + c_{1,0}^3(0;2)x_3(k) \\ \quad + c_{1,0}^3(1;2)x_3(k-1) + c_{2,0}^{33}(0,0;2)x_3^2(k) + c_{3,0}^{333}(0,0,0;2)x_3^3(k) \\ \quad + c_{3,0}^{444}(0,0,0;2)x_4^3(k) \\ x_3(k) = c_{1,0}^2(0;3)x_2(k) + c_{1,0}^1(0;3)x_1(k) \\ x_4(k) = c_{1,0}^2(0;4)x_2(k) + c_{1,0}^2(1;4)x_2(k-1) + c_{1,0}^2(2;4)x_2(k-2) \end{array} \right. \quad (3.35)$$

where  $x_1=x_t$ ,  $x_2=x_s$ , and all of the coefficients are presented in table 3.1.

Table 3.1 Coefficients of (3.35)

$c_{1,0}^1(1;1) = (2m_t + c_t T_s)/D$	$c_{1,0}^1(2;1) = -m_t/D$
$c_{0,1}(0;1) = (k_t T_s^2 + c_t T_s)/D$	$c_{1,0}^2(1;2) = 2$
$c_{0,1}(1;1) = -c_t T_s/D$	$c_{1,0}^2(2;2) = -1$
$c_{1,0}^3(0;2) = (-k_{s1} T_s^2 + c_s T_s)/m_s$	$c_{1,0}^3(1;2) = c_s T/m_s$
$c_{2,0}^{33}(0,0;2) = -k_{s2} T_s^2/m_s$	$c_{1,0}^2(0;3) = 1$
$c_{2,0}^{333}(0,0,0;2) = -k_{s3} T_s^2/m_s$	$c_{1,0}^1(0;3) = -1$
$c_{3,0}^{444}(0,0,0;2) = -c_{s3} T_s^2/m_s$	$c_{1,0}^2(0;4) = -1/T_s^2$
$c_{1,0}^2(2;4) = 1/T_s^2$	$c_{1,0}^2(1;4) = -2/T_s^2$
$D = k_t^2 T_s^2 + c_s T_s + m_t$	$T_s = 1/2000$

From (3.35),  $c_{3,0}^{444}(0,0,0;2) = -c_{s3} T_s^2 / m_s$ , and  $c_{s3}$  is only involved in  $c_{3,0}^{444}(0,0,0;2)$ . Thus the PBoC of  $c_{s3}$  (denoted as  $C_{s3}$ ) can be obtained as

$$C_{s3} = \left( m_s / T_s^2 \right) C_{(3,0;2)}^{444} \quad (3.36)$$

where  $C_{(3,0;2)}^{444}$  is the computed PBoC of  $c_{3,0}^{444}(0,0,0;2)$ . The computation of  $C_{(3,0;2)}^{444}$  can be conducted according to the procedure in Algorithm 2.4. The elements in (2.20) can be obtained according to (2.84)-(2.88), which are given as (as shown in Proposition 2.6,  $j$  can be any value from 1 to 4, and here  $j$  takes 4 in the following

calculation)

$$a_{1,3} = \bar{L}(j\omega) \left[ C_{(3,0;2)}^{333} \left( \frac{\bar{H}_1^{(3)}(j\omega)}{\bar{H}_1^{(4)}(j\omega)} \right)^3 + C_{(3,0;2)}^{444} \right], a_{1,0} = \sum_{j_k=1}^4 \bar{H}_1^{(j_k)}(j\omega)U,$$

$$a_{1,2} = \bar{L}(j\omega)C_{(2,0;2)}^{33} \left( \frac{\bar{H}_1^{(3)}(j\omega)}{\bar{H}_1^{(4)}(j\omega)} \right)^2, a_{1,1} = -\sum_{j_k=1}^4 \frac{\bar{H}_1^{(j_k)}(j\omega)}{\bar{H}_1^{(4)}(j\omega)}$$

$$a_{2,2} = 3a_{1,3}, a_{2,1} = 2a_{1,2}, a_{2,0} = a_{1,1}$$

where  $C_{(3,0;2)}^{333} = |c_{3,0}^{333}(0,0,0;2)|$ ,  $C_{(3,0;2)}^{444} = |c_{3,0}^{444}(0,0,0;2)|$ ,  $C_{(2,0;2)}^{33} = |c_{2,0}^{33}(0,0;2)|$ . The following equation then holds,

$$(27a_{1,0}^2)a_{1,3}^2 + (4a_{1,1}^3 - 18a_{1,2}a_{1,1}a_{1,0})a_{1,3} + (4a_{1,2}^3a_{1,1} - a_{1,2}^2a_{1,3}^2) = 0 \quad (3.37)$$

Equation (3.37) is a quadratic equation of  $a_{1,3}$  with known coefficients. Solving  $a_{1,3}$  from (3.37), the PBoC  $C_{(3,0;2)}^{444}$  can then be obtained,

$$C_{(3,0;2)}^{444} = a_{1,3}/\bar{L}(j\omega) - C_{(3,0;2)}^{333} \left( \bar{H}_1^{(3)}(j\omega)/\bar{H}_1^{(4)}(j\omega) \right)^3. \quad (3.38)$$

When  $C_{(3,0;2)}^{444}$  from (3.38) is smaller than 0, denote  $C_{(3,0;2)}^{444} = 0$  because  $C_{(3,0;2)}^{444}$  is nonnegative. This means that the suspension model with existing nonlinear stiffness is not a Volterra-type nonlinear system. Based on (3.38), the PBoC  $C_{s3}$  can then be computed according to (3.36).

The computed PBoC for  $C_{s3}$  is presented in Fig. 3.10 with the input amplitude given as

$$U = n_0 \sqrt{2G(n_0)}v/f \quad (3.39)$$

where  $G(n_0)$  is the spatial ground displacement power spectral density, which has 8 grades according to ISO/TC108/SC2N67.  $G(n_0)$  is chosen as  $256 \times 10^{-6} \text{ m}^3$  in (3.39), which corresponds to the C grade road profile. The vehicle velocity  $v$  here is 20 m/s,  $f$  is the excited frequency, and  $n_0$  is the reference spatial frequency, which equals 0.1 m in (3.39). The input amplitude  $U$  in (3.39) is closer to the actual road

profile over a constant amplitude in the whole frequency range because the road profile has a higher amplitude at a lower frequency and a lower amplitude at a higher frequency.

From Figure 3.10, the smallest PBoC, which is located at the first resonant frequency, is 20. The estimated convergence bound by numerical simulation is approximately 140. This deviation mainly comes from the large damping ratio in this example, that is,  $\xi = c_s/2\sqrt{k_{s1}m_s} = 0.4$ . In the rest of the frequency range, the PBoC obtained by Proposition 2.6 is very close to the true convergence bound.

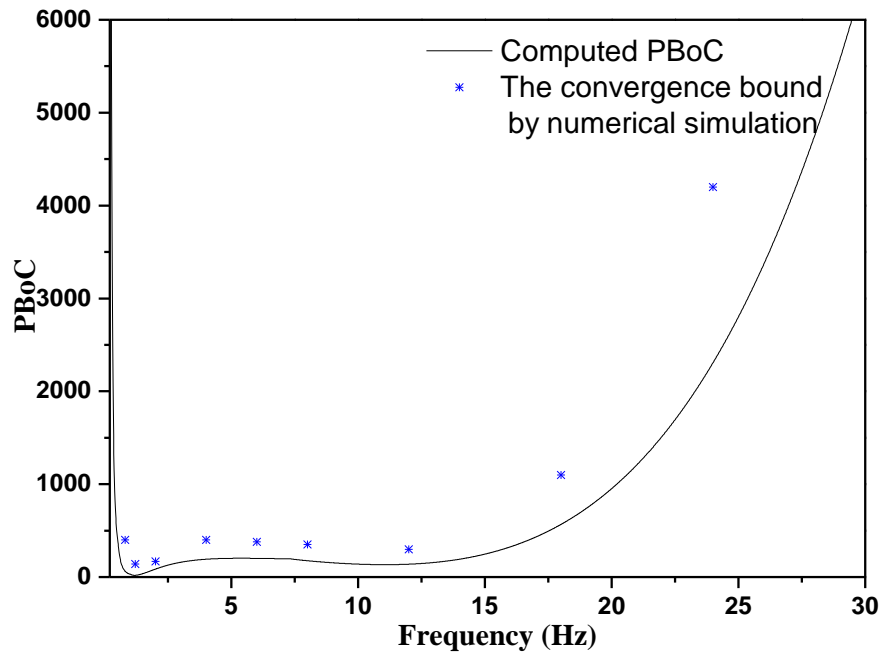


Figure 3.10 The PBoC of  $C_{s3}$

To validate the effectiveness of the result above, the normalized root mean square error (NRMSE) defined in (2.34) is used to measure the closeness between the synthesized output truncated up to the  $N$ th-order and the real output by ode 45.

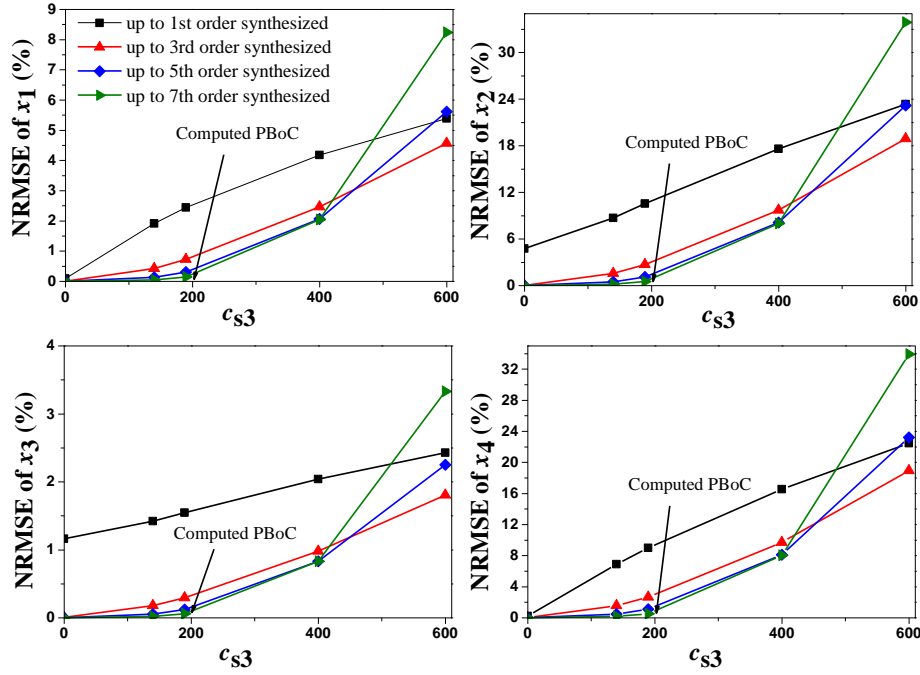


Figure 3.11 The normalized root mean square error when  $f=4$  Hz

From Figure 3.11, when the model parameter  $c_{s3}$  is chosen to be smaller than the computed PBoC, the NRMSEs of all of the outputs in (3.35) dramatically decrease to 0 as the synthesized order increases. For example, when  $f=4$  Hz and  $c_{s3}$  takes 140, which is smaller than the computed PBoC ( i.e., 190 ), the higher the order of the approximation used, the smaller the NRMSEs that can be obtained. This means that the vehicle suspension system (3.35) involves a convergent Volterra series expansion. As the parameter  $c_{s3}$  becomes larger and larger, the synthesized outputs up to the same truncated order also have observably growing NRMSEs. When the model parameter  $c_{s3}$  is taken to be much larger than the computed PBoC, for example, if  $c_{s3}$  equals 600, the NRMSEs of the synthesized outputs become larger and larger after a certain synthesized order (fifth-order in this case), which indicates that the synthesized

outputs diverge. Therefore, within the PBoC range, the suspension system (3.35) is Volterra-type and consequently can be freely analysed with the Volterra-series based methods.

### 3.3.3 Multiple-object performance analysis

The performance of the vehicle suspension system, for example, the ride comfort (the vertical body acceleration)  $y_1 = \ddot{x}_s$ , the relative dynamic tire load  $y_2 = k_t(x_t - u)/(m_s + m_t)g$ , and the suspension stroke  $y_3 = x_s - x_t$ , can be analysed in the frequency domain using the nonlinear output spectrum if the nonlinear model (3.35) is Volterra-type. Any nonlinear output function including the MOP function can be treated with the nCOS (nonlinear characteristic output spectrum) function based method, and thus can be expressed as an explicit and analytic polynomial function of the model parameter of interest [92] (the model parameter is  $c_{s3}$  in this case),

$$\begin{aligned}
Y_i(j\omega) &= Y_{i,1}(j\omega) + Y_{i,2}(j\omega) + \underbrace{Y_{i,3}(j\omega)\Big|_{c_{s3}=0} + c_{s3} \cdot \varphi_{i,3}(c_{s3}; j\omega)}_{Y_{i,3}(j\omega)} \\
&+ \underbrace{Y_{i,4}(j\omega)\Big|_{c_{s3}=0} + c_{s3} \cdot \varphi_{i,4}(c_{s3}; j\omega)}_{Y_{i,4}(j\omega)} \\
&+ \underbrace{Y_{i,5}(j\omega)\Big|_{c_{s3}=0} + c_{s3} \cdot \varphi_{i,5}(c_{s3}; j\omega) + c_{s3}^2 \cdot \varphi_{i,5}(c_{s3}^2; j\omega) + \dots}_{Y_{i,5}(j\omega)} + \dots
\end{aligned} \tag{3.40}$$

where  $Y_{i,m}(j\omega)$  is the  $m$ th-order output spectrum for the output  $y_i$ , and  $\varphi_{i,m}(c_{s3}^k; j\omega)$  is the model parameter independent part in the  $m$ th-order output spectrum, which corresponds to the  $k$ th-order of the model parameters  $c_{s3}$ . When  $c_{s3}$  is taken under the convergence bound, (3.40) is always valid.

For a Volterra-type nonlinear system, there are no jumping or chaotic phenomena because it works around a stable equilibrium. Therefore, the system dynamic response will change continuously with the characteristic parameters, and thus the nCOS in (3.40) at several typical frequencies can well represent the system output spectrum.

**Under cosine wave excitation.** Figure 3.12 presents the performance of vertical body acceleration when the suspension system is subjected to a cosine wave excitation.  $c_{s3}$  here takes 140, and thus, system (3.35) is Volterra-type over the whole frequency range. Figure 3.12 presents the first-order harmonic component of the acceleration, that is, the Fourier transform of the acceleration at the first-order harmonic frequency (the same as the input frequency). It can be observed that the nonlinear controller has much better performance in the frequency range between the two resonant frequencies (e.g., 4-8 Hz, which are most sensitively felt by the human body and are suggested as a nominal frequency range for assessing the ride comfort according to ISO 2361). Another advantage of the nonlinear controller when compared with the skyhook based methods is that it is much easier to measure the acceleration signal than to obtain the absolute velocity or displacement signal. The active suspension controller based on  $H_\infty$  [166] is developed with linear models, and thus they are not available in this case. For those based on fuzzy control [167] and adaptive control [142, 159, 168], more complicated controllers, state estimation and filters are needed. Compared with the methods above, the proposed nonlinear controller is much easier to implement.

Figure 3.12 only shows how the performance varies with the frequency change but does not present how the performance is affected by model parameters. Therefore, the nCOS (nonlinear characteristic output spectrum) function would be much better than the traditional simulation based output spectrum analysis. When it is truncated up to the fifth-order, (3.40) can be rearranged as,

$$Y_i(j\omega) = Y_{i0}(j\omega) + c_{s3}Y_{i1}(j\omega) + c_{s3}^2Y_{i2}(j\omega), \quad i = 1, 2, 3 \quad (3.41)$$

where  $Y_{i0}(j\omega) = Y_{i,1}(j\omega) + Y_{i,2}(j\omega) + Y_{i,3}(j\omega)|_{c_{s3}=0} + Y_{i,4}(j\omega)|_{c_{s3}=0} + Y_{i,5}(j\omega)|_{c_{s3}=0}$ ,  $Y_{i1}(j\omega) = \varphi_{i,3}(c_{s3}; j\omega) + \varphi_{i,4}(c_{s3}; j\omega) + \varphi_{i,5}(c_{s3}; j\omega)$  and  $Y_{i2}(j\omega) = \varphi_{i,5}(c_{s3}^2; j\omega)$ .

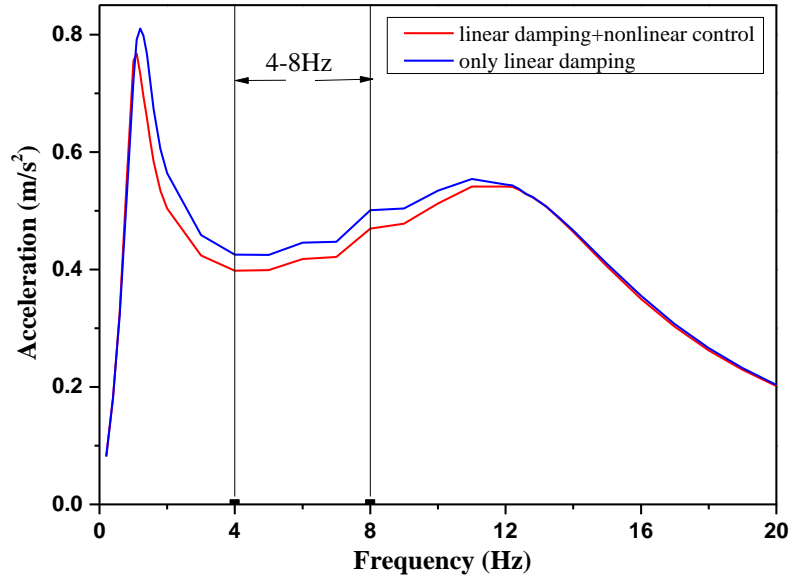


Figure 3.12 Comparison of vertical body acceleration under cosine road excitation

Denote the multiple-object performance (MOP) including vertical body acceleration  $y_1$ , relative dynamic tire load  $y_2$ , and suspension stroke  $y_3$  as,

$$\begin{aligned} z(\mu_1, \mu_2, c_{s3}; \omega) &= \mu_1 \frac{|Y_1(j\omega)|^2}{|Y_{1l}(j\omega)|^2} + \mu_2 \frac{|Y_2(j\omega)|^2}{|Y_{2l}(j\omega)|^2} + (1 - \mu_1 - \mu_2) \frac{|Y_3(j\omega)|^2}{|Y_{3l}(j\omega)|^2} \\ &= z_0(\mu_1, \mu_2; \omega) + c_{s3}z_1(\mu_1, \mu_2; \omega) + c_{s3}^2z_2(\mu_1, \mu_2; \omega) \\ &\quad + c_{s3}^3z_3(\mu_1, \mu_2; \omega) + c_{s3}^4z_4(\mu_1, \mu_2; \omega) \end{aligned} \quad (3.42)$$

where  $z_0, z_1, z_2, z_3,$  and  $z_4$  are independent of  $c_{s3}$ , as presented in table 3.2.  $Y_{il}(j\omega)$  stands for the performance when only linear damping is used, and  $\mu_1, \mu_2, \mu_3=1-\mu_1-\mu_2$  stand for the weight of the vertical body acceleration, the relative tire load, and the suspension stroke in the multiple-object performance function (3.42), respectively. Clearly,  $\mu_1+\mu_2+\mu_3=1$  holds. The MOP function in (3.42) implies the performance improvement of the vehicle suspension by taking all of the three indicators into account.

Table 3.2 Coefficients of (3.42)

$z_0(\mu_1, \mu_2; \omega) = \mu_1 \frac{ Y_{10}(j\omega) ^2}{ Y_{1l}(j\omega) ^2} + \mu_2 \frac{ Y_{20}(j\omega) ^2}{ Y_{2l}(j\omega) ^2} + (1 - \mu_1 - \mu_2) \frac{ Y_{30}(j\omega) ^2}{ Y_{3l}(j\omega) ^2}$
$z_1(\mu_1, \mu_2; \omega) = \mu_1 \frac{2 \operatorname{Re}(Y_{10}(j\omega)Y_{11}^*(j\omega))}{ Y_{1l}(j\omega) ^2} + \mu_2 \frac{2 \operatorname{Re}(Y_{20}(j\omega)Y_{21}^*(j\omega))}{ Y_{2l}(j\omega) ^2} + (1 - \mu_1 - \mu_2) \frac{2 \operatorname{Re}(Y_{30}(j\omega)Y_{31}^*(j\omega))}{ Y_{3l}(j\omega) ^2}$
$z_2(\mu_1, \mu_2; \omega) = \mu_1 \frac{ Y_{11}(j\omega) ^2 + 2 \operatorname{Re}(Y_{10}(j\omega)Y_{12}^*(j\omega))}{ Y_{1l}(j\omega) ^2} + \mu_2 \frac{ Y_{21}(j\omega) ^2 + 2 \operatorname{Re}(Y_{20}(j\omega)Y_{22}^*(j\omega))}{ Y_{2l}(j\omega) ^2} + (1 - \mu_1 - \mu_2) \frac{ Y_{31}(j\omega) ^2 + 2 \operatorname{Re}(Y_{30}(j\omega)Y_{32}^*(j\omega))}{ Y_{3l}(j\omega) ^2}$
$z_3(\mu_1, \mu_2; \omega) = \mu_1 \frac{2 \operatorname{Re}(Y_{11}(j\omega)Y_{12}^*(j\omega))}{ Y_{1l}(j\omega) ^2} + \mu_2 \frac{2 \operatorname{Re}(Y_{21}(j\omega)Y_{22}^*(j\omega))}{ Y_{2l}(j\omega) ^2} + (1 - \mu_1 - \mu_2) \frac{2 \operatorname{Re}(Y_{31}(j\omega)Y_{32}^*(j\omega))}{ Y_{3l}(j\omega) ^2}$
$z_4(\mu_1, \mu_2; \omega) = \mu_1 \frac{ Y_{12}(j\omega) ^2}{ Y_{1l}(j\omega) ^2} + \mu_2 \frac{ Y_{22}(j\omega) ^2}{ Y_{2l}(j\omega) ^2} + (1 - \mu_1 - \mu_2) \frac{ Y_{32}(j\omega) ^2}{ Y_{3l}(j\omega) ^2}$

To estimate the parameter-independent parts in (3.40), the following procedure is given [92]:

**Algorithm 3.1:**

**Step 1.** Given  $c_{s3}$ , for example,  $c_{s3}=10$ , then 5 simulations with different input magnitudes are needed to estimate  $Y_{i,m}(j\omega)$  (because it is truncated up to the fifth-order in (3.40)).

**Step 2.** Take two additional values of  $c_{s3}$ , for example, 50 and 90, and repeat step 1.

**Step 3.** Estimate the model parameter independent part using the different  $Y_{i,m}(j\omega)$  obtained by steps 1 and 2.

It can be observed that only 15 simulations are needed for the estimation of the nCOS function in (3.40) and (3.41) up to the fifth-order with a simple least squares method. Three different  $Y_{i,m}(j\omega)$ s are needed in Procedure 1 because the quadratic term  $c_{s3}^2$  exists in  $Y_{i,5}(j\omega)$  in (3.40). The MOP function can then be studied with different model parameters  $c_{s3}$  and different weights ( $\mu_1$  and  $\mu_2$ ) according to (3.42).

In (3.42),  $\mu_1=1, \mu_2=0$  means that only vertical body acceleration is considered in the MOP function.  $\mu_1=0, \mu_2=1$  and  $\mu_1=0, \mu_2=0$  present the case that only the relative tire load or suspension stroke is taken into account in the MOP function, respectively.  $c_{s3}=0$  stands for the case when only linear damping is used.

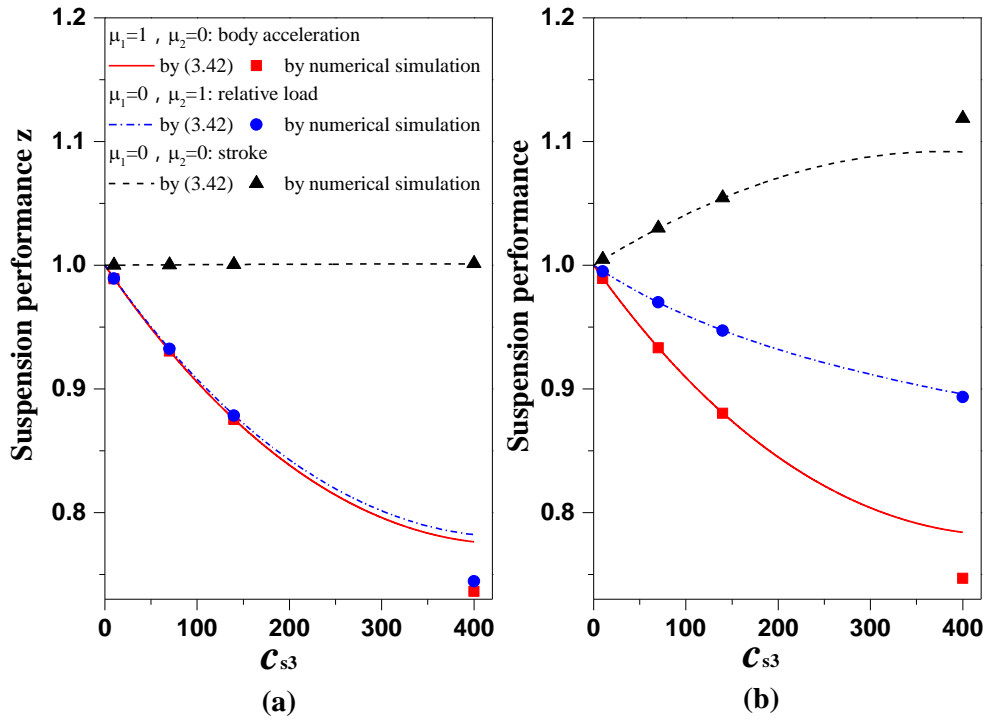


Figure 3.13 Multiple-object performance under cosine excitation: (a) at 4Hz, (b) at 8Hz

Figure 3.13 presents the influence of the model parameter  $c_{s3}$  on the MOP function when only the vertical body acceleration  $y_1$ , relative tire load  $y_2$ , or suspension stroke  $y_3$  is considered. It can be observed that the proposed nonlinear controller can improve both the vertical body acceleration and relative tire load, which correspond to the ride comfort and vehicle handling ability (relates to the ride safety), respectively. The suspension stroke represents the relative motion between the unsprung mass and the sprung mass, and thus usually it is designed to be smaller than a constraint value. The nonlinear controller maintains almost the same suspension stroke as that when only linear damping is used at 4 Hz which leads to a slightly larger suspension stroke at 8 Hz.

The computed PBoC at  $f=4\text{Hz}$  is approximately 190 according to Figure 3.11.

Thus, the results in Figure 3.13 by the MOP function based on the nCOS function

are reliable when  $c_{s3}$  is taken to be smaller than the computed PBoC, and if  $c_{s3}$  is much larger than the computed PBoC, for example, larger than 400, the multiple-object performance (MOP) function based on the nCOS function by (3.42) may result in some errors when compared with those by numerical simulation. This shows the significance and guidance of the results in Proposition 2.6 for the optimization and design of nonlinear systems using the nCOS-based MOP function.

The MOP function considering both vertical body acceleration and relative tire load with different weights  $\mu_1 + \mu_2 = 1$  is presented in Figure 3.14. The MOP function takes 400000 numerical simulations (by ode 45) when  $\mu_1 = 0:0.01:1$  and  $c_{s3} = 0:0.1:400$  for Figure 3.14. However, only 15 simulations are needed for the nCOS method. When more than one model parameter of interest is studied, the efficiency of the nCOS-based method using (3.40) is more obvious. Theoretically, the harmonic balance or perturbation method is available in this case, but the computation complexity makes it impractical. Therefore, if a system is Volterra-type, the advantages of the nCOS-based method including the computational efficiency and the effectiveness for practical applications are obvious, and the results in Proposition 2.6 provide an important guidance for nonlinear analysis, design, and optimization using these Volterra series associated theory and methods.

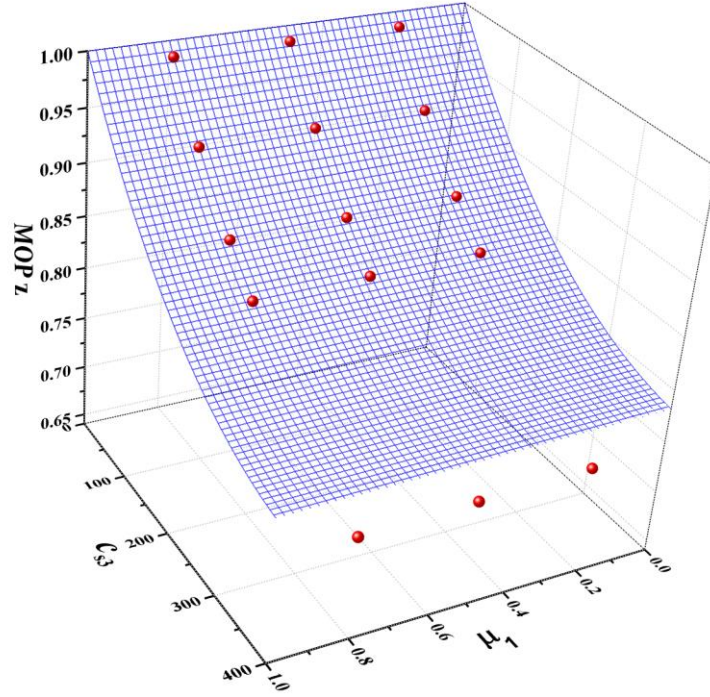


Figure 3.14 Multiple-object performance under cosine excitation at 4 Hz with  $\mu_1+\mu_2=1$ , the red ball is the MOP function by numerical simulation

**Under random road excitation.** The road disturbance is usually considered a random process, and according to ISO/TC108/SC2N67, the road profile can be classified into 8 grades. In this case, the total suspension performance can also be studied according to (3.40)-(3.42).

There also exists other comfort oriented strategies, for example, the acceleration driven damper (ADD) strategy [162] and the improved mixed skyhook and ADD method [164]. The latter has a controller of

$$\begin{cases} c_{in}(t) = c_{\max} & \begin{cases} [(\ddot{x}_s^2 - \alpha^2 \dot{x}_s^2) \leq 0 \wedge \dot{x}_s(\dot{x}_s - \dot{x}_t) > 0] \\ \vee [(\ddot{x}_s^2 - \alpha^2 \dot{x}_s^2) > 0 \wedge \ddot{x}_s(\dot{x}_s - \dot{x}_t) > 0] \end{cases} \\ c_{in}(t) = c_{\min} & \begin{cases} [(\ddot{x}_s^2 - \alpha^2 \dot{x}_s^2) \leq 0 \wedge \dot{x}_s(\dot{x}_s - \dot{x}_t) \leq 0] \\ \vee [(\ddot{x}_s^2 - \alpha^2 \dot{x}_s^2) > 0 \wedge \ddot{x}_s(\dot{x}_s - \dot{x}_t) \leq 0] \end{cases} \end{cases} \quad (3.43)$$

where  $c_{in}(t)$  is the requested damping coefficient. The actual damping coefficient is

obtained by applying a low pass filter on  $c_{in}(t)$ , i.e.,  $\dot{c}(t) = -\beta c(t) + \beta c_{in}(t)$ . The comparison of the performance between the proposed nonlinear controller and that with the mixed skyhook and the ADD method is presented in Figure 3.15. The comparison takes the following coefficients:  $\alpha=11$ ,  $\beta=30$ ,  $c_{min}=300$ ,  $c_{max}=4000$  [164], and  $c_{s3}=140$ . Figure 3.15-(a) presents the performance when the suspension system is subjected to a C level road profile with velocity 20 m/s, and Figure 3.16-(b) presents those with a D level road profile and velocity 20 m/s. The performance with the mixed skyhook and ADD method is close to that with the proposed nonlinear controller when subjected to a C level road profile, but when the road profile deteriorates to D level, the proposed nonlinear controller has a much better performance than that with the mixed skyhook and ADD method.

A unified comparison between the active forces of the proposed nonlinear controller and the hybrid skyhook and ADD method when subjected to a C level road profile is presented in Figure 3.16. The active force with the proposed nonlinear controller is much smoother than that with the hybrid method, and thus the damping force of the hybrid method at high frequency is larger than the proposed one, which leads to a worse performance at high frequency.

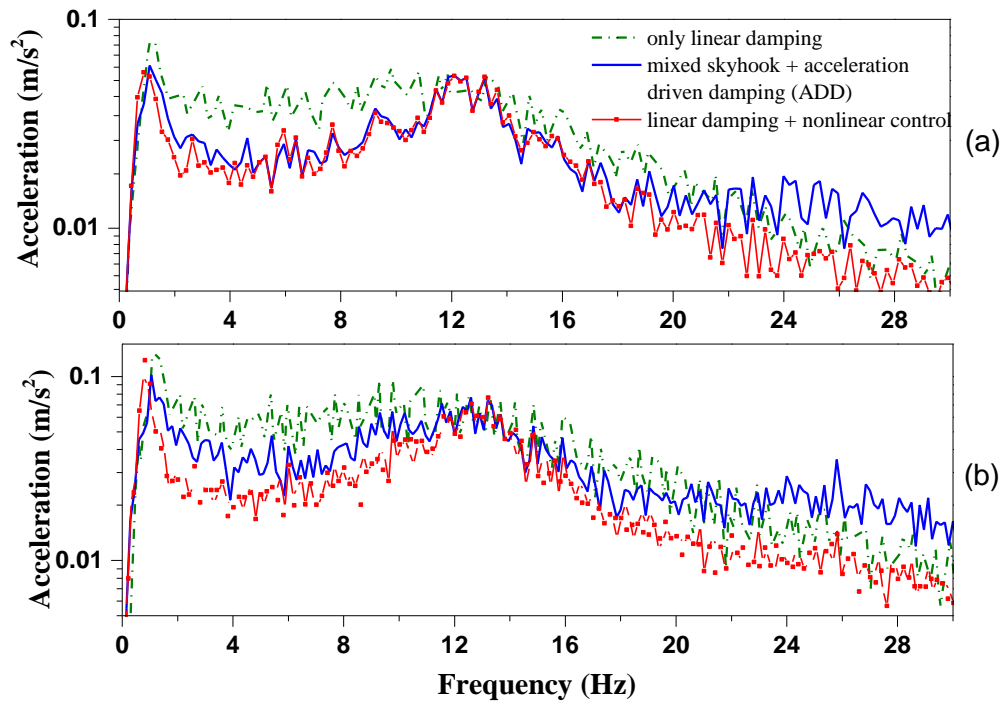


Figure 3.15 Comparison of the performances with different strategies. (a) subjected to C level road profile with 20 m/s, (b) subjected to D level road profile with 20 m/s

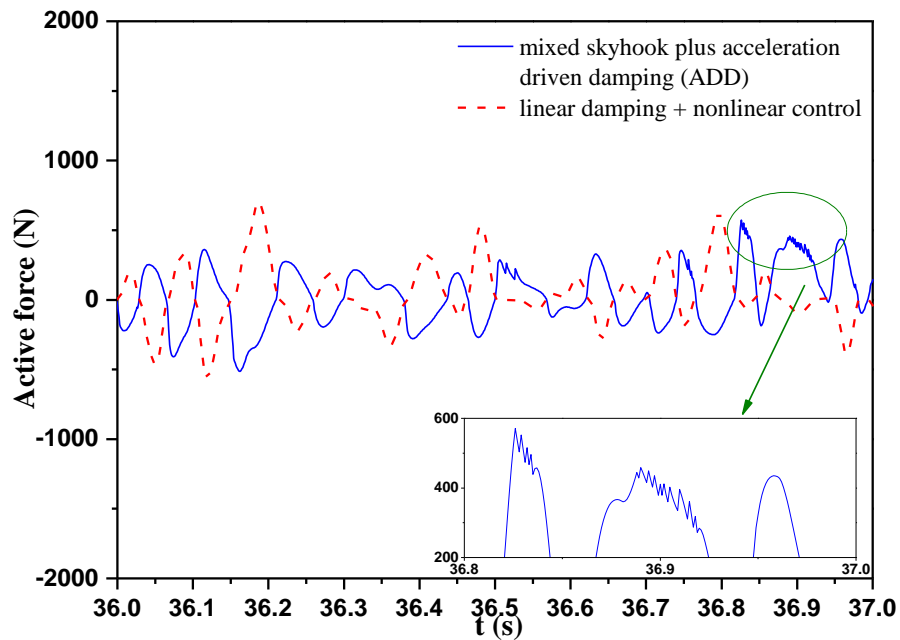


Figure 3.16 Comparison of the active forces

From the results above, the nCOS-based MOP analysis for different excitation inputs indicates clearly that: (1) the proposed nonlinear analysis method provides a

straightforward insight into the nonlinear relationship between the characteristic parameters and system output performance, which can considerably facilitate nonlinear analysis and design and is also computationally efficient; (2) the suspension performance can be effectively improved with the proposed nonlinear acceleration control method, which is much easier to implement than many existing ones; (3) the proposed PBoC can ensure that the system nonlinearity always remains at a Volterra-type level without strong complicated jumping or chaos phenomena.

To provide a straightforward understanding of the proposed nCOS-based MOP analysis method for nonlinear analysis and optimization design in practice, the following general procedure can be followed.

**Algorithm 3.2:**

**Step 1.** Identify the real plant into a NARX model with experimental data. The example in (3.34)-(3.35) shows how to obtain the NARX from a continuous model.

**Step 2.** Determine the characteristic parameters of interest in the design and optimization, e.g., input magnitude or model/controller parameters.

**Step 3.** Compute the PBoC of these characteristic parameters of interest according to Proposition 2.6 to find the parameter ranges to guarantee that the underlying nonlinearity is Volterra-type.

**Step 4.** Determine the nonlinear characteristic output spectrum (nCOS) based multiple-object performance (MOP) function. This can follow Algorithm 3.1.

**Step 5.** Evaluate the MOP function with respect to the characteristic parameters of interest. Examples can be referred to the results in Fig. 3.13-Fig. 3.15

### 3.4 Conclusions

In this chapter, the application of the nCOS method to the analysis and design of nonlinear parameters of interest is shown in two case studies, i.e., the analysis of the proposed nonlinear damping in section 3.2 and the multiple-object optimization of a vehicle suspension in section 3.3. In these two cases, the parametric bound of convergences (PBoC) in Chapter 2 are calculated to guarantee the input-output relationship a convergent Volterra series expansion, which therefore ensure the effectiveness of the nCOS method. Thus, the nCOS method is shown to provide a straightforward insight into the analysis and understanding of the nonlinear systems and also to offer a powerful tool for the design and optimization of nonlinear parameters of interest.

# **4 A new nCOS function for the analysis and design of linear parameters in a nonlinear system**

## **4.1 Introduction**

Many practical systems are inherently nonlinear, for example, a power amplifier [6, 8, 169] or phase lock loop [128]. Nonlinearity often brings difficulties to the analysis and design of these systems. In Chapter 3, it is shown that the nCOS method can significantly facilitate the analysis and design of nonlinear parameters of interest. One weak point of the nCOS method is that it is only applicable to those nonlinear parameters of interest.

A simple linear control or linear component is often preferable in engineering practice for its ease of implementation. How to design linear components and/or how to evaluate the potential influence of linear components or linear feedback control while well considering the inherent system nonlinearity is far from sufficiently investigated in the literature.

In this chapter, a new nCOS function is developed for those linear parameters of interest in a nonlinear system. The linear parameters of interest can be linear components or linear feedback control in engineering practice. The new nCOS function is a significant extension of the existing nCOS method.

In section 4.2, the new nCOS function is developed for a single-input single-output (SISO) nonlinear system. It is shown that the output spectrum of

the nonlinear system can be analytically and explicitly expressed as a polynomial function of those linear parameters of interest. An algorithm for symbolically calculating the coefficients of the new nCOS function is proposed. An example, i.e., the design of linear components in a nonlinear circuit system, is presented to illustrate the application of the proposed new nCOS function.

In section 4.3, the new nCOS function is extended to a multiple-input multiple-output (MIMO) nonlinear system. A numerical algorithm for estimating the coefficients of the new nCOS function is proposed, which can greatly facilitate the application of the new nCOS function to a wide class of engineering practice. Linear feedback control design for a nonlinear vehicle suspension is given as an example to demonstrate the effectiveness of the proposed results.

## 4.2 New nCOS function for linear parameters of interest

The following nonlinear differential equation (NDE) model is considered,

$$\sum_{m=1}^M \sum_{\substack{p=0 \\ p+q=m}}^m \sum_{\substack{L \\ l_1, \dots, l_{p+q}=0}} \bar{c}_{p,q}(l_1, \dots, l_{p+q}) \prod_{i=1}^p \frac{d^{l_i} y(t)}{dt^{l_i}} \prod_{i=p+1}^q \frac{d^{l_i} u(t)}{dt^{l_i}} = 0 \quad (4.1)$$

where  $y(t)$  is the system output,  $u(t)$  is the system input, and  $M$  is the maximum nonlinear order.  $l_i, i=1,2,\dots,p+q$  is the differential order with maximum order  $L$ .  $\bar{c}_{p,q}(l_1, \dots, l_{p+q})$  is the model parameters with nonlinear degree  $p$  in terms of output  $y(t)$  and nonlinear degree  $q$  in terms of input  $u(t)$ .  $\bar{c}_{p,q}(l_1)$  with  $p+q=1$  corresponds to the linear model parameters.

System (4.1) allows a Volterra series expansion of its input-output relationship [48, 51, 53, 56, 170] as

$$y(t) = \sum_{n=1}^{\infty} \int_{-\infty}^{\infty} \dots \int_{-\infty}^{\infty} h_n(\tau_1, \dots, \tau_n) \prod_{i=1}^n u(t - \tau_i) d\tau_i$$

where  $h_n(\tau_1, \dots, \tau_n)$  is the  $n$ th-order Volterra kernel, and  $\tau_i$  is the convolution variable. The input-output relationship can also be expressed in the frequency domain as [70],

$$Y(\Omega) = \sum_{n=1}^{+\infty} \int \dots \int_{\omega_1 + \dots + \omega_n = \Omega} H_n(j\omega_1, \dots, \omega_n) \prod_{i=1}^n U(\omega_i) d\omega_i$$

where  $H_n(j\omega_1, \dots, \omega_n)$  is the  $n$ th-order generalized frequency response function (GFRF) (which is the  $n$ -dimensional Fourier transform of the Volterra kernel  $h_n(\tau_1, \dots, \tau_n)$ ), and  $U(\omega_i)$  is the input spectrum. The  $n$ th-order ( $n \geq 2$ ) GFRF can be calculated as [59, 116]

$$H_n(j\omega_1, \dots, j\omega_n) = \frac{-1}{L_n(\omega_1, \dots, \omega_n)} \sum_{m=p+q=2}^n \sum_{p=0}^m \sum_{(l_1, \dots, l_m)} \left[ \bar{c}_{p,q}(l_1, \dots, l_m) \prod_{i=1}^q (j\omega_{p+i})^{l_{p+i}} H_{n-q,p}(j\omega_1, \dots, j\omega_{n-q}) \right] \quad (4.2)$$

where

$$L_n(\omega_1, \dots, \omega_n) = \sum_{l=0}^L \bar{c}_{1,0}(l) \left( \sum_{i=1}^n j\omega_i \right)^l \quad (4.3)$$

$$H_{n-q,p}(j\omega_1, \dots, j\omega_{n-q}) = \sum_{\substack{r_1, \dots, r_p=1 \\ \sum r_i=n-q}}^{n-q-p+1} \prod_{i=1}^p \left[ \left( \sum_{j=1}^{r_i} \omega_{X_i+j} \right)^{l_i} H_{r_i}(j\omega_{X_i+1}, \dots, j\omega_{X_i+r_i}) \right] \quad (4.4)$$

where  $X_i=r_1+\dots+r_{i-1}$ . In (4.4),  $r_1+\dots+r_p=n$  holds, and thus  $r_i$  is smaller than  $n$ . It is clear from (4.2) that higher-order GFRFs can be recursively calculated from lower-order GFRFs. The first-order GFRF (when all of the nonlinear model parameters equal 0, i.e.,  $c_{p,q}(\cdot)=0$  with  $p+q \geq 2$ ) is given as,

$$H_1(j\omega_1) = - \frac{\sum_{l=0}^L \bar{c}_{0,1}(l) (j\omega_1)^l}{L_1(j\omega_1)} \quad (4.5)$$

For convenience in discussion, denote the linear parameters of (4.1) as two parts, i.e.,

$$\bar{c}_{p,q}(l) = \hat{c}_{p,q}(l) + c_{p,q}(l), \quad p+q=1, \quad l=0,1,\dots,L$$

where  $\hat{c}_{1,0}(l)$  and  $\hat{c}_{0,1}(l)$  denote those existing system inherent linear components or those linear components of no interest, and  $c_{1,0}(l)$  and  $c_{0,1}(l)$  are linear parameters to be analysed and designed (introduced by the linear feedback control or linear circuit components). Moreover, denote  $\boldsymbol{\alpha} = [\alpha_1 \alpha_2 \dots \alpha_L]$ ,  $\boldsymbol{\beta} = [\beta_1 \beta_2 \dots \beta_L]$ ,  $\alpha_l, \beta_l \in \mathbb{N}^+$ ,  $l=0, \dots, L$ .  $\boldsymbol{\omega}_n = [\omega_1 \omega_2 \dots \omega_n]$ . Let  $c^{\boldsymbol{\alpha}, \boldsymbol{\beta}} = \prod_{l=0}^L c_{1,0}^{\alpha_l}(l) c_{0,1}^{\beta_l}(l)$ , which involves only those linear parameters of interest.

### 4.2.1 Explicit polynomial relationship between GFRFs and those linear parameters of interest

**Proposition 4.1:** If  $|\hat{L}_n^{-1}(\boldsymbol{\omega}_n)\delta(\boldsymbol{\omega}_n)| < 1$ ,  $\delta(\boldsymbol{\omega}_n) = \sum_{l=0}^L c_{1,0}(l)(j\omega_1 + \dots + j\omega_n)^l$ , then the following equation holds,

$$L_n^{-1}(\boldsymbol{\omega}_n) = \varphi_n^{0,0}(\boldsymbol{\omega}_n) + \sum_{\alpha_0 + \dots + \alpha_L = 1}^{\infty} \varphi_n^{\alpha,0}(\boldsymbol{\omega}_n) c^{\alpha,0} \quad (4.6)$$

where

$$\varphi_n^{\alpha,0}(\boldsymbol{\omega}_n) = (-1)^{\sum_{l=0}^L \alpha_l} \left[ \hat{L}_n^{-1}(\boldsymbol{\omega}_n) \right]_{l=0}^{\sum_{l=0}^L \alpha_l + 1} (j\omega_1 + \dots + j\omega_n)^{\sum_{l=0}^L l \times \alpha_l} \quad (4.7)$$

$$\varphi_n^{0,0}(\boldsymbol{\omega}_n) = \hat{L}_n^{-1}(\boldsymbol{\omega}_n) = \frac{1}{\sum_{l=0}^L \hat{c}_{1,0}(l)(j\omega_1 + \dots + j\omega_n)^l} \quad (4.8)$$

**Proof:** From (4.3),  $L_n^{-1}(\boldsymbol{\omega}_n) = \hat{L}_n^{-1}(\boldsymbol{\omega}_n) \sum_{i=0}^{\infty} [\hat{L}_n^{-1}(\boldsymbol{\omega}_n)\delta(\boldsymbol{\omega}_n)]^i$ .  $[\delta(\boldsymbol{\omega}_n)]^i = \left[ \sum_{l=0}^L c_{1,0}(l)(j\omega_1 + \dots + j\omega_n)^l \right]^i = \prod_{l=0}^L c_{1,0}^{\alpha_l}(l)(j\omega_1 + \dots + j\omega_n)^{l \times \alpha_l}$  where  $\alpha_1 + \dots + \alpha_L = i$ . This completes the proof.  $\square$

**Remark 4.1:** From (4.7) and (4.8), it is clear that  $\varphi_n^{\alpha,0}(\boldsymbol{\omega}_n)$  only involves those linear parameters of no interest, i.e.,  $\hat{c}_{1,0}(l)$ , so it is independent of those linear parameters to be analysed and designed,  $c_{1,0}(l)$ .  $c^{\alpha,0} = \prod_{l=0}^L c_{1,0}^{\alpha_l}(l)$  only involves those linear parameters of interest.

**Proposition 4.2:** The first-order GFRF of system (4.1) can be given as a polynomial function with respect to the linear parameters of interest as

$$H_1(\omega_1) = \theta_1^{0,0}(\omega_1) + \sum_{\substack{\alpha_0 + \dots + \alpha_L + s_{\beta} = 1, \beta_0 + \dots + \beta_L = 0 \\ s_{\beta} \leq 1}}^{\infty} \sum_{\beta}^{s_{\beta}} \theta_1^{\alpha,\beta}(\omega_1) c^{\alpha,\beta} \quad (4.9)$$

where

$$\theta_1^{\mathbf{a},\mathbf{\beta}}(\omega_1) = -\varphi^{\mathbf{a},\mathbf{0}}(\omega_1) \sum_{l=0}^L \left[ \hat{c}_{0,1}^{1-\beta_l}(l) (j\omega_1)^l \right] \quad (4.10)$$

and  $\theta_1^{\mathbf{0},\mathbf{0}}(\omega_1) = -\varphi^{\mathbf{0},\mathbf{0}}(\omega_1) \sum_{l=0}^L \bar{c}_{0,1}(l) (j\omega_1)^l$  is the first-order GFRF when all of the linear parameters of interest are 0.

**Proof:** Substituting (4.6) into (4.5), the result in Proposition 4.2 is straightforward.  $\square$

For higher-order GFRFs ( $n \geq 2$ ), the following proposition holds:

**Proposition 4.3:** The GFRFs of system (4.1) with order  $n \geq 2$  can also be expressed in the form of a polynomial function with respect to those linear parameters of interest,

$$H_n(\omega_n) = \theta_n^{\mathbf{0},\mathbf{0}}(\omega_n) + \sum_{\substack{\alpha_0 + \dots + \alpha_L + s_\beta = 1, \beta_0 + \dots + \beta_L = 0 \\ s_\beta \leq n}}^{\infty} \sum_{s_\beta}^{\beta_\beta} \theta_n^{\mathbf{a},\mathbf{\beta}}(\omega_n) c^{\mathbf{a},\mathbf{\beta}} \quad (4.11)$$

where

$$\theta_n^{\mathbf{a},\mathbf{\beta}}(\omega_n) = \sum_{\substack{\alpha_1^\varphi + \alpha_1^\beta = \alpha_1 \\ \vdots \\ \alpha_L^\varphi + \alpha_L^\beta = \alpha_L}} \varphi_n^{\mathbf{a}^\varphi, \mathbf{0}}(\omega_n) b_n^{\mathbf{a}^\beta, \mathbf{\beta}}(\omega_n) \quad (4.12)$$

$\alpha^\varphi = [\alpha_1^\varphi \alpha_2^\varphi \dots \alpha_L^\varphi]$  and  $\alpha^\beta = [\alpha_1^\beta \alpha_2^\beta \dots \alpha_L^\beta]$  denote the nonlinear orders of  $c_{1,0}(l)$  in  $\varphi_n(\omega_n)$  and  $b_n(\omega_n)$ , respectively.

$$b_n^{\mathbf{a},\mathbf{\beta}}(\omega_n) = \sum_{p+q=2}^n \sum_{p=0}^n \sum_{(l_1, l_2, \dots, l_{p+q})} \left[ -\bar{c}_{p,q}(l_1, \dots, l_{p+q}) \prod_{i=1}^q (j\omega_{n-q+i})^{l_{p+i}} d_{n-q,p}^{\mathbf{a},\mathbf{\beta}}(\omega_{n-q}) \right] \quad (4.13)$$

and

$$d_{n-q,p}^{\mathbf{a},\mathbf{\beta}}(\omega_{n-q}) = \sum_{\substack{\gamma_1 + \dots + \gamma_p = n-q, \alpha_1^1 + \dots + \alpha_1^p = \alpha_1 \\ \gamma_1, \dots, \gamma_p \geq 1 \\ \vdots \\ \alpha_L^1 + \dots + \alpha_L^p = \alpha_L \\ \beta_1^1 + \dots + \beta_1^p = \beta_1 \\ \vdots \\ \beta_L^1 + \dots + \beta_L^p = \beta_L}} \sum \prod_{i=1}^p \left[ \theta_{\gamma_i}^{\mathbf{a}^i, \mathbf{\beta}^i}(\omega_{X_i}) \left( \sum_{k=1}^{\gamma_i} \omega_{X_i+k} \right)^{\gamma_i} \right] \quad (4.14)$$

where  $\alpha^i = [\alpha_1^i \alpha_2^i \dots \alpha_L^i]$  and  $\beta^i = [\beta_1^i \beta_2^i \dots \beta_L^i]$  are the nonlinear orders of

$\theta_{\gamma_i}(\boldsymbol{\omega}_{X_i})$ ,  $\boldsymbol{\omega}_{X_i} = [\omega_{X_i+1}, \dots, \omega_{X_i+\gamma_i}]$ ,  $X_i = \gamma_1 + \dots + \gamma_{i-1}$  for  $i \geq 2$ , and  $X_1 = 0$ .

**Proof:** In this proof, we first assume that Proposition 4.3 holds for all of the  $n$ th-order GFRFs with  $n < n_0$ , and it is then shown that Proposition 4.3 also holds for  $n = n_0$ .

First,  $d_{n-q,p}^{\alpha,\beta}(\boldsymbol{\omega}_{n-q})$  in (4.14) is derived, and then  $b_n^{\alpha,\beta}(\boldsymbol{\omega}_n)$  in (4.13) is demonstrated. Based on these results,  $\theta_n^{\alpha,\beta}(\boldsymbol{\omega}_n)$  in (4.12) can be obtained, and thus, the  $n$ th-order GFRF in (4.11) is then straightforward to derive. Details are given in Appendix 4.1.  $\square$

**Remark 4.2:**  $\theta_1^{0,0}(\omega_1)$  and  $\theta_n^{0,0}(\omega_n)$  in (4.9) and (4.11) are the GFRFs when all of the linear parameters of interest, i.e.,  $c_{1,0}(l)$  and  $c_{0,1}(l)$ , are 0. The coefficients  $\theta_n^{\alpha,\beta}(\omega_n)$  for  $n=1,2,\dots$  only involve those parameters of no interest, so they are independent of the linear parameters to be analysed and designed, i.e.,  $c_{1,0}(l)$  and  $c_{0,1}(l)$ .

**Remark 4.3:** The GFRFs in (4.9) and (4.11) are given as polynomial function with respect to the linear parameters of interest i.e.,  $c_{1,0}(l)$  and  $c_{0,1}(l)$ . How those linear parameters of interest act on the  $n$ th-order GFRF is then straightforward. Note that those existing relationships between the  $n$ th-order GFRF and the linear parameters in (4.2)-(4.5) involve complicated recursive calculations, so the polynomial functions in (4.9) and (4.11) provide a very straightforward and explicit expression.

**Remark 4.4:** Once the coefficients,  $\theta_n^{\alpha,\beta}(\omega_n)$ , have been calculated, the effects of the different linear parameters of interest on the  $n$ th-order GFRF can all be

obtained via (4.11), and no additional recursive calculation is needed. When recursive computation via (4.2)-(4.5) is adopted, the first-order GFRF should be computed again via (4.5) if the linear parameters of interest change, and then new recursive calculations (4.2)-(4.4) are required. These show the computation efficiency of the results in (4.9) and (4.11).

The following procedure is developed for computing the coefficients  $\theta_n^{\alpha,\beta}(\omega_n)$ :

**Algorithm 4.1: Calculation of coefficients for the  $n$ th-order GFRF**

**Step 1.** Calculate  $\varphi_n^{\alpha,0}(\omega_n)$  and  $\varphi_n^{0,0}(\omega_n)$  via (4.7) and (4.8), respectively.

**Step 2.** Calculate  $\theta_1^{\alpha,\beta}(\omega_1)$  via (4.10) for the first-order GFRF.

**Step 3.** For  $n \geq 2$ , calculate  $d_{n-q,p}^{\alpha,\beta}(\omega_{n-q})$  and  $b_n^{\alpha,\beta}(\omega_n)$  via (4.14) and (4.13), respectively.

**Step 4.** Calculate  $\theta_n^{\alpha,\beta}(\omega_n)$  via (4.12).

Following Algorithm 4.1, the developed characteristic relationship between the  $n$ th-order GFRF and the linear parameters of interest in (4.11) is ready for analysis and design with different linear parameters of interest.

**4.2.2 Nonlinear characteristic output spectrum (nCOS) function with respect to linear parameters of interest**

The analytical and explicit polynomial relationship shown in Proposition 4.1-4.3 provides a straightforward and effective way to study the effects of the linear parameters of interest on the  $n$ th-order GFRF. Note that the GFRFs,

together with the input spectrum, determine the output spectrum of the system, and how those linear parameters of interest affect the nonlinear output spectrum can then be investigated based on the results in section 4.2.1.

**Proposition 4.4:** The nonlinear output spectrum of system (4.1) can be given as a polynomial function with respect to the linear parameters of interest as

$$Y(\omega) = \psi^{0,0}(\omega) + \sum_{\alpha_0 + \dots + \alpha_L + s_\beta = 1}^{\infty} \sum_{\beta_0 + \dots + \beta_L = 0}^{s_\beta} \psi^{\alpha,\beta}(\omega) c^{\alpha,\beta} \quad (4.15)$$

where

$$\psi^{\alpha,\beta}(\omega) = \sum_{\substack{n=1, \\ s_\beta \leq n}}^N \int \dots \int_{\omega = \omega_1 + \dots + \omega_n} \theta_n^{\alpha,\beta}(\omega_n) \prod_{i=1}^n U(\omega_i) d\omega_i \quad (4.16)$$

$N$ , here, is the truncation order. Clearly, the coefficients  $\psi^{\alpha,\beta}(\omega)$  in (4.15) are also independent of those linear parameters of interest.  $\psi^{0,0}(\omega)$  is the case in which all of the linear parameters of interest are 0.

**Proof:**

$$\begin{aligned} Y(\omega) &= \sum_{n=1}^N \int \dots \int_{\omega_1 + \dots + \omega_n = \omega} H_n(j\omega_1, \dots, \omega_n) \prod_{i=1}^n U(\omega_i) d\omega_i \\ &= \sum_{n=1}^N \int \dots \int_{\omega_1 + \dots + \omega_n = \omega} \sum_{\substack{\alpha_0 + \dots + \alpha_L + s_\beta = 0, \\ s_\beta \leq n}}^{\infty} \sum_{\beta_0 + \dots + \beta_L = 0}^{s_\beta} \theta_n^{\alpha,\beta}(\omega_n) c^{\alpha,\beta} \prod_{i=1}^n U(\omega_i) d\omega_i \\ &= \sum_{\alpha_0 + \dots + \alpha_L + s_\beta = 0, \beta_0 + \dots + \beta_L = 0}^{\infty} \sum_{s_\beta = 0}^{s_\beta} \left[ \sum_{\substack{n=1 \\ s_\beta \leq n}}^N \int \dots \int_{\omega_1 + \dots + \omega_n = \omega} \theta_n^{\alpha,\beta}(\omega_n) \prod_{i=1}^n U(\omega_i) d\omega_i \right] c^{\alpha,\beta} \\ &= \sum_{\alpha_0 + \dots + \alpha_L + s_\beta = 0, \beta_0 + \dots + \beta_L = 0}^{\infty} \sum_{s_\beta = 0}^{s_\beta} \psi^{\alpha,\beta}(\omega) c^{\alpha,\beta} \end{aligned}$$

This completes the proof.  $\square$

**Algorithm 4.2:** Calculation of coefficients for the  $n$ th-order nonlinear output

## spectrum

**Step. 1** Calculate coefficients  $\theta_n^{\alpha,\beta}(\omega_n)$  for the  $n$ th-order GFRF via Algorithm 4.1.

**Step. 2** Calculate coefficients  $\Psi^{\alpha,\beta}(\omega)$  via (4.16) for the  $n$ th-order output spectrum.

**Remark 4.5:** The relationship between the nonlinear output spectrum and the linear parameters of interest in Proposition 4.4 is referred to as the nonlinear characteristic output spectrum (nCOS). Proposition 4.4 still has the following advantages: 1. a more straightforward and explicit relationship between the nonlinear output spectrum and the linear parameters of interest, 2. the coefficients of the polynomial function, i.e.,  $\Psi^{\alpha,\beta}(\omega)$ , are independent of those linear parameters of interest, 3. high computational efficiency (especially when a higher truncation order is required for the nonlinear output spectrum), 4. ease of application by symbolic calculation (via Algorithm 4.1-4.2). The results above can greatly facilitate the analysis and design of linear parameters.

**Remark 4.6:** The computation of the coefficients via (4.16) is available for various inputs, for example, harmonic inputs, multiple inputs, random inputs.

**Remark 4.7:** The nonlinear characteristic output spectrum (nCOS) built in (4.15) is a polynomial function of those linear parameters of interest (to design) and is an important extension of the method established in [92, 95, 113, 115].

### 4.2.3 Examples and discussion

#### Example 4.1: Effects of linear parameters of interest on the $n$ th-order GFRFs.

In Fig. 4.1, a current source with conductance  $1/R_s$  and susceptance  $1/j\omega L$  acts on a common-gate amplifier. The drain current  $i_{out}$  can be modelled as

$$y = i_{out} = g_1 v_{gs} + g_2 v_{gs}^2 + g_3 v_{gs}^3$$

where  $v_{gs}$  is the gate-to-source voltage. A capacitor is introduced to suppress the harmonic distortion of the amplifier.  $v_{gs} = -v_s$ , and denote  $x = v_s$ , which is governed by

$$C_{gs} \ddot{x} + \left(\frac{1}{R_s} + g_1\right) \dot{x} + \frac{1}{L} x - \frac{1}{R_s} \dot{u} - 2g_2 x \dot{x} + 3g_3 x^2 \dot{x} + C \ddot{x} = 0$$

where  $\hat{c}_{1,0}(2) = C_{gs}$ ,  $\hat{c}_{1,0}(1) = 1/R_s + g_1$ ,  $\hat{c}_{1,0}(0) = 1/L$ ,  $\hat{c}_{0,1}(1) = -1/R_s$ ,  $\bar{c}_{2,0}(0,1) = -2g_2$ , and  $\bar{c}_{3,0}(0,0,1) = 3g_3$ . Only one linear parameter is of interest in this case study, i.e.,  $c_{1,0}(2) = C$ .

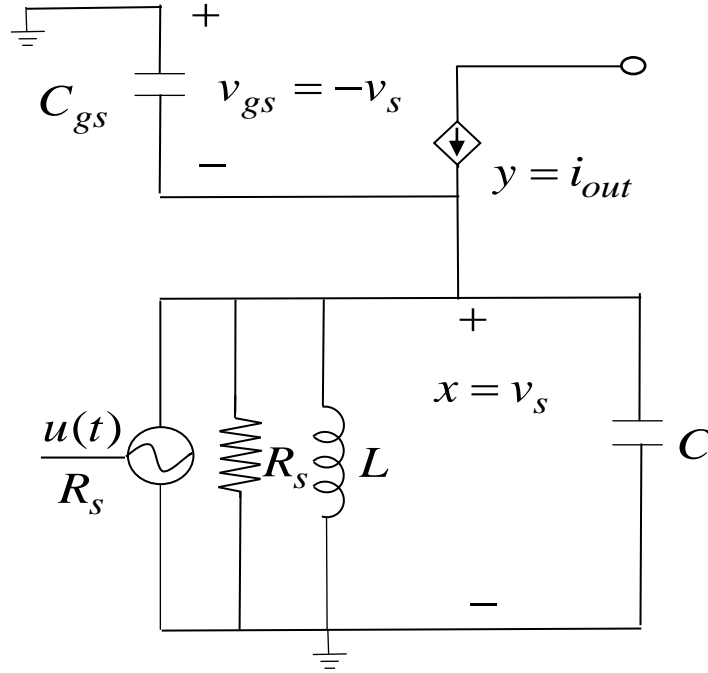


Figure 4.1 The equivalent circuit model of a common-gate amplifier

In the following, the parameters are borrowed from [7] with a 65nm CMOS process as,  $C_{gs}=500$  fF,  $g_1=7.3$  mS,  $g_2=0.0598$  S/V,  $g_3=0.2628$  S/V<sup>2</sup>,  $R_s=50$   $\Omega$ ,  $L=4$   $\mu$ H,  $u(t)=U\sin(2\pi ft)$ , and  $f=5$  MHz.

In this case study, only the linear parameter  $c_{1,0}(2)$ , the capacitance, is of interest as an example to show the results, so that  $\alpha = [00\alpha_2]$ ,  $\beta = \mathbf{0}$ . For convenience in the following study, the notation  $\alpha, \beta$  is simplified as  $\alpha_2$ , where  $\alpha_2$  denotes the nonlinear order of the linear parameter  $c_{1,0}(2)$ .

Following Algorithm 4.1,  $\varphi_n^{\alpha,0}(\omega_n)$  and  $\varphi_n^{0,0}(\omega_n)$  should be calculated first. According to (4.8),

$$\varphi_1^0(\omega_1) = \hat{c}_{1,0}(2)(j\omega_1)^2 + \hat{c}_{1,0}(1)(j\omega_1) + \hat{c}_{1,0}(0).$$

From (4.7),

$$\varphi_1^1(\omega_1) = -1 \times (\varphi_1^0(\omega_1))^2 (j\omega_1)^2,$$

$$\varphi_1^2(\omega_1) = (\varphi_1^0(\omega_1))^3 (j\omega_1)^4,$$

$$\varphi_1^3(\omega_1) = -1 \times (\varphi_1^0(\omega_1))^4 (j\omega_1)^6, \text{ and}$$

$$L_1^{-1}(\omega_1) = \varphi_1^0(\omega_1) + \varphi_1^1(\omega_1)c_{1,0}(2) + \varphi_1^2(\omega_1) \left(c_{1,0}(2)\right)^2 + \dots$$

For the first-order GFRF, according to (4.10),

$$\theta_1^0(\omega_1) = -\varphi_1^0(\omega_1)\hat{c}_{1,0}(1)(j\omega_1),$$

$$\theta_1^1(\omega_1) = -\varphi_1^1(\omega_1)\hat{c}_{1,0}(1)(j\omega_1),$$

$$\theta_1^2(\omega_1) = -\varphi_1^2(\omega_1)\hat{c}_{1,0}(1)(j\omega_1), \dots$$

From (4.9),

$$H_1(\omega_1) = \theta_1^0(\omega_1) + \theta_1^1(\omega_1)c_{1,0}(2) + \theta_1^2(\omega_1) \left(c_{1,0}(2)\right)^2 + \dots$$

Table 4.1 Coefficients  $\theta_1^{\alpha_2}(\omega_1)$  at  $\omega_1 = 2\pi \times 5 \times 10^6 \text{ rad/s}$

$\alpha_2$	$\theta_1^{\alpha_2}(\omega_1)$	$\alpha_2$	$\theta_1^{\alpha_2}(\omega_1)$
0	0.6748 +0.1961i	1	4.1561e+08 -6.5479e+08i
2	-5.6602e+17 -6.4217e+17i	3	-8.5496e+26 +4.0215e+26i
4	1.6293e+35 +1.0300e+36i		

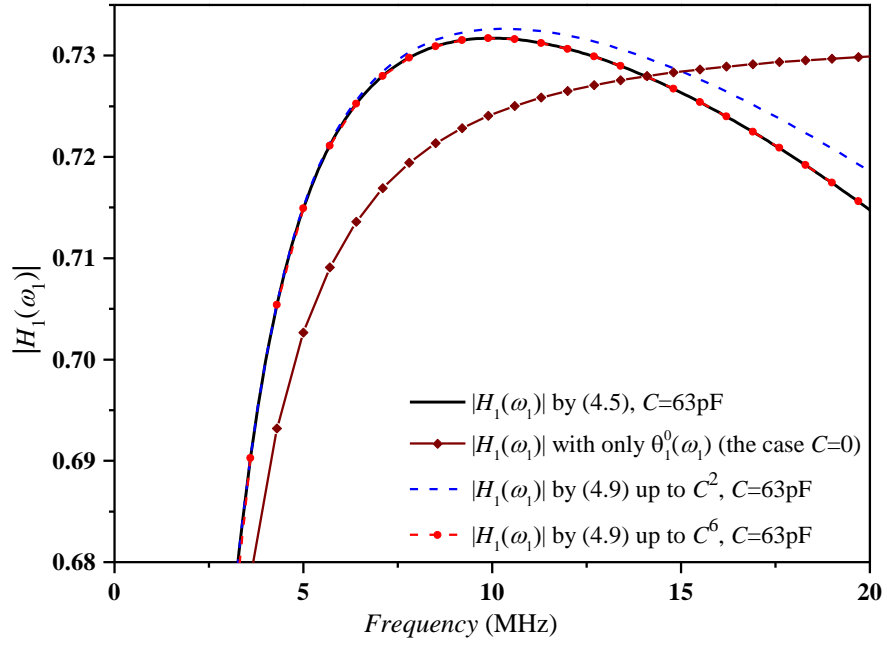


Figure 4.2 Validation of Proposition 4.2 with  $c_{1,0}(2)=C=63\text{pF}$ . 63pF is adopted here because it is the optimal value for the suppression of the harmonic distortion in example 2.

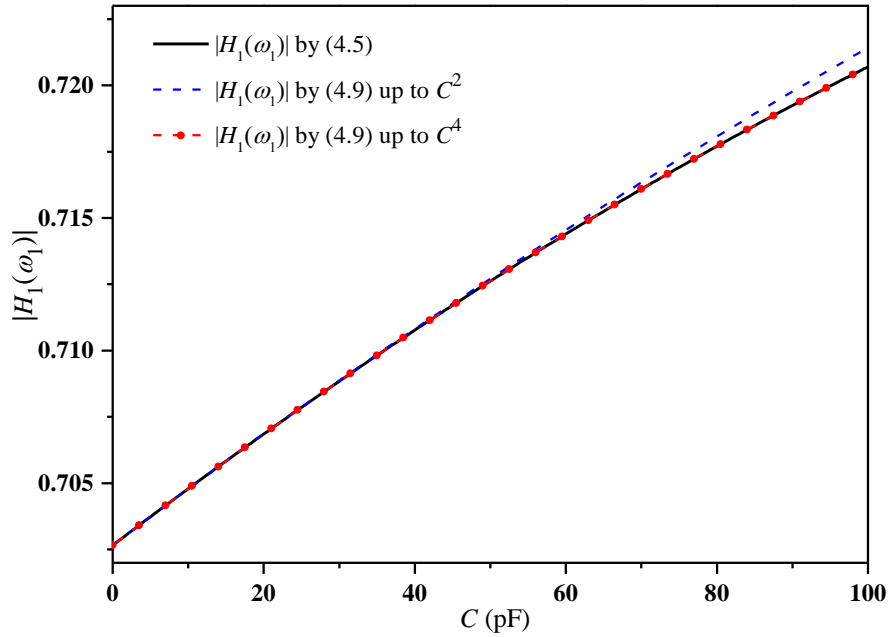


Figure 4.3 Magnitude of  $H_1(\omega_1)$  with different capacitance values at  $\omega_1 = 2\pi \times 5 \times 10^6 \text{ rad/s}$

Fig. 4.2 shows the first-order GFRF, i.e.,  $H_1(\omega_1)$ , with different frequency variables, and Fig. 4.3 presents  $H_1(\omega_1)$  with different introduced capacitance  $C$  values, having the coefficients calculated at  $\omega_1 = 2\pi \times 5 \times 10^6 \text{ rad/s}$  shown in

table 4.1. From these two figures, it can be observed that as the truncated order of capacitance  $C$  increases,  $H_1(\omega_1)$  calculated by (4.9) quickly converges to that by direct application of the existed result via (4.5), which verifies the effectiveness of the results in Proposition 4.2. From the above calculation, the advantage shown in Remark 4.2 can be observed, that is, the coefficients  $\theta_1^1(\omega_1), \theta_1^2(\omega_1), \dots$  are independent of the linear parameters of interest. Those advantages in Remark 4.3 and Remark 4.4 will be more obvious when higher-order GFRFs are considered, for example,  $H_3(\omega_1, \omega_2, \omega_3)$ .

For the third-order GFRF,  $H_3(\omega_1, \omega_2, \omega_3)$ , according to step 3 in Algorithm 4.1,  $d_{3,2}^{\alpha_2}(\omega_3)$  and  $d_{3,3}^{\alpha_2}(\omega_3)$  should be calculated first.

$$d_{3,2}^0(\omega_3) = (j\omega_2 + j\omega_3)\theta_1^0(\omega_1)\theta_2^0(\omega_2, \omega_3) + (j\omega_3)\theta_2^0(\omega_1, \omega_2)\theta_1^0(\omega_3),$$

$$d_{3,2}^1(\omega_3) = (j\omega_2 + j\omega_3)\theta_1^0(\omega_1)\theta_2^1(\omega_2, \omega_3) + (j\omega_2 + j\omega_3)\theta_1^1(\omega_1)\theta_2^0(\omega_2, \omega_3) +$$

$$(j\omega_3)\theta_2^0(\omega_1, \omega_2)\theta_1^1(\omega_3) + (j\omega_3)\theta_2^1(\omega_1, \omega_2)\theta_1^0(\omega_3),$$

$$d_{3,2}^2(\omega_3) = (j\omega_2 + j\omega_3)\theta_1^0(\omega_1)\theta_2^2(\omega_2, \omega_3) + (j\omega_2 + j\omega_3)\theta_1^1(\omega_1)\theta_2^1(\omega_2, \omega_3) +$$

$$(j\omega_2 + j\omega_3)\theta_1^2(\omega_1)\theta_2^0(\omega_2, \omega_3) + (j\omega_3)\theta_2^0(\omega_1, \omega_2)\theta_1^2(\omega_3) +$$

$$(j\omega_3)\theta_2^1(\omega_1, \omega_2)\theta_1^1(\omega_3) + (j\omega_3)\theta_2^2(\omega_1, \omega_2)\theta_1^0(\omega_3),$$

...

Similarly, according to (4.14),

$$d_{3,3}^0(\omega_3) = (j\omega_3)\theta_1^0(\omega_1)\theta_1^0(\omega_2)\theta_1^0(\omega_3),$$

$$d_{3,3}^1(\omega_3) = (j\omega_3)\theta_1^1(\omega_1)\theta_1^0(\omega_2)\theta_1^0(\omega_3) + (j\omega_3)\theta_1^0(\omega_1)\theta_1^1(\omega_2)\theta_1^0(\omega_3) +$$

$$(j\omega_3)\theta_1^0(\omega_1)\theta_1^0(\omega_2)\theta_1^1(\omega_3),$$

$$d_{3,3}^2(\omega_3) = (j\omega_3)\theta_1^2(\omega_1)\theta_1^0(\omega_2)\theta_1^0(\omega_3) + (j\omega_3)\theta_1^0(\omega_1)\theta_1^2(\omega_2)\theta_1^0(\omega_3) +$$

$$(j\omega_3)\theta_1^0(\omega_1)\theta_1^0(\omega_2)\theta_1^2(\omega_3) + (j\omega_3)\theta_1^1(\omega_1)\theta_1^1(\omega_2)\theta_1^0(\omega_3) + \\ (j\omega_3)\theta_1^1(\omega_1)\theta_1^0(\omega_2)\theta_1^1(\omega_3) + (j\omega_3)\theta_1^0(\omega_1)\theta_1^1(\omega_2)\theta_1^1(\omega_3) \dots$$

Then  $b_3^{\alpha_2}(\omega_3)$  can be calculated according to (4.13) as,

$$b_3^0(\omega_3) = -\bar{c}_{2,0}(0,1)d_{3,2}^0(\omega_3) - \bar{c}_{3,0}(0,0,1)d_{3,3}^0(\omega_3),$$

$$b_3^1(\omega_3) = -\bar{c}_{2,0}(0,1)d_{3,2}^1(\omega_3) - \bar{c}_{3,0}(0,0,1)d_{3,3}^1(\omega_3), \dots$$

Finally, the coefficients  $\theta_n^{\alpha,\beta}(\omega_n)$  can be calculated in a straightforward manner according to (4.12) as

$$\theta_3^0(\omega_3) = \varphi_3^0(\omega_3)b_3^0(\omega_3),$$

$$\theta_3^1(\omega_3) = \varphi_3^0(\omega_3)b_3^1(\omega_3) + \varphi_3^1(\omega_3)b_3^0(\omega_3),$$

$$\theta_3^2(\omega_3) = \varphi_3^0(\omega_3)b_3^2(\omega_3) + \varphi_3^1(\omega_3)b_3^1(\omega_3) + \varphi_3^2(\omega_3)b_3^0(\omega_3) \dots$$

and

$$H_3(\omega_3) = \theta_3^0(\omega_3) + \theta_3^1(\omega_3)c_{1,0}(2) + \theta_3^2(\omega_3) \left( c_{1,0}(2) \right)^2 + \dots$$

Table 4.2 Coefficients of  $\theta_3^{\alpha_2}(\omega_3)$

$\alpha_2$	$\theta_3^{\alpha_2}(\omega_3)$	$\alpha_2$	$\theta_3^{\alpha_2}(\omega_3)$
0	-0.4280 +0.2060i	1	7.8371e+09 +5.9585e+08i
2	3.2996e+18 -6.7376e+19i	3	-3.7399e+29 -5.3968e+28i
4	-4.4446e+38 +1.6680e+39i		

From the computation of the third-order GFRF,  $H_3(\omega_1, \omega_2, \omega_3)$ , above, it is clear that the coefficients of the polynomial function in (4.11),  $\theta_3^{\alpha_2}(\omega_3)$ , are independent of the linear parameter of interest  $c_{1,0}(2) = C$ . Thus, once the

coefficients  $\theta_3^{\alpha_2}(\boldsymbol{\omega}_3)$  have been calculated,  $H_3(\omega_1, \omega_2, \omega_3)$  with different linear parameters of interest can all be obtained, and no additional recursive calculation is required (each of the coefficients require only one calculation), which shows an obvious advantage over that by recursive calculation via (4.2)-(4.4). In the latter case, once the linear parameter of interest changes, new recursive computations are required. The recursive calculation in (4.2)-(4.4) not only makes the computation of higher-order GFRFs less efficient but also causes an inexplicit relationship between the higher-order GFRF and the linear parameters of interest. The relationship built in (4.11) in the form of a power series is more straightforward and explicit. The coefficients  $\theta_3^{\alpha_2}(\boldsymbol{\omega}_3)$  are shown in table 4.2, and from Fig. 4.4 it can be observed that the 4th truncation order is enough for the characteristic relationship between the  $n$ th-order GFRF and the linear parameters of interest.

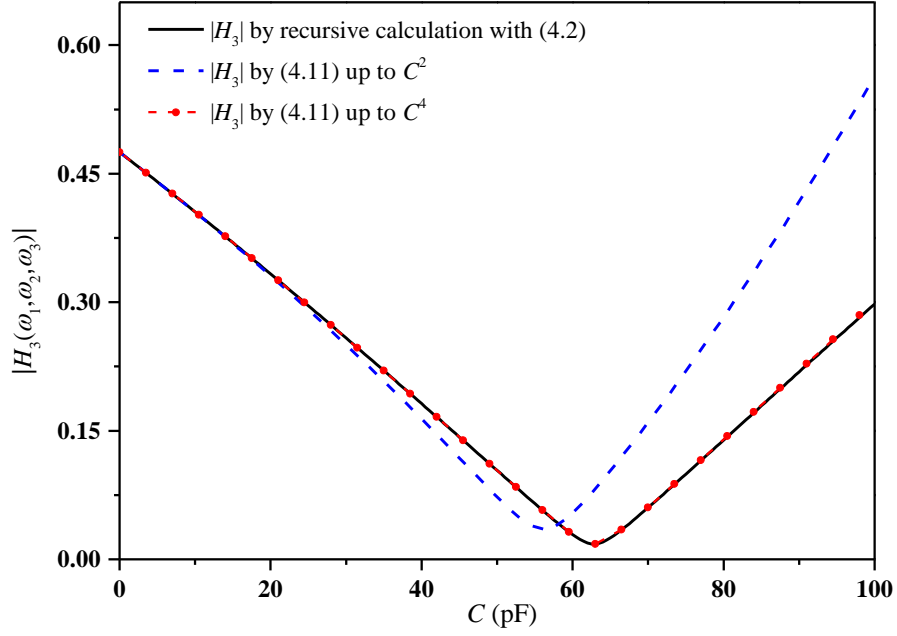


Figure 4.4 Magnitude of  $H_3(\omega_1, \omega_2, \omega_3)$  with different capacitance values at  $\omega_1 = \omega_2 = \omega_3 = 2\pi \times 5 \times 10^6 \text{ rad / s}$

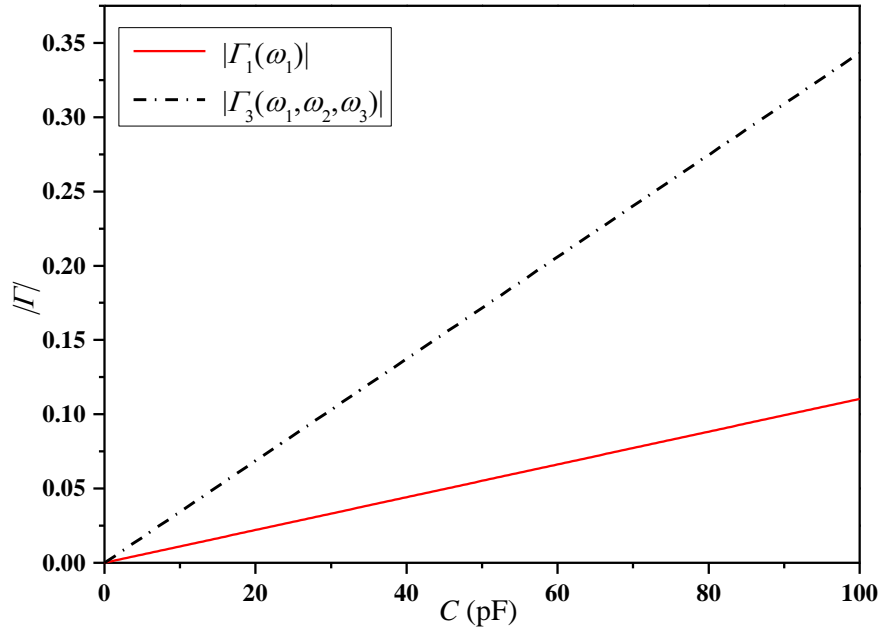


Figure 4.5  $\Gamma_1 = |\hat{L}_1^{-1}(\omega_1)\delta(\omega_1)|$  and  $\Gamma_3 = |\hat{L}_3^{-1}(\omega_3)\delta(\omega_3)|$

The validation of Proposition 4.1-4.3 in Fig. 4.2-4.4 requires that  $|\hat{L}_n^{-1}(\omega_n)\delta(\omega_n)| < 1$  holds. For the first-order GFRF and the third-order GFRF,

it is shown in Fig. 4.5 that the linear parameter of interest satisfies this condition.

**Example 4.2: Optimal suppression of the harmonic distortion of the common-gate amplifier.**

The third-order harmonic distortion is defined as  $HD_3 = |Y(3\Omega)|/|Y(\Omega)|$ , where  $Y(\Omega)$  and  $Y(3\Omega)$  are the output spectra at frequencies  $\Omega$  and  $3\Omega$ , respectively. First, the response of the voltage  $x = v_s$  is required. According to Proposition 4.2, the output spectrum can be calculated in the form of a polynomial function as  $X(\omega) = \Psi_x^0(\omega) + \Psi_x^1(\omega)c_{1,0}(2) + \Psi_x^2(\omega)(c_{1,0}(2))^2 + \dots$ , with the coefficients  $\Psi_x^{\alpha_2}(\omega)$  independent of the linear parameters of interest. Similar to the case in example 4.1, the notation  $\alpha, \beta$  is simplified as  $\alpha_2$  for convenience. Then, the output spectrum of the current  $y = i_{out}$  can be computed as

$$Y(\omega) = \Psi_y^0(\omega) + \Psi_y^1(\omega)c_{1,0}(2) + \Psi_y^2(\omega)(c_{1,0}(2))^2 + \dots$$

where  $\Psi_y^0(\omega) = U(\omega)/R_s + (j\omega C_{gs} + 1/j\omega L + 1/R_s)\Psi_x^0(\omega)$  ,  $\Psi_y^{\alpha_2}(\omega) = (j\omega C_{gs} + 1/j\omega L + 1/R_s)\Psi_x^{\alpha_2}(\omega) + (j\omega)\Psi_x^{\alpha_2-1}(\omega)$ ,  $\alpha_2 > 1$ .

Once the coefficients  $\Psi_y^{\alpha_2}(\omega)$  have been calculated as shown above, the study of the harmonic distortion can be conducted with the following straightforward and explicit expression

$$HD_3 = \frac{Y(3\Omega)}{Y(\Omega)} = \frac{\Psi_y^0(3\Omega) + \Psi_y^1(3\Omega) \times c_{1,0}(2) + \dots + \Psi_y^N(3\Omega) \times (c_{1,0}(2))^N}{\Psi_y^0(\Omega) + \Psi_y^1(\Omega) \times c_{1,0}(2) + \dots + \Psi_y^N(\Omega) \times (c_{1,0}(2))^N} \quad (4.17)$$

From (4.17), how the linear parameter of interest  $c_{1,0}(2)$ , the capacitance,

affects the harmonic distortion is ready for study. All of the coefficients in (4.17) can be symbolically calculated, as shown in Table 4.3 (computed with the model parameters given in example 4.1).

Table 4.3 Coefficients of (4.17)

$\alpha_2$	$\Psi_y^{\alpha_2}(\Omega)$	$\Psi_y^{\alpha_2}(3\Omega)$
0	-7.4217e-06+2.1565e-06i	-2.7079e-11+1.7670e-11i
1	-4.5714e+03+7.2021e+03i	0.4687e-00-0.1648e-00i
2	6.2256e+12+7.0633e+12i	-5.5927e+08-2.0840e+09i
3	9.4037e+21-4.4233e+21i	-4.2874e+18+6.9534e+17i
4	-1.7921e+30-1.1329e+31i	1.8328e+27-2.4603e+27i

Table 4.3 shows the coefficients in (4.17), which are constant and thus independent of the introduced capacitance. With these calculated coefficients, the third-order harmonic distortion can be freely analysed and optimized with different introduced capacitance  $C$  values. From Fig. 4.6-4.8, it can be observed that the output spectra ( $Y(\Omega)$  and  $Y(3\Omega)$ ) and the third-order harmonic distortion  $HD_3$  given in the coefficients of (4.17) all have good agreement with those obtained by numerical simulation (ode 45 and Fourier transform), and as the truncation order increases (up to the fourth-order in Fig. 4.6-4.8), the output spectrum and harmonic distortion by (4.17) converge quickly to those obtained by the recursive computation of the Volterra series using (4.2)-(4.5), which shows the effectiveness of the third-order harmonic distortion given in (4.17) and

also the new nCOS relationship developed in (4.15).

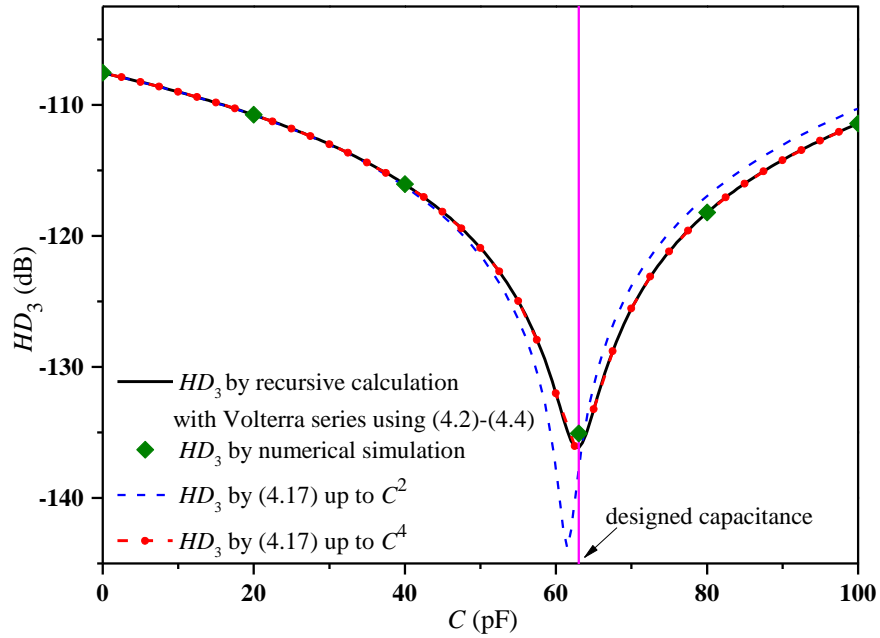


Figure 4.6 Third-order harmonic distortion with different parameters of interest

It is obvious in Fig. 4.6 that the third-order harmonic distortion has a minimum value when the introduced capacitance equals 63pF, and from Fig 4.7-4.8, it can be observed that this optimal value can greatly reduce the third-order output component  $Y(3\Omega)$  without deteriorating the first-order output component  $Y(\Omega)$ , so a good suppression of harmonic distortion is achieved.

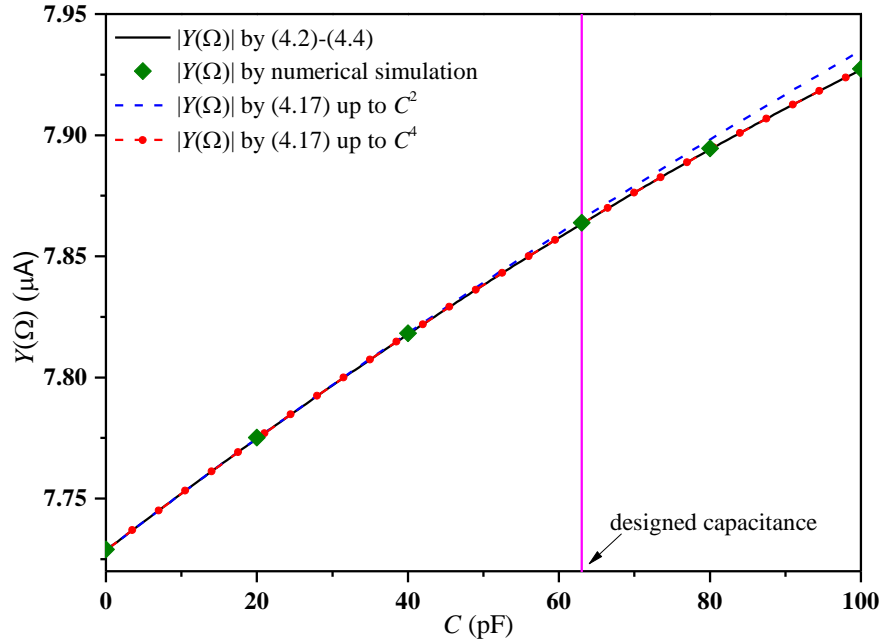


Figure 4.7 Output spectrum with different parameters of interest at  $\Omega$

For the output spectrum and harmonic distortion by pure numerical simulation (ode45) or the direct application of the Volterra series via (4.2)-(4.5), once the introduced capacitance  $C$  changes, a new numerical simulation or a new recursive calculation via (4.2)-(4.5) is required. Clearly, the expression in (4.17) in the form of a polynomial function with the calculated coefficients in table 4.3 is more efficient because each coefficient requires only one calculation (resulting from the characteristic that the coefficients are independent of those linear parameters of interest). The efficiency of the relationship developed in (4.17) would be more obvious in the cases where there is more than one linear parameters of interest, if a higher nonlinear order is considered for higher accuracy of the nonlinear output spectrum, or if a system with a multi-tone harmonic input or wideband-modulated signal input is investigated. Moreover, a pure numerical simulation method or direct application of the Volterra series via

(4.2)-(4.5) (involves recursive computation) cannot provide the straightforward, analytical, and explicit relationship shown in (4.17) for facilitating the analysis and design of the linear parameters of interest with consideration of the system's inherent nonlinearity.

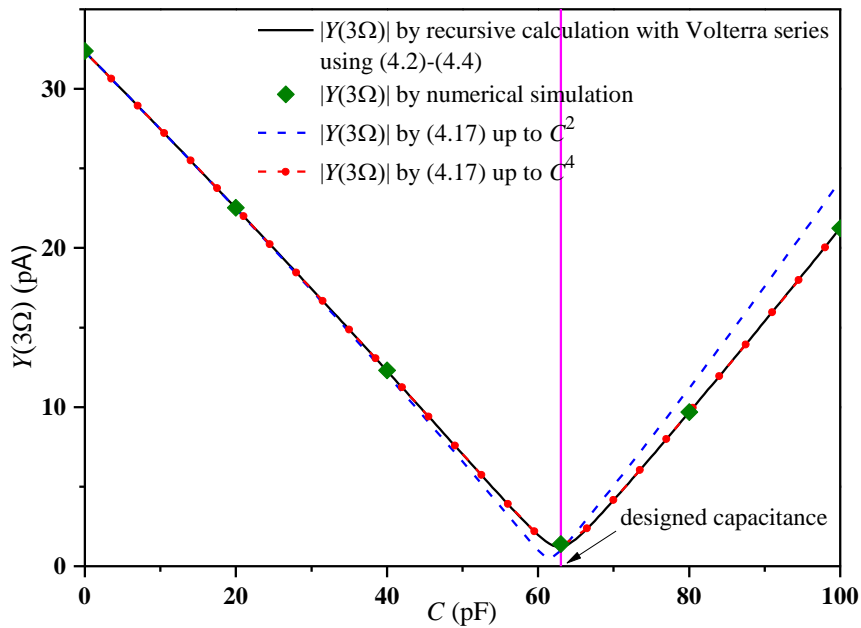


Figure 4.8 Output spectrum with different parameters of interest at  $3\Omega$

**Remark 4.8:** Linearization is frequently used in radio frequency (RF) circuit design, and various reports have studied harmonic distortion and intermodulation distortion. For those results with the direct application of the Volterra series [7, 11, 171-177], Taylor series expansion [178], harmonic balance [179], or perturbation method [180], usually a system having only up to third-order nonlinearity together with a single-tone or double-tone harmonic input can be considered. The results often fail to study the wideband modulated signal in the real world [181-183] and also cannot be used to investigate those scenarios when a higher nonlinear order is required [181]. Even for those cases with third-order

nonlinearity and single-tone or double-tone harmonic inputs, the results may still be complicated because of the recursive computation of the Volterra series, as shown in(4.2)-(4.5). Some assumptions are thus required for simplifying the analysis [7, 172-177], which strongly depends on the engineer's experience, and the results are only available for those specific cases.

The proposed results of this study are developed for a wide class of nonlinear systems governed by the SISO NDE, which provides a straightforward, efficient and explicit relationship between the nonlinear output spectrum and those linear parameters of interest (see (4.15) also an example in (4.17)). This can greatly facilitate the analysis and design of nonlinear systems with only linear feedback control or linear components.

### 4.3 The new nCOS function based linear feedback design for MIMO nonlinear systems

#### 4.3.1 The system under consideration

Consider the following nonlinear multiple-input multiple-output (MIMO) plant:

$$\dot{\mathbf{x}} = \mathbf{A}\mathbf{x} + \mathbf{B}_1\mathbf{w} + \mathbf{P}(\mathbf{x}, \mathbf{w}) + \mathbf{B}_2\mathbf{u} \quad (4.18)$$

$$\mathbf{y} = \mathbf{C}\mathbf{x} + \mathbf{D}\mathbf{w} + \mathbf{Q}(\mathbf{x}, \mathbf{w}) \quad (4.19)$$

where  $\mathbf{x} \in \mathcal{R}^{r \times 1}$ ,  $\mathbf{y} \in \mathcal{R}^{s \times 1}$ ,  $\mathbf{w} \in \mathcal{R}^v \times 1$ , and  $\mathbf{u} \in \mathcal{R}^{t \times 1}$  are the state vector, output vector, system external input, and control input, respectively.  $\mathbf{A}$ ,  $\mathbf{B}_1$ ,  $\mathbf{B}_2$ ,  $\mathbf{C}$ ,  $\mathbf{D}$  are nonzero real matrices with proper dimensions. For convenience in practical application, it is supposed that only a linear state feedback controller is expected to be designed for the nonlinear plant as

$$\mathbf{u} = -\mathbf{K}\mathbf{x} \quad (4.20)$$

$\mathbf{K} \in \mathcal{R}^{t \times r}$  is the linear feedback gain to design. Denote as  $x_j$ ,  $y_\eta$ , and  $w_\mu$  the  $j$ th element of  $\mathbf{x}$ , the  $\eta$ th element of  $\mathbf{y}$ , and the  $\mu$ th element of  $\mathbf{w}$ , respectively.  $\mathbf{P}(\mathbf{x}, \mathbf{w})$  and  $\mathbf{Q}(\mathbf{x}, \mathbf{w})$  are vectors with dimensions  $r \times 1$  and  $s \times 1$ , respectively. The  $i$ th element in  $\mathbf{P}(\mathbf{x}, \mathbf{w})$  and the  $\eta$ th element in  $\mathbf{Q}(\mathbf{x}, \mathbf{w})$  are given as

$$P_i(\mathbf{x}, \mathbf{w}) = \sum_{n=p+q=2}^{N_p} \sum_{\substack{\beta_1, \dots, \beta_r, \alpha_1, \dots, \alpha_v \geq 0 \\ \beta_1 + \dots + \beta_r + \alpha_1 + \dots + \alpha_v = q}} \left[ c_{p,q}(\boldsymbol{\alpha}, \boldsymbol{\beta}; i) \prod_{j=1}^r x_j^{\beta_j} \prod_{\mu=1}^v w_\mu^{\alpha_\mu} \right] \quad (4.21)$$

$$Q_\eta(\mathbf{x}, \mathbf{w}) = \sum_{n=2}^{N_Q} \sum_{\substack{\beta_1, \dots, \beta_r, \alpha_1, \dots, \alpha_v \geq 0 \\ \beta_1 + \dots + \beta_r + \alpha_1 + \dots + \alpha_v = n}} \left[ d_{0,n}(\boldsymbol{\alpha}, \boldsymbol{\beta}; \eta) \prod_{j=1}^r x_j^{\beta_j} \prod_{\mu=1}^v w_\mu^{\alpha_\mu} \right] \quad (4.22)$$

where  $1 \leq i \leq r$  and  $1 \leq \eta \leq s$ .  $\boldsymbol{\alpha} = \alpha_1 \alpha_2 \dots \alpha_v$ , and  $\boldsymbol{\beta} = \beta_1 \beta_2 \dots \beta_r$  in (4.21) and (4.22)

denote the nonlinear degrees of the system external inputs  $w_1, \dots, w_\mu$  and the state

variables  $x_1, \dots, x_r$ , respectively.  $c_{p,q}(\boldsymbol{\alpha}, \boldsymbol{\beta}; i)$  in (4.21) is the nonlinear model parameter in the  $i$ th element of  $\mathbf{P}(\mathbf{x}, \mathbf{w})$  corresponding to the nonlinear term which has  $p$  order in terms of state variable  $x_j$  with nonlinear degree  $\beta_j$  and  $q$  order in terms of external input  $w_\mu$  with nonlinear degree  $\alpha_\mu$ .  $d_{0,n}(\boldsymbol{\alpha}, \boldsymbol{\beta}; \eta)$  in (4.22) indicates the  $n$ th-order nonlinear parameter in the  $\eta$ th element of  $\mathbf{Q}(\mathbf{x}, \mathbf{w})$  of a nonlinear term having  $\beta_j$  terms of  $x_j$  and  $\alpha_\mu$  terms of  $w_\mu$ .  $N_P$  and  $N_Q$  are the maximum nonlinear degree in  $\mathbf{P}(\mathbf{x}, \mathbf{w})$  and  $\mathbf{Q}(\mathbf{x}, \mathbf{w})$ . An example is given to illustrate the notations in (4.21) and (4.22).

**Example 4.3:** A nonlinear model with one external disturbance  $w$ , one output  $y$ , one control input  $u$ , and two state variables is considered here:

$$\dot{\mathbf{x}} = \begin{pmatrix} a_{11} & a_{12} \\ a_{21} & a_{22} \end{pmatrix} \begin{bmatrix} x_1 \\ x_2 \end{bmatrix} + \begin{bmatrix} b_{11} \\ b_{12} \end{bmatrix} w + \begin{bmatrix} b_{21} \\ b_{22} \end{bmatrix} u + \begin{bmatrix} e_1 x_1^2 + e_2 x_1 x_2 w \\ e_3 x_1^2 x_2 \end{bmatrix} \quad (4.23)$$

$$y = [c_{11} \ c_{12}] \begin{bmatrix} x_1 \\ x_2 \end{bmatrix} + d_{11} w + e_4 x_1 x_2 w \quad (4.24)$$

The model parameters ( $e_1$  to  $e_4$ ) can be represented as

$$c_{2,0}(0, 20; 1) = e_1, \quad c_{2,1}(1, 11; 1) = e_2, \quad c_{3,0}(0, 21; 2) = e_3, \quad d_{0,3}(1, 11; 1) = e_4$$

**Remark 4.9:** The system under consideration, i.e., (4.18)-(4.20), is a general nonlinear system. Many practical nonlinear vibration systems can be modelled or identified into such a nonlinear differential equation model. A vehicle suspension system in section IV will show in detail how to describe a real engineering problem with equations (4.18)-(4.20).

**Remark 4.10:** This study focuses on the design of the linear state feedback gain  $\mathbf{K}$ . For those unobservable systems, an observer can be constructed to estimate

the state variables. Moreover, it can be easily shown that all of the conclusions for the design of  $\mathbf{K}$  also hold for the design of the matrices  $\mathbf{A}$  and  $\mathbf{B}_2$ . That is, the method developed here is applicable for the design of all model parameters of the linear dynamics of the system.

**Remark 4.11:** It is supposed that the nonlinear dynamics of the system (4.18)-(4.19) with the linear feedback control in (4.20) is overall Volterra-type and thus allows a convergent Volterra series expansion of the input-output relationship. The parameter ranges to guarantee the Volterra series expansion can be determined with the methods in [138, 139].

This paper aims at providing an explicit and analytic relationship between the system output  $y$  and the system linear dynamics ( $\mathbf{K}$ ,  $\mathbf{A}$ , and  $\mathbf{B}_2$ ) and developing a straightforward method, i.e., the new nCOS function, to facilitate the analysis and design of the system linear dynamics ( $\mathbf{K}$ ,  $\mathbf{A}$ , and  $\mathbf{B}_2$ ) with full consideration of the system's inherent nonlinearity ( $\mathbf{P}(\mathbf{x}, \mathbf{w})$  and  $\mathbf{Q}(\mathbf{x}, \mathbf{w})$ ).

### 4.3.2 Nonlinear output spectrum

The nonlinear output spectrum of MIMO nonlinear systems can follow those for SISO nonlinear systems in [70, 95, 113, 115]. The nonlinear output spectrum of the  $\eta$ th output  $y_\eta$  in (4.19), i.e.,  $Y_\eta(\Omega)$ , can be computed as,

$$Y_\eta(\Omega) = \sum_{n=1}^N \sum_{\substack{\beta_1, \dots, \beta_r, \alpha_1, \dots, \alpha_v \geq 0 \\ \beta_1 + \dots + \beta_r + \alpha_1 + \dots + \alpha_v = n}} \int \cdots \int_{\sum_{i=1}^n \omega_i = \Omega} G_n^\eta(\boldsymbol{\alpha}, \boldsymbol{\beta}; \omega_1, \dots, \omega_n) \\ \times \prod_{j=1}^r \left[ \prod_{z=1}^{\beta_j} X_j(\omega_{nX_j+z}) \right] \prod_{\mu=1}^v \left[ \prod_{z=1}^{\alpha_\mu} W_\mu(\omega_{nW_\mu+z}) \right] d\omega_1 \cdots d\omega_n \quad (4.25)$$

where  $G_n^\eta(\boldsymbol{\alpha}, \boldsymbol{\beta}; \omega_1, \dots, \omega_n)$  is the  $n$ th-order generalized frequency response function (GFRF) of the  $\eta$ th output in equation (4.19), and  $N$  the truncation order.  $\boldsymbol{\alpha} = \alpha_1 \alpha_2 \dots \alpha_\nu$ , and  $\boldsymbol{\beta} = \beta_1 \beta_2 \dots \beta_r$  are the numbers of  $W_1(\omega), \dots, W_\nu(\omega)$  and  $X_1(\omega), \dots, X_r(\omega)$  appearing in the  $n$ -dimensional convolution, respectively.  $X_j(\omega)$  and  $W_\mu(\omega)$  are the Fourier transforms of the state variable  $x_j$  and external input  $w_\mu$ , respectively.  $nX_j = \beta_1 + \dots + \beta_{j-1}$ ,  $nX_1 = 0$ ,  $nW_\mu = nX_r + \alpha_1 + \dots + \alpha_{\mu-1}$ .

Given that the output equation (4.19) has pure input nonlinearity (considering that the spectrum of state vector  $X(\omega)$  can be computed by equation (4.18)), the generalized frequency response function (GFRF) in (4.25) can then be computed as (see also discussion in [59, 65, 115]),

$$G_n^\eta(\boldsymbol{\alpha}, \boldsymbol{\beta}; \omega_1, \dots, \omega_n) = d_{0,n}(\boldsymbol{\alpha}, \boldsymbol{\beta}; \eta) \quad (4.26)$$

$$G_1^\eta(\boldsymbol{\alpha}_\mu, \mathbf{0}; \omega_1) = D(\eta, \mu) \quad (4.27)$$

$$G_1^\eta(\mathbf{0}, \boldsymbol{\beta}_j; \omega_1) = C(\eta, j) \quad (4.28)$$

where  $G_1^\eta(\boldsymbol{\alpha}_\mu, \mathbf{0}; \omega_1)$  and  $G_1^\eta(\mathbf{0}, \boldsymbol{\beta}_j; \omega_1)$  are the first-order transfer function of the  $\eta$ th output with respect to the  $\mu$ th external input  $w_\mu$  and the  $j$ th state variable  $x_j$ , respectively.  $C(\eta, j)$  is the element of  $\mathbf{C}$  in the  $\eta$ th row and  $j$ th column, and  $D(\eta, \mu)$  indicates the element of  $\mathbf{D}$  in the  $\eta$ th row and  $\mu$ th column.  $\boldsymbol{\alpha}_\mu = 0 \dots 1 \dots 0$ , which means that only the  $\mu$ th element equals 1 and all of the other elements are 0.  $\boldsymbol{\beta}_j$  has the same meaning.

**Example 4.4:** Taking the system in (4.23) and (4.24) as an example, the output spectrum can be computed according to (4.25) as

$$Y_1(\Omega) = G_1^1(0,10;\Omega)X_1(\Omega) + G_1^1(0,01;\Omega)X_2(\Omega) + G_1^1(1,00;\Omega)W(\Omega) \\ + \iint \int_{\omega_1+\omega_2+\omega_3=\Omega} G_3^1(1,11;\omega_1,\omega_2,\omega_3)X_1(\omega_1)X_2(\omega_2)W(\omega_3)d\omega_1d\omega_2d\omega_3$$

where  $X_1(\Omega)$  and  $X_2(\Omega)$  are the spectra of state variable  $x_1$  and  $x_2$ , respectively,

and

$$G_1^1(0,10;\Omega) = c_{11}, G_1^1(0,01;\Omega) = c_{12}, G_1^1(1,00;\Omega) = d_{11}, G_3^1(1,11;\omega_1,\omega_2,\omega_3) = e_4$$

Considering the  $j$ th state variable  $x_j$  as an output of (4.18), the spectrum of the state variable can be calculated as

$$X_j(\Omega) = \sum_{n=1}^N \sum_{\tilde{\alpha}_1, \dots, \tilde{\alpha}_v \geq 0, \tilde{\alpha}_1 + \dots + \tilde{\alpha}_v = n} \int \dots \int_{\sum_{i=1}^n \omega_i = \Omega} H_n^j(\tilde{\alpha}; \omega_1, \dots, \omega_n) \\ \times \prod_{\mu=1}^v \left[ \prod_{z=1}^{\tilde{\alpha}_\mu} W_\mu(\omega_{nW_\mu+z}) \right] d\omega_1 \dots d\omega_n \quad (4.29)$$

where  $nW_i = \tilde{\alpha}_1 + \dots + \tilde{\alpha}_{i-1}$  and  $nW_1 = 0$ .  $\tilde{\alpha} = \tilde{\alpha}_1 \tilde{\alpha}_2 \dots \tilde{\alpha}_v$  means that  $\tilde{\alpha}_\mu$  terms of external input  $W_\mu(\omega)$  are involved in the convolution for  $\mu=1, \dots, v$ .

$H_n^j(\tilde{\alpha}; \omega_1, \dots, \omega_n)$  is the  $n$ th-order generalized frequency response function (GFRF) for the  $j$ th state vector  $x_j$  with respect to external input  $\tilde{\alpha}$ , which can be computed as

$$\mathbf{H}_n(\tilde{\alpha}) = \begin{bmatrix} H_n^1(\tilde{\alpha}; \omega_1, \dots, \omega_n) \\ H_n^2(\tilde{\alpha}; \omega_1, \dots, \omega_n) \\ \vdots \\ H_n^r(\tilde{\alpha}; \omega_1, \dots, \omega_n) \end{bmatrix} = \left[ (i\omega_1 + \dots + i\omega_n) \mathbf{I} - (\mathbf{A} - \mathbf{B}_2 \mathbf{K}) \right]^{-1} \begin{bmatrix} V_{1,n}(\tilde{\alpha}) \\ V_{2,n}(\tilde{\alpha}) \\ \vdots \\ V_{r,n}(\tilde{\alpha}) \end{bmatrix} \quad (4.30) \\ = \mathbf{L}_n(\omega_1, \dots, \omega_n) \mathbf{V}_n$$

where  $i$  is the imaginary unit, and the elements in  $\mathbf{V}_n$  can be computed following the methods demonstrated in [59, 65, 115],

$$V_{j,n}(\tilde{\alpha}) = c_{0,n}(\tilde{\alpha}, \mathbf{0}; j) + \sum_{m=p+q=2}^n \sum_{p=1}^m \sum_{\substack{\beta_1, \dots, \beta_r, \alpha_1, \dots, \alpha_v \geq 0 \\ \beta_1 + \dots + \beta_r = p, \alpha_1 + \dots + \alpha_v = q}} c_{p,q}(\boldsymbol{\alpha}, \boldsymbol{\beta}, i) \\ \times H_{n-q,p}(\tilde{\alpha} - \boldsymbol{\alpha}, \boldsymbol{\beta}; \omega_1, \dots, \omega_{n-q}) \quad (4.31)$$

where the first part considers the pure input nonlinearity and the second part involves the cross input-output nonlinearity and pure output nonlinearity,  $\tilde{\alpha}_\mu - \alpha_\mu, \mu = 1, \dots, v$ , in which  $\tilde{\alpha} - \alpha$  means that  $\alpha_\mu$  terms of external input  $w_\mu$  have already been considered with the input nonlinearity, and

$$H_{n-q,p}(\tilde{\alpha} - \alpha, \beta; \omega_1, \dots, \omega_{n-q}) = \sum_{\substack{\beta_1, \dots, \beta_r \geq 0 \\ \beta_1 + \dots + \beta_r = p}} \sum_{\substack{\gamma_{jz} \geq 0, \sum \gamma_{jz} = n-q}} \left( \prod_{j=1}^r \prod_{z=1}^{\beta_j} H_{\gamma_{jz}}^j(\sigma_{jz}; \omega_{X_{jz}+1}, \dots, \omega_{X_{jz}+\gamma_{jz}}) \right) \sum_{jz} \sigma_{jz}^{\tilde{\alpha}_v - \alpha_v} \dots \sum_{i:z} \sigma_{i:z}^{\tilde{\alpha}_1 - \alpha_1} \quad (4.32)$$

where  $\sigma_v^{jz} + \sigma_{v-1}^{jz} + \dots + \sigma_1^{jz} = \gamma_{jz}$ ,  $\sigma_{jz} = \sigma_1^{jz} \sigma_2^{jz} \dots \sigma_v^{jz}$ . Denote  $\prod_{i=1}^0(\cdot) = 1$ .  $H_{\gamma_{jz}}^j$  stands for the  $\gamma_{jz}$ th-order GFRF of the  $j$ th state variable  $x_j$  with respect to the external input having  $\sigma_\mu^{jz}$  terms of  $w_\mu$ ,  $\mu = 1, 2, \dots, v$ .  $\sum \gamma_{jz} = n - q$  indicates that the multiplication  $\prod_{j=1}^r \prod_{z=1}^{\beta_j}(\cdot)$  results in a  $(n-q)$ th-order GFRF.  $\gamma_{jz}$  is a positive integer that is smaller than  $n-q$ . It is thus clear that a higher-order GFRF can be recursively computed from lower-order GFRFs.  $\beta_1 + \dots + \beta_r = p$  indicates that there are overall  $p$  terms of  $H_{\gamma_{jz}}^j$  in the product  $\prod_{j=1}^r \prod_{z=1}^{\beta_j}(\cdot)$ .

**Example 4.5:** For the system in (4.23) and (4.24),  $V_{j,m}(\tilde{\alpha})$  can be computed according to (4.31) and (4.32) as

$$\begin{aligned} V_{1,2}(2) &= c_{2,0}(0, 20; 1)H_{2,2}(2, 20; \omega_1, \omega_2) = e_1 H_1^1(1; \omega_1) H_1^1(1; \omega_2), \\ V_{1,3}(3) &= c_{2,0}(0, 20; 1)H_{3,2}(3, 20; \omega_1, \omega_2, \omega_3) + c_{2,1}(1, 11; 1)H_{2,2}(2, 11; \omega_1, \omega_2) \\ &= e_1 \left[ H_1^1(\omega_1) H_2^1(\omega_2, \omega_3) + H_2^1(\omega_1, \omega_2) H_1^1(\omega_3) \right] + e_2 H_1^1(\omega_1) H_1^2(\omega_2), \\ V_{2,3}(3) &= c_{3,0}(0, 21; 2)H_{3,3}(3, 21; \omega_1, \omega_2, \omega_3) = e_3 H_1^1(\omega_1) H_1^1(\omega_2) H_1^2(\omega_3) \end{aligned}$$

The first-order generalized frequency response function (GFRF) can be directly obtained,

$$\mathbf{H}_1(\boldsymbol{\alpha}_\mu) = \begin{bmatrix} H_1^1(\boldsymbol{\alpha}_\mu; \omega_1) \\ H_1^2(\boldsymbol{\alpha}_\mu; \omega_1) \\ \vdots \\ H_1^r(\boldsymbol{\alpha}_\mu; \omega_1) \end{bmatrix} = [(i\omega_1)\mathbf{I} - (\mathbf{A} - \mathbf{B}_2\mathbf{K})]^{-1} \mathbf{B}_1 \mathbf{E}_\mu = \mathbf{L}_1^{-1}(\omega_1) \mathbf{B}_1 \mathbf{E}_\mu \quad (4.33)$$

where  $\mathbf{I}$  is the identity matrix,  $i$  is the imaginary unit, and  $\mathbf{E}_\mu$  is a  $v \times 1$  column vector with the  $\mu$ th element equals 1 and all other elements 0.  $\boldsymbol{\alpha}_\mu$  is the same as that in (4.27).

### 4.3.3 The nCOS function with respect to the linear feedback gain $\mathbf{K}$

Let  $\tilde{\mathbf{L}}_n^{-1}(\omega_1, \dots, \omega_n)$ ,  $\tilde{\mathbf{H}}_n(\boldsymbol{\alpha}, \boldsymbol{\beta}; \omega_1, \dots, \omega_n)$ ,  $\tilde{\mathbf{G}}_n(\boldsymbol{\alpha}, \boldsymbol{\beta}; \omega_1, \dots, \omega_n)$  and  $\tilde{\mathbf{Y}}(\Omega)$  be the  $\mathbf{L}_n^{-1}$  matrix,  $n$ th-order GFRF of state equations (4.18),  $n$ th-order GFRF of output equations (4.19), and output spectrum with the open loop case, i.e., linear feedback gain matrix  $\mathbf{K}=0$ , respectively, where the  $\mathbf{L}_n$  matrix is defined in (4.30).

**Lemma 4.1:** If the inequality  $\rho(\mathbf{K}\tilde{\mathbf{L}}_1^{-1}\mathbf{B}_2) < 1$  holds, the first-order GFRF of the state equation (4.18) can be computed using the feedback gain matrix  $\mathbf{K}$  as a perturbation on the open-loop transfer function a

$$\mathbf{H}_1(\boldsymbol{\alpha}_\mu; \omega_1) = \tilde{\mathbf{H}}_1(\boldsymbol{\alpha}_\mu; \omega_1) - \boldsymbol{\chi} \quad (4.34)$$

where  $\rho(\mathbf{K}\tilde{\mathbf{L}}_1^{-1}\mathbf{B}_2)$  is the spectral radius of  $\mathbf{K}\tilde{\mathbf{L}}_1^{-1}\mathbf{B}_2$ ,  $\boldsymbol{\chi} = \boldsymbol{\delta}\mathbf{B}_1\mathbf{E}_\mu$ ,  $\boldsymbol{\delta} = \sum_{i=0}^{\infty} [(-1)^i \tilde{\mathbf{L}}_1^{-1} \mathbf{B}_2 \boldsymbol{\varepsilon}^i \mathbf{K} \tilde{\mathbf{L}}_1^{-1}]$ ,  $\boldsymbol{\varepsilon} = \mathbf{K}\tilde{\mathbf{L}}_1^{-1}\mathbf{B}_2$ , and  $\tilde{\mathbf{L}}_1^{-1} = ((j\omega_1)\mathbf{I} - \mathbf{A})^{-1}$ .  $\boldsymbol{\chi}$  is an  $r \times 1$  vector with the element  $\chi_i$ ,  $1 \leq i \leq r$ , as

$$\chi_i = \sum_{l=1}^{\infty} \sum_{\tau_{1,1} + \dots + \tau_{t,r} = l} \left( \varphi_{\tau_{1,1}, \dots, \tau_{t,r}} k_{1,1}^{\tau_{1,1}} k_{1,2}^{\tau_{1,2}} \dots k_{t,r}^{\tau_{t,r}} \right) \quad (4.35)$$

where  $k_{i,j}$  is the element of  $\mathbf{K}$ ,  $\tau_{i,j}$  is the order of  $k_{i,j}$ , and  $\tau_{i,j} \in \mathcal{N}$ ,  $0 \leq i \leq t$ ,  $0 \leq j \leq r$ .  $\varphi_{\tau_{1,1}, \dots, \tau_{t,r}}$  is a scalar independent of  $k_{i,j}$ .

**Proof:** See Appendix 4.2.

**Remark 4.13:** The perturbation  $\chi$  in Lemma 4.1 can be theoretically computed with symbolic manipulations, which then provides an explicit analytical expression for the first-order GFRF based on the open loop transfer function.

**Proposition 4.5:** The  $n$ th-order GFRF of state equation (4.18) can be regarded as a perturbation on the open loop  $n$ th-order GFRF as,

$$\mathbf{H}_n(\tilde{\alpha}) = \tilde{\mathbf{H}}_n(\tilde{\alpha}) - \chi^{(n)} \quad (4.36)$$

when the spectral radius  $\rho(\mathbf{K}\tilde{\mathbf{L}}_1^{-1}\mathbf{B}_2) < 1$  holds, and  $\chi^{(n)}$  is an  $r \times 1$  vector with elements having coefficient  $\varphi_{\tau_{1,1}\dots\tau_{t,r}}^{(n)}$ ,

$$\chi_i^{(n)} = \sum_{l=1}^{\infty} \sum_{\tau_{1,1}+\dots+\tau_{t,r}=l} \left( \varphi_{\tau_{1,1},\dots,\tau_{t,r}}^{(n)} k_{1,1}^{\tau_{1,1}} k_{1,2}^{\tau_{1,2}} \dots k_{t,r}^{\tau_{t,r}} \right) \quad (4.37)$$

where  $\tau_{i,j} \in \mathcal{N}; i \in [0, t], j \in [0, r]; \varphi_{\tau_{1,1}\dots\tau_{t,r}}^{(n)}$  is independent of  $k_{i,j}$ .

**Proof:** See Appendix 4.3.

**Proposition 4.6:** When the spectral radius  $\rho(\mathbf{K}\tilde{\mathbf{L}}_1^{-1}\mathbf{B}_2) < 1$  holds, the spectrum of state variable  $x_j$  in (4.18) at any frequency  $\Omega$  of interest can be computed as a perturbation on the open loop spectrum, so the perturbation can be given as a polynomial function with respect to the elements of the feedback gain  $\mathbf{K}$ .

$$X_j(\Omega) = \tilde{X}_j(\Omega) + \sum_{l=1}^{\infty} \sum_{\tau_{1,1}+\dots+\tau_{t,r}=l} \left( \varphi_{\tau_{1,1},\dots,\tau_{t,r}}^{x_j} k_{1,1}^{\tau_{1,1}} k_{1,2}^{\tau_{1,2}} \dots k_{t,r}^{\tau_{t,r}} \right) \quad (4.38)$$

where  $\tilde{X}_j(\Omega)$  is the open loop output spectrum of the  $j$ th state variable, and  $\varphi_{\tau_{1,1}\dots\tau_{t,r}}^{x_j}$  is the coefficient independent of the feedback gain matrix  $\mathbf{K}$ .

**Proof:** See Appendix 4.4.

**Corollary 4.1:** The spectrum of the output at any frequency  $\Omega$  can be computed via a correction (which can be given as a polynomial function with respect to the elements of the feedback gain matrix  $\mathbf{K}$ ) on the open loop output spectrum,

$$Y_\eta(\Omega) = \tilde{Y}_\eta(\Omega) + \sum_{l=1}^{\infty} \sum_{\tau_{1,1} + \dots + \tau_{t,r} = l} \left( \varphi_{\tau_{1,1}, \dots, \tau_{t,r}}^{y_\eta} k_{1,1}^{\tau_{1,1}} k_{1,2}^{\tau_{1,2}} \dots k_{t,r}^{\tau_{t,r}} \right) \quad (4.39)$$

where  $\tilde{Y}_\eta(\Omega)$  is the open loop output spectrum, and  $\varphi_{\tau_{1,1}, \dots, \tau_{t,r}}^{y_\eta}$  is a coefficient that is independent of  $\mathbf{K}$ .

**Proof:** The output equation (4.19) has only pure input nonlinearity. Thus, substituting (4.38) into (4.25), the result in Corollary 4.1 is straightforward. This completes the proof.  $\square$

**Remark 4.14:** Coefficient  $\varphi_{\tau_{1,1}, \dots, \tau_{t,r}}^{y_\eta}$  in Corollary 4.1 is independent of the elements of matrix  $\mathbf{K}$ . If  $\varphi_{\tau_{1,1}, \dots, \tau_{t,r}}^{y_\eta}$  is determined, the output spectrum of the system (4.18)-(4.20) can then be freely analysed and designed via (4.39) with a different feedback gain matrix  $\mathbf{K}$ . The nonlinear output spectrum in (4.39) is referred to as the new nCOS function with respect to the linear model parameters of interest, which explicitly unveils for the first time the analytical relationship between the system output spectrum and the linear feedback gain matrix  $\mathbf{K}$ . This is a significant extension of the previous results on the nCOS method for nonlinear analysis and design in the frequency domain [92, 95, 113, 115].

**Remark 4.15:** Alternatively, the output spectrum,  $Y_\eta(\Omega)$ , could also be simply expanded with respect to the elements of the feedback gain matrix  $\mathbf{K}$  using Taylor series. However, the coefficients of the resulting Taylor series are still functions of the elements of  $\mathbf{K}$ , and thus the analytical relationship between the nonlinear

output spectrum and linear feedback gain cannot be revealed as clearly as that via (4.39).

**Remark 4.16:** In (4.39), the coefficient  $\varphi_{\tau_{1,1}\dots\tau_{t,r}}^{y_\eta}$  also describes the sensitivity (influence) of the elements of matrix  $\mathbf{K}$  to the output spectrum, which can then help to determine the dominant elements of matrix  $\mathbf{K}$  and thus reduce the design complexity. This will greatly facilitate the analysis and design of feedback gain matrix  $\mathbf{K}$ , especially when  $\mathbf{K}$  has large dimensions.

The coefficient  $\varphi_{\tau_{1,1}\dots\tau_{t,r}}^{y_\eta}$  in (4.39) can be symbolically calculated, but the calculation could be computationally intensive. To overcome this weak point and to facilitate practical application, a numerical algorithm is given to estimate the coefficient  $\varphi_{\tau_{1,1}\dots\tau_{t,r}}^{y_\eta}$  as follows (**Algorithm 4.3**):

$$\begin{bmatrix} \tilde{Y}_\eta(\Omega) \\ \varphi_{1,0,\dots,0}^{y_\eta} \\ \varphi_{0,1,\dots,0}^{y_\eta} \\ \vdots \\ \varphi_{m_{1,1},\dots,m_{t,r}}^{y_\eta} \end{bmatrix} = \begin{bmatrix} 1 & (k_{1,1}^{(1)})^1 (k_{1,2}^{(1)})^0 \cdots (k_{t,r}^{(1)})^0 & \cdots & (k_{1,1}^{(1)})^{m_{1,1}} (k_{1,2}^{(1)})^{m_{1,2}} \cdots (k_{t,r}^{(1)})^{m_{t,r}} \\ & \vdots & \vdots & \vdots \\ 1 & (k_{1,1}^{(\bar{M})})^1 (k_{1,2}^{(\bar{M})})^0 \cdots (k_{t,r}^{(\bar{M})})^0 & \cdots & (k_{1,1}^{(\bar{M})})^{m_{1,1}} (k_{1,2}^{(\bar{M})})^{m_{1,2}} \cdots (k_{t,r}^{(\bar{M})})^{m_{t,r}} \end{bmatrix}^{-1} \begin{bmatrix} Y_\eta^{(1)}(\Omega) \\ Y_\eta^{(2)}(\Omega) \\ \vdots \\ Y_\eta^{(\bar{M})}(\Omega) \end{bmatrix} \quad (4.40)$$

where  $m_{i,j}$  is the truncation order with respect to  $k_{i,j}$ ,  $k_{1,1}^{(1)}k_{1,2}^{(1)}\dots k_{t,r}^{(1)}$  to  $k_{1,1}^{(\bar{M})}k_{1,2}^{(\bar{M})}\dots k_{t,r}^{(\bar{M})}$  are  $\bar{M}$  different sets of elements in  $\mathbf{K}$ , and  $Y_\eta^{(i)}(\Omega)$  is the output spectrum with the  $i$ th feedback gain matrix  $\mathbf{K}$  (i.e.,  $k_{1,1}^{(i)}k_{1,2}^{(i)}\dots k_{t,r}^{(i)}$ ). Clearly,  $\bar{M} = (1 + m_{1,1}) \times \dots \times (1 + m_{t,r})$ .

The  $\bar{M}$  different feedback gain matrix  $\mathbf{K}$  should be properly chosen such that the inverse of the matrix in (4.40) exists (e.g., nonsingular).

**Remark 4.17:** If the spectral radius  $\rho(\mathbf{K}\tilde{\mathbf{L}}_1^{-1}\mathbf{B}_2)$  is close to 0, a small truncation order  $\bar{l}=m_{1,1}+m_{1,2}+\dots+m_{t,r}$  can provide a good approximation of (4.39), where  $m_{i,j}$  in (4.40) is the truncation order of  $\tau_{i,j}$  in (4.39), while a large truncation order  $\bar{l}$  is required if spectral radius  $\rho(\mathbf{K}\tilde{\mathbf{L}}_1^{-1}\mathbf{B}_2)$  is more close to 1.

**Remark 4.18:** There also exist some other control methods for system (4.18)-(4.19), for example, feedback linearization [45], which requires full knowledge of the system and is not so easy to implement because the controller is nonlinear. Moreover, not all nonlinear systems in (4.18)-(4.19) can be linearized, and the linearization method may sometimes lose sight of the potential benefits of the underlying nonlinear dynamics in vibration control [7,9]. The proposed method in this paper has the following advantages: 1) ease of implementation because of the simple linear feedback controller adopted; 2) full consideration of the nonlinear influence on system response; 3) convenience in practical application with Algorithm 4.3, with which the coefficient  $\varphi_{\tau_{1,1}\dots\tau_{t,r}}^{y_\eta}$  in the new nCOS function (4.39) can be identified with input-output data, without a full knowledge of model (4.18)-(4.19).

#### 4.3.4 A case study on vehicle suspension control

Active control of vehicle suspension systems is a very hot topic in the literature [140, 142, 184, 185]. To illustrate the design of a simple linear feedback controller for a nonlinear system for performance improvement via the proposed new nCOS function, a suspension system with nonlinear stiffness is

studied in this section.

The governing equation of the system in Fig. 4.9 is

$$\begin{cases} m_t \ddot{x}_t = k_t(\bar{w} - x_t) + c_t(\dot{\bar{w}} - \dot{x}_t) + f_s + c_{s1}(\dot{x}_s - \dot{x}_t) + u \\ m_s \ddot{x}_s = -f_s - c_{s1}(\dot{x}_s - \dot{x}_t) - u \end{cases} \quad (4.41)$$

where  $f_s = k_{s1}(x_s - x_t) + k_{s2}(x_s - x_t)^2 + k_{s3}(x_s - x_t)^3$  is the nonlinear spring force,  $\bar{w}$  is the road disturbance, and  $u$  is the control. The model actually is identified from the Hyundai Elantra front suspension with parameters [1]:  $m_s=240$  kg,  $m_t=25$  kg,  $k_t=160$  kN/m,  $c_t=10$  N/m·s<sup>-1</sup>,  $c_s=1385$  N/m·s<sup>-1</sup>,  $k_{s1}=12$  kN/m,  $k_{s2}=-73696$  N/m<sup>2</sup>, and  $k_{s3}=3170400$  N/m<sup>3</sup>.

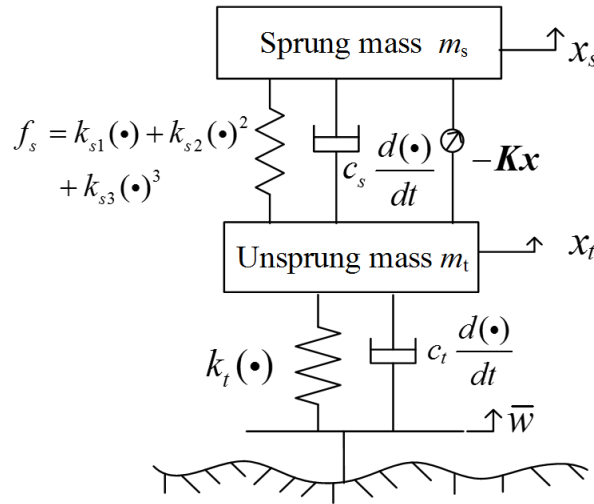


Figure 4.9 A nonlinear vehicle suspension system

The governing equation in (4.41) can be transferred into state space equations

by using  $x_1 = x_s - x_t$ ,  $x_2 = x_t - \bar{w}$ ,  $x_3 = \dot{x}_s$ ,  $x_4 = \dot{x}_t$ , and  $w = \bar{w}$  as

$$\dot{\mathbf{x}} = \begin{bmatrix} \dot{x}_1 \\ \dot{x}_2 \\ \dot{x}_3 \\ \dot{x}_4 \end{bmatrix} = \begin{bmatrix} 0 & 0 & 1 & -1 \\ 0 & 0 & 0 & 1 \\ -\frac{k_{s1}}{m_s} & 0 & -\frac{c_{s1}}{m_s} & \frac{c_{s1}}{m_s} \\ \frac{k_{s1}}{m_t} & -\frac{k_t}{m_t} & \frac{c_{s1}}{m_t} & \frac{-c_{s1} - c_t}{m_t} \end{bmatrix} \begin{bmatrix} x_1 \\ x_2 \\ x_3 \\ x_4 \end{bmatrix} + \begin{bmatrix} 0 \\ 0 \\ -\frac{k_{s2}}{m_s} \\ \frac{k_{s2}}{m_t} \end{bmatrix} x_1^2 + \begin{bmatrix} 0 \\ 0 \\ -\frac{k_{s3}}{m_s} \\ \frac{k_{s3}}{m_t} \end{bmatrix} x_1^3 + \begin{bmatrix} 0 \\ -1 \\ 0 \\ \frac{c_t}{m_t} \end{bmatrix} w + \begin{bmatrix} 0 \\ 0 \\ -\frac{1}{m_s} \\ \frac{1}{m_t} \end{bmatrix} u \quad (4.42)$$

where the linear state feedback controller is defined as  $u = -\mathbf{K}\mathbf{x} = -[k_1 \ k_2 \ k_3 \ k_4]\mathbf{x}$ .  $k_3$  and  $k_4$  in the feedback gain matrix corresponds to  $x_3=\dot{x}_s$ , and  $x_4=\dot{x}_t$ , which can be observed as the damping coefficients in vibration control and thus are more important. For convenience in analysis, parameters  $k_1$  and  $k_2$  are supposed to be already known, i.e.,  $k_1=k_2=0$ . According to ISO/TC108/SC2N67, the C level road profile corresponds to the average road profile, so it is considered here as the external road disturbance  $\bar{w}$  with a vehicle velocity 15 m/s.

There are three indicators for evaluating the performance of a suspension system, i.e., the body acceleration (relates to ride comfort), the relative tire load (corresponds to vehicle handling ability), and the suspension stroke (describes the deflection of the suspension). To apply the nCOS function based method with (4.39) for the analysis and design of the state feedback controller, these three indicators are first presented as three outputs as

$$\begin{aligned} y_1 &= \ddot{x}_s = \dot{x}_3 = \left[ \begin{array}{ccc} -\frac{k_{s1}}{m_s} & 0 & -\frac{c_{s1}}{m_s} \quad \frac{c_{s1}}{m_s} \end{array} \right] \mathbf{x} - \frac{k_{s2}}{m_s} x_1^2 - \frac{k_{s3}}{m_s} x_1^3 - \frac{1}{m_s} u \\ y_2 &= k_t x_2 / (m_s + m_t) g \\ y_3 &= x_1 \end{aligned} \quad (4.43)$$

From Corollary 4.1, the output spectrum  $Y_i(\Omega)$  can be expressed as an analytical polynomial with respect to the elements of the feedback gain matrix  $\mathbf{K}$ . The nCOS function can be obtained according to (4.39) (with truncation order 2) as,

$$Y_i(j\Omega) = \tilde{Y}_i(j\Omega) + \varphi_{0,0,1,0}^{y_i} k_3 + \varphi_{0,0,0,1}^{y_i} k_4 + \varphi_{0,0,2,0}^{y_i} k_3^2 + \varphi_{0,0,1,1}^{y_i} k_3 k_4 + \varphi_{0,0,0,2}^{y_i} k_4^2 \quad (4.44)$$

where  $\tilde{Y}_i(j\Omega)$  is the output spectrum with the open loop system. The coefficients

of variables  $k_3$  and  $k_4$  can be estimated by the following procedure (Note that all of parameters  $k_1, k_2, k_3$ , and  $k_4$  can be considered together in (4.39) with the same procedure, but only  $k_3$  and  $k_4$  are focused on here for convenience in illustration).

**Algorithm 4.4:**

**Step 1.** Calculate the matrices  $\tilde{L}_1^{-1}$  (defined in Lemma 1) and  $B_2$ .

**Step 2.** Choose the first value set for  $k_3$  and  $k_4$ , and make sure that

$$\rho(K\tilde{L}_1^{-1}B_2) < 1 \text{ holds. Simulate the system with ode45, and then take the Fourier transform. Denote the output spectrum as } Y^{(1)}(\Omega).$$

**Step 3.** Given the other 5 sets of  $k_3$  and  $k_4$ , repeat step 2.

**Step 4.** Check if the inverse of the matrix in (4.45) exists; if not, try another set of  $k_3$  and  $k_4$ .

**Step 5.** Identify the associated coefficients by (4.45).

$$\begin{bmatrix} \tilde{Y}_i(j\Omega) \\ \varphi_{0,0,1,0}^{y_i} \\ \varphi_{0,0,0,1}^{y_i} \\ \varphi_{0,0,2,0}^{y_i} \\ \varphi_{0,0,1,1}^{y_i} \\ \varphi_{0,0,0,2}^{y_i} \end{bmatrix} = \begin{bmatrix} 1 & k_3^{(1)} & k_4^{(1)} & (k_3^{(1)})^2 & k_3^{(1)}k_4^{(1)} & (k_4^{(1)})^2 \\ 1 & k_3^{(2)} & k_4^{(2)} & (k_3^{(2)})^2 & k_3^{(2)}k_4^{(2)} & (k_4^{(2)})^2 \\ 1 & k_3^{(3)} & k_4^{(3)} & (k_3^{(3)})^2 & k_3^{(3)}k_4^{(3)} & (k_4^{(3)})^2 \\ 1 & k_3^{(4)} & k_4^{(4)} & (k_3^{(4)})^2 & k_3^{(4)}k_4^{(4)} & (k_4^{(4)})^2 \\ 1 & k_3^{(5)} & k_4^{(5)} & (k_3^{(5)})^2 & k_3^{(5)}k_4^{(5)} & (k_4^{(5)})^2 \\ 1 & k_3^{(6)} & k_4^{(6)} & (k_3^{(6)})^2 & k_3^{(6)}k_4^{(6)} & (k_4^{(6)})^2 \end{bmatrix}^{-1} \begin{bmatrix} Y_i^{(1)}(\Omega) \\ Y_i^{(2)}(\Omega) \\ Y_i^{(3)}(\Omega) \\ Y_i^{(4)}(\Omega) \\ Y_i^{(5)}(\Omega) \\ Y_i^{(6)}(\Omega) \end{bmatrix} \quad (4.45)$$

With the estimated coefficients  $\varphi_{\bullet}^{y_i}$  in (4.45), the nCOS function (4.44) can then be freely used for the analysis and design of the controller.

The three outputs above are then combined together to form a multiple-object function as a performance output for the design of the linear feedback gain

matrix  $K$ ,

$$Y_4(j\Omega) = \sum_{i=1}^3 \mu_i \frac{Y_i(j\Omega)}{\tilde{Y}_i(j\Omega)} = \sum_{i=1}^3 \mu_i + \left( \sum_{i=1}^3 \mu_i \frac{\varphi_{0,0,1,0}^{y_i}}{\tilde{Y}_i(j\Omega)} \right) k_3 + \left( \sum_{i=1}^3 \mu_i \frac{\varphi_{0,0,0,1}^{y_i}}{\tilde{Y}_i(j\Omega)} \right) k_4 \quad (4.46)$$

$$+ \left( \sum_{i=1}^3 \mu_i \frac{\varphi_{0,0,2,0}^{y_i}}{\tilde{Y}_i(j\Omega)} \right) k_3^2 + \left( \sum_{i=1}^3 \mu_i \frac{\varphi_{0,0,1,1}^{y_i}}{\tilde{Y}_i(j\Omega)} \right) k_3 k_4 + \left( \sum_{i=1}^3 \mu_i \frac{\varphi_{0,0,0,2}^{y_i}}{\tilde{Y}_i(j\Omega)} \right) k_4^2$$

where  $\tilde{Y}_i(j\Omega)$  and  $Y_i(j\Omega)$  are the output spectra for the open loop case and closed loop case, respectively.  $\mu_i$ ,  $i=1,2,3$  are weights for the three indicators with  $\mu_1+\mu_2+\mu_3=1$ .  $Y_4(j\Omega)$  stands for the performance improvement of the feedback control suspension in the open loop case with full consideration of the vehicle body acceleration, the relative tire load, and the suspension stroke.

If system (4.41) possesses Volterra-type nonlinearity, nonlinear phenomena such as jump phenomena, bifurcation, and chaos will not exist, so that the following four frequencies can successfully describe the characteristics of the system outputs and then be seen as frequencies of interest, i.e., the first and second resonant frequencies ( $\Omega_1$  and  $\Omega_2$ ), the frequencies between the two resonant frequencies ( $\Omega_3$ ), and the frequencies larger than the second resonant frequency ( $\Omega_4$ ). In the following discussion, these frequencies are chosen:  $\Omega_1=2\pi \times 1.2$  rad/s,  $\Omega_2=2\pi \times 13$  rad/s,  $\Omega_3=2\pi \times 7$  rad/s, and  $\Omega_4=2\pi \times 25$  rad/s.

Following the procedure above, given  $(k_3, k_4)$  as: (37, 89), (137, 280), (23, 490), (167, 680), (42, 890), and (183, 1080), the associated independent coefficients for the three indicators,  $y_1$ ,  $y_2$ , and  $y_3$  at all four frequencies of interest can be estimated by (4.45) and are given in table 4.4. Because the ISO C level road profile involves all of the frequency components, all of the independent

associated coefficients in table 4.4 can be identified with only 6 numerical simulations (ode45 and the corresponding Fourier transform), which shows the efficiency of the proposed theoretical results.

With the independent coefficients obtained in table 4.4, all the three indicators  $y_1$ ,  $y_2$ , and  $y_3$ , can be freely analysed with different feedback gain parameters, i.e.,  $(k_3, k_4)$ , via (4.45). Fig. 4.10 presents the estimated acceleration by nCOS at all four frequencies of interest with different  $k_3$  and  $k_4$ . It can be observed that the accelerations by numerical simulation (Fourier transform of the output by ode45) are in good agreement with those predicted via the nCOS function (4.44), which shows the effectiveness of the proposed results. The nCOS functions for  $y_2$  and  $y_3$  also work well but are omitted here for space limitations. The spectral radius  $\rho(\mathbf{K}\tilde{\mathbf{L}}_1^{-1}\mathbf{B}_2) < 1$  holds for all frequencies of interest, and only the case of  $\Omega_3$  is presented in Fig. 4.11 for space limitations.

Note that with the nCOS function given in (4.44), only 6 simulations are needed for the estimation of the associated independent coefficients. Taking Fig. 4.10 as an example, when the parameter step is 10, then  $k_3$  has 21 points, and  $k_4$  has 101 numbers, so that more than 2000 simulations are needed for ode 45 if using a pure simulation-based method. The efficiency of the proposed results can then be demonstrated. The proposed results with (4.44) and (4.46) can provide an explicit analytical relationship between the output (performance objective function) and the linear feedback gain matrix, which will greatly facilitate the analysis and design of the linear feedback controller.

Table 4.4 Estimation of Parameters of Interest-Independent Part

	$\bar{Y}_i(j\Omega)$	$\Phi_{0,0,1,0}^{y_i}$	$\Phi_{0,0,0,1}^{y_i}$	$\Phi_{0,0,2,0}^{y_i}$	$\Phi_{0,0,1,1}^{y_i}$	$\Phi_{0,0,0,2}^{y_i}$
$Y_1(j\Omega_1)$	0.0180 +0.0281i	-1.488e-5 -2.090e-5i	3.243e-6 -1.766e-5i	7.617e-9 +3.841e-9i	-3.401e-10 +1.304e-8i	2.914e-10 +2.331e-9i
$Y_1(j\Omega_2)$	0.0120 -0.0141i	1.746e-6 -3.378e-7i	-5.003e-6 +1.080e-5i	-1.537e-9 +7.272e-9i	-4.953e-10 -6.306e-10i	-3.409e-9 -2.686e-9i
$Y_1(j\Omega_3)$	0.0163 +0.0168i	-4.946e-7 -8.201e-7i	-1.568e-6 +5.622e-7i	-1.947e-9 +5.728e-9i	4.195e-9 -1.881e-9i	4.011e-9 -2.700e-9i
$Y_1(j\Omega_4)$	-0.0037 -0.0004i	-5.871e-8 -1.905e-7i	2.097e-6 +1.684e-6i	8.100e-10 +7.736e-10i	-1.172e-10 -4.596e-10i	5.430e-10 -8.527e-10i
$Y_2(j\Omega_1)$	0.0016 +0.0028i	-1.394e-6 -1.947e-6i	2.978e-7 -1.649e-6i	7.402e-10 +3.480e-10i	-2.999e-11 +1.218e-9i	2.420e-11 +2.208e-10i
$Y_2(j\Omega_2)$	0.0020 -0.0004i	2.230e-7 -3.265e-8i	-6.621e-7 +1.418e-6i	-1.560e-10 +8.825e-10i	-6.460e-11 -6.665e-11i	-4.577e-10 -3.249e-10i
$Y_2(j\Omega_3)$	-0.0013 +0.0038i	1.038e-6 +1.514e-6i	3.500e-6 -3.427e-7i	4.574e-9 -9.434e-9i	-9.424e-9 +2.431e-9i	-9.087e-9 +3.897e-9i
$Y_2(j\Omega_4)$	-0.0002 -0.0010i	4.709e-9 -5.1108e-9i	-6.746e-8 -4.190e-8i	4.230e-11 +4.557e-11i	4.580e-12 -2.128e-13i	-1.453e-11 +2.276e-12i
$Y_3(j\Omega_1)$	-4.444e-4 -1.429e-4i	2.471e-7 +3.353e-7i	-5.133e-8 +2.872e-7i	-1.244e-10 -6.146e-11i	2.889e-12 -2.121e-10i	-3.918e-12 -3.765e-11i
$Y_3(j\Omega_2)$	4.123e-5 +5.726e-5i	2.954e-9 -4.885e-10	-8.147e-9 +1.800e-8i	-1.812e-12 +1.064e-11i	-8.601e-13 -1.175e-12i	-5.642e-12 -3.925e-12i
$Y_3(j\Omega_3)$	-4.481e-5 +3.137e-5i	1.700e-8 +2.462e-8i	5.704e-8 -5.342e-9i	7.451e-11 -1.540e-10i	-1.536e-10 +3.951e-11i	-1.481e-10 +6.364e-11i
$Y_3(j\Omega_4)$	7.103e-7 -4.005e-6i	1.001e-10 -1.125e-10i	-1.904e-9 -5.91e-10i	-7.267e-13 +7.298e-13i	8.233e-14 -1.028e-13i	-2.551e-13 +6.041e-14i

The performance function (4.46) fully considers all three indicators (acceleration  $y_1$ , relative tire load  $y_2$ , and suspension stroke  $y_3$ ) at the four frequencies of interest and is thus seen as an objective function for feedback design. Consider the controller as a ride comfort oriented controller and give the weights as  $\mu_1=0.75$ ,  $\mu_2=0.15$ ,  $\mu_3=0.1$ . The performance function with different feedback gain parameters is presented in Fig. 4.12, from which the optimal performance can be achieved with parameters  $(k_3, k_4) = (140, 940)$ .

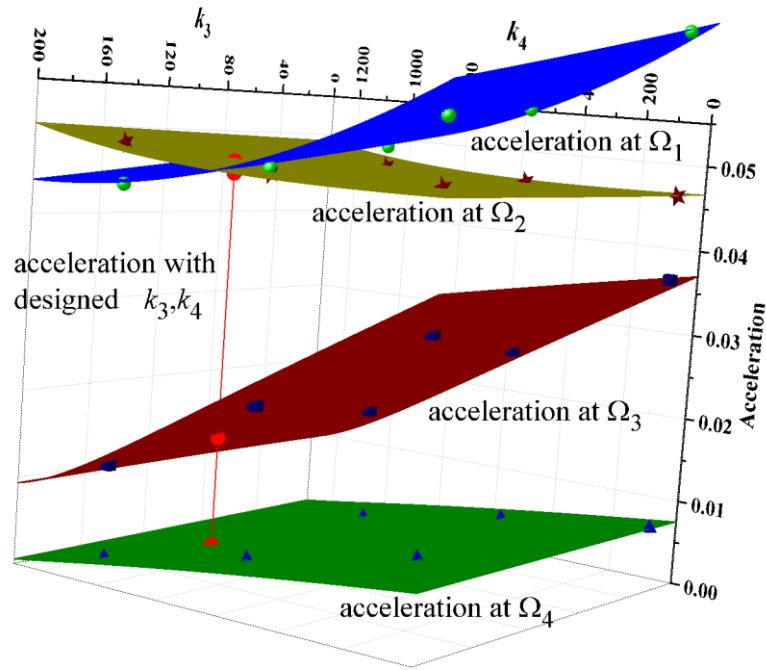


Figure 4.10 The estimated nCOS function by (4.44) with different sets of  $k_3$  and  $k_4$  at the four frequencies of interest. The symbols (ball, star, cubic, and tetrahedron) stand for the accelerations at the corresponding frequencies and the parameters by numerical simulation. The red balls represent the accelerations with the design parameters.

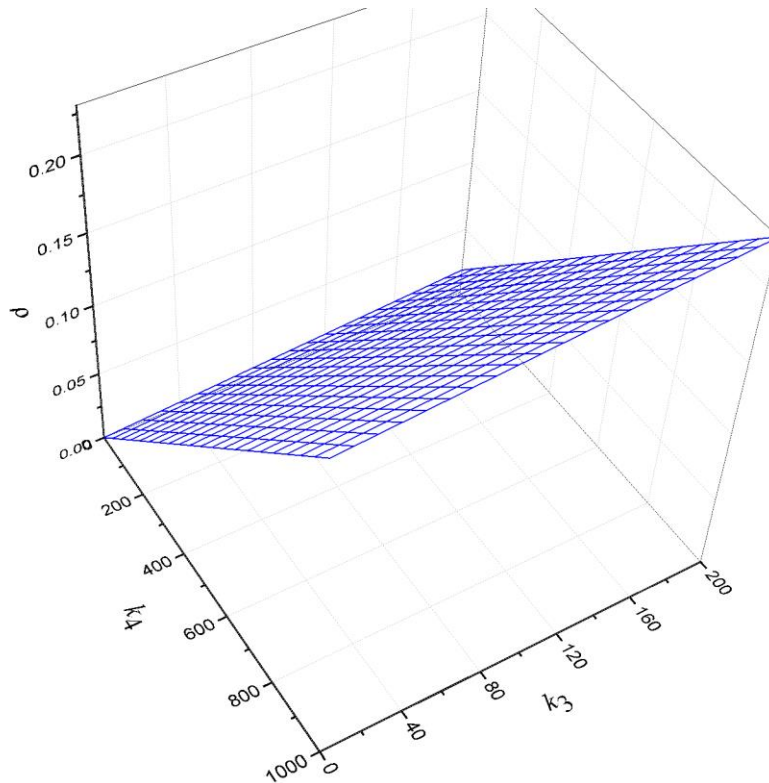


Figure 4.11 The value of  $\rho = |\mathbf{K}\tilde{\mathbf{L}}_1^{-1}\mathbf{B}_2|$

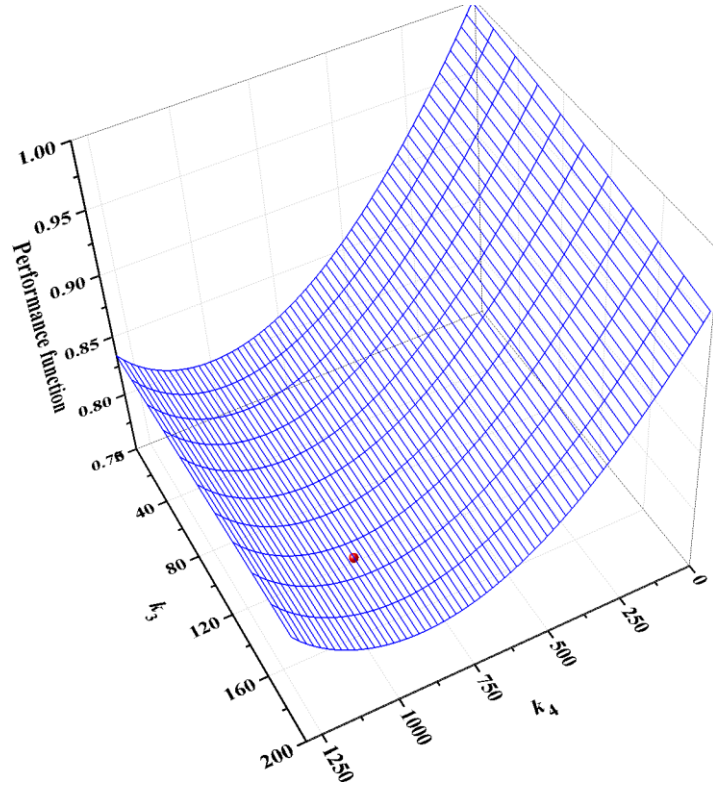


Figure 4.12 Performance function (4.46) with different feedback gain parameters. The red ball is the performance with the optimal design parameters.

For comparison, a recently developed ride comfort oriented control, i.e., the mixed skyhook and acceleration driven damper (ADD) method [164], is adopted here, which is given by

$$\begin{cases} c_{in}(t) = c_{\max} & \left[ (\ddot{x}_s^2 - \alpha^2 \dot{x}_s^2) \leq 0 \wedge \dot{x}_s(\dot{x}_s - \dot{x}_t) > 0 \right] \\ & \vee \left[ (\ddot{x}_s^2 - \alpha^2 \dot{x}_s^2) > 0 \wedge \ddot{x}_s(\dot{x}_s - \dot{x}_t) > 0 \right] \\ c_{in}(t) = c_{\min} & \left[ (\ddot{x}_s^2 - \alpha^2 \dot{x}_s^2) \leq 0 \wedge \dot{x}_s(\dot{x}_s - \dot{x}_t) \leq 0 \right] \\ & \vee \left[ (\ddot{x}_s^2 - \alpha^2 \dot{x}_s^2) > 0 \wedge \ddot{x}_s(\dot{x}_s - \dot{x}_t) \leq 0 \right] \end{cases}$$

where  $c_{in}(t)$  is the required damping coefficient, and  $\alpha=11$ ,  $\beta=30$ ,  $c_{\min}=300$ ,  $c_{\max}=4000$  [164]. The actual damping coefficient  $c(t)$  is followed by

$$\dot{c}(t) = -\beta c(t) + \beta c_{in}(t) .$$

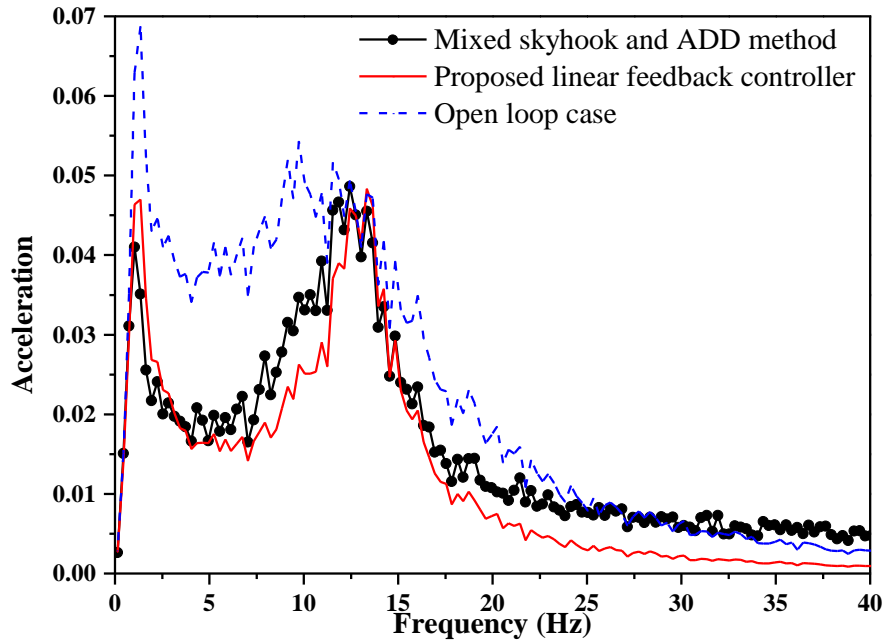


Figure 4.13 Comparison of the performance with/without controller when subjected to ISO C level road profile.

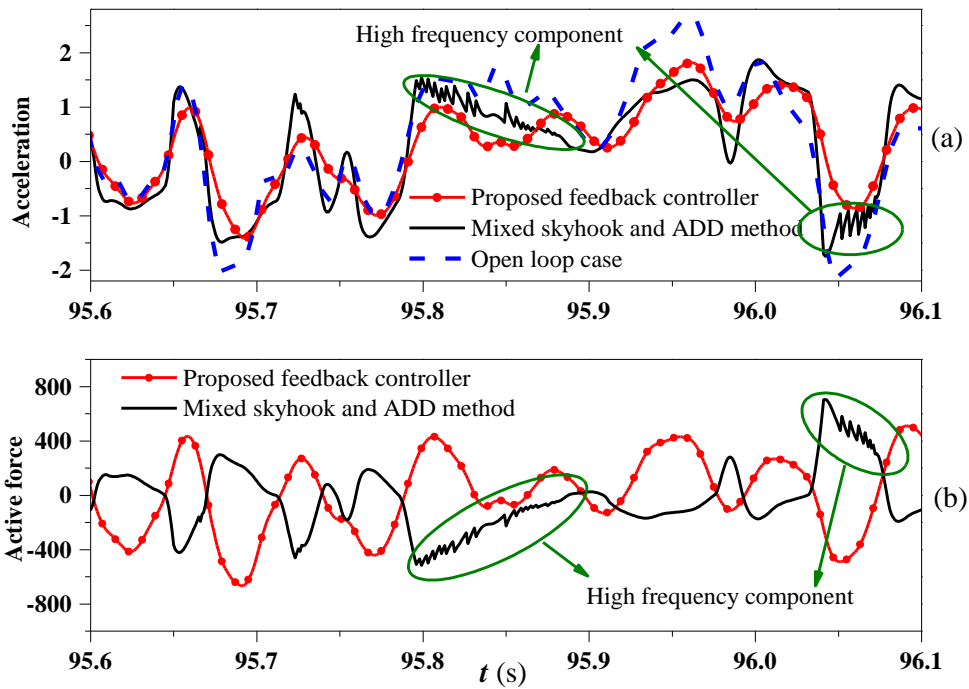


Figure 4.14 (a) Comparison of the accelerations when subjected to ISO C level road profile in the time domain. (b) Comparison of the active force in the time domain.

Comparisons are conducted between the proposed nCOS-based method and the mixed skyhook and ADD method under very close active forces (with  $\mathbf{K}=[0 \ 0$

140 940]). It is well known that a large damping in the open loop case, for example,  $c_s=2000 \text{ N/m}\cdot\text{s}^{-1}$ , will deteriorate the performance in the frequencies between the two resonant frequencies and also the frequencies larger than the second resonant frequency, while a smaller damping coefficient, for example,  $600 \text{ N/m}\cdot\text{s}^{-1}$ , leads to a performance deterioration around the first and second resonant frequencies. Both controllers have better performance than the open loop case, but the proposed one provides much better performance in the frequencies between the two resonant frequencies and also at high frequencies (larger than the second resonant frequency), as is presented in Fig. 5. In Fig. 6, the high-frequency components can be clearly observed in both accelerations and active force with the ADD method, which again verifies the better performance at frequencies larger than the second resonant frequency with the proposed nCOS-based method in Fig. 4.13.

The following procedure is summarized to help understand the proposed new nCOS function for a MIMO nonlinear system and to facilitate the application of the new nCOS function to the analysis and design of those linear parameters of interest.

**Algorithm 4.5 (Application of the new nCOS function to the design of linear feedback controller)**

**Step 1.** Construct the system output and performance objective function; examples can be seen in (4.43) and (4.46).

**Step 2.** Estimate the associated independent coefficients in (4.39) with Algorithm

4.3; an example can be seen in (4.44) with Algorithm 4.4.

**Step 3.** Determine the feedback gain matrix with the performance objective function via the nCOS method; examples can be seen with (4.46) and Fig. 4.12.

#### 4.4 Conclusions

In this chapter, a new nCOS function is developed for those linear parameters of interest in nonlinear systems as a useful extension of the existing nCOS function (which is only available for nonlinear parameters of interest). The new nCOS function is analytically developed for SISO nonlinear systems, and a numerical algorithm for estimating the nCOS function is proposed for MIMO nonlinear systems. Two examples, i.e., linear component design in a nonlinear circuit and linear feedback design for a vehicle suspension system, are given to illustrate the proposed new nCOS function. Note that the linear parameter of interest can be a linear component or a linear controller in engineering practice, so the proposed new nCOS function is thus of great significance.

# 5 An extension to exponential type nonlinear systems

## 5.1 Introduction

Many of the nonlinear systems can be described with an exponential-type nonlinearity (nonlinearity described by  $e^{f(\cdot)}$ ), and examples can be seen in the input-output relationship of the bipolar/CMOS amplifier [11, 178], the clearance nonlinearity in mechanical engineering or controller design [186], the saturation problem in an actuator [140, 161], and the basis function in a neural network [187]. To study this exponential-type nonlinearity via the Volterra series associated method, the exponential-type nonlinearity should first be approximated with a Taylor series expansion to transform the exponential-type nonlinearity into a polynomial-type nonlinearity. This is because the algorithms for calculating the generalized frequency response function (GFRF) are only developed for polynomial nonlinearities in the literature. The Taylor series approximation requires a large truncation order for a high-approximation accuracy, so a large number of parameters are involved in the nonlinear analysis.

The method of transforming the exponential nonlinearity into a polynomial-type nonlinearity in the Volterra series based analysis and design results in two problems: low computational efficiency and high analysis complexity. To overcome these two problems, a low truncation order is usually

used in practical application, for example, a third-order approximation in amplifier dynamics modelling [6, 7]. This simplification obviously leads to a description of system dynamics with less accuracy, and can even miss some interesting results [181]. An effective and efficient method for the analysis and design of an exponential-type nonlinear system is thus of great significance.

In this chapter, a new algorithm for calculating the generalized frequency response function (GFRF) is first proposed for an exponential-type nonlinearity. Compared with the method using a Taylor series approximation discussed above, the proposed algorithm can calculate GFRFs with many fewer parameters, and the advantages of the proposed algorithm, for example, its high computational efficiency and being straightforward and easy to implement, can then be demonstrated. Based on the proposed algorithm for calculating the GFRFs, the nCOS method can be applied to analyse and design the exponential-type nonlinear systems. Two examples, the suppression of harmonic distortion in an amplifier and the analysis of a radial-basis function neural network, are given to illustrate the proposed results. It is shown that the proposed algorithm in section 5.2.1 can effectively calculate the GFRFs for exponential-type nonlinear systems with many fewer parameters and thereby greatly facilitate the analysis and design of exponential-type nonlinear systems with the new nCOS function.

## 5.2 Calculation of the GFRFs and the nCOS-based analysis of exponential-type nonlinear systems

The following exponential-type nonlinear system is considered,

$$g_1(\mathbf{x}, \mathbf{u}) + g_2(\mathbf{x}, \mathbf{u})e^{f_1(\mathbf{x}, \mathbf{u})} + g_3(\mathbf{x}, \mathbf{u})e^{f_2(\mathbf{u})} = \sum_{l=0}^L \frac{d^l u}{dt^l} \quad (5.1)$$

where  $g_1(\mathbf{x}, \mathbf{u}), g_2(\mathbf{x}, \mathbf{u}), g_3(\mathbf{x}, \mathbf{u}), f_1(\mathbf{x}, \mathbf{u})$  are polynomial functions of system output  $\mathbf{x}$  and system input  $\mathbf{u}$ , and  $f_2(\mathbf{u})$  is a polynomial function of  $\mathbf{u}$ .

$l$  denotes the differential order with a maximum order  $L$ .

$$\mathbf{x} = \left\{ x, \frac{d^1 x}{dt^1}, \frac{d^2 x}{dt^2}, \dots, \frac{d^L x}{dt^L} \right\}, \quad \text{and} \quad \mathbf{u} = \left\{ u, \frac{d^1 u}{dt^1}, \frac{d^2 u}{dt^2}, \dots, \frac{d^L u}{dt^L} \right\}. \quad \text{When}$$

$g_2(\mathbf{x}, \mathbf{u}) = g_3(\mathbf{x}, \mathbf{u}) = 0$ , system (5.1) reduces to a polynomial nonlinear system, which has been studied in [59].

The following comes to develop a new algorithm for calculating the generalized frequency response function (GFRF) for an exponential-type nonlinear system (5.1).

### 5.2.1 Algorithm for Calculating Generalized Frequency Response Functions (GFRF)

**Proposition 5.1:** The exponential-type nonlinear system (5.1) can be analytically transformed into the following polynomial nonlinear system as,

$$\begin{cases} g_1(\mathbf{x}, \mathbf{u}) + g_2(\mathbf{x}, \mathbf{u})x_2 + g_3(\mathbf{x}, \mathbf{u})x_3 = \sum_{l=0}^L \frac{d^l u}{dt^l} \\ \dot{x}_2 = x_2 \frac{df_1(\mathbf{x}, \mathbf{u})}{dt} \\ \dot{x}_3 = x_3 \frac{df_2(\mathbf{u})}{dt} \end{cases} \quad (5.2)$$

**Proof:** Denote  $x_2 = e^{f_1(x,u)}$ , and take the derivative with respect to the time variable of both sides, and the following equation can be obtained

$$\dot{x}_2 = e^{f_1(x,u)} \frac{df_1(x,u)}{dt}$$

It is easy to see that the second equation in (5.2) holds. By denoting  $x_3 = e^{f_2(u)}$ , the third equation in (5.2) is also straightforward. Note that  $f_1(x,u)$  and  $f_2(u)$  are polynomial nonlinear functions, so that model (5.2) is a polynomial nonlinear system. This completes the proof.

**Remark 5.1:** By introducing these two auxiliary equations, the nonlinear system described by an exponential nonlinearity can be analytically transformed into a single-input three-output polynomial nonlinear system. The problem between the approximation accuracy and the truncation order in the Taylor series expansion can thus be overcome.

Denote as  $M_{g_1}, M_{g_2}, M_{g_3}, M_{f_1}, M_{f_2}$  the number of coefficients in  $g_1(x,u), g_2(x,u), g_3(x,u), f_1(x,u)$ , and  $f_2(u)$ , respectively. Denote as  $N_{f_1}$  and  $N_{f_2}$  the truncation orders of the Taylor series expansions of  $e^{f_1(x,u)}$  and  $e^{f_2(u)}$  in (5.1), respectively.

**Remark 5.2:** The transformation in Proposition 5.1 results in  $M_{g_1} + M_{g_2} + M_{g_3} + 2M_{f_1} + M_{f_2} + L + 3$  coefficients of interest, while the direct Taylor series expansion of  $e^{f_1(x,u)}$  and  $e^{f_2(u)}$  in (5.1) leads to  $M_{g_1} + M_{g_2} \times \frac{1+N_{f_1}}{2} N_{f_1} + M_{g_3} \times N_{f_2} + L$  coefficients of interest. The polynomial nonlinear system in Proposition 5.1 thus with many fewer coefficients than that by Taylor series expansion. This advantage will be more obvious when a large

truncation order  $N_{f_1}$  or  $N_{f_2}$  is required.

The polynomial nonlinear system (5.2) can be rearranged as the following single-input three-output polynomial equations as

$$\left\{ \begin{array}{l} \sum_{l=0}^L c_{1,0}^{100}(l;1) \frac{d^l x_1}{dt^l} + \sum_{l=0}^L c_{1,0}^{010}(l;1) \frac{d^l x_2}{dt^l} + \sum_{l=0}^L c_{1,0}^{001}(l;1) \frac{d^l x_3}{dt^l} = \sum_{l=0}^L c_{0,1}(l) \frac{d^l u}{dt^l} + \\ \dot{x}_1 = \sum_{m=p+q=2}^N \sum_{p=0}^m \sum_{s_1+s_2+s_3=p} \sum_{l_1, \dots, l_{p+q}=0}^L c_{p,q}^{s_1 s_2 s_3}(l_1, \dots, l_{p+q}; 1) \prod_{i=1}^{s_1} \frac{d^{l_i} x_1}{dt^{l_i}} \prod_{i=s_1+1}^{s_1+s_2} \frac{d^{l_i} x_2}{dt^{l_i}} \prod_{i=s_1+s_2+1}^{s_1+s_2+s_3} \frac{d^{l_i} x_3}{dt^{l_i}} \prod_{i=p+1}^{p+q} \frac{d^{l_i} u}{dt^{l_i}} \\ \dot{x}_2 = \sum_{m=p+q=2}^N \sum_{p=1}^m \sum_{s_1+s_2+s_3=p} \sum_{l_1, \dots, l_{p+q}=0}^L c_{p,q}^{s_1 s_2 s_3}(l_1, \dots, l_{p+q}; 2) \prod_{i=1}^{s_1} \frac{d^{l_i} x_1}{dt^{l_i}} \prod_{i=s_1+1}^{s_1+s_2} \frac{d^{l_i} x_2}{dt^{l_i}} \prod_{i=s_1+s_2+1}^{s_1+s_2+s_3} \frac{d^{l_i} x_3}{dt^{l_i}} \prod_{i=p+1}^{p+q} \frac{d^{l_i} u}{dt^{l_i}} \\ \dot{x}_3 = \sum_{m=p+q=2}^N \sum_{p=1}^m \sum_{s_1+s_2+s_3=p} \sum_{l_1, \dots, l_{p+q}=0}^L c_{p,q}^{s_1 s_2 s_3}(l_1, \dots, l_{p+q}; 3) \prod_{i=1}^{s_1} \frac{d^{l_i} x_1}{dt^{l_i}} \prod_{i=s_1+1}^{s_1+s_2} \frac{d^{l_i} x_2}{dt^{l_i}} \prod_{i=s_1+s_2+1}^{s_1+s_2+s_3} \frac{d^{l_i} x_3}{dt^{l_i}} \prod_{i=p+1}^{p+q} \frac{d^{l_i} u}{dt^{l_i}} \end{array} \right. \quad (5.3)$$

where  $x_i$  is the  $i$ th output,  $i=1,2,3$ .  $N$  is the maximum nonlinear order in terms of output  $x$  and input  $u$ .  $c_{p,q}^{s_1 s_2 s_3}(l_1, \dots, l_{p+q}; j)$  is the model parameter of the

corresponding term  $\prod_{i=1}^{s_1} \frac{d^{l_i} x_1}{dt^{l_i}} \prod_{i=s_1+1}^{s_1+s_2} \frac{d^{l_i} x_2}{dt^{l_i}} \prod_{i=s_1+s_2+1}^{s_1+s_2+s_3} \frac{d^{l_i} x_3}{dt^{l_i}} \prod_{i=p+1}^{p+q} \frac{d^{l_i} u}{dt^{l_i}}$  in the  $j$ th equation,

which has a nonlinear degree  $p+q$  ( $p$  order in terms of the outputs  $x_1, x_2, x_3$ , and  $q$  order in terms of the input  $u$ ), and  $l_i$  is the differential order, with the

maximum order  $L$ .  $s_1, s_2, s_3 \in \mathbb{N}$ , which are the nonlinear degrees of  $x_1, x_2, x_3$

in the nonlinear term  $\prod_{i=1}^{s_1} \frac{d^{l_i} x_1}{dt^{l_i}} \prod_{i=s_1+1}^{s_1+s_2} \frac{d^{l_i} x_2}{dt^{l_i}} \prod_{i=s_1+s_2+1}^{s_1+s_2+s_3} \frac{d^{l_i} x_3}{dt^{l_i}} \prod_{i=p+1}^{p+q} \frac{d^{l_i} u}{dt^{l_i}}$ , respectively.

Denote  $\prod_{i=s+1}^s (\cdot) = 1$  when  $s=0, s_1, s_1+s_2$  holds.

**Remark 5.3:** The equilibrium of the exponential-type nonlinear system is not zero, which means that there exist constant terms (i.e., dc components) when the input  $u$  is zero, so that the results in [65] derived for multiple-input

multiple-output nonlinear differential equations are not applicable for system (5.3).

**Proposition 5.2:** Denote as  $H_0^1, H_0^2, H_0^3$  the equilibria of  $x_1, x_2, x_3$  in (5.3), respectively. The  $n$ th-order generalized frequency response function (GFRF) can be calculated as

$$H_n = \begin{bmatrix} H_n^1(j\omega_1, \dots, j\omega_n) \\ H_n^2(j\omega_1, \dots, j\omega_n) \\ H_n^3(j\omega_1, \dots, j\omega_n) \end{bmatrix} = \begin{bmatrix} l_{1,1} & l_{1,2} & l_{1,3} \\ l_{2,1} & l_{2,2} & l_{2,3} \\ l_{3,1} & l_{3,2} & l_{3,3} \end{bmatrix}^{-1} \begin{bmatrix} A_{1,n} \\ A_{2,n} \\ A_{3,n} \end{bmatrix} = L_n^{-1} \begin{bmatrix} A_{1,n} \\ A_{2,n} \\ A_{3,n} \end{bmatrix} \quad (5.4)$$

where

$$\begin{aligned} l_{1,1} &= \sum_{l=0}^L c_{1,0}^{100}(l;1)(j\omega_1 + \dots + j\omega_n)^l - \sum_{p=2}^N \sum_{\substack{l_2+l_3=p-1 \\ l_2 \leq s_2, l_3 \leq s_3}} c_{p,0}^{1l_2l_3}(l_1, 0, \dots, 0;1)(j\omega_1 + \dots + j\omega_n)^l (H_0^2)^{l_2} (H_0^3)^{l_3} \\ l_{1,2} &= \sum_{l=0}^L c_{1,0}^{010}(l;1)(j\omega_1 + \dots + j\omega_n)^l - \sum_{p=2}^N \sum_{\substack{l_1+l_3=p-1 \\ l_1 \leq s_1, l_3 \leq s_3}} c_{p,0}^{l_1l_3}(0, \dots, l_2, \dots, 0;1)(j\omega_1 + \dots + j\omega_n)^l (H_0^1)^{l_1} (H_0^3)^{l_3} \\ l_{1,3} &= \sum_{l=0}^L c_{1,0}^{001}(l;1)(j\omega_1 + \dots + j\omega_n)^l - \sum_{p=2}^N \sum_{\substack{l_1+l_2=p-1 \\ l_1 \leq s_1, l_2 \leq s_2}} c_{p,0}^{l_1l_2}(0, \dots, 0, l_3;1)(j\omega_1 + \dots + j\omega_n)^l (H_0^1)^{l_1} (H_0^2)^{l_2} \\ l_{2,1} &= - \sum_{p=2}^N \sum_{\substack{l_2+l_3=p-1 \\ l_2 \leq s_2, l_3 \leq s_3}} c_{p,0}^{1l_2l_3}(l_1, 0, \dots, 0;2)(j\omega_1 + \dots + j\omega_n)^l (H_0^2)^{l_2} (H_0^3)^{l_3} \\ l_{2,2} &= c_{1,0}^{010}(1;1)(j\omega_1 + \dots + j\omega_n) - \sum_{p=2}^N \sum_{\substack{l_1+l_3=p-1 \\ l_1 \leq s_1, l_3 \leq s_3}} c_{p,0}^{l_1l_3}(0, \dots, l_2, \dots, 0;2)(j\omega_1 + \dots + j\omega_n)^l (H_0^1)^{l_1} (H_0^3)^{l_3} \\ l_{2,3} &= - \sum_{p=2}^N \sum_{\substack{l_1+l_2=p-1 \\ l_1 \leq s_1, l_2 \leq s_2}} c_{p,0}^{l_1l_2}(0, \dots, 0, l_3;2)(j\omega_1 + \dots + j\omega_n)^l (H_0^1)^{l_1} (H_0^2)^{l_2} \\ l_{3,1} &= - \sum_{p=2}^N \sum_{\substack{l_2+l_3=p-1 \\ l_2 \leq s_2, l_3 \leq s_3}} c_{p,0}^{1l_2l_3}(l_1, 0, \dots, 0;3)(j\omega_1 + \dots + j\omega_n)^l (H_0^2)^{l_2} (H_0^3)^{l_3} \\ l_{3,2} &= - \sum_{p=2}^N \sum_{\substack{l_1+l_3=p-1 \\ l_1 \leq s_1, l_3 \leq s_3}} c_{p,0}^{l_1l_3}(0, \dots, l_2, \dots, 0;3)(j\omega_1 + \dots + j\omega_n)^l (H_0^1)^{l_1} (H_0^3)^{l_3} \\ l_{3,3} &= c_{1,0}^{001}(1;1)(j\omega_1 + \dots + j\omega_n) - \sum_{p=2}^N \sum_{\substack{l_1+l_2=p-1 \\ l_1 \leq s_1, l_2 \leq s_2}} c_{p,0}^{l_1l_2}(0, \dots, 0, l_3;3)(j\omega_1 + \dots + j\omega_n)^l (H_0^1)^{l_1} (H_0^2)^{l_2} \end{aligned} \quad (5.5)$$

and

$$\begin{aligned}
A_{i,n} &= c_{0,n}^{000}(l_1, \dots, l_n; i) \prod_{i=1}^n (j\omega_i)^{l_i} + \sum_{m=p+q=2}^n \sum_{p=1}^m \sum_{\substack{t=t_1+t_2+t_3=0 \\ t_1 \leq s_1, t_2 \leq s_2 \\ t_3 \leq s_3}}^{p-1} \sum_{l_1, \dots, l_{p+q}=0}^L c_{p,q}^{s_1 s_2 s_3}(l_1, \dots, l_{p+q}; i) \\
&\quad \times (H_0^1)^{t_1} (H_0^2)^{t_2} (H_0^3)^{t_3} \prod_{i=1}^q (j\omega_{n-q+i})^{l_{n-q+i}} H_{n-q,p-t}^{t_1 t_2 t_3}(\omega_1, \dots, \omega_{n-q})
\end{aligned} \tag{5.6}$$

$$\begin{aligned}
H_{n-q,p-t}^{t_1 t_2 t_3}(\omega_1, \dots, \omega_{n-q}) &= \sum_{i=0}^{t_1} (\omega_1 + \dots + \omega_i)^{l_{i+1}} H_i^1(\omega_1, \dots, \omega_i) H_{n-q-i,p-t-1}^{(t_1-i)t_2 t_3}(\omega_{i+1}, \dots, \omega_{n-q}) \\
&\quad + \sum_{i=0}^{t_2} (\omega_1 + \dots + \omega_i)^{l_{i+2}+1} H_i^2(\omega_1, \dots, \omega_i) H_{n-q-i,p-t-1}^{t_1(t_2-i)t_3}(\omega_{i+1}, \dots, \omega_{n-q}) \\
&\quad + \sum_{i=0}^{t_3} (\omega_1 + \dots + \omega_i)^{l_{i+3}+t_3+1} H_i^3(\omega_1, \dots, \omega_i) H_{n-q-i,p-t-1}^{t_1 t_2(t_3-i)}(\omega_{i+1}, \dots, \omega_{n-q})
\end{aligned} \tag{5.7}$$

where  $\sum_{i=0}^0 (\cdot) = 0$ , and  $t_1' = s_1 - t_1, t_2' = s_2 - t_2, t_3' = s_3 - t_3$ . The recursion in (5.7)

ends when  $p=1$  holds, i.e.,

$$\begin{aligned}
H_{n,1}^{100}(\omega_1, \dots, \omega_n) &= (\omega_1 + \dots + \omega_n)^{s_1} H_n^{100}(\omega_1, \dots, \omega_n) \\
H_{n,1}^{010}(\omega_1, \dots, \omega_n) &= (\omega_1 + \dots + \omega_n)^{s_1+s_2} H_n^{010}(\omega_1, \dots, \omega_n) \\
H_{n,1}^{001}(\omega_1, \dots, \omega_n) &= (\omega_1 + \dots + \omega_n)^{s_1+s_2+s_3} H_n^{001}(\omega_1, \dots, \omega_n)
\end{aligned} \tag{5.8}$$

For the first-order GFRF,

$$\begin{aligned}
A_{1,1} &= \sum_{l=0}^L c_{0,1}(l; 1)(j\omega_1)^l \\
&\quad + \sum_{p=1}^{N-1} \sum_{s_1+s_2+s_3=p}^L \sum_{l_{p+1}=0}^L c_{p,1}^{s_1 s_2 s_3}(0, \dots, 0, l_{p+1}; 1) (H_0^1)^{s_1} (H_0^2)^{s_2} (H_0^3)^{s_3} (j\omega_1)^{l_{p+1}} \\
A_{2,1} &= \sum_{p=1}^{N-1} \sum_{s_1+s_2+s_3=p}^L \sum_{l_{p+1}=0}^L c_{p,1}^{s_1 s_2 s_3}(0, \dots, 0, l_{p+1}; 2) (H_0^1)^{s_1} (H_0^2)^{s_2} (H_0^3)^{s_3} (j\omega_1)^{l_{p+1}} \\
A_{3,1} &= \sum_{p=1}^{N-1} \sum_{s_1+s_2+s_3=p}^L \sum_{l_{p+1}=0}^L c_{p,1}^{s_1 s_2 s_3}(0, \dots, 0, l_{p+1}; 3) (H_0^1)^{s_1} (H_0^2)^{s_2} (H_0^3)^{s_3} (j\omega_1)^{l_{p+1}}
\end{aligned} \tag{5.9}$$

**Proof:** See Appendix 5.1.

The  $L_n$  matrix in (5.4) can be singular when  $\omega_1 + \dots + \omega_n = 0$  holds (which means that the GFRFs are calculated at dc components). For this case, the following algorithm is proposed for an approximation of the inverse matrix  $L_n^{-1}$ :

**Algorithm 5.1:**

**Step 1.** For the  $n$ th-order GFRF, approximate  $\omega_i$  by  $\omega'_i = \omega_i + \frac{\Delta}{n}$  for  $i = 1, 2, \dots, n$ , where  $\Delta$  is a small perturbation close to 0 which makes the inverse matrix  $L_n^{-1}(j\omega'_1 + \dots + j\omega'_n) = L_n^{-1}(j\Delta)$  exist.

**Step 2.** Approximate  $H_n^i(\omega_1, \dots, \omega_n)$  with  $H_n^i(\omega'_1, \dots, \omega'_n)$ .

**Remark 5.4:** The point  $(\omega'_1, \dots, \omega'_n)$  is chosen in the normal direction of the hyperplane  $\omega_1 + \dots + \omega_n = 0$  with a distance  $d = \frac{\Delta}{\sqrt{n}}$  to the frequencies  $(\omega_1, \dots, \omega_n)$ . After  $\Delta$  is chosen,  $L_n^{-1}(j\Delta)$  will be the same for a different order  $n$ , that is,  $L_1^{-1}(j\Delta) = L_2^{-1}(j\Delta) = \dots$ . Note that the distance  $d$  decreases as the order  $n$  increases, so the approximation of  $H_n^i(\omega_1, \dots, \omega_n)$  with  $H_n^i(\omega'_1, \dots, \omega'_n)$  would thus be more accurate as the order  $n$  increases.

To illustrate the theoretical results above, the following example is given and discussed.

**Example 5.1 Pure input nonlinearity**

Consider the exponential nonlinear system described by

$$x = e^{au}$$

where  $u$  is the system input and  $x$  is the system output. This exponential nonlinearity can be expanded with a Taylor series as

$$x = 1 + au + \frac{a^2 u^2}{2!} + \frac{a^3 u^3}{3!} + \dots \quad (5.10)$$

When the nonlinear equation is truncated to  $u^3$ , there are 4 parameters to analyse. The GFRFs can be computed as

$$\begin{aligned}
H_0 &= 1, \\
H_1 &= 1, \\
H_2 &= \frac{a^2}{2!}, \\
H_3 &= \frac{a^3}{3!}, \dots
\end{aligned} \tag{5.11}$$

With the results in Proposition 5.1, the exponential nonlinearity  $x = e^{au}$  can be analytically transformed into the following single-input single-output polynomial nonlinear system

$$\dot{x} = axi \tag{5.12}$$

In (5.12), there exists only one coefficient  $a$ . The GFRFs can then be computed with Proposition 5.2 as

$$\begin{aligned}
H_0^{asym} &= 1, \\
H_1^{asym}(\omega_1) &= \frac{a(j\omega_1)H_0^{asym}}{j\omega_1}, \\
H_2^{asym}(\omega_1, \omega_2) &= \frac{a(j\omega_1)H_1^{asym}(j\omega_2)}{j\omega_1 + j\omega_2}, \\
H_3^{asym}(\omega_1, \omega_2, \omega_3) &= \frac{a(j\omega_1)H_2^{asym}(\omega_2, \omega_3)}{j\omega_1 + j\omega_2 + j\omega_3} \dots
\end{aligned} \tag{5.13}$$

The GFRFs in (5.13) are asymmetrical, but can be symmetrized as,

$$H_0^{sym} = 1, H_1^{sym}(\omega_1) = a, H_2^{sym}(\omega_1, \omega_2) = \frac{a^2}{2!}, H_3^{sym}(\omega_1, \omega_2, \omega_3) = \frac{a^3}{3!} \dots \tag{5.14}$$

The GFRFs in (5.14) are the same as those in (5.11), thereby verifying the effectiveness of the result in Proposition 5.2. It is clear that the polynomial nonlinear system in (5.12) has many fewer parameters (only one parameter) than that by the Taylor series expansion in (5.10) (4 parameters). The other advantages of the proposed algorithm, for example, its high computational efficiency and being straightforward and easy to implement, will be more obvious for pure output

nonlinear systems or cross input-output nonlinear systems, which will be illustrated and discussed in the next section.

### 5.2.2 The nCOS-based analysis and design for exponential-type nonlinear systems

It has been shown in Chapter 3 and Chapter 4 that the output spectrum of a nonlinear system can be expressed as a polynomial function with respect to those parameters of interest, referred to as nCOS functions for nonlinear parameters of interest in Chapter 3 and new nCOS functions for linear parameters of interest in Chapter 4.

Assuming that there are 3 parameters of interest, denoted as  $c_1, c_2, c_3$ , the output spectrum can then be given as

$$Y(\omega) = \varphi_1^1(\omega)c_1 + \varphi_2^1(\omega)c_2 + \varphi_3^1(\omega)c_3 + \varphi_{11}^2(\omega)(c_1)^2 + \varphi_{12}^2(\omega)c_1c_2 + \varphi_{13}^2(\omega)c_1c_3 + \varphi_{22}^2(\omega)(c_2)^2 + \dots \quad (5.15)$$

where  $\varphi_{ij}^{(k)}(\omega)$  is the coefficient of the polynomial function, which is independent of the parameters of interest, i.e.,  $c_1, c_2, c_3$ . When the nCOS function in (5.15) is truncated by up to third-order, there are 39 coefficients for calculation. The problem would be even worse when a higher truncation order is required or more parameters are of interest in the nonlinear analysis and design.

The proposed new algorithm in section 5.2.1 can calculate the GFRFs of an exponential-type nonlinearity with many fewer parameters, which will significantly facilitate the analysis and design of an exponential-type nonlinear

system via the new nCOS function. An example for studying the harmonic distortion of a bipolar amplifier is discussed in the following.

**Example 5.2 Suppression of harmonic distortion via the new nCOS function**

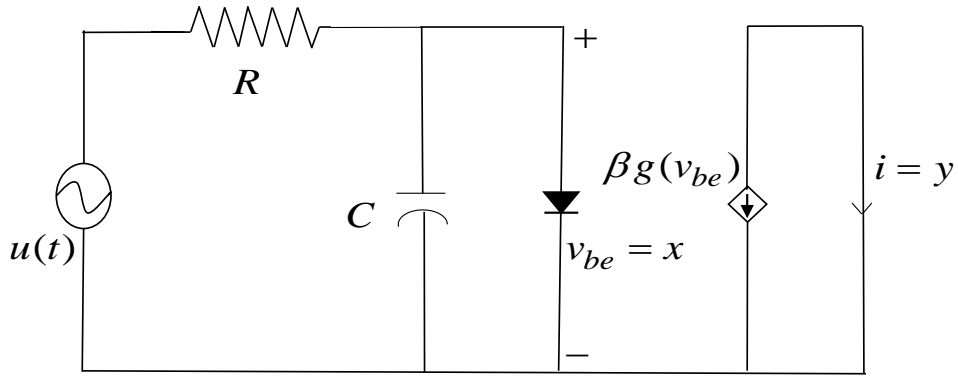


Figure 5.1 Equivalent model of bipolar amplifier

The input-output dynamics of the common emitter amplifier are governed by the exponential-type nonlinearity as

$$\frac{u - x}{R} = C\dot{x} + I_{BQ} (e^{\frac{x}{V_T}} - 1) \quad (5.16)$$

$$y = -\beta I_{BQ} (e^{\frac{x}{V_T}} - 1) \quad (5.17)$$

where  $u = U \sin \omega t$ , and  $I_{BQ}$  is the reverse saturation current, which always varies with temperature. It is thus necessary and of great interest to study how the amplifier performance, for example, the linearity described by the harmonic distortion, is affected by this reverse saturation current.

In the literature, the exponential-type nonlinearity is often approximated by a third-order Taylor series expansion as

$$g(x) = I_{BQ} (e^{x/V_T} - 1) = \sum_{i=1}^3 \frac{I_{BQ}}{i! V_T^i} x^i = \frac{I_{BQ}}{V_T} x + \frac{I_{BQ}}{2V_T^2} x^2 + \frac{I_{BQ}}{6V_T^3} x^3 \quad (5.18)$$

From (5.18), it can be seen that  $I_{BQ}$  is involved in all 3 parameters, so that the number of parameters to analyse via the Volterra series associated method is 3.

Denote  $x_2 = I_{BQ}(e^{\frac{x_1}{V_T}} - 1)$ , and take the derivative with respect to time of both sides, and  $\dot{x}_2 = \frac{I_{BQ}}{V_T}\dot{x}_1 + \frac{1}{V_T}\dot{x}_1x_2$  will hold. (5.17) can then be given as  $y = -\beta x_2$ .

(5.16) can be rearranged into a single-input double-output set of equations as

$$\begin{cases} \frac{1}{R}x_1 + Cx_1 + x_2 = \frac{1}{R}u \\ -\frac{I_{BQ}}{V_T}\dot{x}_1 + \dot{x}_2 = \frac{1}{V_T}\dot{x}_1x_2 \end{cases} \quad (5.19)$$

The GFRFs can then be computed according to Proposition 5.2 as

$$H_0^1 = H_0^2 = 0 \quad (5.20)$$

$$\begin{bmatrix} H_1^1(j\omega_1) \\ H_1^2(j\omega_1) \end{bmatrix} = \begin{bmatrix} \frac{1}{R} + C(j\omega_1) & 1 \\ -\frac{I_{BQ}}{V_T}(j\omega_1) & (j\omega_1) \end{bmatrix}^{-1} \begin{bmatrix} \frac{1}{R} \\ 0 \end{bmatrix} \quad (5.21)$$

$$\begin{bmatrix} H_n^1(\omega_1, \dots, \omega_n) \\ H_n^2(\omega_1, \dots, \omega_n) \end{bmatrix} = \begin{bmatrix} \frac{1}{R} + C(j\omega_1 + \dots + j\omega_n) & 1 \\ -\frac{I_{BQ}}{V_T}(j\omega_1 + \dots + j\omega_n) & (j\omega_1 + \dots + j\omega_n) \end{bmatrix}^{-1} \begin{bmatrix} 0 \\ A_{2,n} \end{bmatrix}, n \geq 2 \quad (5.22)$$

where

$$A_{2,2} = \frac{1}{V_T}(j\omega_1)H_1^1(j\omega_1)H_1^2(j\omega_2),$$

$$A_{2,3} = \frac{1}{V_T} \left[ (j\omega_1)H_1^1(\omega_1)H_2^2(\omega_2, \omega_3) + (j\omega_1 + j\omega_2)H_2^1(\omega_1, \omega_2)H_1^2(\omega_3) \right]$$

$$\begin{aligned} A_{2,4} = \frac{1}{V_T} & \left[ (j\omega_1)H_1^1(\omega_1)H_3^2(\omega_2, \omega_3, \omega_4) + (j\omega_1 + j\omega_2)H_2^1(\omega_1, \omega_2)H_2^2(\omega_3 + \omega_4) \right. \\ & \left. + (j\omega_1 + j\omega_2 + j\omega_3)H_3^1(\omega_1, \omega_2, \omega_3)H_1^2(\omega_4) \right] \end{aligned}$$

$$A_{2,5} = \frac{1}{V_T} \left[ (j\omega_1)H_1^1(\omega_1)H_4^2(\omega_2, \omega_3, \omega_4, \omega_5) + (j\omega_1 + j\omega_2)H_2^1(\omega_1, \omega_2)H_3^2(\omega_3, \omega_4, \omega_5) \right. \\ \left. + (j\omega_1 + j\omega_2 + j\omega_3)H_3^1(\omega_1, \omega_2, \omega_3)H_2^2(\omega_4, \omega_5) \right. \\ \left. + (j\omega_1 + j\omega_2 + j\omega_3 + j\omega_4)H_4^1(\omega_1, \omega_2, \omega_3, \omega_4)H_1^2(\omega_5) \right]$$

...

The calculation of the GFRFs for (5.19) is more efficient and straightforward than that by the Taylor series expansion in (5.18) because there exists only one nonlinear parameter,  $\frac{1}{V_T}$ , in (5.19), while at least two nonlinear parameters,  $\frac{I_{BQ}}{V_T}$  and  $\frac{I_{BQ}}{2V_T^2}$ , are involved in the calculation of GFRFs for the system approximated by the Taylor series expansion (5.18).

In (5.19), it is clear that only one parameter,  $-\frac{I_{BQ}}{V_T}$ , is of interest to analyse.

Denote  $c = -\frac{I_{BQ}}{V_T}$  for ease of notation in the following illustration. According to the new nCOS function developed in Chapter 4 for the analysis and design of those linear parameters of interest, the output spectrum can be expressed as a polynomial function of linear parameter  $c$  as

$$Y(\omega) = \varphi_0(\omega) + \varphi_1(\omega)c + \varphi_2(\omega)c^2 + \varphi_3(\omega)c^3 + \varphi_4(\omega)c^4 + \dots \quad (5.23)$$

where the coefficients  $\varphi_0(\omega), \varphi_1(\omega), \dots$  are independent of the linear parameter  $c$ .

The third-order harmonic distortion can then be calculated as

$$HD_3 = \frac{\varphi_0(3\Omega) + \varphi_1(3\Omega)c + \varphi_2(3\Omega)c^2 + \varphi_3(3\Omega)c^3 + \varphi_4(3\Omega)c^4 + \dots}{\varphi_0(\Omega) + \varphi_1(\Omega)c + \varphi_2(\Omega)c^2 + \varphi_3(\Omega)c^3 + \varphi_4(\Omega)c^4 + \dots} \quad (5.24)$$

where  $\varphi_0(3\Omega), \varphi_1(3\Omega), \dots$  are coefficients at the third-order harmonic frequency,

and  $\varphi_0(\Omega), \varphi_1(\Omega), \dots$  are coefficients at frequency  $\Omega$ .

The application of the new nCOS function is under the assumption that the input-output relationship of the nonlinear system allows a convergent Volterra series expansion. Given the model parameters of  $V_T = 26\text{mV}$ ,  $\beta = 180$ ,  $R = 100\Omega$ ,  $C = 10\text{pF}$ , and input frequency  $\omega = 2\pi \times 5 \times 10^6 \text{ rad/s}$ , the input magnitude bound is 42mV according to the results in section 2.4.

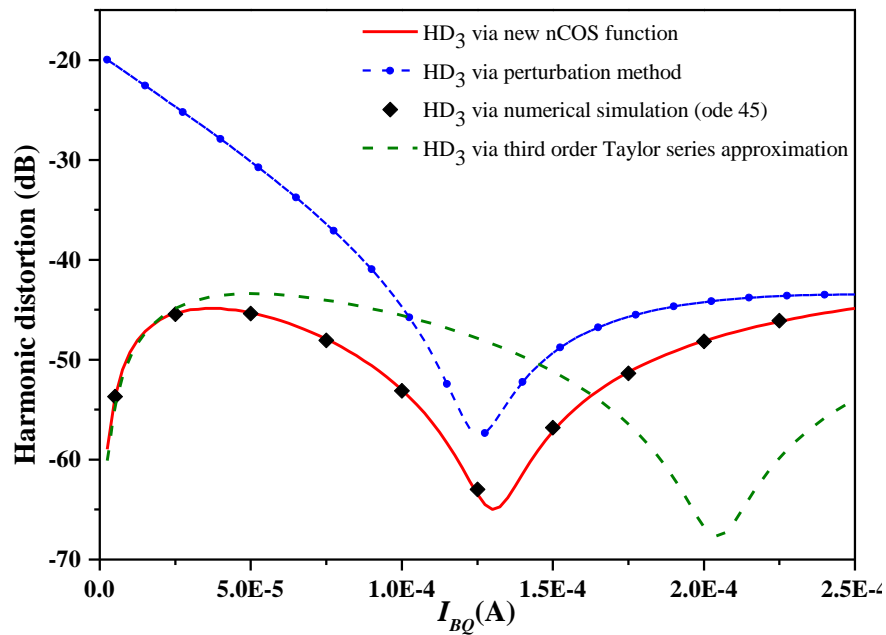


Figure 5.2 Comparison of third-order harmonic distortion with different methods

Linearization is a hot topic in the literatures for the analysis and design of amplifier [6-11, 180]. Usually, a third-order Taylor series expansion is used to approximate the exponential nonlinearity. The Taylor series is truncated up to the third-order to simplify the analysis and design (as only three parameters are involved in the analysis and design). This simplification may leads to an inaccurate or wrong result. In Figure 5.2, the harmonic distortion by the third-order Taylor series expansion is quite different from that by numerical simulation. To improve the accuracy of the result, the exponential nonlinearity

should be approximated with a higher-order Taylor series expansion, but in this case, the number of parameters to analyse and design would increase, which will greatly complicate the analysis and also reduce the computational efficiency. In Proposition 5.1, the exponential-type nonlinear system can be analytically transformed into a polynomial nonlinear system. This transformation produces many fewer parameters to analyse and design (only one linear parameter  $-\frac{I_{BQ}}{V_T}$  in this example), which will significantly facilitate the analysis and design of the nonlinear system described by the exponential nonlinearity. From Figure 5.2, it can be observed that based on the analytical transformation in Proposition 5.1, the harmonic distortion via the new nCOS function has good agreement with that by numerical simulation. As a comparison, the harmonic distortion by the perturbation method proposed in [180] is also presented in Figure 5.2, which is also quite different from that by numerical simulation.

### **Example 5.3 nCOS-based analysis of neural network**

Artificial neural networks are a hot topic in the literature for system modelling, identification, and control. The study of neural networks can also be conducted in the frequency domain. In [188, 189], the basis functions of the neural network were first approximated with a truncated Taylor series expansion to transform the basis functions from exponential-type nonlinearities into polynomial-type nonlinearities, so that the generalized frequency response functions of the neural network can be computed, and the Volterra series associated methods can be

applied to the analysis of the neural network. The Taylor series expansion of the exponential-type basis functions results in too many parameters (including linear parameters and nonlinear parameters) to analyse and design, which greatly complicates the Volterra series based study in the frequency domain. In the following, it will be shown that the proposed algorithm in section 5.2.1 can calculate the GFRFs of the neural network with many fewer parameters of interest and to facilitate the analysis and design of the neural network with the nCOS-based method.

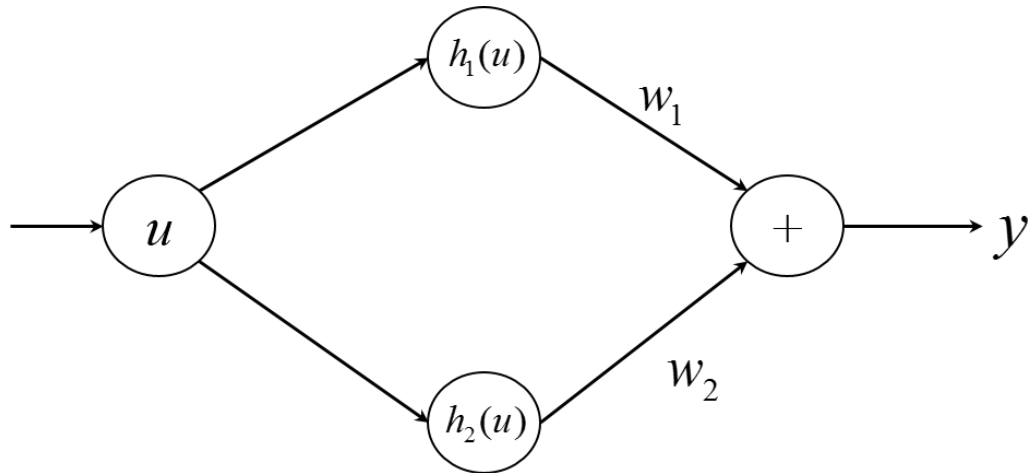


Figure 5.3 A three-layer radial-basis function neural network

In Figure 5.3, a three-layer radial-basis function neural network is shown.

$w_1, w_2$  are weight values, and  $h_1, h_2$  are radial-basis functions

$$h_i(u) = e^{-\frac{(u-c_i)^2}{2b_i^2}}, i=1,2. \quad (5.25)$$

where  $c_i$  and  $b_i$  are the centre point and the width of the Gaussian function, respectively.  $u$  is the network input.

The following comes to study the effects of the parameters  $c_i$  and  $b_i$  on the neural network output  $y$ . With the results in [188, 189], the basis function

in (5.25) should be expanded with a truncated Taylor series as

$$x_i = a_{i0} + a_{i1}u + a_{i2}u^2 + a_{i3}u^3 + \cdots, i = 1, 2. \quad (5.26)$$

where

$$\begin{aligned} a_{i0} &= e^{-\frac{c_i^2}{2b_i^2}}, \\ a_{i1} &= \frac{c_i}{b_i^2} e^{-\frac{c_i^2}{2b_i^2}}, \\ a_{i2} &= \left( \frac{c_i^2}{b_i^4} - \frac{1}{b_i^2} \right) e^{-\frac{c_i^2}{2b_i^2}}, \\ &\dots \end{aligned}$$

From (5.26), it can be observed that the parameters of interest, i.e.,  $c_i$  and  $b_i$ , are involved in all of the coefficients  $a_{i0}, a_{i1}, a_{i2}, a_{i3}, \dots$ . Obviously, a large number of coefficients in (5.26) would complicate the analysis of the neural network in Figure 5.3.

Denote  $x_i = h_i(u)$ , and take the derivative with respect to time of both sides, and the following equation holds

$$\dot{x}_i = -\frac{1}{b_i^2} x_i u \dot{u} + \frac{c_i}{b_i^2} x_i \dot{u}. \quad (5.27)$$

In (5.27), obviously only two parameters are of interest, i.e.,  $-\frac{1}{b_i^2}$  and  $\frac{c_i}{b_i^2}$ . The

GFRFs can be calculated according to Proposition 5.2 as

$$H_0^i = e^{-\frac{c_i^2}{2b_i^2}} \quad (5.28)$$

and

$$H_n^i = L_{i,n}^{-1} A_{i,n} \quad (5.29)$$

where

$$L_{i,n}^{-1} = \frac{1}{j\omega_1 + \dots + j\omega_n} \quad (5.30)$$

$$\begin{aligned} A_{i,1} &= \frac{c_i}{b_i^2} H_0^i, \\ A_{i,2} &= \frac{c_i}{b_i^2} (j\omega_2) \times H_1^i(\omega_1) - \frac{j\omega_2}{b_i^2} H_0^i, \\ A_{i,3} &= \frac{c_i}{b_i^2} (j\omega_3) \times H_2^i(\omega_1, \omega_2) - \frac{j\omega_3}{b_i^2} H_1^i(\omega_1), \\ A_{i,4} &= \frac{c_i}{b_i^2} (j\omega_4) \times H_3^i(\omega_1, \omega_2, \omega_3) - \frac{j\omega_4}{b_i^2} H_2^i(\omega_1, \omega_2), \\ A_{i,5} &= \frac{c_i}{b_i^2} (j\omega_5) \times H_4^i(\omega_1, \omega_2, \omega_3, \omega_4) - \frac{j\omega_5}{b_i^2} H_3^i(\omega_1, \omega_2, \omega_3), \\ &\dots \end{aligned} \quad (5.31)$$

Denote  $f_i = -\frac{1}{b_i^2}$  and  $g_i = \frac{c_i}{b_i^2}$ , and the calculated GFRFs can then be given in

the form of characteristic functions as

$$\begin{aligned} H_1^i(\omega_1) &= g_i H_0^i, \\ H_2^i(\omega_1, \omega_2) &= \left[ (g_i)^2 + f_i \right] H_0^i \times \frac{\omega_2}{\omega_1 + \omega_2}, \\ H_3^i(\omega_1, \omega_2, \omega_3) &= \left[ (g_i)^3 + f_i g_i \right] H_0^i \times \frac{\omega_2 \omega_3}{(\omega_2 + \omega_3)(\omega_1 + \omega_2 + \omega_3)}, \\ H_4^i(\omega_1, \omega_2, \omega_3, \omega_4) &= (g_i)^4 H_0^i \times \frac{\omega_2 \omega_3 \omega_4}{(\omega_2 + \omega_3)(\omega_1 + \omega_2 + \omega_3)(\omega_1 + \omega_2 + \omega_3 + \omega_4)} \\ &+ f_i (g_i)^2 H_0^i \times \left[ \frac{\omega_2 \omega_3 \omega_4}{(\omega_2 + \omega_3)(\omega_1 + \omega_2 + \omega_3)(\omega_1 + \omega_2 + \omega_3 + \omega_4)} + \frac{\omega_2 \omega_4}{(\omega_1 + \omega_2)(\omega_1 + \omega_2 + \omega_3 + \omega_4)} \right] \\ &+ (f_i)^2 H_0^i \times \frac{\omega_2 \omega_4}{(\omega_1 + \omega_2)(\omega_1 + \omega_2 + \omega_3 + \omega_4)}, \\ &\dots \end{aligned} \quad (5.32)$$

The output spectrum can then be given as

$$\begin{aligned} X_i(\omega) &= \varphi_0(\omega) H_0^i + \varphi_{01}(\omega) f_i H_0^i + \varphi_{10}(\omega) g_i H_0^i \\ &+ \varphi_{02}(\omega) (f_i)^2 H_0^i + \varphi_{11}(\omega) f_i g_i H_0^i + \varphi_{20}(\omega) (g_i)^2 H_0^i + \dots, \end{aligned} \quad (5.33)$$

and

$$Y(\omega) = X_1(\omega) + X_2(\omega) \quad (5.34)$$

which are nCOS functions, and the coefficients  $\varphi_{\bullet}$  are independent of those

parameters of interest, i.e.,  $f_i$  and  $g_i$ .

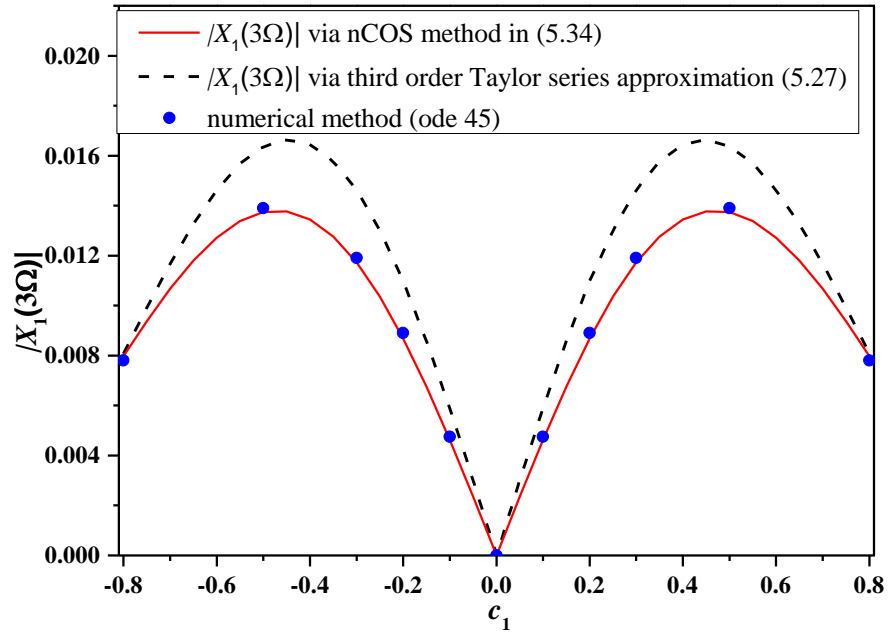


Figure 5.4 Amplitude of  $X_1(3\Omega)$  via different methods

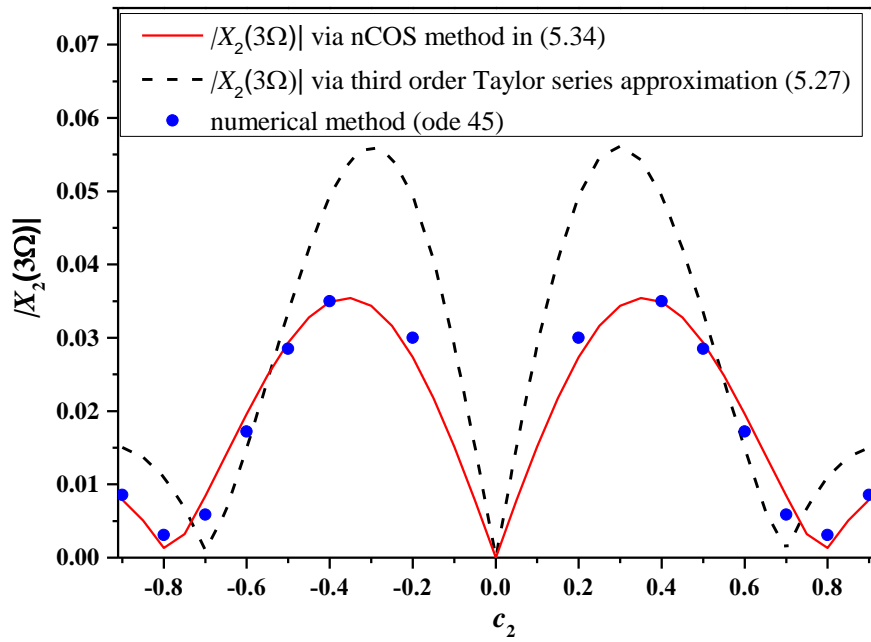


Figure 5.5 Amplitude of  $X_2(3\Omega)$  via different methods

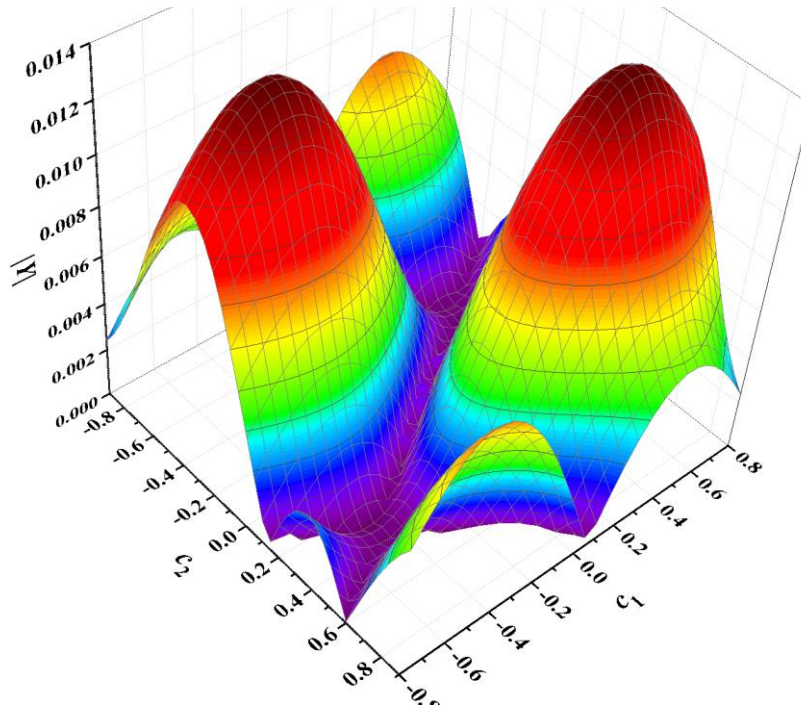


Figure 5.6 Amplitude of  $Y(3\Omega)$  with different parameters of interest

Given  $u = 0.5 \sin(2\pi \times 20t)$ , and  $b_1 = 0.6, b_2 = 0.4$ , the spectra of  $X_1(\omega)$  and  $X_2(\omega)$  with different parameters of interest can be obtained via (5.33). The coefficients  $\varphi_i$  in (5.33) can be analytically calculated. Both Figure 5.4 and Figure 5.5 show that the spectrum via the nCOS method has good agreement with that by numerical simulation, but the third-order Taylor series approximation of the radial-basis function in (5.26) leads to an inaccurate result. To improve the accuracy of the result by Taylor series expansion, a higher truncation order is therefore required, which will of course introduce more parameters to the nonlinear analysis and complicate the analysis. The output spectrum  $Y(3\Omega)$  can then be easily calculated with different parameters of interest, as is shown in Figure 5.6. It can be observed that the proposed results in section 5.2.1 can calculate the GFRFs of the radial-basis neural network with many fewer parameters of interest and thereby greatly facilitate the analysis of the neural

network via the nCOS method in the frequency domain. The nCOS method provides an effective and straightforward way to analyse the neural networks.

### 5.3 Conclusion

In this chapter, the nCOS method is extended for the analysis and design of nonlinear systems described by exponential nonlinearities. First, the exponential-type nonlinear system is analytically transformed into a polynomial nonlinear system, which results in many fewer parameters to analyse and design when compared with that by a Taylor series approximation. Then, a new algorithm is developed to calculate the generalized frequency response functions (GFRFs) of the targeted polynomial nonlinear system with dc terms (with non-zero equilibria). This new algorithm greatly facilitates the nCOS-based analysis and design of the exponential-type nonlinear system because many fewer parameters are involved in the nonlinear analysis and design.

# 6 Conclusions and future work

## 6.1 Conclusions

The Volterra series and its associated methods for nonlinear analysis and design have been extensively studied and well applied to various engineering practices. This thesis addresses several issues of the Volterra series associated method raised in practical applications.

In Chapter 2, the convergence bound of the Volterra series expansion is studied for a wide class of nonlinear systems described by a nonlinear auto-regressive with exogenous input (NARX) model. The proposed parametric bound of convergence (PBoC) can be easily computed with the proposed algorithms and can provide a very useful guidance for the parameter optimization and/or system design of nonlinear systems for any characteristic parameters (including the model parameters, input magnitude, and frequency variable). The parametric convergence margin (PCM) is proposed to evaluate the extent of a given nonlinear system to which the system has a convergent Volterra series expansion. The result of PBoC is then extended to the NARX model with a general input and also to the single-input multiple-output (SIMO) NARX model. The results in this chapter are great extensions of those convergent results in the literatures, where the convergence bound is only studied for the input magnitude.

In Chapter 3, the applications of the nonlinear characteristic output spectrum (nCOS) method involves two parts. First, a nonlinear damping defined as a

function of both position and velocity is proposed to tackle the dilemma relating to linear damping. The performance of the nonlinear damping is derived using the nCOS method, and the proposed nonlinear damping shows advantages under both force excitation and base excitation. Then, the multiple-object optimization problem in vibration control is investigated. The multiple-object function is first cast into a nonlinear characteristic output spectrum function, which can then be freely analysed and designed within the parametric convergence region computed with the results in Chapter 2. A nonlinear vehicle suspension system is given for illustration.

The nCOS method in Chapter 3 is only applicable to those nonlinear parameters of interest. In Chapter 4, the new nCOS function is developed for those linear parameters of interest in nonlinear systems. This extension is of great significance because the linear component or linear controller is usually easy to implement. First, the generalized frequency response function (GFRF) is expressed as a polynomial function of linear parameters of interest. The coefficients of the polynomial function is independent of those linear parameters of interest and can be symbolically determined with the proposed procedures. The new nCOS function is then developed, which shows great advantages such as high computational efficiency and straightforward insight into understanding nonlinear systems. For nonlinear state equations (which can be observed as multiple-input multiple-output system) in control design, the symbolical determination of the coefficients in the new nCOS function may be complicated,

so a numerical identification method is developed for facilitating the application of the extended nCOS method in practical engineering problems.

Finally, in Chapter 5, the nCOS method is extended to those nonlinear systems with exponential-type nonlinearity. A novel algorithm is developed for calculating the generalized frequency response function (GFRF) for exponential-type nonlinear systems. The proposed algorithm transforms the exponential-type nonlinearity into a polynomial-type nonlinearity by introducing two auxiliary equations. Compared with that by directly approximating the exponential-type nonlinearity with a Taylor series expansion, the proposed algorithm results in many fewer parameters to analyse and design, which greatly facilitates the application of the nCOS method. This chapter provides a powerful tool for the analysis and design of those systems involving exponential-type nonlinearities.

## **6.2 Future work**

1. The concept of the parametric convergence margin (PCM) is developed as an indicator to quantitatively evaluate whether or not a given nonlinear system has a convergent Volterra series expansion. A controller to transfer a system with strong nonlinearity into a mild nonlinear system can thus be developed using the concept of PCM. This would be of interest because in some circumstances, complex phenomena such as jump phenomena are not likely to exist in the designed or optimized system.

2. With the novel algorithm for calculating the GFRFs for exponential-type nonlinearities, a controller with full consideration of the actuator saturation or clearance nonlinearity can be analysed and designed in the frequency domain with the nCOS method to provide a straightforward insight into the analysis and design of the controller.
3. The exponential-type nonlinearity is an important basis function in neural networks and fuzzy systems. The results in Chapter 5 provide a useful and fundamental basis for developing training methods or controllers with neural networks or fuzzy methods in the frequency domain.

## 7 Appendix

### Appendix 2.1: Proof of Proposition 2.1

$$\begin{aligned}
& \frac{1}{\underline{L}(\omega)} \sum_{m=2}^{+\infty} \sum_{p=1}^m U^q C(p, q) (\bar{Y}(U)_\omega)^p + \frac{1}{\underline{L}(\omega)} \sum_{q=m=2}^{+\infty} C(0, m) U^m \\
&= \frac{1}{\underline{L}(\omega)} \sum_{m=2}^{+\infty} \sum_{p=1}^m C(p, q) \left( \sum_{i=1}^{+\infty} \bar{H}_i(j\omega_1, \dots, j\omega_i) U^i \right)^p U^q + \frac{1}{\underline{L}(\omega)} \sum_{q=m=2}^{+\infty} C(0, m) U^m \\
&= \sum_{n=2}^{+\infty} \left( \frac{1}{\underline{L}(\omega)} \left( C(0, n) + \sum_{m=2}^n \sum_{p=1}^m C(p, q) \sum_{r_i=1, \sum r_i=n-q}^{n-m+1} \prod_{i=1}^p \bar{H}_{r_i}(j\omega_1, \dots, j\omega_{r_i}) \right) \right) U^n \\
&= \sum_{n=2}^{+\infty} \bar{H}_n(j\omega_1, \dots, j\omega_n) U^n
\end{aligned}$$

then, the following equation holds for  $p + q \geq 2$

$$\frac{1}{\underline{L}(\omega)} \sum_{m=2}^{+\infty} \sum_{p=1}^m U^q C(p, q) (\bar{Y}(U)_\omega)^p + \frac{1}{\underline{L}(\omega)} \sum_{q=m=2}^{+\infty} C(0, m) U^m = \bar{Y}(U)_\omega - \bar{H}_1(j\omega) U \quad (\text{A-1})$$

Denote  $x(\omega, U) = \bar{Y}(U)_\omega = \sum_{n=1}^{+\infty} \bar{H}_n(j\omega_1, \dots, j\omega_n) U^n$ , and rearrange (A-1), (2.17)

can be obtained. The result in (2.18) is straightforward according to (2.17). This

completes the proof.  $\square$

## Appendix 2.2: Proof of Proposition 2.2

When the input amplitude  $U$  increases with the model parameters fixed, the upper bound of the nonlinear output spectrum  $x = \sum_{n=1}^{+\infty} \bar{H}_n(j\omega_1, \dots, j\omega_n) U^n$  also increases. When any nonlinear model parameter increases with the other model parameters and the input amplitude  $U$  fixed, according to (2.14), the bound of the  $n$ th order GFRF  $\bar{H}_n(j\omega_1, \dots, j\omega_n)$  also increases. Therefore, the upper bound of the nonlinear output spectrum  $x$  increases accordingly. Both these cases make the function  $\Gamma$  increase.

It is clear that  $\Gamma = 0$  when the input amplitude  $U = 0$  or all of the nonlinear model parameters are zero ( $C(p, q) = 0$ ). When the Volterra series expansion is divergent, the upper bound of the nonlinear output spectrum  $x \rightarrow \infty$ , thus

$$\Gamma = \frac{1}{\underline{L}(\omega)} \sum_{p=1}^{M_p} \sum_{q=0}^{\infty} p C(p, q) U^q x^{p-1} \rightarrow \infty.$$

For the case that only the nonlinear terms

with index  $p=1$  or together with the pure input nonlinear terms are included in the NARX model, it is obvious that there exist some  $(U, C(1, q))$  such that

$$\Gamma = \frac{1}{\underline{L}(\omega)} \sum_{q=1}^{\infty} C(1, q) U^q > 1 \text{ holds.}$$

Because  $\Gamma$  is a continuous and

monotonically increasing function with respect to the input amplitude  $U$  or any nonlinear model parameter, then  $\Gamma = 1$  exists for some  $U$  and  $C(p, q)$ .

According to (2.11)-(2.13), it is clear that  $\underline{L}(\omega)$ ,  $\bar{H}_1(j\omega)$ , and  $C(p, q)$  are no functions of the input amplitude  $U$ . When the model parameters are given, the upper bound of the nonlinear output spectrum is only a function of the input magnitude  $U$ . Calculate the derivative with respect to  $U$  in (2.17), the following

equation holds,

$$\sum_{p=1}^{M_p} \sum_{q=0}^{\infty} C(p, q) q U^{q-1} x^p + \sum_{p=1}^{M_p} \sum_{q=0}^{\infty} C(p, q) U^q p x^{p-1} \frac{dx}{dU} - \underline{L}(\omega) \frac{dx}{dU} + \underline{L}(\omega) \bar{H}_1(j\omega) + \sum_{m=2}^{\infty} C(0, m) m U^{m-1} = 0, \quad p + q \geq 2$$

From this equation,  $\frac{dx}{dU}$  can be obtained. And then the derivative of the inverse

function  $U(x)$  is given by  $\frac{dU}{dx} = \frac{1}{dx/dU} = \frac{\underline{L}(\omega) - \sum_{p=1}^{M_p} \sum_{q=0}^{\infty} C(p, q) U^q p x^{p-1}}{\sum_{p=1}^{M_p} \sum_{q=0}^{\infty} C(p, q) q U^{q-1} x^p + \underline{L}(\omega) \bar{H}_1(\omega)}$ . When  $\Gamma = 1$ ,

according to (2.19),  $\sum_{p=1}^{M_p} \sum_{q=0}^{\infty} C(p, q) U^q p x^{p-1} = \underline{L}(\omega)$  holds. Because  $\underline{L}(\omega)$ ,  $\bar{H}_1(j\omega)$ ,

$C(p, q)$  and  $U$  are nonnegative, thus the denominator is always larger than 0, and then  $\frac{dU}{dx} = 0$  holds.

According to the Analytic Inversion Lemma in [137]: An analytic function locally admits an analytic inverse near any point where its first derivative is non-zero. However, a function cannot be analytically inverted in a neighbourhood of a point where its first derivative vanishes. Because the output bound  $x = \sum_{n=1}^{+\infty} \bar{H}_n(j\omega_1, \dots, j\omega_n) U^n$  is a power series of input amplitude  $U$ , and it is known that the power series is analytic in the convergence region, which means that there does not exist singularity in the convergence region.

From the discussion above, when  $0 \leq \Gamma < 1$ ,  $\frac{dU}{dx} \neq 0$  holds, which means that no singularity exists in this region, thus  $x$  (described by an infinite power series  $x = \sum_{n=1}^{+\infty} \bar{H}_n(j\omega_1, \dots, j\omega_n) U^n$ ) is convergent in this region. When  $\Gamma = 1$ , the output bound  $x$  is divergent. Because  $\Gamma$  increases as the input amplitude  $U$

increases or the nonlinear model parameters function  $C(p,q)$  increases, so when  $\Gamma > 1$ , there exists a smaller input amplitude  $U$  or smaller function  $C(p,q)$  which can bring  $\Gamma$  back to  $\Gamma = 1$ , clear indicating that the output bound  $x$  is divergent for  $\Gamma > 1$ . This completes the proof.  $\square$

### Appendix 2.3: Proof of Proposition 2.3

The upper bound of the nonlinear output spectrum  $x$  reaches the convergent bound when  $I=1$  holds. In the case that the NARX model does not only involve the type of nonlinear term with index  $p=1$  or together with the pure input nonlinear term, the following condition holds,

$$\sum_{p=1}^{M_p} \left( p \sum_{q=0}^{\infty} C(p,q)U^q \right) x^{p-1} = \underline{L}(\omega), \quad p+q \geq 2, \quad (\text{C-1})$$

By substituting (C-1) into (2.17), it can be obtained that

$$\sum_{p=1}^{M_p} \left( (p-1) \sum_{q=0}^{\infty} C(p,q)U^q \right) x^p = \underline{L}(\omega)\bar{H}_1(j\omega)U + \sum_{m=2}^{\infty} C(0,m)U^m, \quad p+q \geq 2, \quad (\text{C-2})$$

Define the formal function  $f(x) = a_n x^n + \dots + a_1 x + a_0$ , and  $g(x) = b_m x^m + \dots + b_1 x + b_0$ . The Sylvester matrix of  $f(x)$  and  $g(x)$  is defined as,

$$Syl(f, g) = \begin{matrix} m \text{ rows} \\ \\ \\ \\ \\ \\ \\ \\ \\ n \text{ rows} \end{matrix} \left\{ \begin{matrix} \left[ \begin{matrix} a_n & \dots & a_0 \\ & \dots & \\ & & a_n & a_0 \\ b_m & \dots & b_0 \\ & \dots & \\ & & b_m & \dots & b_0 \end{matrix} \right]_{(m+n) \times (m+n)} \end{matrix} \right. \quad (\text{C-3})$$

The sufficient and necessary condition for the existence of a solution to the equations

$$\begin{cases} f(x) = 0 \\ g(x) = 0 \end{cases} \text{ is that the Sylvester Resultant equals to 0 [190], that is,}$$

$$Res(f, g) = \det(Syl(f, g)) = 0 \quad (\text{C-4})$$

where  $\det(\bullet)$  means the determinant of the matrix, and  $Res(\bullet)$  means the

Sylvester Resultant of the functions. Equation (C-1) and (C-2) are rewritten as

$$\begin{cases} \sum_{p=1}^{M_p} \left( (p-1) \sum_{q=0}^{\infty} C(p, q) U^q \right) x^p = \underline{L}(\omega) \bar{H}_1(j\omega) U + \sum_{m=2}^{\infty} C(0, m) U^m \\ \sum_{p=1}^{M_p} \left( p \sum_{q=0}^{\infty} C(p, q) U^q \right) x^{p-1} = \underline{L}(\omega) \end{cases}, \quad p+q \geq 2,$$

(C-5)

Equation (2.17) always holds no matter whether  $x$  is convergent or divergent. If there exists a  $(C(p, q), U, \underline{L}(\omega), x)$  that satisfies (C-1), it also satisfies (2.17), and thus (C-2) holds for this  $(C(p, q), U, \underline{L}(\omega), x)$ . Therefore, there exists an  $x$  that satisfies (C-5). Then according to the analysis above, (C-4) holds (the Sylvester Resultant is equal to 0 in this case). According to (C-5), the Sylvester matrix in (C-3) and (C-4) can be obtained by defining the elements in (2.21)-(2.24).

For the case that the NARX model only involves the type of nonlinear terms with  $p=1$  and the pure input nonlinear term, the result in (2.25) is straightforward.

This completes the proof.  $\square$

## Appendix 2.4: Proof of Proposition 2.4

Rearrange (2.19), the following equation holds,

$$\sum_{p=1}^{M_p} \left( p \sum_{q=0}^{\infty} C(p, q) U^q \right) x^{p-1} - \Gamma \underline{L}(\omega) = 0, \quad p + q \geq 2, \quad (\text{D-1})$$

If there is a  $(C(p, q), U, \underline{L}(\omega), x, \Gamma)$  that satisfies (D-1), the corresponding part, i.e.,  $(C(p, q), U, \underline{L}(\omega), x)$  also satisfies (2.17). Thus there exists a solution for  $x$  in the following equations,

$$\begin{cases} \sum_{p=1}^{M_p} \left( \sum_{q=0}^{\infty} C(p, q) U^q \right) x^p - \underline{L}(\omega) x + \underline{L}(\omega) \bar{H}_1(j\omega) U + \sum_{m=2}^{\infty} C(0, m) U^m = 0 \\ \sum_{p=1}^{M_p} \left( p \sum_{q=0}^{\infty} C(p, q) U^q \right) x^{p-1} - \Gamma \underline{L}(\omega) = 0 \end{cases}, \quad p + q \geq 2 \quad (\text{D-2})$$

which means that the Sylvester Resultant of equations (D-2) is equal to 0, and then similarly to Appendix 2.3, (2.20) and (2.27)-(2.31) hold.

For the case of the NARX model with only the type of nonlinear terms with index  $p = 1$  or together with pure input nonlinearity, the result is straightforward. This completes the proof.  $\square$

## Appendix 2.5 Proof of Lemma 2.3

Considering an infinite order, i.e.,  $N=\infty$ ,

$$|Y(j\omega)| \leq \sum_{n=1}^{\infty} |Y_n(j\omega)| \quad (\text{E-1})$$

$$\begin{aligned} |Y_n(j\omega)| &\leq \frac{1}{(2\pi)^{n-1}} \underbrace{\int_{-\infty}^{\infty} \cdots \int_{-\infty}^{\infty}}_{n-1} \Xi d\omega_1 \cdots d\omega_{n-1} \\ &= \bar{H}_n \frac{1}{(2\pi)^{n-1}} \left| \underbrace{\int_{-\infty}^{\infty} \cdots \int_{-\infty}^{\infty}}_{n-1} |U_n(j\omega, j\omega_1, \dots, j\omega_{n-1})| d\omega_1 \cdots d\omega_{n-1} \right| \end{aligned} \quad (\text{E-2})$$

$$\begin{aligned} &\underbrace{\int_{-\infty}^{\infty} \cdots \int_{-\infty}^{\infty}}_{n-1} |U_n(j\omega, j\omega_1, \dots, j\omega_{n-1})| d\omega_1 \cdots d\omega_{n-1} \\ &= \rho^n \underbrace{\int_{-\infty}^{\infty} \cdots \int_{-\infty}^{\infty}}_{n-1} |U(j\omega_1)| \cdots |U(j\omega_{n-1})| |U_n(j\omega - j\omega_1 - \dots - j\omega_{n-1})| d\omega_1 \cdots d\omega_{n-1} \\ &\leq \rho^n \left| \underbrace{\int_{-\infty}^{\infty} \cdots \int_{-\infty}^{\infty}}_{n-1} |U_\rho(j\omega_1)| \cdots |U_\rho(j\omega_{n-1})| d\omega_1 \cdots d\omega_{n-1} \right| \end{aligned} \quad (\text{E-3})$$

where  $|U(j\omega - j\omega_1 - \dots - j\omega_{n-1})| \leq 1$  is used in (E-3). From (E-2) and (E-3), it can

be derived that

$$\begin{aligned} |Y_n(j\omega)| &\leq \bar{H}_n \frac{\rho^n}{(2\pi)^{n-1}} \underbrace{\int_{-\infty}^{\infty} \cdots \int_{-\infty}^{\infty}}_{n-1} |U_\rho(j\omega_1)| \cdots |U_\rho(j\omega_{n-1})| d\omega_1 \cdots d\omega_{n-1} \\ &= \bar{H}_n \frac{\rho^n}{(2\pi)^{n-1}} \left[ \int_{-\infty}^{+\infty} |U_\rho(j\omega_1)| d\omega_1 \right]^{n-1} \\ &= \bar{H}_n \frac{\rho^n}{(2\pi)^{n-1}} \left[ 2 \int_0^{+\infty} |U_\rho(j\omega_1)| d\omega_1 \right]^{n-1} \\ &= \frac{1}{\sigma} \bar{H}_n \gamma^n \end{aligned} \quad (\text{E-4})$$

From (E-1) and (E-4), (2.57) can be obtained. From Lemma 1 in [97], for  $n \geq 2$ ,

$$|H_n(j\omega_1, \dots, j\omega_{n-1}, j(\omega - \omega_1 - \dots - \omega_{n-1}))| \leq \bar{H}_n = \frac{1}{\underline{L}_{R_\omega}} \sum_{m=2}^n \sum_{\substack{p+q=m \\ 0 \leq p, q \leq m}} C(p, q) \left( \sum_{\substack{r_1 \cdots r_p=1 \\ \sum r_i = n-q}}^{n-q-p+1} \prod_{i=1}^p \bar{H}_{r_i} \right)$$

Then, it can be further obtained from (2.57) that

$$\begin{aligned}
\sigma|Y(j\omega)| &\leq \sigma\bar{Y} = \tilde{Y} = \bar{H}_1\gamma + \sum_{n=2}^{\infty} \frac{1}{\underline{L}_{R_\omega}} \sum_{m=2}^n \sum_{\substack{p+q=m \\ 0 \leq p, q \leq m}} C(p, q) \left( \sum_{\substack{r_1 \cdots r_p=1 \\ \sum r_i=n-q}}^{n-q-p+1} \prod_{i=1}^p \bar{H}_{r_i} \right) \gamma^n \\
&= \bar{H}_1\gamma + \frac{1}{\underline{L}_{R_\omega}} \sum_{n=2}^{\infty} \sum_{m=2}^n \sum_{\substack{p+q=m \\ 0 \leq p, q \leq m}} C(p, q) \left( \sum_{\substack{r_1 \cdots r_p=1 \\ \sum r_i=n-q}}^{n-q-p+1} \prod_{i=1}^p \bar{H}_{r_i} \right) \gamma^n \\
&= \bar{H}_1\gamma + \frac{1}{\underline{L}_{R_\omega}} \sum_{m=2}^{\infty} \sum_{\substack{p+q=m \\ 0 \leq p, q \leq m}} C(p, q) \sum_{n=m}^{\infty} \left( \sum_{\substack{r_1 \cdots r_p=1 \\ \sum r_i=n-q}}^{n-q-p+1} \prod_{i=1}^p \bar{H}_{r_i} \right) \gamma^n \\
&= \bar{H}_1\gamma + \frac{1}{\underline{L}_{R_\omega}} \sum_{m=2}^{\infty} \sum_{\substack{p+q=m \\ 0 \leq p, q \leq m}} C(p, q) \sum_{n=m}^{\infty} \left( \sum_{\substack{r_1 \cdots r_p=1 \\ \sum r_i=n-q}}^{n-q-p+1} \prod_{i=1}^p \bar{H}_{r_i} \gamma^{n-q} \right) \gamma^q
\end{aligned} \tag{E-5}$$

Also from (2.57),  $\tilde{Y}^p = \left( \sum_{i=1}^{\infty} \bar{H}_i \gamma^i \right)^p = \sum_{\kappa=p}^{\infty} \left( \sum_{\substack{r_1 \cdots r_p=1 \\ \sum r_i=\kappa}}^{\kappa-p+1} \bar{H}_{r_1} \bar{H}_{r_2} \cdots \bar{H}_{r_p} \right) \gamma^\kappa$ . Take

$\kappa = n - q$ , it gives

$$\tilde{Y}^p = \left( \sum_{i=1}^{\infty} \bar{H}_i \gamma^i \right)^p = \sum_{n=p+q}^{\infty} \left( \sum_{\substack{r_1 \cdots r_p=1 \\ \sum r_i=n-q}}^{n-q-p+1} \bar{H}_{r_1} \bar{H}_{r_2} \cdots \bar{H}_{r_p} \right) \gamma^{n-q} \tag{E-6}$$

Substitute (E-6) into (E-5), it gives

$$\tilde{Y} = \bar{H}_1\gamma + \frac{1}{\underline{L}_{R_\omega}} \sum_{m=2}^{\infty} \sum_{\substack{p+q=m \\ 0 \leq p, q \leq m}} C(p, q) \tilde{Y}^p \gamma^q$$

Considering the maximum nonlinear degree, i.e.,  $m \leq M$ , it gives (2.58). Similar results can be derived for multi-tone input, which is omitted here. Moreover, for a single-tone input, from [98] the bound of  $|H_n(\cdot)|$  can be written as

$$|H_n(\cdot)| \leq \bar{H}_n(\omega) = a_0 + a_1 |H_1(j\omega)| + \cdots + a_n |H_1(j\omega)|^n$$

where  $a_i$  for  $i=0,1,\dots,n$  can be referred to [97, 98]. Therefore,  $\bar{H}_1$  can be replaced by  $|H_1(j\omega)|$  in (2.57) and (2.58), and  $\bar{H}_n$  in (2.57) can be replaced by  $\bar{H}_n(\omega)$ . This completes the proof.  $\square$

## Appendix 2.6: Proof of Lemma 2.4

According to (2.68), the following inequality holds,

$$\|H_n\| \leq \|L_n(j\omega_1, \dots, j\omega_n)\| \|A_n\| \quad (\text{F-1})$$

that is,

$$\sum_{j_k=1}^M \|H_n^{(j_k)}(j\omega_1, \dots, j\omega_n)\| \leq \|L_n(j\omega_1, \dots, j\omega_n)\| \sum_{j_k=1}^M \|A_{j_k, n}\| \leq \bar{L}(\omega) \sum_{j_k=1}^M \|A_{j_k, n}\|.$$

According to (2.70)-(2.73),

$$\begin{aligned} \|A_{j_k, n}\| &= \left\| \sum_{m=2}^n \sum_{p=1}^m \sum_{j_1=1}^M \sum_{j_2=j_1}^M \cdots \sum_{j_p=j_{p-1}}^M \sum_{k_1, \dots, k_{p+q}=0}^K \left[ \left( \sum_{k_1, \dots, k_{p+q}=0}^K c_{0,n}(k_1, \dots, k_n; j_k) e^{-j \sum_{i=1}^n k_i \omega_i} \right) \right. \right. \\ &\quad \left. \left. + \left( c_{p,q}^{j_p j_{p-1} \dots j_1}(k_1, \dots, k_{p+q}; j_k) e^{-\sum_{i=1}^q j \omega_{n-q+i} k_{p+i}} H_{n-q,p}^{(j_p j_{p-1} \dots j_1)}(j\omega_1, \dots, j\omega_{n-q}) \right) \right] \right\| \\ &\leq \sum_{m=2}^n \sum_{p=1}^m \sum_{j_1=1}^M \sum_{j_2=j_1}^M \cdots \sum_{j_p=j_{p-1}}^M \sum_{k_1, \dots, k_{p+q}=0}^K \left[ C_{(0,n;j_k)} + \|c_{p,q}^{j_p j_{p-1} \dots j_1}(k_1, \dots, k_{p+q}; j_k)\| \right] \\ &\quad \times \sum_{r_1, \dots, r_p=1, \sum_{i=1}^p r_i=n}^{n-p+1} \left( \prod_{i=1}^p \|H_{r_i}^{(j_i)}(j\omega_{X+1}, \dots, j\omega_{X+r_i})\| \right) \leq \sum_{m=2}^n \sum_{p=1}^m \sum_{j_1=1}^M \sum_{j_2=j_1}^M \cdots \sum_{j_p=j_{p-1}}^M \\ &\quad \left( C_{(0,n;j_k)} + C_{(p,q;j_k)}^{j_p j_{p-1} \dots j_1} \sum_{r_1, \dots, r_p=1, \sum_{i=1}^p r_i=n}^{n-p+1} \left( \prod_{i=1}^p \bar{H}_{r_i}^{(j_i)}(j\omega_{X+1}, \dots, j\omega_{X+r_i}) \right) \right) \end{aligned} \quad (\text{F-2})$$

By substituting (F-2) into (F-1), (2.80) can be obtained. When  $n=1$ , (2.81) is straightforward. When turns to the upper bound of the nonlinear output spectrum of the  $j_k$ th subsystem at  $\Omega=k\omega$ , for  $k \in \mathbb{N}^+$ ,

$$\begin{aligned} Y_{\Omega=k\omega}^{(j_k)}(U) &\leq \sum_{n=1}^{+\infty} \left[ \frac{2}{2^{k+2(n-1)}} \sum_{\Omega=k\omega} \left( \bar{H}_{k+2(n-1)}^{(j_k)}(j\omega_1, \dots, \omega_n) \prod_{i=1}^{k+2(n-1)} \|A(\omega_i)\| \right) \right] \\ &\leq \sum_{n=1}^{+\infty} \left( \frac{C_{k+2(n-1)}^{n-1}}{2^{k+2(n-1)-1}} \bar{H}_{k+2(n-1)}^{(j_k)}(j\omega_1, \dots, j\omega_{k+2(n-1)}) U^{k+2(n-1)} \right). \end{aligned}$$

For  $k=0$ , the result is straightforward. This completes the proof.  $\square$

**Appendix 2.7:** Proof of Lemma 2.6

Denote  $L_{jk}$  as the  $j_k$ th row of  $L_n(j\omega_1, \dots, j\omega_n)$ . According to (2.68),  $H_n^{(j)}(j\omega_1, \dots, j\omega_n)$  can be seen as the column vector  $A_n$  projects on to the vector  $L_j$ , and  $\|H_n^{(j)}(j\omega_1, \dots, j\omega_n)\| \leq \|L_j\| \|A_n\|$ . When  $\bar{H}_n^{(j)}(j\omega_1, \dots, j\omega_n)$  diverges as order  $n$  increases, in this case, because  $\bar{L}_j(\omega) \leq \bar{L}(\omega) < \infty$ , thus  $\|A_n\| \rightarrow \infty$  as  $n \rightarrow \infty$ , then  $\forall j_k=1, \dots, M$ ,  $\bar{H}_n^{(j_k)}(j\omega_1, \dots, j\omega_n) \rightarrow \infty$  as  $n \rightarrow \infty$ . Then Lemma 2.6 is straightforward. This completes the proof.  $\square$

**Appendix 2.8:** Proof of Lemma 2.7

$$\begin{aligned}
& \bar{L}(\omega) \sum_{j_k=1}^M \left[ \sum_{m=2}^{+\infty} \sum_{p=1}^m \sum_{j_1=1}^M \sum_{j_2=j_1}^M \cdots \sum_{j_p=j_{p-1}}^M \left( U^q C_{(p,q;j_k)}^{j_p j_{p-1} \cdots j_1} \prod_{i=1}^p \bar{Y}_\omega^{(j_i)}(U) \right) + \sum_{m=2}^{+\infty} C_{(0,m;j_k)} U^m \right] \\
&= \bar{L}(\omega) \sum_{j_k=1}^M \left[ \sum_{n=2}^{+\infty} C_{(0,n;j_k)} U^n + \right. \\
&\quad \left. \sum_{m=2}^{+\infty} \sum_{p=1}^m \sum_{j_1=1}^M \sum_{j_2=j_1}^M \cdots \sum_{j_p=j_{p-1}}^M \left( U^q C_{(p,q;j_k)}^{j_p j_{p-1} \cdots j_1} \prod_{i=1}^p \left( \sum_{l=1}^{+\infty} \bar{H}_l^{(j_i)}(j\omega_1, \dots, j\omega_l) U^n \right) \right) \right] \\
&= \bar{L}(\omega) \sum_{j_k=1}^M \left[ \sum_{n=2}^{+\infty} C_{(0,n;j_k)} U^n + \sum_{n=2}^{+\infty} \sum_{m=2}^n \sum_{p=1}^m \sum_{j_1=1}^M \sum_{j_2=j_1}^M \cdots \sum_{j_p=j_{p-1}}^M \right. \\
&\quad \left. \left( C_{(p,q;j_k)}^{j_p j_{p-1} \cdots j_1} \sum_{r_1, \dots, r_p=1, \sum r_i=n-q}^{n-m+1} \prod_{i=1}^p \bar{H}_{r_i}^{(j_i)}(j\omega_{X+1}, \dots, j\omega_{X+r_i}) \right) U^n \right] \\
&= \sum_{n=2}^{+\infty} \left\{ \bar{L}(\omega) \sum_{j_k=1}^M \left[ C_{(0,n;j_k)} + \sum_{m=2}^n \sum_{p=1}^m \sum_{j_1=1}^M \sum_{j_2=j_1}^M \cdots \sum_{j_p=j_{p-1}}^M \right. \right. \\
&\quad \left. \left. \left( C_{(p,q;j_k)}^{j_p j_{p-1} \cdots j_1} \sum_{r_1, \dots, r_p=1, \sum r_i=n-q}^{n-m+1} \prod_{i=1}^p \bar{H}_{r_i}^{(j_i)}(j\omega_{X+1}, \dots, j\omega_{X+r_i}) \right) \right] \right\} U^n \\
&= \sum_{j_k=1}^M \bar{Y}_\omega^{(j_k)}(U) - \sum_{j_k=1}^M \left( \bar{H}_1^{(j_k)}(j\omega_1) U \right)
\end{aligned}$$

This completes the proof.  $\square$

## Appendix 2.9: Proof of Proposition 2.6

The solution of nonlinear differential equations or nonlinear difference equations can be seen as the perturbation of the solution of the corresponding linear equations [39], thus assume that

$$\frac{\bar{Y}_\omega^{(j_k)}(U)}{\bar{Y}_\omega^{(j_i)}(U)} = \frac{\bar{H}_1^{(j_k)}(\omega)U}{\bar{H}_1^{(j_i)}(\omega)U} = \frac{\bar{H}_1^{(j_k)}(\omega)}{\bar{H}_1^{(j_i)}(\omega)}, 1 \leq j_k, j_i \leq M \quad (\text{I-1})$$

Substitute (I-1) into (2.83) in Lemma 2.7, the following equation holds,

$$\begin{aligned} \bar{L}(\omega) \sum_{j_k=1}^M \sum_{m=2}^{+\infty} \sum_{p=1}^m \sum_{j_1=1}^M \sum_{j_2=j_1}^M \cdots \sum_{j_p=j_{p-1}}^M \left[ U^q C_{(p,q;j_k)}^{j_p j_{p-1} \cdots j_1} \left( \prod_{i=1}^p \frac{\bar{H}_1^{(j_i)}(\omega)}{\bar{H}_1^{(j)}(\omega)} \right) \left( \bar{Y}_\omega^{(j)}(U) \right)^p \right] - \\ \sum_{j_k=1}^M \left( \frac{\bar{H}_1^{(j_k)}(\omega)}{\bar{H}_1^{(j)}(\omega)} \bar{Y}_\omega^{(j)}(U) \right) + \sum_{j_k=1}^M \left( \bar{H}_1^{(j_k)}(j\omega_1)U \right) + \bar{L}(\omega) \sum_{j_k=1}^M \sum_{m=2}^{+\infty} \left( C_{(0,m;j_k)} U^m \right) = 0. \end{aligned} \quad (\text{I-2})$$

Based on the results in Lemma 2.6, the superscript  $j$  in (I-2) can be any value where  $1 \leq j \leq M$ . Denote  $x = \bar{Y}_\omega^{(j)}(U)$ , which is an infinite power series. In the convergence region, the infinite power series is analytic, which means that there does not exist any singularity. When there exists some values  $(C_{(p,q;j)}^{j_p j_{p-1} \cdots j_1}, U, \omega)$  which make the infinite power series singular, the closest point  $(C_{(p,q;j)}^{j_p j_{p-1} \cdots j_1}, U, \omega)$  to the expanded center can then be seen as the divergence bound, thus the divergence condition of the infinite power series can be equivalent to the singularity condition (finding the closest singular point to the expanded center).

According to the Analytic Inversion Lemma in [137], the singular condition of  $x = \bar{Y}_\omega^{(j)}(U)$  is  $dU/dx=0$ .  $C_{(p,q;j)}^{j_p j_{p-1} \cdots j_1}$  and  $\bar{L}(\omega)$  are all independent of input magnitude  $U$ , thus take the derivative with respect to  $U$  in both sides of (I-2),  $dx/dU$  can be obtained, then the derivative of inverse function  $U(x)$  can be given

as

$$\begin{aligned}
\frac{dU}{dx} = \frac{1}{dx/dU} &= \left[ \sum_{j_k=1}^M \frac{\bar{H}_1^{(j_k)}(\omega)}{\bar{H}_1^{(j)}(\omega)} - \bar{L}(\omega) \sum_{j_k=1}^M \sum_{m=2}^{+\infty} \sum_{p=1}^m \sum_{j_1=1}^M \sum_{j_2=j_1}^M \cdots \sum_{j_p=j_{p-1}}^M \right. \\
&\left. \left( U^q C_{(p,q;j_k)}^{j_p j_{p-1} \cdots j_1} \left( \prod_{i=1}^p \frac{\bar{H}_1^{(j_i)}(\omega)}{\bar{H}_1^{(j)}(\omega)} \right) p x^{p-1} \right) \right] / \left\{ \sum_{j_k=1}^M \left( \bar{H}_1^{(j_k)}(j\omega_1) \frac{dU}{dx} \right) \right\} + \\
\bar{L}(\omega) &\left[ \sum_{j_k=1}^M \sum_{m=2}^{+\infty} C_{(0,m;j_k)} m U^{m-1} + \sum_{j_k=1}^M \sum_{m=2}^{+\infty} \sum_{p=1}^m \sum_{j_1=1}^M \sum_{j_2=j_1}^M \cdots \sum_{j_p=j_{p-1}}^M \right. \\
&\left. \left( q U^{q-1} C_{(p,q;j_k)}^{j_p j_{p-1} \cdots j_1} \left( \prod_{i=1}^p \frac{\bar{H}_1^{(j_i)}(\omega)}{\bar{H}_1^{(j)}(\omega)} \right) x^p \right) \right] \Bigg\} \quad (\text{I-3})
\end{aligned}$$

When the nominator of (I-3) is equal to 0, that is,

$$\bar{L}(\omega) \sum_{j_k=1}^M \sum_{m=2}^{+\infty} \sum_{p=1}^m \sum_{j_1=1}^M \sum_{j_2=j_1}^M \cdots \sum_{j_p=j_{p-1}}^M \left( U^q C_{(p,q;j_k)}^{j_p j_{p-1} \cdots j_1} \left( \prod_{i=1}^p \frac{\bar{H}_1^{(j_i)}(\omega)}{\bar{H}_1^{(j)}(\omega)} \right) p x^{p-1} \right) - \sum_{j_k=1}^M \frac{\bar{H}_1^{(j_k)}(\omega)}{\bar{H}_1^{(j)}(\omega)} = 0 \quad (\text{I-4})$$

$dU/dx=0$  holds because  $U, C_{(p,q;j)}^{j_p j_{p-1} \cdots j_1}, \bar{L}(\omega), x$  are all positive and the denominator

is also positive. The nominator of (I-2) decreases when increasing  $C_{(p,q;j)}^{j_p j_{p-1} \cdots j_1}$

or  $U$ . When any  $(C_{(p,q;j)}^{j_p j_{p-1} \cdots j_1}, U, \omega)$  makes  $dU/dx > 0$  holds, no singularity exists,

and thus the upper bound of the nonlinear output spectrum

( $x = \bar{Y}_\omega^{(j)}(U) = \sum_{n=1}^{+\infty} \bar{H}_n^{(j)}(j\omega_1, \dots, j\omega_n) U^n$ ) is analytic and convergent; when

increase  $C_{(p,q;j)}^{j_p j_{p-1} \cdots j_1}$  or  $U$  making  $dU/dx=0$  holds, the upper bound of the

nonlinear output spectrum of the  $j$ th subsystem diverges because some

singularity exist in this case; when  $dU/dx$  is smaller than 0, there exists some

smaller values of  $(C_{(p,q;j)}^{j_p j_{p-1} \cdots j_1}, U, \omega)$  which can bring back to  $dU/dx=0$ , and thus

the infinite power series  $\bar{Y}_\omega^{(j)}(U) = \sum_{n=1}^{+\infty} \bar{H}_n^{(j)}(j\omega_1, \dots, j\omega_n) U^n$  also diverges.

When a set  $(C_{(p,q;j)}^{j_p j_{p-1} \cdots j_1}, U, \omega)$  makes the nonlinear system reaches the

parametric bound of convergence (PBoC), (I-2) and (I-4) hold, following the

proof in Appendix 2.3, the result is straightforward. This completes the proof.  $\square$

### Appendix 3.1

$H_n^J(j\omega_1, \dots, j\omega_n)$  can be obtained as:

$$H_1^2(j\omega_1) = (1 + j\omega_1 \xi_1) H_1^1(j\omega_1)$$

$$H_n^2(j\omega_1, \dots, j\omega_n) = -(j\omega_1 + \dots + j\omega_n)^2 H_n^1(j\omega_1, \dots, j\omega_n) \quad n = 2, \dots, N$$

$$H_1^1(j\omega_1) = \frac{-1}{L(j\omega_1)}$$

$$H_3^1(j\omega_1, j\omega_2, j\omega_3) = \beta_2 \frac{\prod_{i=1}^3 H_1^1(j\omega_i)}{L(j\omega_1 + j\omega_2 + j\omega_3)}(j\omega_1)$$

$$H_{2n}^1(j\omega_1, \dots, j\omega_{2n}) = 0 \quad n = 1, \dots, \lfloor N/2 \rfloor$$

$$H_{2n+1}^1(j\omega_1, \dots, j\omega_{2n+1}) = \frac{\prod_{i=1}^{2n+1} H_1^1(j\omega_i)}{L(j\omega_1 + \dots + j\omega_{2n+1})} \sum_{z=1}^{N_{\bar{n}}} \frac{\prod_{k=1}^n [j\omega_{l_k(1)}^z + \dots + j\omega_{l_k(j_k)}^z]}{\prod_{i=1}^{n-1} L[j\omega_{l_i(1)}^z + \dots + j\omega_{l_i(j_i)}^z]}$$

$$n = 1, \dots, \lfloor N/2 \rfloor$$

$$L[(j\omega_1 + \dots + j\omega_n)] = -[1 + \xi_1(j\omega_1 + \dots + j\omega_n) + (j\omega_1 + \dots + j\omega_n)^2]$$

### Appendix 3.2: Proof of Proposition 3.1

(I)  $P_n(j\Omega)$  can be calculated as,

$$\begin{aligned} |P_n(j\Omega)| &= \left| \frac{1}{2^{2n}} \frac{-j\Omega^2}{|L(j\Omega)|^{2n} [L(j\Omega)]^2} \sum_{\omega_1+\dots+\omega_{2n+1}=\Omega} \sum_{z=1}^{N_{\bar{n}}} \frac{\prod_{k=1}^n [j\omega_{l_k(1)}^z + \dots + j\omega_{l_k(j_k^n)}^z]}{\prod_{i=1}^{n-1} L[j\omega_{l_i(1)}^z + \dots + j\omega_{l_i(j_i^n)}^z]} \right| \\ &\leq \frac{1}{2^{2n}} \frac{\Omega^2}{\left(\sqrt{(1-\Omega^2)^2} + (\xi_1\Omega)^2\right)^{2n+2}} \sum_{\omega_1+\dots+\omega_{2n+1}=\Omega} \sum_{z=1}^{N_{\bar{n}}} \frac{\prod_{k=1}^n [j\omega_{l_k(1)}^z + \dots + j\omega_{l_k(j_k^n)}^z]}{\prod_{i=1}^{n-1} L\left[1 + \left(j\omega_{l_i(1)}^z + \dots + j\omega_{l_i(j_i^n)}^z\right)^2 + \xi_1 \left(j\omega_{l_i(1)}^z + \dots + j\omega_{l_i(j_i^n)}^z\right)\right]} \end{aligned}$$

When  $\Omega \ll 1$

$$|P_n(j\Omega)| \leq \frac{1}{2^{2n}} \Omega^2 \sum_{\omega_1+\dots+\omega_{2n+1}=\Omega} \sum_{z=1}^{N_{\bar{n}}} \prod_{k=1}^n \left[ j\omega_{l_k(1)}^z + \dots + j\omega_{l_k(j_k^n)}^z \right] = \frac{1}{2^{2n}} \Omega^{n+2} c1(n)$$

where  $c1(n) = \sum_{\omega_1+\dots+\omega_{2n+1}=\Omega} \sum_{z=1}^{N_{\bar{n}}} \prod_{k=1}^n \left| \frac{j\omega_{l_k(1)}^z + \dots + j\omega_{l_k(j_k^n)}^z}{\Omega} \right|$  is a bounded constant which is a

$n$  dependent but independent of  $\Omega$ . So when  $\Omega \ll 1$ ,

$$|P_n(j\Omega)| \leq \frac{1}{2^{2n}} \Omega^{n+2} c1(n) \approx 0, \text{ for } n = 1, 2, \dots, \lfloor N/2 \rfloor$$

When  $\Omega \gg 1$

$$\begin{aligned} |P_n(j\Omega)| &\leq \frac{1}{2^{2n}} \frac{\Omega^2}{\left(\sqrt{(1-\Omega^2)^2} + (\xi_1\Omega)^2\right)^{2n+2}} \sum_{\omega_1+\dots+\omega_{2n+1}=\Omega} \sum_{z=1}^{N_{\bar{n}}} \frac{\prod_{k=1}^n [j\omega_{l_k(1)}^z + \dots + j\omega_{l_k(j_k^n)}^z]}{\prod_{i=1}^{n-1} L\left[1 + \left(j\omega_{l_i(1)}^z + \dots + j\omega_{l_i(j_i^n)}^z\right)^2 + \xi_1 \left(j\omega_{l_i(1)}^z + \dots + j\omega_{l_i(j_i^n)}^z\right)\right]} \\ &\approx \frac{1}{2^{2n}} \frac{\Omega^2}{\Omega^{4n+4}} \frac{\Omega^n}{\Omega^{2n-2}} \sum_{\omega_1+\dots+\omega_{2n+1}=\Omega} \sum_{z=1}^{N_{\bar{n}}} \prod_{k=1}^n \left| \frac{j\omega_{l_k(1)}^z + \dots + j\omega_{l_k(j_k^n)}^z}{\Omega} \right| = \frac{1}{2^{2n}} \frac{1}{\Omega^{5n}} c2(n) \end{aligned}$$

where  $c2(n) = \sum_{\omega_1+\dots+\omega_{2n+1}=\Omega} \sum_{z=1}^{N_{\bar{n}}} \prod_{k=1}^n \left| \frac{j\omega_{l_k(1)}^z + \dots + j\omega_{l_k(j_k^n)}^z}{\Omega} \right|$  is a bounded constant which is a

$n$  dependent but independent of  $\Omega$ . So when  $\Omega \gg 1$ ,

$$|P_n(j\Omega)| \leq \frac{1}{2^{2n}} \frac{1}{\Omega^{5n}} c_{2(n)} \approx 0, \text{ for } n = 1, 2, \dots, \lfloor N/2 \rfloor$$

So the conclusion (I) of Proposition 3.1 holds.

(II) The proof is given in theorem 3 in Ref. [79].

### Appendix 3.3: Proof of Proposition 3.2

$P_n(j\Omega)$  for the force transmissibility under base displacement excitation can be calculated as,

$$|P_n(j\Omega)| = \left| \frac{1}{2^{2n}} \frac{-j\Omega^{4n+4}}{|L(j\Omega)|^{2n} [L(j\Omega)]^2} \sum_{\omega_1+\dots+\omega_{2n+1}=\Omega} \sum_{z=1}^{N_{\bar{n}}} \prod_{k=1}^n \frac{[j\omega_{l_k(1)}^z + \dots + j\omega_{l_k(j_k^n)}^z]}{\prod_{i=1}^{n-1} L[j\omega_{l_i(1)}^z + \dots + j\omega_{l_i(j_i^n)}^z]} \right| \leq \frac{1}{2^{2n}} \times$$

$$\frac{\Omega^{4n+4}}{\left(\sqrt{(1-\Omega^2)^2 + (\xi_1\Omega)^2}\right)^{2n+2}} \sum_{\omega_1+\dots+\omega_{2n+1}=\Omega} \sum_{z=1}^{N_{\bar{n}}} \frac{\prod_{k=1}^n \left[ |j\omega_{l_k(1)}^z + \dots + j\omega_{l_k(j_k^n)}^z| \right]}{\prod_{i=1}^{n-1} \left| L \left[ 1 + \left( j\omega_{l_i(1)}^z + \dots + j\omega_{l_i(j_i^n)}^z \right)^2 + \xi_1 \left( j\omega_{l_i(1)}^z + \dots + j\omega_{l_i(j_i^n)}^z \right) \right] \right|}$$

(I) When  $\Omega \ll 1$

$$|P_n(j\Omega)| \leq \frac{1}{2^{2n}} \Omega^{4n+4} \sum_{\omega_1+\dots+\omega_{2n+1}=\Omega} \sum_{z=1}^{N_{\bar{n}}} \prod_{k=1}^n \left[ |j\omega_{l_k(1)}^z + \dots + j\omega_{l_k(j_k^n)}^z| \right] = \frac{1}{2^{2n}} \Omega^{5n+4} c1(n)$$

where  $c1(n) = \sum_{\omega_1+\dots+\omega_{2n+1}=\Omega} \sum_{z=1}^{N_{\bar{n}}} \prod_{k=1}^n \left| \frac{j\omega_{l_k(1)}^z + \dots + j\omega_{l_k(j_k^n)}^z}{\Omega} \right|$  is a bounded constant which is a

$n$  dependent but independent of  $\Omega$ . So when  $\Omega \ll 1$ ,

$$|P_n(j\Omega)| \leq \frac{1}{2^{2n}} \Omega^{5n+4} c1(n) \approx 0, \text{ for } n = 1, 2, \dots, \lfloor N/2 \rfloor$$

(2) When  $\Omega \gg 1$ ,

$$|P_n(j\Omega)| \leq \frac{1}{2^{2n}} \frac{1}{\Omega^{n-2}} \sum_{\omega_1+\dots+\omega_{2n+1}=\Omega} \sum_{z=1}^{N_{\bar{n}}} \prod_{k=1}^n \left| \frac{j\omega_{l_k(1)}^z + \dots + j\omega_{l_k(j_k^n)}^z}{\Omega} \right| = \frac{1}{2^{2n}} \frac{1}{\Omega^{n-2}} c1(n)$$

Where  $c1(n) = \sum_{\omega_1+\dots+\omega_{2n+1}=\Omega} \sum_{z=1}^{N_{\bar{n}}} \prod_{k=1}^n \left| \frac{j\omega_{l_k(1)}^z + \dots + j\omega_{l_k(j_k^n)}^z}{\Omega} \right|$  is a bounded constant which is a

$n$  dependent but independent of  $\Omega$ . So when  $\Omega \gg 1$ ,

$$|P_n(j\Omega)| \leq \frac{1}{2^{2n}} \frac{1}{\Omega^{n-2}} c1(n) \approx 0, \text{ for } n = 3, 4, \dots, \lfloor N/2 \rfloor$$

(III) The proof is given in [79].

This completes the proof.  $\square$

### Appendix 3.4: Proof of Proposition 3.4

Similar to the proof in Appendix 3.3,  $P_n(j\Omega)$  for the absolute transmissibility under base displacement excitation approaches 0 when  $\Omega \ll 1$  or  $\Omega \gg 1$ .

$$P_0(j\Omega) = -j - \frac{-j\Omega^2}{L(j\Omega)} = \frac{-j + \xi_1\Omega}{1 - \Omega^2 + j\xi_1\Omega}$$

This completes the proof.  $\square$

### Appendix 4.1: Proof of Proposition 4.3

Suppose that Proposition 4.3 holds for all of the  $n$ th-order GFRF with  $n < n_0$ , the following then comes to prove that it also holds for  $n = n_0$ . It is clear from (4.4) that  $H_{n_0-q,p}(\boldsymbol{\omega}_{n_0-q})$  can be computed with lower-order GFRF, i.e.,  $\gamma_1 + \dots + \gamma_p = n_0 - q$  and  $1 \leq \gamma_1, \dots, \gamma_p \leq n_0 - q - p + 1$ . Thus substitute (4.11) into (4.4), the following equation holds,

$$\begin{aligned}
H_{n_0-q,p}(\boldsymbol{\omega}_{n_0-q}) &= \sum_{\substack{\gamma_1, \dots, \gamma_p=1, \\ \sum \gamma_i = n_0 - q}}^{n_0 - q - p + 1} \prod_{i=1}^p \left[ \left( \sum_{k=1}^{\gamma_i} \omega_{X_{i+k}} \right)^{\gamma_i} H_{\gamma_i}(\boldsymbol{\omega}_{X_i}) \right] \\
&= \sum_{\substack{\gamma_1, \dots, \gamma_p=1, \\ \sum \gamma_i = n_0 - q}}^{n_0 - q - p + 1} \prod_{i=1}^p \left[ \left( \sum_{k=1}^{\gamma_i} \omega_{X_{i+k}} \right)^{\gamma_i} \sum_{\substack{\alpha_0^i + \dots + \alpha_L^i + s_\beta^i = 0, \\ s_\beta^i \leq \gamma_i}}^{\infty} \sum_{\beta_0^i + \dots + \beta_L^i = 0}^{s_\beta^i} \theta_{\gamma_i}^{\boldsymbol{\alpha}^i, \boldsymbol{\beta}^i}(\boldsymbol{\omega}_{X_i}) c^{\boldsymbol{\alpha}^i, \boldsymbol{\beta}^i} \right] \\
&= \sum_{\substack{\alpha_0 + \dots + \alpha_L + s_\beta = 0, \\ s_\beta \leq n_0 - q}}^{\infty} \sum_{\beta_0 + \dots + \beta_L = 0}^{s_\beta} \sum_{\substack{\gamma_1, \dots, \gamma_p=1, \\ \sum \gamma_i = n_0 - q}}^{n_0 - q - p + 1} \sum_{\substack{\alpha_1^1 + \dots + \alpha_1^p = \alpha_1 \\ \vdots \\ \alpha_L^1 + \dots + \alpha_L^p = \alpha_L \\ \beta_1^1 + \dots + \beta_1^p = \beta_1 \\ \vdots \\ \beta_L^1 + \dots + \beta_L^p = \beta_L}} \prod_{i=1}^p \left[ \left( \sum_{k=1}^{\gamma_i} \omega_{X_{i+k}} \right)^{\gamma_i} \theta_{\gamma_i}^{\boldsymbol{\alpha}^i, \boldsymbol{\beta}^i}(\boldsymbol{\omega}_{X_i}) \right] c^{\boldsymbol{\alpha}, \boldsymbol{\beta}} \\
&= \sum_{\substack{\alpha_0 + \dots + \alpha_L + s_\beta = 0, \\ s_\beta \leq n_0 - q}}^{\infty} \sum_{\beta_0 + \dots + \beta_L = 0}^{s_\beta} d_{n_0-q,p}^{\boldsymbol{\alpha}, \boldsymbol{\beta}}(\boldsymbol{\omega}_{n_0-q}) c^{\boldsymbol{\alpha}, \boldsymbol{\beta}}
\end{aligned}$$

where  $c^{\boldsymbol{\alpha}, \boldsymbol{\beta}} = \prod_{l=0}^L c_{1,0}^{\alpha_l}(l) c_{0,1}^{\beta_l}(l)$  and  $d_{n_0-q,p}^{\boldsymbol{\alpha}, \boldsymbol{\beta}}(\boldsymbol{\omega}_{n_0-q})$  is the corresponding coefficient of  $c^{\boldsymbol{\alpha}, \boldsymbol{\beta}}$ . From the above,  $d_{n-q,p}^{\boldsymbol{\alpha}, \boldsymbol{\beta}}(\boldsymbol{\omega}_{n-q})$  in (4.14) holds.

From (4.2),

$$\begin{aligned}
& L_{n_0}(\boldsymbol{\omega}_{n_0})H_{n_0}(\boldsymbol{\omega}_{n_0}) = \\
& - \sum_{m=p+q=2}^{n_0} \sum_{p=0}^m \sum_{(l_1, \dots, l_m)} \left[ \bar{c}_{p,q}(l_1, \dots, l_{p+q}) \prod_{i=1}^q (j\omega_{p+i})^{l_{p+i}} H_{n_0-q,p}(\boldsymbol{\omega}_{n_0-q}) \right] \\
& = - \sum_{m=p+q=2}^{n_0} \sum_{p=0}^m \sum_{(l_1, \dots, l_m)} \left[ \bar{c}_{p,q}(l_1, \dots, l_{p+q}) \prod_{i=1}^q (j\omega_{p+i})^{l_{p+i}} \right. \\
& \qquad \qquad \qquad \times \sum_{\substack{\alpha_0 + \dots + \alpha_L + s_\beta = 0, \beta_0 + \dots + \beta_L = 0 \\ s_\beta \leq n_0 - q}}^{\infty} \sum_{s_\beta}^{s_\beta} d_{n_0-q,p}^{\alpha,\beta}(\boldsymbol{\omega}_{n_0-q}) c^{\alpha,\beta} \left. \right] \\
& = \sum_{\substack{\alpha_0 + \dots + \alpha_L + s_\beta = 0, \beta_0 + \dots + \beta_L = 0 \\ s_\beta \leq n_0 - q}}^{\infty} \sum_{s_\beta}^{s_\beta} \sum_{m=p+q=2}^{n_0} \sum_{p=0}^m \sum_{(l_1, \dots, l_m)} \\
& \qquad \qquad \qquad \left[ -\bar{c}_{p,q}(l_1, \dots, l_{p+q}) \prod_{i=1}^q (j\omega_{p+i})^{l_{p+i}} d_{n_0-q,p}^{\alpha,\beta}(\boldsymbol{\omega}_{n_0-q}) \right] c^{\alpha,\beta} \\
& = \sum_{\substack{\alpha_0 + \dots + \alpha_L + s_\beta = 0, \beta_0 + \dots + \beta_L = 0 \\ s_\beta \leq n_0}}^{\infty} \sum_{s_\beta}^{s_\beta} b_{n_0}^{\alpha,\beta}(\boldsymbol{\omega}_{n_0}) c^{\alpha,\beta}
\end{aligned}$$

Thus  $b_n^{\alpha,\beta}(\boldsymbol{\omega}_n)$  in (4.13) holds. Substitute (4.6) into the above equation,

$$\begin{aligned}
H_{n_0}(\boldsymbol{\omega}_{n_0}) &= L_{n_0}^{-1}(\boldsymbol{\omega}_{n_0}) \sum_{\substack{\alpha_0 + \dots + \alpha_L + s_\beta = 0, \beta_0 + \dots + \beta_L = 0 \\ s_\beta \leq n_0 - q}}^{\infty} \sum_{s_\beta}^{s_\beta} b_{n_0}^{\alpha^b, \beta}(\boldsymbol{\omega}_{n_0}) c^{\alpha^b, \beta} \\
&= \sum_{\alpha_0^a + \dots + \alpha_L^a = 0}^{\infty} \varphi_{n_0}^{\alpha^a, 0}(\boldsymbol{\omega}_{n_0}) c^{\alpha^a, 0} \sum_{\substack{\alpha_0^b + \dots + \alpha_L^b + s_\beta^b = 0, \beta_0^b + \dots + \beta_L^b = 0 \\ s_\beta^b \leq n_0}}^{\infty} \sum_{s_\beta^b}^{s_\beta^b} b_{n_0}^{\alpha^b, \beta}(\boldsymbol{\omega}_{n_0}) c^{\alpha^b, \beta} \\
&= \sum_{\substack{\alpha_0 + \dots + \alpha_L + s_\beta = 0, \beta_0 + \dots + \beta_L = 0 \\ s_\beta \leq n_0}}^{\infty} \sum_{s_\beta}^{s_\beta} \left[ \sum_{\substack{\alpha_1^a + \alpha_1^b = \alpha_1 \\ \vdots \\ \alpha_L^a + \alpha_L^b = \alpha_L}} \varphi_{n_0}^{\alpha^a, 0}(\boldsymbol{\omega}_{n_0}) b_{n_0}^{\alpha^b, \beta}(\boldsymbol{\omega}_{n_0}) \right] c^{\alpha,\beta} \\
&= \sum_{\substack{\alpha_0 + \dots + \alpha_L + s_\beta = 0, \beta_0 + \dots + \beta_L = 0 \\ s_\beta \leq n_0}}^{\infty} \sum_{s_\beta}^{s_\beta} \theta_{n_0}^{\alpha,\beta}(\boldsymbol{\omega}_{n_0}) c^{\alpha,\beta}
\end{aligned}$$

$\theta_n^{\alpha,\beta}(\boldsymbol{\omega}_n)$  in (4.12) thus holds, and the  $n$ th-order GFRF in (4.11) is then

straightforward. This completes the proof.  $\square$

## Appendix 4.2. Proof of Lemma 4.1

According to the Woodbury formula[191], the  $L_1$  matrix in (4.33) can be computed as

$$L_1^{-1} = [\tilde{L}_1 + B_2 K]^{-1} = \tilde{L}_1^{-1} - \tilde{L}_1^{-1} B_2 (I + K \tilde{L}_1^{-1} B_2)^{-1} K \tilde{L}_1^{-1} = \tilde{L}_1^{-1} - \delta \quad (\text{K-1})$$

It is clear from (K-1) that the close loop  $L_1^{-1}$  can be seen as a perturbation on the open loop matrix  $\tilde{L}_1^{-1}$ . Based on this, the first-order GFRF in (4.33), i.e.,  $H_1(\tilde{\alpha}_\mu) = L_1^{-1} B_1 E_\mu = (\tilde{L}_1^{-1} - \delta) B_1 E_\mu = \tilde{H}_1(\tilde{\alpha}_\mu) - \delta B_1 E_\mu$  can also be seen as a perturbation on the open loop transfer function  $\tilde{H}_1(\tilde{\alpha}_\mu)$ .

Denote  $\varepsilon = K \tilde{L}_1^{-1} B_2$ , in which the element can be seen as linear combination of the element of  $K$ , i.e.,  $\varepsilon_{m,n} = \sum_{i,j} \varphi_{m_i, n_j} k_{i,j}$ , then the element of the  $l$ th-order matrix  $\varepsilon^l$  can be given as  $\varepsilon_{m,n}^{(l)} = \sum_{\tau_{1,1} + \dots + \tau_{t,r} = l} \varphi_{\tau_{1,1} \dots \tau_{t,r}}^{(m,n)} k_{1,1}^{\tau_{1,1}} k_{1,2}^{\tau_{1,2}} \dots k_{t,r}^{\tau_{t,r}}$ , which is thus a  $l$ th-order nonlinear polynomial with respect to  $k_{i,j}$ .

Denote  $\vartheta = I + K \tilde{L}_1^{-1} B_2 = I + \varepsilon$ . Then  $\vartheta^{-1} = (I + \varepsilon)^{-1} = \sum_{i=0}^{\infty} (-1)^i \varepsilon^i$  converges if the spectral radius  $\rho(\varepsilon) < 1$  holds.

$$\delta = \tilde{L}_1^{-1} B_2 (I + \varepsilon)^{-1} K \tilde{L}_1^{-1} = \sum_{i=0}^{\infty} \left[ (-1)^i \tilde{L}_1^{-1} B_2 \varepsilon^i K \tilde{L}_1^{-1} \right] \quad (\text{K-2})$$

From(K-2), the element of  $\delta$  can then be given as the sum of infinite series with respect to the elements of linear feedback gain matrix  $K$ ,

$$\delta_{m,n} = \sum_{l=1}^{\infty} \sum_{\tau_{1,1} + \dots + \tau_{t,r} = l} \left( \tilde{\varphi}_{\tau_{1,1} \dots \tau_{t,r}} k_{1,1}^{\tau_{1,1}} k_{1,2}^{\tau_{1,2}} \dots k_{t,r}^{\tau_{t,r}} \right) \quad (\text{K-3})$$

The result in Lemma 4.1 is then straightforward. This completes the proof.  $\square$

### Appendix 4.3. Proof of Proposition 4.5

Assuming that Proposition 4.5 holds for all  $n < n_0$ , the following then comes to prove that it still holds for  $n = n_0$ .

From (4.31) and (4.32), the  $n$ th-order GFRF can be recursively calculated with lower-order GFRF. From the assumption above, Proposition 1 holds for all lower-order GFRF, i.e.,  $H_\gamma^j(\boldsymbol{\alpha}; \omega_1, \dots, \omega_\gamma) = \tilde{H}_\gamma^j(\boldsymbol{\alpha}; \omega_1, \dots, \omega_\gamma) + \chi_j^{(\gamma)}$ ,  $\gamma < n_0$ .

Substitute these equations into (4.32),

$$\begin{aligned} \prod_{j=1}^r \prod_{z=1}^{\beta_j} H_{\gamma_{jz}}^j(\boldsymbol{\sigma}_{jz}) &= \prod_{j=1}^r \prod_{z=1}^{\beta_j} \left( \tilde{H}_{\gamma_{jz}}^j(\boldsymbol{\sigma}_{jz}) + \chi_j^{(\gamma_{jz})} \right) = \prod_{j=1}^r \prod_{z=1}^{\beta_j} \tilde{H}_{\gamma_{jz}}^j(\boldsymbol{\sigma}_{jz}) + \sum_j \sum_z \xi_j^1 \chi_j^{(\gamma_{jz})} \\ &+ \sum_{j_1, j_2} \sum_z \xi_{j_1 j_2} \left( \prod_{l=1}^2 \chi_{j_l}^{(\gamma_{j_l z})} \right) + \dots + \sum_{j_1, \dots, j_p} \sum_z \xi_{j_1, \dots, j_p} \left( \prod_{l=1}^p \chi_{j_l}^{(\gamma_{j_l z})} \right) \end{aligned} \quad (\text{K-3})$$

where  $\xi_{j_1 j_2} = \sum \left( \prod_{j=1}^\gamma \prod_{z=1}^{\beta_j} H_{\gamma_{jz}}^j(\boldsymbol{\sigma}_{jz}) \right)$ ,  $\beta_1 + \dots + \beta_\gamma = p - \tau$ , which is the sum of monomials obtained by multiplication of  $p - \tau$  terms lower-order GFRF.

Substitute (K-3) into (4.31) and (4.32), and considering that the inverse of  $\mathbf{L}_n$  matrix in (4.30) can be given as  $\mathbf{L}_n^{-1} = \tilde{\mathbf{L}}_n^{-1} - \boldsymbol{\delta}$ , where  $\boldsymbol{\delta} = \sum_{i=0}^{\infty} [(-1)^i \tilde{\mathbf{L}}_n^{-1} \mathbf{B}_2 \boldsymbol{\varepsilon}^i \mathbf{K} \tilde{\mathbf{L}}_n^{-1}]$ , and  $\boldsymbol{\varepsilon} = \mathbf{K} \tilde{\mathbf{L}}_n^{-1} \mathbf{B}_2$ . Proposition is straightforward according to (4.30). This completes the proof.  $\square$

#### Appendix 4.4. Proof of Proposition 4.6

From Proposition 4.5,  $H_n^j(\boldsymbol{\alpha}; \omega_1, \dots, \omega_n) = \tilde{H}_n^j(\boldsymbol{\alpha}; \omega_1, \dots, \omega_n) + \chi_j^{(n)}$  .

Substituting these equations into (4.29)

$$\begin{aligned}
X_j(\Omega) &= \sum_{n=1}^N \sum_{\substack{\tilde{\alpha}_1, \dots, \tilde{\alpha}_v \geq 0 \\ \tilde{\alpha}_1 + \dots + \tilde{\alpha}_v = n}} \int \cdots \int_{\sum_{i=1}^n \omega_i = \Omega} \left( \tilde{H}_n^j(\tilde{\boldsymbol{\alpha}}) + \chi_j^{(n)} \right) \prod_{\mu=1}^v \left[ \prod_{z=1}^{\tilde{\alpha}_\mu} W_\mu(\omega_{nW_\mu+z}) \right] d\omega_1 \cdots d\omega_n \\
&= \tilde{X}_j(\Omega) + \sum_{n=1}^N \int \cdots \int \left[ \sum_{l=1}^{\infty} \sum_{\tau_{1,1} + \dots + \tau_{r,r} = l} \left( \varphi_{\tau_{1,1}, \dots, \tau_{r,r}}^{(n)} k_{1,1}^{\tau_{1,1}} k_{1,2}^{\tau_{1,2}} \cdots k_{r,r}^{\tau_{r,r}} \right) \prod_{\mu=1}^v \left[ \prod_{z=1}^{\tilde{\alpha}_\mu} W_\mu(\omega_{nW_\mu+z}) \right] \right] d\omega_1 \cdots d\omega_n \\
&= \tilde{X}_j(\Omega) + \sum_{l=1}^{\infty} \sum_{\tau_{1,1} + \dots + \tau_{r,r} = l} \left[ k_{1,1}^{\tau_{1,1}} k_{1,2}^{\tau_{1,2}} \cdots k_{r,r}^{\tau_{r,r}} \left( \sum_{n=1}^N \int \cdots \int \varphi_{\tau_{1,1}, \dots, \tau_{r,r}}^{(n)} \prod_{\mu=1}^v \left[ \prod_{z=1}^{\tilde{\alpha}_\mu} W_{\mu_i}(\omega_{nW_\mu+z}) \right] d\omega_1 \cdots d\omega_n \right) \right] \\
&= \tilde{X}_j(\Omega) + \sum_{l=1}^{\infty} \sum_{\tau_{1,1} + \dots + \tau_{r,r} = l} \varphi_{\tau_{1,1}, \dots, \tau_{r,r}}^{x_j} k_{1,1}^{\tau_{1,1}} k_{1,2}^{\tau_{1,2}} \cdots k_{r,r}^{\tau_{r,r}}
\end{aligned}$$

This completes the proof.  $\square$

### Appendix 5.1: Proof of Proposition 5.2.

For the first-order GFRF, assuming that the input is given as  $u = e^{j\omega t}$ , the output of system (5.3) can be expressed as

$$x_i = H_0^i + H_1^i(\omega_1)e^{j\omega_1 t}, i = 1, 2, 3. \quad (\text{L-1})$$

Substituting (L-1) into (5.3) and equating the coefficients of  $e^{j\omega t}$  to zero, the results are straightforward.

For  $n$ th-order GFRF, giving the input as  $u = e^{j\omega_1 t + \dots + j\omega_n t}$ , the output can then be given as

$$\begin{aligned} x_i = & H_0^i + \sum_{\substack{\text{all combinations} \\ \text{of } \omega_{i1} \text{ in } \boldsymbol{\omega}}} H_1^i(\omega_{i1})e^{j\omega_{i1} t} + \sum_{\substack{\text{all permutations} \\ \text{of } (\omega_{i1}, \omega_{i2})}} \sum_{\substack{\text{all combinations} \\ \text{of } (\omega_{i1}, \omega_{i2}) \text{ in } \boldsymbol{\omega}}} H_2^i(\omega_{i1}, \omega_{i2})e^{j\omega_{i1} t + j\omega_{i2} t} \\ & + \sum_{\substack{\text{all permutations} \\ \text{of } (\omega_{i1}, \omega_{i2}, \omega_{i3})}} \sum_{\substack{\text{all combinations} \\ \text{of } (\omega_{i1}, \omega_{i2}, \omega_{i3}) \text{ in } \boldsymbol{\omega}}} H_3^i(\omega_{i1}, \omega_{i2}, \omega_{i3})e^{j\omega_{i1} t + j\omega_{i2} t + j\omega_{i3} t} + \dots \\ & + \sum_{\substack{\text{all permutations} \\ \text{of } (\omega_{i1}, \dots, \omega_{in})}} \sum_{\substack{\text{all combinations} \\ \text{of } (\omega_{i1}, \dots, \omega_{in}) \text{ in } \boldsymbol{\omega}}} H_n^i(\omega_{i1}, \dots, \omega_{in})e^{j\omega_{i1} t + \dots + j\omega_{in} t} \end{aligned} \quad (\text{L-2})$$

where  $\boldsymbol{\omega} = (\omega_1, \dots, \omega_n)$ . Substituting (L-2) into (5.3) and equating the coefficients of  $e^{j\omega_1 t + \dots + j\omega_n t}$  to zero, the results in Proposition 5.2 can then be obtained. This completes the proof.  $\square$

## 8 Reference

- [1] M. Shokrieh and D. Rezaei, "Analysis and optimization of a composite leaf spring," *Composite Structures*, vol. 60, pp. 317-325, 2003.
- [2] X. Zhu, X. Jing, and L. Cheng, "A magnetorheological fluid embedded pneumatic vibration isolator allowing independently adjustable stiffness and damping," *Smart Materials and Structures*, vol. 20, p. 085025, 2011.
- [3] X. Zhu, X. Jing, and L. Cheng, "Systematic design of a magneto-rheological fluid embedded pneumatic vibration isolator subject to practical constraints," *Smart Materials and Structures*, vol. 21, p. 035006, 2012.
- [4] X. Zhu, X. Jing, and L. Cheng, "Magnetorheological fluid dampers: A review on structure design and analysis," *Journal of Intelligent Material Systems and Structures*, 2012.
- [5] S. Shin, S. Park, J. Kim, and S. Ko, "New quasi-analytic BER estimation technique on the nonlinear satellite communication channels," *Communications, IEE Proceedings-*, vol. 146, pp. 68-72, 1999.
- [6] C. Crespo-Cadenas, J. Reina-Tosina, M. Madero-Ayora, and M. Munoz-Cruzado, "A New Approach to Pruning Volterra Models for Power Amplifiers," *Signal Processing, IEEE Transactions on*, vol. 58, pp. 2113-2120, 2010.
- [7] N. Kim, V. Aparin, and L. Larson, "Analysis of IM3 Asymmetry in MOSFET Small-Signal Amplifiers," *Circuits and Systems I: Regular Papers, IEEE Transactions on*, vol. 58, pp. 668-676, 2011.
- [8] C. Crespo-Cadenas, J. Reina-Tosina, M. Madero-Ayora, and M. Allegue-Martinez, "A Volterra-Based Procedure for Multi-Port and Multi-Zone GaN FET Amplifier CAD Simulation," *Circuits and Systems I: Regular Papers, IEEE Transactions on*, vol. 60, pp. 3022-3032, 2013.
- [9] M. Rawat, F. Ghannouchi, and K. Rawat, "Three-Layered Biased Memory Polynomial for Dynamic Modeling and Predistortion of Transmitters With Memory," *Circuits and Systems I: Regular Papers, IEEE Transactions on*, vol. 60, pp. 768-777, 2013.
- [10] D. Sira and T. Larsen, "Process, Voltage and Temperature Compensation Technique for Cascode Modulated PAs," *Circuits and Systems I: Regular Papers, IEEE Transactions on*, vol. 60, pp. 2511-2520, 2013.
- [11] H. Yu, K. El-Sankary, and E. El-Masry, "Distortion Analysis Using Volterra Series and Linearization Technique of Nano Scale Bulk Driven CMOS RF Amplifier," *Circuits and Systems I: Regular Papers, IEEE Transactions on*, vol. PP, pp. 1-10, 2014.
- [12] A. Carrella, M. Brennan, and T. Waters, "Static analysis of a passive vibration isolator with quasi-zero-stiffness characteristic," *Journal of Sound and Vibration*, vol. 301, pp. 678-689, 2007.

- [13] I. Kovacic, J. Brennan, and T. Waters, "A study of a nonlinear vibration isolator with a quasi-zero stiffness characteristic," *Journal of Sound and Vibration*, vol. 315, pp. 700-711, 2008.
- [14] A. Carrella, M. Brennan, I. Kovacic, and T. Waters, "On the force transmissibility of a vibration isolator with quasi-zero-stiffness," *Journal of Sound and Vibration*, vol. 322, pp. 707-717, 2009.
- [15] I. Kovacic, J. Brennan, and B. Lineton, "Effect of a static force on the dynamic behaviour of a harmonically excited quasi-zero stiffness system," *Journal of Sound and Vibration*, vol. 325, pp. 870-883, 2009.
- [16] G. Gatti, I. Kovacic, and M. Brennan, "On the response of a harmonically excited two degree-of-freedom system consisting of a linear and a nonlinear quasi-zero stiffness oscillator," *Journal of Sound and Vibration*, vol. 329, pp. 1823-1835, 2010.
- [17] D. Xu, Q. Yu, J. Zhou, and S. Bishop, "Theoretical and experimental analyses of a nonlinear magnetic vibration isolator with quasi-zero-stiffness characteristic," *Journal of Sound and Vibration*, vol. 332, pp. 3377-3389, 2013.
- [18] X. Liu, X. Huang, and H. Hua, "On the characteristics of a quasi-zero stiffness isolator using Euler buckled beam as negative stiffness corrector," *Journal of Sound and Vibration*, vol. 332, pp. 3359-3376, 2013.
- [19] X. Sun, X. Jing, J. Xu, and L. Cheng, "A Quasi-Zero-Stiffness-Based Sensor System in Vibration Measurement," *Industrial Electronics, IEEE Transactions on*, vol. 61, pp. 5606-5614, 2014.
- [20] C. Lan, S. Yang, and Y. Wu, "Design and experiment of a compact quasi-zero-stiffness isolator capable of a wide range of loads," *Journal of Sound and Vibration*, vol. 333, pp. 4843-4858, 2014.
- [21] X. Sun, X. Jing, J. Xu, and L. Cheng, "Vibration isolation via a scissor-like structured platform," *Journal of Sound and Vibration*, vol. 333, pp. 2404-2420, 2014.
- [22] X. Sun, X. Jing, L. Cheng, and X. J., "A 3-D Quasi-Zero-Stiffness-Based Sensor System for Absolute Motion Measurement and Application in Active Vibration Control," *Mechatronics, IEEE/ASME Transactions on*, vol. 20, pp. 254-262, 2015.
- [23] Z. Xiao, X. Jing, and L. Cheng, "The transmissibility of vibration isolators with cubic nonlinear damping under both force and base excitations," *Journal of Sound and Vibration*, vol. 332, pp. 1335-1354, 2013.
- [24] Z. Lang, X. Jing, S. Billings, and etc., "Theoretical study of the effects of nonlinear viscous damping on vibration isolation of sdof systems," *Journal of Sound and Vibration*, vol. 323, pp. 352-365, 2009.
- [25] G. Adomian, *Nonlinear stochastic systems theory and application to physics* vol. 46: Springer, 1989.
- [26] J. Hsu, H. Lai, and C. Chen, "An innovative eigenvalue problem solver

- for free vibration of uniform Timoshenko beams by using the Adomian modified decomposition method," *Journal of Sound and Vibration*, vol. 325, pp. 451-470, 2009.
- [27] Q. Mao and S. Pietrzko, "Design of shaped piezoelectric modal sensor for beam with arbitrary boundary conditions by using Adomian decomposition method," *Journal of Sound and Vibration*, vol. 329, pp. 2068-2082, 2010.
- [28] Q. Mao, "Free vibration analysis of elastically connected multiple-beams by using the Adomian modified decomposition method," *Journal of Sound and Vibration*, vol. 331, pp. 2532-2542, 2012.
- [29] R. Ramana and B. R. Prasad, "Modified Adomian Decomposition Method for Van der Pol equations," *International Journal of Non-Linear Mechanics*, vol. 65, pp. 121-132, 2014.
- [30] Y. Cherruault, G. Saccomandi, and B. Some, "New results for convergence of Adomian's method applied to integral equations," *Mathematical and Computer Modelling*, vol. 16, pp. 85-93, 1992.
- [31] Y. Cherruault and G. Adomian, "Decomposition methods: A new proof of convergence," *Mathematical and Computer Modelling*, vol. 18, pp. 103-106, 1993.
- [32] S. Liao, *Beyond perturbation: introduction to the homotopy analysis method*: CRC press, 2003.
- [33] S. Abbasbandy, "Homotopy analysis method for heat radiation equations," *International Communications in Heat and Mass Transfer*, vol. 34, pp. 380-387, 3// 2007.
- [34] S. Abbasbandy, "The application of homotopy analysis method to solve a generalized Hirota–Satsuma coupled KdV equation," *Physics Letters A*, vol. 361, pp. 478-483, 2007.
- [35] J. Cheng, S. Liao, R. Mohapatra, and K. Vajravelu, "Series solutions of nano boundary layer flows by means of the homotopy analysis method," *Journal of Mathematical Analysis and Applications*, vol. 343, pp. 233-245, 2008.
- [36] S. Hoseini, T. Pirbodaghi, M. Asghari, G. Farrahi, and M. Ahmadian, "Nonlinear free vibration of conservative oscillators with inertia and static type cubic nonlinearities using homotopy analysis method," *Journal of Sound and Vibration*, vol. 316, pp. 263-273, 2008.
- [37] Y. Chen, G. Meng, J. Liu, and J. Jing, "Homotopy Analysis Method for Nonlinear Dynamical System of an Electrostatically Actuated Microcantilever," *Mathematical Problems in Engineering*, vol. 2011, p. 14, 2011.
- [38] A. Nayfeh, *Perturbation methods*: John Wiley & Sons, 2000.
- [39] A. Nayfeh and D. Mook, *Nonlinear oscillations*: Wiley-VCH, 2008.
- [40] R. Mahaffey, "Anharmonic oscillator description of plasma oscillations," *Physics of Fluids (1958-1988)*, vol. 19, pp. 1387-1391, 1976.
- [41] J. Peyton, "Automatic computation of polyharmonic balance equations

- for non-linear differential systems," *International Journal of Control*, vol. 76, pp. 355-365, 2003.
- [42] J. Peyton and I. Çankaya, "Polyharmonic Balance Analysis of Nonlinear Ship Roll Response," *Nonlinear Dynamics*, vol. 35, pp. 123-146, 2004.
- [43] D. Akgün, I. Çankaya, and J. Peyton, "A symbolic algorithm for the automatic computation of multitone-input harmonic balance equations for nonlinear systems," *Nonlinear Dynamics*, vol. 56, pp. 179-191, 2009.
- [44] J. Slotine and W. Li, *Applied nonlinear control* vol. 199: Prentice-Hall Englewood Cliffs, NJ, 1991.
- [45] H. Khalil, *Nonlinear systems* vol. 3: Prentice hall Upper Saddle River, 2002.
- [46] J. Peyton and S. Billings, "Describing functions, Volterra series, and the analysis of non-linear systems in the frequency domain," *International Journal of Control*, vol. 53, pp. 871-887, 1991.
- [47] J. Peyton, "Mapping nonlinear integro-differential equations to a generalized describing function form," *International Journal of Control*, vol. 62, pp. 1145-1160, 1995.
- [48] V. Volterra, "Theory of functionals and of integral and integro-differential equations," 1959.
- [49] M. Brilliant, "Theory of the analysis of nonlinear systems," Technical report 345, 1958.
- [50] R. Brockett, "Volterra series and geometric control theory," *Automatica*, vol. 12, pp. 167-176, 1976.
- [51] I. Sandberg, "Expansions for nonlinear systems," *Bell Syst. Tech. J.*, vol. 61, pp. 159-199, 1982.
- [52] I. Sandberg, "On Volterra expansions for time-varying nonlinear systems," *Circuits and Systems, IEEE Transactions on*, vol. 30, pp. 61-67, 1983.
- [53] I. Sandberg, "The mathematical foundations of associated expansions for mildly nonlinear systems," *Circuits and Systems, IEEE Transactions on*, vol. 30, pp. 441-455, 1983.
- [54] I. Sandberg, "Volterra-like expansions for solutions of nonlinear integral equations and nonlinear differential equations," *Circuits and Systems, IEEE Transactions on*, vol. 30, pp. 68-77, 1983.
- [55] S. Boyd, L. Chua, and C. Desoer, "Analytical Foundations of Volterra Series," *IMA Journal of Mathematical Control and Information*, vol. 1, pp. 243-282, 1984.
- [56] S. Boyd and L. Chua, "Fading memory and the problem of approximating nonlinear operators with Volterra series," *Circuits and Systems, IEEE Transactions on*, vol. 32, pp. 1150-1161, 1985.
- [57] D. George, "Continuous nonlinear systems," *Technical report (Massachusetts Institute of Technology. Research Laboratory of Electronics) ; 355.*, 1959.
- [58] J. Peyton and S. Billings, "Recursive algorithm for computing the

- frequency response of a class of non-linear difference equation models," *International Journal of Control*, vol. 50, pp. 1925-1940, 1989.
- [59] S. Billings and J. Peyton, "Mapping non-linear integro-differential equations into the frequency domain," *International Journal of Control*, vol. 52, pp. 863-879, 1990.
- [60] H. Zhang, S. Billings, and Q. Zhu, "Frequency response functions for nonlinear rational models," *International Journal of Control*, vol. 61, pp. 1073-1097, 1995.
- [61] J. P. Billings, "Mean levels in nonlinear analysis and identification," *International Journal of Control*, vol. 58, pp. 1033-1052, 1993.
- [62] J. Peyton and K. Choudhary, "Efficient computation of higher order frequency response functions for nonlinear systems with, and without, a constant term," *International Journal of Control*, vol. 85, pp. 578-593, 2012.
- [63] S. Billings and H. Zhang, "Computation of non-linear transfer functions when constant terms are present," *Mechanical Systems and Signal Processing*, vol. 9, pp. 537-553, 1995.
- [64] K. Worden, G. Manson, and G. Tomlinson, "A Harmonic Probing Algorithm for the Multi-input Volterra Series," *Journal of Sound and Vibration*, vol. 201, pp. 67-84, 1997.
- [65] A. Swain and S. Billings, "Generalized frequency response function matrix for MIMO non-linear systems," *International Journal of Control*, vol. 74, pp. 829-844, 2001.
- [66] Y. Guo, L. Guo, S. Billings, D. Coca, and Z. Lang, "Volterra Series Approximation of a Class of Nonlinear Dynamical Systems Using the Adomian Decomposition Method," *Nonlinear Dynamics*, vol. 74, pp. 359-371, 2013.
- [67] R. Bayma and Z. Lang, "A New Method for Determining the Generalised Frequency Response Functions of Nonlinear Systems," *Circuits and Systems I: Regular Papers, IEEE Transactions on*, vol. 59, pp. 3005-3014, 2012.
- [68] J. Peyton, "Simplified computation of the Volterra frequency response functions of non-linear systems," *Mechanical Systems and Signal Processing*, vol. 21, pp. 1452-1468, 2007.
- [69] B. Zhang, S. Billings, Z. Lang, and G. Tomlinson, "Analytical Description of the Frequency Response Function of the Generalized Higher Order Duffing Oscillator Model," *Circuits and Systems I: Regular Papers, IEEE Transactions on*, vol. 56, pp. 224-232, 2009.
- [70] Z. Lang and S. Billings, "Output frequency characteristics of nonlinear systems," *International Journal of Control*, vol. 64, pp. 1049-1067, 1996.
- [71] Z. Lang and S. Billings, "Output frequencies of nonlinear systems," *International Journal of Control*, vol. 67, pp. 713-730, 1997.
- [72] X. Wu, Z. Lang, and S. Billings, "Analysis of Output Frequencies of Nonlinear Systems," *Signal Processing, IEEE Transactions on*, vol. 55,

- pp. 3239-3246, 2007.
- [73] X. Jing, Z. Lang, and S. Billings, "Output frequency properties of nonlinear systems," *International Journal of Non-Linear Mechanics*, vol. 45, pp. 681-690, 2010.
  - [74] J. Peyton and S. Billings, "Interpretation of non-linear frequency response functions," *International Journal of Control*, vol. 52, pp. 319-346, 1990.
  - [75] J. Peyton and K. Choudhary, "Output frequency response characteristics of nonlinear systems. Part I: general multi-tone inputs," *International Journal of Control*, vol. 85, pp. 1263-1278, 2012.
  - [76] J. Peyton and K. Choudhary, "Output frequency response characteristics of nonlinear systems. Part II: overlapping effects and commensurate multi-tone excitations," *International Journal of Control*, vol. 85, pp. 1279-1292, 2012.
  - [77] R. Yue, S. Billings, and Z. Lang, "An investigation into the characteristics of non-linear frequency response functions. Part 1: Understanding the higher dimensional frequency spaces," *International Journal of Control*, vol. 78, pp. 1031-1044, 2005.
  - [78] R. Yue, S. Billings, and Z. Lang, "An investigation into the characteristics of non-linear frequency response functions. Part 2: New analysis methods based on symbolic expansions and graphical techniques," *International Journal of Control*, vol. 78, pp. 1130-1149, 2005.
  - [79] X. Jing, Z. Lang, and S. Billings, "Nonlinear influence in the frequency domain: Alternating series," *Systems & Control Letters*, vol. 60, pp. 295-309, 2011.
  - [80] X. Wu, Z. Lang, and S. Billings, "The design of energy transfer filters for energy focus filtering," *International Journal of Control*, vol. 81, pp. 214-226, 2008.
  - [81] X. Wu, Z. Lang, and S. Billings, "A new method for the design of energy transfer filters," *International Journal of Control*, vol. 79, pp. 968-981, 2006.
  - [82] Z. Lang and S. Billings, "Energy transfer properties of non-linear systems in the frequency domain," *International Journal of Control*, vol. 78, pp. 345-362, 2005.
  - [83] S. Billings and Z. Lang, "Non-linear systems in the frequency domain: Energy transfer filters," *International Journal of Control*, vol. 75, pp. 1066-1081, 2002.
  - [84] G. Tomlinson, Z. Lang, S. Billings, and F. Xie, "Suppressing resonant vibrations via energy transfer concepts," *Structural Control and Health Monitoring*, vol. 13, pp. 523-535, 2006.
  - [85] X. Jing and Z. Lang, "Frequency domain analysis of a dimensionless cubic nonlinear damping system subject to harmonic input," *Nonlinear Dynamics*, vol. 58, pp. 469-485, 2009.
  - [86] X. Jing, Z. Lang, S. Billings, and etc., "Frequency domain analysis for suppression of output vibration from periodic disturbance using

- nonlinearities," *Journal of Sound and Vibration*, vol. 314, pp. 536-557, 2008.
- [87] Z. Peng, Z. Lang, and S. Billings, "Non-linear output frequency response functions for multi-input non-linear Volterra systems," *International Journal of Control*, vol. 80, pp. 843-855, 2007.
- [88] Z. Peng, Z. Lang, and S. Billings, "Crack detection using nonlinear output frequency response functions," *Journal of Sound and Vibration*, vol. 301, pp. 777-788, 2007.
- [89] Z. Peng, Z. Lang, and S. Billings, "Nonlinear parameter estimation for multi-degree-of-freedom nonlinear systems using nonlinear output frequency-response functions," *Mechanical Systems and Signal Processing*, vol. 22, pp. 1582-1594, 2008.
- [90] Z. Peng, Z. Lang, F. Chu, and G. Meng, "Locating Nonlinear Components in Periodic Structures using Nonlinear Effects," *Structural Health Monitoring*, vol. 9, pp. 401-411, September 1, 2010 2010.
- [91] X. Jing, "Truncation order and its effect in a class of nonlinear systems," *Automatica*, vol. 48, pp. 2978-2985, 2012.
- [92] X. Jing, "Nonlinear Characteristic Output Spectrum for Nonlinear Analysis and Design," *Mechatronics, IEEE/ASME Transactions on*, vol. 19, pp. 171-183, 2012.
- [93] X. Jing, Z. Lang, and S. Billings, "Determination of the analytical parametric relationship for output spectrum of Volterra systems based on its parametric characteristics," *Journal of Mathematical Analysis and Applications*, vol. 351, pp. 694-706, 2009.
- [94] X. Jing, Z. Lang, and S. Billings, "Output frequency response function-based analysis for nonlinear Volterra systems," *Mechanical Systems and Signal Processing*, vol. 22, pp. 102-120, 2008.
- [95] Z. Lang, S. Billings, R. Yue, and etc., "Output frequency response function of nonlinear Volterra systems," *Automatica*, vol. 43, pp. 805-816, 2007.
- [96] X. Jing, Z. Lang, and S. Billings, "Frequency-dependent magnitude bounds of the generalized frequency response functions for NARX model," *European journal of control*, vol. 15, pp. 68-83, 2009.
- [97] X. Jing, Z. Lang, and S. Billings, "Magnitude bounds of generalized frequency response functions for nonlinear Volterra systems described by NARX model," *Automatica*, vol. 44, pp. 838-845, 2008.
- [98] X. Jing, Z. Lang, and S. Billings, "New bound characteristics of NARX model in the frequency domain," *International Journal of Control*, vol. 80, pp. 140-149, 2006.
- [99] J. Peyton, "Practical frequency response analysis of non-linear time-delayed differential or difference equation models," *International Journal of Control*, vol. 78, pp. 65-79, 2005.
- [100] A. Swain, E. Mendes, and S. Nguang, "Analysis of the effects of time delay in nonlinear systems using generalised frequency response

- functions," *Journal of Sound and Vibration*, vol. 294, pp. 341-354, 2006.
- [101] Y. Guo, L. Guo, S. Billings, D. Coca, and Z. Lang, "A parametric frequency response method for non-linear time-varying systems," *International Journal of Systems Science*, vol. 45, pp. 2133-2144, 2013.
- [102] L. Guo, S. Billings, and D. Coca, "Identification of partial differential equation models for a class of multiscale spatio-temporal dynamical systems," *International Journal of Control*, vol. 83, pp. 40-48, 2009.
- [103] Y. Guo, L. Guo, S. Billings, D. Coca, and Z. Lang, "Characterizing Nonlinear Spatio-temporal Systems in the Frequency Domain," *International Journal of Bifurcation and Chaos*, vol. 22, p. 1230009, 2012.
- [104] L. Guo, Y. Guo, S. Billings, D. Coca, and Z. Lang, "A Volterra series approach to the frequency domain analysis of non-linear viscous Burgers' equation," *Nonlinear Dynamics*, vol. 70, pp. 1753-1765, 2012.
- [105] L. Guo, Y. Guo, S. Billings, D. Coca, and Z. Lang, "Spatial frequency range analysis for the nonlinear Schrödinger equation," *Nonlinear Dynamics*, vol. 78, pp. 93-102, 2014.
- [106] L. Guo, Y. Guo, Y. Zhao, S. Billings, D. Coca, and Z. Lang, "A Spatial Frequency Domain Analysis of the Belousov–Zhabotinsky Reaction," *International Journal of Bifurcation and Chaos*, vol. 24, p. 1450031, 2014.
- [107] O. Boaghe and S. Billings, "Subharmonic oscillation modeling and MISO Volterra series," *Circuits and Systems I: Fundamental Theory and Applications, IEEE Transactions on*, vol. 50, pp. 877-884, 2003.
- [108] L. Li and S. Billings, "Discrete time subharmonic modelling and analysis," *International Journal of Control*, vol. 78, pp. 1265-1284, 2005.
- [109] S. Billings and O. Boaghe, "The response spectrum map, a frequency domain equivalent to the bifurcation diagram," *International Journal of Bifurcation and Chaos*, vol. 11, pp. 1961-1975, 2001.
- [110] L. Li and S. Billings, "Analysis of nonlinear oscillators using Volterra series in the frequency domain," *Journal of Sound and Vibration*, vol. 330, pp. 337-355, 2011.
- [111] L. Li and S. Billings, "Piecewise Volterra modeling of the Duffing oscillator in the frequency-domain," *Mechanical Systems and Signal Processing*, vol. 26, pp. 117-127, 2012.
- [112] X. Jing and Z. Lang, *Frequency Domain Analysis and Design of Nonlinear Systems based on Volterra Series Expansion: A Parametric Characteristic Approach*: Springer, 2015.
- [113] X. Jing, Z. Lang, S. Billings, and etc., "The parametric characteristic of frequency response functions for nonlinear systems," *International Journal of Control*, vol. 79, pp. 1552-1564, 2006.
- [114] X. Jing, Z. Lang, and S. Billings, "Frequency domain analysis for non-linear Volterra systems with a general non-linear output function," *International Journal of Control*, vol. 81, pp. 235-251, 2008.

- [115] X. Jing, Z. Lang, and S. Billings, "Mapping from parametric characteristics to generalized frequency response functions of non-linear systems," *International Journal of Control*, vol. 81, pp. 1071-1088, 2008.
- [116] X. Jing and Z. Lang, "On the Generalized Frequency Response Functions of Volterra Systems," *Journal of dynamic systems, measurement, and control*, vol. 131, p. 061002, 2009.
- [117] X. Jing, Z. Lang, and S. Billings, "Parametric Characteristic Analysis for Generalized Frequency Response Functions of Nonlinear Systems," *Circuits, Systems, and Signal Processing*, vol. 28, pp. 699-733, 2009.
- [118] F. Bullo, "Series expansions for analytic systems linear in control," *Automatica*, vol. 38, pp. 1425-1432, 2002.
- [119] G. Tomlinson, G. Manson, and G. Lee, "A Simple Criterion for Establishing an Upper Limit to the Harmonic Excitation Level of the Duffing Oscillator Using the Volterra Series," *Journal of Sound and Vibration*, vol. 190, pp. 751-762, 1996.
- [120] Z. Peng and Z. Lang, "On the convergence of the Volterra-series representation of the Duffing's oscillators subjected to harmonic excitations," *Journal of Sound and Vibration*, vol. 305, pp. 322-332, 2007.
- [121] T. Helie and B. Laroche, "Computation of Convergence Bounds for Volterra Series of Linear-Analytic Single-Input Systems," *Automatic Control, IEEE Transactions on*, vol. 56, pp. 2062-2072, 2011.
- [122] H. Hélie and B. Laroche, "Computable convergence bounds of series expansions for infinite dimensional linear-analytic systems and application," *Automatica*, vol. 50, pp. 2334-2340, 2014.
- [123] M. Asyali and M. Juusola, "Use of Meixner functions in estimation of Volterra kernels of nonlinear systems with delay," *Biomedical Engineering, IEEE Transactions on*, vol. 52, pp. 229-237, 2005.
- [124] G. Li, C. Wen, W. Zheng, and Y. Chen, "Identification of a Class of Nonlinear Autoregressive Models With Exogenous Inputs Based on Kernel Machines," *Signal Processing, IEEE Transactions on*, vol. 59, pp. 2146-2159, 2011.
- [125] M. Inagaki and H. Mochizuki, "Bilinear system identification by Volterra kernels estimation," *Automatic Control, IEEE Transactions on*, vol. 29, pp. 746-749, 1984.
- [126] S. Kotsios, "Transformation of finite degree discrete Volterra systems with cross products to finite input-output forms," *Automatic Control, IEEE Transactions on*, vol. 44, pp. 1460-1464, 1999.
- [127] D. Mirri, G. Iuculano, F. Filicori, and etc., "A modified Volterra series approach for nonlinear dynamic systems modeling," *Circuits and Systems I: Fundamental Theory and Applications, IEEE Transactions on*, vol. 49, pp. 1118-1128, 2002.
- [128] J. Nichols, "Frequency Distortion of Second- and Third-Order Phase-Locked Loop Systems Using a Volterra-Series Approximation,"

- Circuits and Systems I: Regular Papers, IEEE Transactions on*, vol. 56, pp. 453-459, 2009.
- [129] Q. Zheng and E. Zafiriou, "A local form of small gain theorem and analysis of feedback Volterra systems," *Automatic Control, IEEE Transactions on*, vol. 44, pp. 635-640, 1999.
- [130] S. Chen and S. Billings, "Representations of non-linear systems: the NARMAX model," *International Journal of Control*, vol. 49, pp. 1013-1032, 1989.
- [131] I. Leontaritis and S. Billings, "Input-output parametric models for non-linear systems Part I: deterministic non-linear systems," *International Journal of Control*, vol. 41, pp. 303-328, 1985.
- [132] I. Leontaritis and S. Billings, "Input-output parametric models for non-linear systems Part II: stochastic non-linear systems," *International Journal of Control*, vol. 41, pp. 329-344, 1985.
- [133] D. Jiang, C. Pierre, and S. Shaw, "Nonlinear normal modes for vibratory systems under harmonic excitation," *Journal of Sound and Vibration*, vol. 288, pp. 791-812, 2005.
- [134] G. Kerschen, M. Peeters, J. Golinval, and A. Vakakis, "Nonlinear normal modes, Part I: A useful framework for the structural dynamicist," *Mechanical Systems and Signal Processing*, vol. 23, pp. 170-194, 2009.
- [135] M. Peeters, R. Viguié, G. Séréndour, G. Kerschen, and J. Golinval, "Nonlinear normal modes, Part II: Toward a practical computation using numerical continuation techniques," *Mechanical Systems and Signal Processing*, vol. 23, pp. 195-216, 2009.
- [136] X. Jing, "Frequency domain analysis and identification of block-oriented nonlinear systems," *Journal of Sound and Vibration*, vol. 330, pp. 5427-5442, 2011.
- [137] P. Flajolet and R. Sedgewick, *Analytic combinatorics*: Cambridge Univ Pr, 2009.
- [138] Z. Xiao, X. Jing, and L. Cheng, "Parameterized Convergence Bounds for Volterra Series Expansion of NARX Models," *Signal Processing, IEEE Transactions on*, vol. 61, pp. 5026-5038, 2013.
- [139] Z. Xiao, X. Jing, and L. Cheng, "Estimation of parametric convergence bounds for Volterra series expansion of nonlinear systems," *Mechanical Systems and Signal Processing*, vol. 45, pp. 28-48, 2014.
- [140] W. Sun, Z. Zhao, and H. Gao, "Saturated Adaptive Robust Control for Active Suspension Systems," *Industrial Electronics, IEEE Transactions on*, vol. 60, pp. 3889-3896, 2013.
- [141] C. Kim and P. Ro, "A sliding mode controller for vehicle active suspension systems with non-linearities," *Proceedings of the Institution of Mechanical Engineers, Part D: Journal of Automobile Engineering*, vol. 212, pp. 79-92, 1998.
- [142] R. Lian, "Enhanced Adaptive Self-Organizing Fuzzy Sliding-Mode Controller for Active Suspension Systems," *Industrial Electronics, IEEE*

- Transactions on*, vol. 60, pp. 958-968, 2013.
- [143] Y. Jin, P. Chang, M. Jin, and D. Gweon, "Stability Guaranteed Time-Delay Control of Manipulators Using Nonlinear Damping and Terminal Sliding Mode," *Industrial Electronics, IEEE Transactions on*, vol. 60, pp. 3304-3317, 2013.
  - [144] J. Kovacsics, J. Piedboeuf, and C. Lange, "Dynamics modeling and simulation of constrained robotic systems," *Mechatronics, IEEE/ASME Transactions on*, vol. 8, pp. 165-177, 2003.
  - [145] T. Hu, K. Low, L. Shen, and X. Xu, "Effective Phase Tracking for Bioinspired Undulations of Robotic Fish Models: A Learning Control Approach," *Mechatronics, IEEE/ASME Transactions on*, vol. 19, pp. 191-200, 2014.
  - [146] L. Garbuio, M. Lallart, D. Guyomar, C. Richard, and D. Audigier, "Mechanical Energy Harvester With Ultralow Threshold Rectification Based on SSHI Nonlinear Technique," *Industrial Electronics, IEEE Transactions on*, vol. 56, pp. 1048-1056, 2009.
  - [147] W. Lan, C. Thum, and B. Chen, "A Hard-Disk-Drive Servo System Design Using Composite Nonlinear-Feedback Control With Optimal Nonlinear Gain Tuning Methods," *Industrial Electronics, IEEE Transactions on*, vol. 57, pp. 1735-1745, 2010.
  - [148] R. Dhaouadi and K. Kubo, "A nonlinear control method for good dynamic performance elastic drives," *Industrial Electronics, IEEE Transactions on*, vol. 46, pp. 868-870, 1999.
  - [149] Z. Yao and L. Xiao, "Control of Single-Phase Grid-Connected Inverters With Nonlinear Loads," *Industrial Electronics, IEEE Transactions on*, vol. 60, pp. 1384-1389, 2013.
  - [150] P. Thureau, D. Lecler, and J. Grosjean, *An introduction to the principles of vibrations of linear systems*: Thornes, 1981.
  - [151] S. Rao and F. Yap, *Mechanical vibrations* vol. 4: Addison-Wesley New York, 1995.
  - [152] R. Ibrahim, "Recent advances in nonlinear passive vibration isolators," *Journal of Sound and Vibration*, vol. 314, pp. 371-452, 2008.
  - [153] B. Ravindra and A. Mallik, "Performance of Non-linear Vibration Isolators Under Harmonic Excitation," *Journal of Sound and Vibration*, vol. 170, pp. 325-337, 1994.
  - [154] R. Jazar, R. Houim, A. Narimani, and M. Golnaraghi, "Frequency Response and Jump Avoidance in a Nonlinear Passive Engine Mount," *Journal of Vibration and Control*, vol. 12, pp. 1205-1237, 2006.
  - [155] G. Popov and S. Sankar, "Modelling and analysis of non-linear orifice type damping in vibration isolators," *Journal of Sound and Vibration*, vol. 183, pp. 751-764, 1995.
  - [156] P. Yang, J. Yang, and J. Ding, "Dynamic Transmissibility of a Complex Nonlinear Coupling Isolator," *Tsinghua Science Technology*, vol. 11, pp. 538-542, 2006.

- [157] Z. Milovanovic, I. Kovacic, and M. Brennan, "On the Displacement Transmissibility of a Base Excited Viscously Damped Nonlinear Vibration Isolator," *Journal of Vibration and Acoustics*, vol. 131, pp. 054502-7, 2009.
- [158] R. Dixit and G. Buckner, "Sliding mode observation and control for semiactive vehicle suspensions," *Vehicle System Dynamics*, vol. 43, pp. 83-105, 2005.
- [159] W. Sun, H. Gao, and O. Kaynak, "Adaptive Backstepping Control for Active Suspension Systems With Hard Constraints," *Mechatronics, IEEE/ASME Transactions on*, vol. 18, pp. 1072-1079, 2013.
- [160] M. Zapateiro, F. Pozo, H. Karimi, and N. Luo, "Semiactive Control Methodologies for Suspension Control With Magnetorheological Dampers," *Mechatronics, IEEE/ASME Transactions on*, vol. 17, pp. 370-380, 2012.
- [161] W. Sun, H. Gao, and O. Kaynak, "Vibration Isolation for Active Suspensions With Performance Constraints and Actuator Saturation," *Mechatronics, IEEE/ASME Transactions on*, vol. PP, pp. 1-9, 2014.
- [162] S. Savaresi, E. Silani, and S. Bittanti, "On performance evaluation methods and control strategies for semi-active suspension systems," in *Decision and Control, 2003. Proceedings. 42nd IEEE Conference on*, 2003, pp. 2264-2269 Vol.3.
- [163] S. Savaresi, E. Silani, and S. Bittanti, "Acceleration-Driven-Damper (ADD): An optimal control algorithm for comfort-oriented semiactive suspensions," *Journal of dynamic systems, measurement, and control*, vol. 127, pp. 218-229, 2005.
- [164] S. Savaresi and C. Spelta, "Mixed sky-hook and ADD: Approaching the filtering limits of a semi-active suspension," *Journal of dynamic systems, measurement, and control*, vol. 129, pp. 382-392, 2007.
- [165] M. Milanese and C. Novara, "Structured Set Membership identification of nonlinear systems with application to vehicles with controlled suspension," *Control Engineering Practice*, vol. 15, pp. 1-16, 2007.
- [166] R. Amirifar and N. Sadati, "Low-order H infinity controller design for an active suspension system via LMIs," *Industrial Electronics, IEEE Transactions on*, vol. 53, pp. 554-560, 2006.
- [167] H. Li, J. Yu, C. Hilton, and etc., "Adaptive Sliding-Mode Control for Nonlinear Active Suspension Vehicle Systems Using TS Fuzzy Approach," *Industrial Electronics, IEEE Transactions on*, vol. 60, pp. 3328-3338, 2013.
- [168] H. Gao, W. Sun, and P. Shi, "Robust Sampled-Data H infinity Control for Vehicle Active Suspension Systems," *Control Systems Technology, IEEE Transactions on*, vol. 18, pp. 238-245, 2010.
- [169] F. del-Aguila-Lopez, P. Pala-Schonwalder, P. Molina-Gaudo, and A. Mediano-Heredia, "A Discrete-Time Technique for the Steady-State Analysis of Nonlinear Class-E Amplifiers," *Circuits and Systems I:*

- Regular Papers, IEEE Transactions on*, vol. 54, pp. 1358-1366, 2007.
- [170] M. Schetzen, "The Volterra and Wiener theories of nonlinear systems," 1980.
- [171] M. Mollaalipour and H. Miar-Naimi, "An Improved High Linearity Active CMOS Mixer: Design and Volterra Series Analysis," *Circuits and Systems I: Regular Papers, IEEE Transactions on*, vol. 60, pp. 2092-2103, 2013.
- [172] T. Kim, "A Common-gate Amplifier With Transconductance Nonlinearity Cancellation and Its High Frequency Analysis Using the Volterra Series," *Microwave Theory and Techniques, IEEE Transactions on*, vol. 57, pp. 1461-1469, 2009.
- [173] B. Toole, C. Plett, and M. Cloutier, "RF circuit implications of moderate inversion enhanced linear region in MOSFETs," *Circuits and Systems I: Regular Papers, IEEE Transactions on*, vol. 51, pp. 319-328, 2004.
- [174] Y. Miao and Z. Y., "Distortion Modeling of Feedback Two Stage Amplifier Compensated With Miller Capacitor and Nulling Resistor," *Circuits and Systems I: Regular Papers, IEEE Transactions on*, vol. 59, pp. 93-105, 2012.
- [175] S. Cannizzaro, G. Palumbo, and S. Pennisi, "Effects of nonlinear feedback in the frequency domain," *Circuits and Systems I: Regular Papers, IEEE Transactions on*, vol. 53, pp. 225-234, 2006.
- [176] G. Palumbo and S. Pennisi, "High frequency harmonic distortion in feedback amplifiers: analysis and applications," *Circuits and Systems I: Fundamental Theory and Applications, IEEE Transactions on*, vol. 50, pp. 328-340, 2003.
- [177] S. Cannizzaro, G. Palumbo, and S. Pennisi, "Distortion analysis of Miller compensated three stage amplifiers," *Circuits and Systems I: Regular Papers, IEEE Transactions on*, vol. 53, pp. 961-976, 2006.
- [178] M. Kim and T. Yun, "Analysis and Design of Feedforward Linearity Improved Mixer Using Inductive Source Degeneration," *Microwave Theory and Techniques, IEEE Transactions on*, vol. 62, pp. 323-331, 2014.
- [179] W. Cheng, M. Alink, A. Annema, J. Croon, and B. Nauta, "RF Circuit Linearity Optimization Using a General Weak Nonlinearity Model," *Circuits and Systems I: Regular Papers, IEEE Transactions on*, vol. 59, pp. 2340-2353, 2012.
- [180] A. Buonomo and A. L. Schiavo, "Perturbation analysis of nonlinear distortion in analog integrated circuits," *Circuits and Systems I: Regular Papers, IEEE Transactions on*, vol. 52, pp. 1620-1631, 2005.
- [181] N. Boulejfen, A. Harguem, and M. Ghannouchi, "New closed-form expressions for the prediction of multitone intermodulation distortion in fifth-order nonlinear RF circuits/systems," *Microwave Theory and Techniques, IEEE Transactions on*, vol. 52, pp. 121-132, 2004.
- [182] J. Martins, N. Carvalho, and J. Pedro, "Intermodulation Distortion of

- Third Order Nonlinear Systems With Memory Under Multisine Excitations," *Microwave Theory and Techniques, IEEE Transactions on*, vol. 55, pp. 1264-1271, 2007.
- [183] S. Farsi, P. Draxler, H. Gheidi, and B. Nauwelaers, "Characterization of Intermodulation and Memory Effects Using Offset Multisine Excitation," *Microwave Theory and Techniques, IEEE Transactions on*, vol. 62, pp. 645-657, 2014.
- [184] S. Lee, M. Jeon, and V. Shin, "Distributed Estimation Fusion With Application to a Multisensory Vehicle Suspension System With Time Delays," *Industrial Electronics, IEEE Transactions on*, vol. 59, pp. 4475-4482, 2012.
- [185] W. Sun, Y. Zhao, J. Li, L. Zhang, and H. Gao, "Active Suspension Control With Frequency Band Constraints and Actuator Input Delay," *Industrial Electronics, IEEE Transactions on*, vol. 59, pp. 530-537, 2012.
- [186] N. Wouw, H. Pastink, M. Heertjes, A. Pavlov, and H. Nijmeijer, "Performance of convergence-based variable-gain control of optical storage drives," *Automatica*, vol. 44, pp. 15-27, 2008.
- [187] S. Haykin, *Neural networks and learning machines* vol. 3. Upper Saddle River: Pearson Education, 2009.
- [188] J. Chance, K. Worden, and G. Tomlinson, "Frequency domain analysis of NARX neural networks," *Journal of Sound and Vibration*, vol. 213, pp. 915-941, 1998.
- [189] C. Fung, S. Billings, and H. Zhang, "Generalised transfer functions of neural networks," *Mechanical Systems and Signal Processing*, vol. 11, pp. 843-868, 1997.
- [190] B. Roth, "Computations in kinematics," *Computational Kinematics*, pp. 3-14, 1993.
- [191] G. Golub and C. V. Loan, *Matrix computations* vol. 3: JHU Press, 2012.